Université de Montréal

Biomimetic Materials for *In Situ* Corneal Tissue Regeneration

Par

Fiona Simpson

Département de pharmacologie et physiologie
Institut de génie biomédical
Faculté de médecine

Thèse présentée en vue de l'obtention du grade de
Philosophiæ Doctor (Ph.D.)
en Génie Biomédical

octobre 2021

© Fiona Simpson, 2021

Université de Montréal

Faculté des études supérieures et postdoctorales

Cette thèse intitulée

Biomimetic Materials for *In Situ* Corneal Tissue Regeneration

présentée par

Fiona Simpson

a été évaluée par un jury composé des personnes suivantes :

Dr. Houman Savoji
(président-rapporteur)

Dr. May Griffith
(directeur de recherche)

Dr. Marie-Claude Robert
(co-directeur)

Dr. Marc Lavertu
(membre du jury)

Dr. Che Connon
(examinateur externe)

Dr. Alain Vinet
(représentant du doyen de la FESP)

Thèse acceptée le :
4 octobre 2021

Sommaire

La cécité cornéenne touche 12,7 millions personnes globalement. Il y a une pénurie des cornées de donneurs humains (CDH), et donc les tissues disponibles sont implanté préférentiellement dans les patients avec des troubles cornéens à faible risque comme le kératocône et la dystrophie endothéliale de Fuchs. Les patients qui ont un risque élevé d'inflammation, comme ceux avec des brûlures acides, alcalines et thermiques, des infections et des ulcères, ne reçoivent pas de greffes pour leurs maladies cornéennes.

Les biomatériaux offrent une alternative aux CDH en permettant le développement de solutions de régénération cornéenne avec une longue durée de conservation, une thermostabilité pour un déploiement en zone rurale, et biocompatibilité chez les patients à haut risque.

Les biomatériaux peuvent être développés sous forme d'implants cornéens solides à greffer dans des opacités cornéennes ou sous forme de liquides gélifiants injectables qui peuvent sceller des petites perforations cornéennes. Les implants cornéens solides conviennent aux chirurgiens ophtalmologiques, mais les produits de comblement liquides peuvent être utilisés par les prestataires de médecine d'urgence ou le personnel médical non spécialisé dans les zones où les chirurgiens ophtalmologistes ne sont pas disponibles.

Cette thèse explore les formulations de biomatériaux pour les cornéens solides et gélifiants in situ, leurs performances en tant que dispositifs composites, l'ajout de la stérilisation terminale à la fabrication d'implants cornéens solides et le développement de futures protéines mimétiques du collagène pour la formulation d'hydrogel.

Le premier objectif de cette thèse était de développer un implant cornéen solide adapté à l'implantation chez les patients cornéens à haut risque. Les implants cornéens peptide-mimant-le-collagène-polyéthylène glycol-phosphorylcholine (PMC-PEG-MPC) et

les implants recombinants de collagène humain de type III-phosphorylcholine (RCHIII-MPC) ont réussi à régénérer les cornées de mini-porcs et de lapins, respectivement. La phosphorylcholine présente dans la formulation PMC-PEG-MPC a diminué l'inflammation et fourni une alternative cornéenne viable dans les brûlures alcalines à haut risque. Des nanoparticules d'argent coiffées de peptides étaient fabriquées avec succès à la surface d'un implant cornéen solide de collagène porcin de type I. Ces implants ont inhibé *P. aeruginosa*, *S. aureus* et *S. epidermidis in vitro* et empêché la formation de biofilm à l'interface air-liquide. Ces implants cornéens solides élargissent la gamme d'efficacité pour inclure les personnes souffrant de brûlures alcalines et d'infections. Finalement, on a validé une méthode de stérilisation terminale des implants cornéens solides. Le RCHIII-MPC a été stérilisé en phase terminale avec succès à l'aide d'une irradiation par faisceau d'électrons, offrant une future voie pour la stérilisation terminale des implants cornéens solides à base de biomatériaux.

Le deuxième objectif était de concevoir un hydrogel qui se solidifierait *in situ* pour sceller les perforations cornéennes. Le PMC-PEG était combiné avec du fibrinogène pour former "LiQD Cornea", le premier produit de comblement cornéen liquide à être chimiquement réticulé avec succès *in situ* pour sceller les perforations cornéennes et les plaies chirurgicales chez le lapin et les mini-porcs.

Pour le troisième objectif, ce projet fournit également une méthodologie future pour la production de protéines mimétiques de collagène personnalisées pour les futures formulations d'hydrogel.

Dans l'ensemble, le collagène et les biomatériaux inspirés du collagène se sont révélés être des greffes et des scellants cornéens prometteurs avec des voies viables de fabrication commerciale.

Mots clés: cornée, biomatériaux, médecine régénérative

Summary

Corneal blindness and opacities affect 12.7 million people globally. There is a shortage of human donor corneas (HDCs), which are prioritized for patients with low risk corneal disorders like keratoconus and Fuch's endothelial dystrophy. Patients with high-risk inflammatory conditions like acid, alklai and thermal burns, infections and ulcers are often unable to receive transplants to treat their corneal disorders.

Biomaterials provide an alternative to HDCs by allowing the development of corneal regenerative solutions with a long-shelf life, thermostability for deployment in rural areas and biocompatibility in high-risk patients. Biomaterials can be developed as solid corneal implants to graft into large corneal opacities or as injectable *in situ* gelling liquids that can seal small corneal perforations. Solid corneal implants are suited for use by ophthalmic surgeons, but liquid fillers can be used by emergency medicine providers or non-specialized medical personnel in areas where ophthalmic surgeons are not available.

This thesis explores biomaterials formulations for solid and *in situ* gelling corneal biomaterials, their performance as composite devices, the addition of terminal sterilization to the manufacture of solid corneal implants, and the development of future collagen mimetic proteins for hydrogel formulations.

The first objective of this thesis was to develop a solid corneal implant suitable for implantation in high-risk corneal patients. Collagen-like-peptide-polyethylene glycol-phosphorylcholine (CLP-PEG-MPC) corneal implants and recombinant human collagen type III-phosphorylcholine implants were successful in regenerating the corneas of mini-pigs and rabbits, respectively. The phosphorylcholine present in the CLP-PEG-MPC formulation decreased inflammation and provided a viable corneal alternative in high-risk alkali burns. Peptide-capped nanoparticles were successfully fabricated on the surface of a porcine collagen type I solid corneal implant. These implants inhibited *P.aeruginosa*, *S. aureus*,

and *S. epidermidis in vitro* and prevented biofilm formation at the air-liquid interface. These solid corneal implants expand the range of efficacy to include individuals with alkali burns and infections. This thesis validated a method of terminal sterilization for solid corneal implants. RHCIII-MPC was successfully terminally sterilized using electron-beam irradiation, providing a future avenue for terminal sterilization of biomaterials-based solid corneal implants.

The second objective was to design a hydrogel that will solidify *in situ* to seal corneal perforations. CLP-PEG was combined with fibrinogen to form LiQD Cornea, the first liquid corneal filler to be successfully chemically crosslinked *in situ* to seal corneal perforations and surgical wounds in rabbit and mini-pigs.

For the third objective, this project also provides future methodology for the production of custom collagen mimetic proteins for future hydrogel formulations.

Overall, collagen and collagen-inspired biomaterials were demonstrated to be promising corneal grafts and sealants with viable pathways to commercial manufacture.

Keywords: cornea, biomaterials, regenerative medicine

Contents

Sommaire v

Summary vii

List of tables xiii

List of figures xv

Abbreviations and Acronyms xvii

Acknowledgements 1

Chapter 1. Introduction 3

1.1. The Cornea 3

1.1.1. Corneal Anatomy 3

1.2. Corneal Damage and Blindness and Currently Available Treatments 7

1.2.1. Causes of Corneal Blindness 7

1.2.1.1. Corneal Transplantation and its Challenges 7

1.2.2. Alternatives to Donor Transplantation in Clinical Use 11

1.2.2.1. Keratoprostheses 11

1.2.3. Therapeutic Cell Grafting and Role of Biomaterials 11

1.2.3.1. Autologous Cell Therapies for Epithelium 12

1.2.3.2. Autologus Cell Therapies for Stroma 13

1.2.3.3. Autologous Cell Therapies for Endothelium 13

1.3. Biomaterials in Regenerative Medicine for the Cornea 14

1.3.1. Naturally Derived Biomaterials 14

1.3.1.1. Decellularized corneas 14
1.3.1.2. Culture-derived ECM matrices 24

1.4. Keratoprostheses with Regenerative Properties 31

1.5. Biosynthetic-Based Implants 32
1.5.1. Collagen-Based Biomaterials 32
1.5.2. Collagen Mimetic Peptide-Based Biomaterials 42
1.5.3. Peptide Ampiphile-Based Biomaterials 43

1.6. Fabricating Biomaterials for Delivery 46
1.6.1. Molding 46
1.6.2. 3D Printing 46
1.6.3. Injectable Hydrogels 47

1.7. Anti-infective Additives for Corneal Implants 48

Chapter 2. Thesis Research Summary 49

2.1. Rationale 49

2.2. Objectives and Hypotheses 49

2.3. Summary of Research Papers and Contributions 50

Chapter 3. Collagen analogs with phosphorylcholine as inflammation-suppressing scaffolds for corneal regeneration in high-risk alkali burns 55

Chapter 4. Nanoengineering the surface of corneal implants: Towards functional anti-microbial and biofilm materials 121

Chapter 5. Electron-Beam Irradiated Recombinant Human Collagen-Phosphorylcholine Corneal Implants Retain Pro-Regeneration Capacity 147

Chapter 6. LiQD Cornea: Pro-Regeneration Collagen Mimetics as Patches and Alternatives to Corneal Transplantation 177

Chapter 7. Synthesis and application of collagens for assembling a corneal implant 227

Chapter 8. Discussion 249

8.1. Solid Corneal Implants 249
8.1.1. Impact of phosphorylcholine on cornea regeneration 249
8.1.2. Suitability of collagen-based constructs for anti-bacterial additives 250
8.1.3. Effect of e-beam on collagen-derived biomaterials 251

8.2. Liquid Corneal Fillers 251
8.2.1. Adhesive Properties 251
8.2.2. Tissue Regeneration by CLP-PEG-fibrinogen 252

8.3. Design of Collagen Mimetics 252

8.4. Perspectives 253
8.4.1. Collagen vs. Peptide Implants 253
8.4.2. Primary Matrix Design of Liquid-to-Solid Hydrogel Formulations 255
8.4.3. General Design for *in situ* tissue regeneration 256
8.4.4. Should sterilization technique be integral to biomaterials design? 256
8.4.5. Recommendation of sterilization methods for future efforts 257

8.5. Future Work 258
8.5.1. Primary Hydrogel Components 258
8.5.2. Anti-Inflammatory Properties 258
8.5.3. Adhesives 258
8.5.4. Anti-microbial Properties 259

Chapter 9. References 261

Appendix A. *In situ* Tissue Regeneration in the Cornea from Bench-to-Bedside ..... A-i

Appendix B. Plant Recombinant Human Collagen Type I Hydrogels for Corneal Regeneration ..... B-i

List of tables

1.1 Decellularized Materials for Epithelial Repair 16
1.2 Decellularized Tissues for Stromal Repair 18
1.3 Decellularized Tissues for Endothelial Repair 21
1.4 Decellularized Tissue Particles for Stromal Repair 22
1.5 Hydrogels Derived from Decellularized Tissues for Epithelial and Stromal Repair 23
1.6 Decellularized Materials as Tissue Culture Substrates 25
1.7 Cultured Tissue-Engineered Corneas 27
1.8 Xenogeneic Collagen-Based Biomaterials 35
8.1 Summary of Mechanical Properties for Solid and Liquid Corneal Biomaterials .. 255

List of figures

1.1 Anatomy of the cornea with schematic representation of its five main layers. 3

1.2 Collagen Fibril Structure 5

1.3 Patient corneas before and after grafting with RHCIII-MPC implants at last follow-up..... 42

1.4 RHCIII-MPC and CLP-PEG corneal implants and their performance in mini-pigs 44

Abbreviations and Acronyms

α-SMA - α-smooth muscle actin

AFM - atomic force microscopy

APS - ammonium persulfate

aSLATE - aligned self-lifting auto-generated tissue equivalent

BCI - bovine collagen, type I

bFBF - basic fibroblast growth factor

BDDGE - 1, 4-butanediol diglycidyl ether

BMDC - bone marrow-derived dendritic cell

BMDM - bone marrow-derived macrophage

CD - cluster of differentiation

CEnC - corneal endothelial cell

CEpC - corneal epithelial cell

CLP - collagen-like peptide

CSF - corneal stromal fibroblast

CSK - corneal stromal keratocytes

CSSC - corneal stromal stem cell

DAMP - damage-associated molecular patterns

DAPI - 4',6-diamidino-2-phenylindole

DBCO-sulfo-NHS - Dibenzocyclooctyne-sulfo-N-hydroxysuccinimidyl ester

dECM - decellularized extracellular matrix

DOX - doxycycline

DMTMM - 4-(4,6-Dimethoxy-1,3,5-triazin-2-yl)-4-methylmorpholinium chloride

DSC - differential scanning calorimeter

ECM - extracellular matrix

EDC - N-(3-Dimethylaminopropyl)-N'-ethylcarbodiimide hydrochloride

EDTA - ethylenediaminetetraacetic acid

EGF - epidermal growth factor

EV - extracellular vesicles

FBS - fetal bovine serum

FIJI - FIJI is just ImageJ

FTIR - Fourier transformed infrared spectroscopy

GAG - glycosaminoglycan

GelMA - gelatin methacrylate

GFP - green fluorescent protein

H & E - hematoxylin and eosin

HA - hyaluronic acid

hAM - human amniotic membrane

HCEpC - human corneal epithelial cell

HDC - human donor cornea

HMPEI - N,N-hexyl,methyl-polyethylenimine

HUVEC - human umbilical vein epithelial cell

IFN - interferon

IL - interleukin

IOP - intraocular pressure

IVCM - *in vivo* confocal microscopy

KPa - kilopascal

KPro - keratoprosthesis

LESC - limbal epithelial stem cell

LN - liquid nitrogen

LPS - lipopolysaccharide

LYVE1 - lymphatic vessel endothelial hyaluronan receptor 1

MHC-II - major histocompatibility complex-II

miRNA - micro RNA

MMP - matrix metalloproteinase

MPC - 2-methacryloyloxyethyl phosphorylcholine

MSC - mesenchymal stromal cell

mRNA - messenger RNA

MUA - 11-mercaptoundecanoic acid

MWCO - molecular weight cut-off

NHS - N-hydroxysuccinimide

NP - nanoparticle

PA - peptide ampiphile

PBS - phosphate buffered saline

PCI - porcine collagen, type I

PDGF - platelet-derived growth factor

PDMS - polydimethylsiloxane

PEG - polyethylene glycol

PFA - paraformaldehyde

pHEMA - poly(hydroxyethyl) methacrylate

PLA2 - phospholipase A_2

pMMA - polymethyl methacrylate

POC - point of care

PTFE - polytetrafluoroethylene

PVA - polyvinyl alcohol

RCI - rat collagen, type I

RHCI - recombinant human collagen, type I

RHCIII - recombinant human collagen, type III

RNA -ribonucleic acid

SBF - simulated body fluid

SEM - scanning electron microscope or standard error of the mean

SD - standard deviation

SLATE - self-lifting auto-generated tissue equivalent

TCP - tissue culture plastic

TEM - transmission electron microscope

TEMED - N,N,N',N'-Tetramethylethylenediamine

TGF-α - transforming growth factor-α

TGF-β - transforming growth factor-β

T_m - melting temperature

UV - ultraviolet

VEGF - vascular endothelial growth factor

VEGFR - vascular endothelial growth factor receptor

Acknowledgements

I would like to thank my supervisor, Dr. May Griffith, for giving me my first international job and guiding me through my PhD, so I could make my dream of working in industry a reality. I would like to thank my co-supervisor Dr. Marie-Claude Robert for many hours spent doing test surgeries for new biomaterials and her feedback and support for new formulations.

I would like to thank my wife, Elle, for being my biggest cheerleader and most critical reviewer. I would not have managed to finish my doctorate without her invaluable help in polymer chemistry and statistics, as well as her love and support.

I would like to thank my parents for believing in me more than I have always believed in myself and for always saying yes when I wanted to go to French Immersion, or extra science classes in Toronto. I would like to thank my Mom for taking me to meet a Nobel Prize winner when I was 10 and always validating my curiosity about the world and my Dad for taking me to science class in Toronto. I would like to congratulate my little sister Madeline for beating me to a PhD. I would also like to thank Fenris for her invaluable help chasing the mouse while counting vesicles and Hel for sitting on my laptop and judging me when I was not writing fast enough.

I would like to thank Dr. Ashok Grover for giving me my first job in research and many early mornings spent reviewing his grants. I would not have had nearly as successful a scientific career without his early guidance.

Chapter 1

Introduction

1.1. The Cornea

1.1.1. Corneal Anatomy

The human cornea is the transparent front of the eye that transmits light through the lens and onto the retina. Together with the surrounding white of the eye, the sclera, that is overlain with a thin conjunctiva, the cornea also forms the protective outer surface of the eye. Unlike the conjunctiva or sclera, the cornea is avascular. The cornea is the most highly

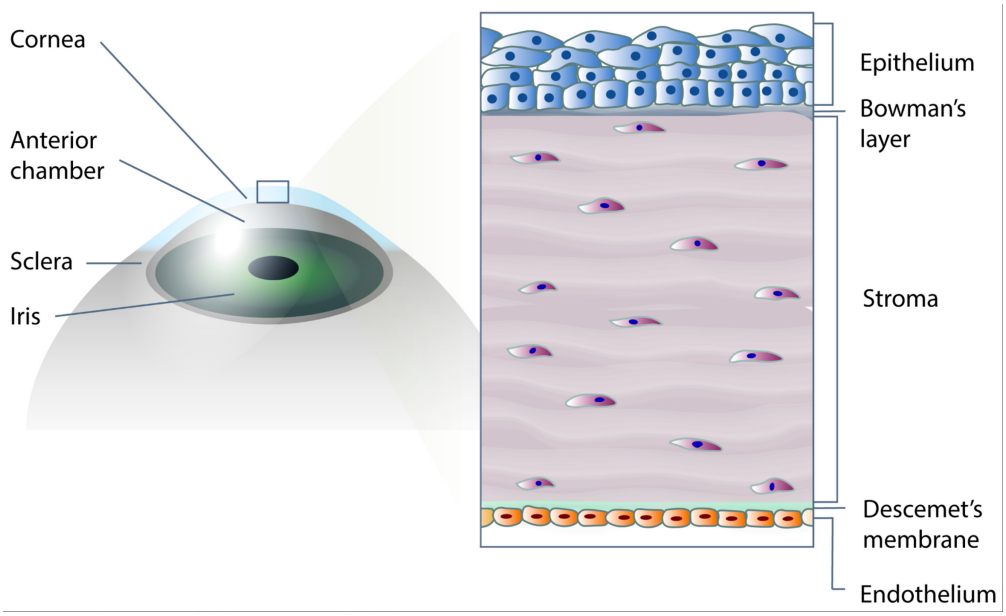

Fig. 1.1. Epithelial cells are indicated in blue, stromal keratocytes in purple and endothelial cells in orange. *Reproduced under a CC BY license from Formisano et al. [1].*

innervated tissue in the human body with sensory, sympathetic and parasympathetic nerves that regulate homeostasis and the link response [2, 3].

The cornea is composed of three cellular layers: epithelium, stroma, and endothelium (Fig 1). It also has two acellular membranes: the Bowman's layer between the epithelium and the stroma, and the Descemet's membrane between the stroma and the endothelium. A somewhat controversial third membrane, the pre-Descemet's membrane or Dua layer has been reported; it lies between the stroma and Descemet's membrane [4]. The corneal epithelium is the anterior chamber's protective layer; this is renewed every ten days. Epithelial progenitor or stem cells are located at the peripheral boundary of the cornea, called the limbus. These cells, known as limbal epithelial stem cells (LESCs), migrate from the periphery of the cornea to the center. LESCs differentiate into five to six layers of stratified, non-keratinizing corneal epithelial cells (CEpCs) [5–9]. The tear film enables the barrier function of the epithelium by lubricating the surface and carrying protective and wound healing factors [10]. It is an aqueous solution that contains mucins and lipids. The wound healing factors in the tear film include tumor growth factor (TGF)-α, TGF-β, epidermal growth factor (EGF), platelet-derived growth factor (PDGF), and vascular endothelial growth factor (VEGF) [10]. Tear film also contains host defense peptides, such as lysozyme, lactoferrin, lipocalin and the cathelecidin LL37 that protect against infections [11–14].

The Bowman's layer maintains the separation of the corneal epithelium and stroma in the cornea of most primate species [15]. The Bowman's layer is a dense acellular network of randomly arranged collagen type I and V fibrils [16–18]. The dense collagen network provides mechanical strength to help the cornea maintain its shape. It also acts as a barrier between the corneal epithelium and stroma, limiting the passage of pathogens and growth factors [19].

The corneal stroma is composed of an extracellular matrix (ECM) surrounding corneal stromal keratocytes (CSKs). Corneal ECM is composed of collagens and glycosaminoglycans (GAGs) organized in a tightly packed structure of approximately 250 lamellae that allows light transmission with minimal scatter. The primary component of a healthy corneal extracellular matrix is collagen fibrils, composed of collagens I and V [20–23]. Pro-collagens are secreted by CSKs, and the N- and C-terminal regions are cleaved. The collagen forms short protofibrils in close proximity to the cell surface, which are then organized into continuous,

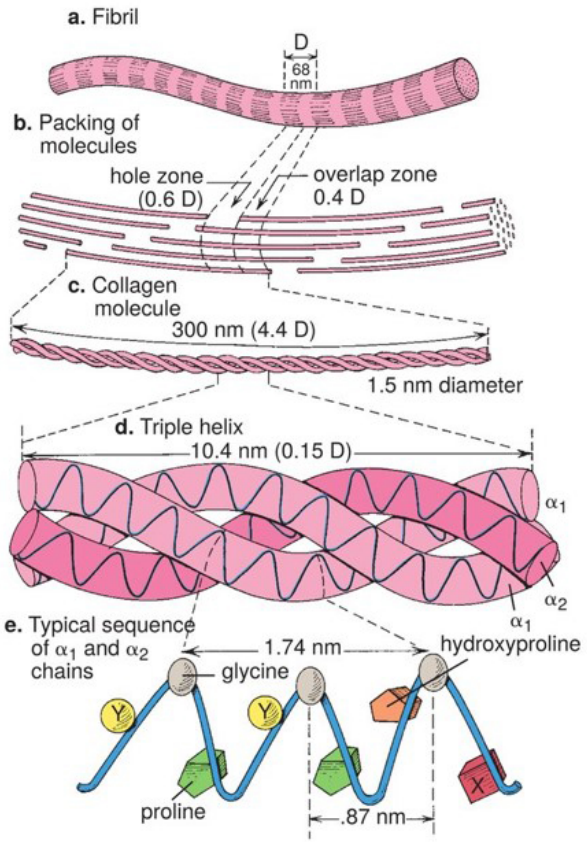

Fig. 1.2. Single collagen fibril reflecting the banding patterns with d–spacing (67 [nm]). Each fibril is assembled by collagen molecules featuring a triple helix. The triple helix, measuring about 300 [nm] in length and 1.5 [nm] in thickness, is made up of α–chains with every third amino acid of the chain being a glycine. The positions X and Y are predominantly proline and hydroxyproline, respectively. *Reproduced from Gültekin, 2018 under a CC BY 4.0 license [26].*

mature collagen fibrils in the ECM. The fibrillar assembly is stabilized by small leucine-rich repeat proteoglycans which interact with the CSK surface, collagen fibrils and other ECM proteins to organize fibrillar diameter and spacing [24, 25].

In a healthy cornea, the ECM is maintained by a balance in collagen secretion, ECM crosslinking by lysyl oxidase, and ECM degradation by matrix metalloproteinases (MMPs). Lysyl oxidase is an amine oxidase protein that crosslinks collagen and elastin to form and repair the ECM [27, 28]. Lysyl oxidase is not an abundant protein in the human eye, but it is critical for the formation of a healthy corneal stroma, and deficits in lysyl oxidase are

associated with corneal thinning in keratoconus [27, 29, 30]. Elevated levels of MMPs are associated with ECM proteolysis, angiogenesis and inflammation [31–35].

The Descemet's membrane separates the stroma and the endothelium. It is composed of three layers of collagen type IV and laminin [36, 37]. The layers of the Descement's membrane are described by the banded or non-banded appearance of their collagen fibrils in electron micrographs. Adjacent to the stroma is a thin, non-banded zone that is 0.3 μm thick. The central layer is a 2-4 μm banded zone. The endothelium-adjacent layer is >4 μm and nonbanded.The Descemet's membrane protects and isolates the corneal endothelium, as well as providing structural support for the mono-layer of cells that composes the endothelium.

The endothelium is responsible for osmoregulation of the cornea. Corneal endothelial cells (CEnCs) are hexagonal in shape and non-proliferative. The integrity of the corneal endothelium is maintained by a network of tight junctions between adjacent CEnCs that block paracellular osmotic transfer[38]. Tight junctions composed of claudin, occludin, junctional adhesion molecules and cadherins are anchored to the cytoskeleton by zonula occludens-1 at the apical junction of the monolayer. This directs regulation of the osmotic balance to ion channels, exchangers and pumps located at the apical and basolateral cell membranes. CEnCs also actively transport glucose into the corneal stroma and remove lactate [39, 40]. Endothelial tight junctions are complemented by the gap junction protein, Connexin 43, which allows the the passage of electrical signals and molecules less than 1 kDa [41]. The gap junctions allow for intracellular communication between CEnCs, while preserving the osmotic integrity of the monolayer. CEnCs keep the corneal stroma relatively dehydrated by pumping water from the stroma into the anterior chamber to compensate for the osmotic pressure of the GAGs present in the stroma [42]. Their activity helps preserve corneal transparency.

Together the three layers of the cornea work synergistically to protect and maintain the optical transparency needed to transmit light for vision, and to maintain the integrity of the corneal surface to protect the more delicate inner parts of the eye.

1.2. Corneal Damage and Blindness and Currently Available Treatments

1.2.1. Causes of Corneal Blindness

Due to the superficial location of the cornea, it is exposed to the environment and prone to injury and infection. Although the human cornea is capable of wound healing (see Section 1.2.1.1), this process does not always result in restoration of the lamellar structure of stromal ECM. In severe damage due to disease or injury, the result is scar formation or ulceration and ultimately, loss of transparency, potentially leading to blindness.

Most recent available estimates report that there are 12.7 million people awaiting corneal transplantation gobally [43, 44]. Corneal opacities causing complete vision loss and moderate to severe vision loss are most common in North Africa/Middle East, Oceania, Southeast Asia, and Central sub-Saharan Africa[45]. Overall, the majority of patients with corneal blindness live in low to medium income countries in the world. Corneal visual impairment has been named by the WHO as a priority eye disease [46]. Major causes of corneal opacity have traditionally been attributed to trachoma, xerophthalmia, measles, neonatal ophthalmia, and leprosy [44]. Damage from injuries that lead to ulceration and infection is being increasingly reported. In developed regions, including Canada, the USA, and Europe, corneal blindness tends to originate from degenerative or inherited disorders. Keratoconus results from thinning of the central stroma leading to an irregular cone-shaped, rather than smoothly curved, sphere-shaped cornea [47]. Fuchs' endothelial dystrophy is an autosomal dominant corneal dystrophy that causes the loss of CEnCs and excressences of the Descemet's membrane leading to a loss of endothelial regulatory function and severe corneal edema [48]. Corneal infections caused by contact lens misuse are also a common pathology [49].

1.2.1.1. *Corneal Transplantation and its Challenges*

The current gold standard therapy is the replacement of the pathological tissue with a human donor cornea (HDC). Corneal transplantation is the most common tissue transplant globally, as corneal tissue can be harvested up to 24 hours post-mortem and stored for 4 weeks prior to surgery [50]. The most common transplantation technique is a surgical technique called a penetrating keratoplasty. In penetrating keratoplasty, a full thickness corneal

button containing the the pathologic area within its margin is excised and replaced with the HDC [51]. However, as the globe is opened to the environment, PK is associated with a number of challenges such as peri-operative infection. Improvements in surgical technique have allowed for the lamellar corneal replacement techniques favoured more recently. Replacement of the front epithelium and part of the stroma uses a technique called anterior lamellar keratoplasty, where the healthy, intact corneal endothelium is left in place [52]. This technique was further refined into a deep anterior lamellar keratoplasty which removes all but a thin layer of stroma and endothelium. Corneal allografts are also used to replace the posterior endothelium when the anterior tissues are healthy. The two most common endothelial cell replacement procedures are: Descemet membrane endothelial keratoplasty and Descemet stripping automated endothelial keratoplasty [53]. In both procedures, the patient's Descemet's membrane and corneal endothelium are removed, leaving the epithelium and anterior stroma intact to allow space to graft new tissue. In Descemet membrane endothelial keratoplasty, only the Descemet's membrane and endothelium are grafted. In Descemet stripping automated endothelial keratoplasty, the Descemet's membrane and endothelium are re-grafted with a layer of corneal stromal cells.

Corneal transplants are most successful in low-risk diseases like keratoconus and Fuchs' endothelial dystrophy, where HDC allografts have a 2 year survival rate of 98% and 92%, respectively [54]. The long-term survival of HDC transplants declines with time, decreasing to 73% at 5 years, 62% at 10 years and 55% at 15 years [55]. Graft failure is very common, especially in high-risk patients [56–58]. These patients present with significant corneal inflammation and vascularization, often due to ocular Herpes simplex virus-1, bullous keratopathy, or a prior graft [59]. A 2018 study of the UK corneal transplant registry showed that 21.1% of transplant procedures were re-grafts during the 17 year study period [60]. The most common reasons for re-graft were endothelial decompensation, irreversible rejection, and primary graft failure. Primary grafts had a five year survival rate of 72.5% (95%CI, 71.7%-73.2%). The five year survival for a second corneal graft was reduced to 53.4% (95% CI, 51.4%-55.4%).

Patients cannot be regrafted in the immediate aftermath of trauma like a physical injury, acid or alkali burn or infection. Instead surgeons often wait until the ocular surface is stable and quiescent before considering a transplant. During this time inflammation can

cause abnormal wound healing in the cornea, leading to scarring (seen as corneal haze) and neovascularization.

In corneas with epithelial and stromal trauma, the immune system plays a significant role in wound healing. Langerhans cells that are positive for major histocompatibility complex-II (MHC-II) migrate from the limbus to the central corneal epithelium four hours after epithelial trauma and DCs in the central cornea upregulate MHC-II [61–63]. Neutrophils infiltrate the wound site in two waves, 18 and 30 hours after trauma [64]. Neutrophil deficient mice have impaired corneal re-epithelialization and decreased corneal nerve infiltration, likely due to the absence of the neurotrophic effects of their VEGF-A secretion [64–67]. Macrophages clear the wound site of debris and apoptotic cells, but they are also strong mediators of angiogenesis and stimulators of myofibroblast transformation, contributing to fibrotic response and corneal ECM dysregulation [68, 69]. Natural killer cells also infiltrate the corneal stroma, peaking at 24 hours after epithelial trauma. They may play a role in reducing neutrophil infiltration via a NKG2D-dependent modulatory effect on an innate acute inflammatory process [70]. They also increase the presence of DCs in the cornea via IFN-γ stimulation [71].

The corneal epithelium is repaired via flattening and centripetal migration of the adjacent cells into the wound site. The epithelial layer is then restored via differentiation and migration of LESCs from the periphery of the cornea into the central cornea. This is a rapid process that usually takes under two weeks in the absence of ulcer formation.

Corneal stromal healing is a significantly slower process. In the immediate aftermath of injury, the normally quiescent corneal keratocytes differentiate into fibroblasts to migrate into the wound site [72]. This process can be stimulated by the release of PDGF and TGF-β from epithelial cells that travels through the damaged basement-membrane [73–76]. Bone marrow-derived fibrocytes also migrate into the wound and differentiate into fibroblasts three to five days after injury [77, 78]. The conversion of either lineage of fibroblasts into myofibroblasts is a dual-edged sword. Myofibroblasts are contractile fibroblasts that can interact with the ECM to maintain corneal structural integrity. This cell type is marked by the expression of α-smooth muscle actin ($\alpha-$SMA), vimentin, and desmin [79–83]. Myofibroblasts are problematic for corneal wound healing because they secrete disorganized ECM that causes corneal haze and opacity [84, 85]. The myofibroblasts are maintained by secretion of TGF-β

and the presence of myofibroblasts in the stroma markedly decreases after the basement membrane is restored and stromal TGF-β decreases [86–88].

Corneal nerves and epithelial cells have a synergistic relationship, where trophic factors secreted by nerves (substance P, calcitonin-gene related peptide, norepinephrine, acetylcholine) stimulate CEpC proliferation and migration, while CEpCs secrete nerve growth factor and glial cell-derived neurotrophic factor, which promote neurite extension and survival [3, 89–93]. During wound healing, the factors secreted by both cell types promote neurite extension into the damaged area, which in turn supports CEpC regeneration.

Neovascularization of the cornea occurs when the inflammatory cytokines interleukin-1 (IL)-1 and IL-6 secreted in the immediate aftermath of trauma stimulate production of pro-angiogenic factors such as VEGF, basic fibroblast growth factor (bFGF), MMPs, and PDGF [94]. These factors act to stimulate vascular endothelial cell proliferation and migration into the cornea, as well as causing enzymatic breakdown of the corneal ECM, which facilitates vessel penetration.

VEGF is a family of growth factors (VEGF-A, VEGF-B, VEGF-C, and VEGF-D) that bind the three VEGF-receptors (VEGFR). In cornea, VEGF-A is the primary driver of angiogenesis, binding to VEGFR-1 and VEGFR-2 on vascular endothelial cells and causing vascular leakage that allows the vascular endothelial cells to migrate from the vessels at the periphery into the central cornea [95]. VEGF-A also stimulates macrophage infiltration, leading to a feed-forward loop of macrophage-secreted VEGF-A [96, 97]. VEGF-C and VEGF-D are also associated with VEGFR-3 mediated angiogenesis [98].

The secretion of VEGFs explains the chemo-attraction of vascular endothelial cells to the cornea, but not their ability to penetrate deep into the lamellae. MMPs are zinc-containing endopeptidases that are primarily associated with breakdown of the corneal ECM. MMP-2 and MMP-9 both cleave the collagen IV found in the basement membrane [99], weakening the barrier between the endothelium and the stroma and allowing for secretion of TGF-β and PDGF from the epithelium into the stroma. MMP-2 and MMP-9 precede the infiltration of vascular endothelial cells into the cornea during abnormal wound healing [100, 101]. They can increase chemoattraction of vascular endothelial cells by releasing VEGF from inhibitory binding proteins in the ECM [102]. Overall, they break down the corneal ECM allowing vascular endothelial cells to penetrate into the stroma.

Wound healing in an inflamed cornea can lead to haze and neovascularization that permanently decreases corneal transparency leading to loss of vision or complete corneal blindness.

1.2.2. Alternatives to Donor Transplantation in Clinical Use

There is a severe global shortage of donor tissue that leaves 12.7 million people awaiting transplantation [43]. In addition, HDC transplantation is most successful in patients when there is no inflammation, e.g. in keratoconus or healed scars from infections which are conditions that carry a low risk of graft failure or rejection [56–58]. Patients with inflammation or severe pathologies (e.g., chemical burns, active infections or previous rejected grafts) tend to have a high risk for graft rejection or failure. High-risk patients are often contraindicated for transplantation with HDCs due to the severe worldwide shortage of donor tissues, and the allocation of donor allografts for cases with higher chances of success [43].

1.2.2.1. *Keratoprostheses*

High-risk patients can be treated with corneal prosthetic device called a keratoprosthesis (KPro) that restores minimum function, such as light transmission into the eye for vision and protection of the more delicate inner structures of the globe [103, 104]. The most commonly used KPro is the Boston KPro. The standard Type I Boston KPro has a central, transparent polymethylmethacrylate (pMMA) core, surrounded by a titanium back plate and titanium locking ring that anchor the KPro to the cornea. They are inserted into a HDC which is then grafted into the patient's eye, using the HDC tissue to encourage integration around the surgical site. The Type II device is even more complicated and is implanted through the upper eyelid. KPro transplantation is often complex, necessitating lifelong need for antibiotics and carries severe side effects such as glaucoma that could result in permanent blindness; therefore, KPros are only used in end-stage eyes [105, 106].

1.2.3. Therapeutic Cell Grafting and Role of Biomaterials

Apart from KPros, biomaterials have also been in clinical use for delivery of therapeutic cells for regenerating damaged corneas. These are described below.

1.2.3.1. *Autologous Cell Therapies for Epithelium*

Corneal epithelial replacement is the only layer of the cornea that has regulatory-approval for cell therapy. Holoclar™ is an advanced therapy medicinal product comprising cleanroom expanded stem cells that is used in Europe for "restoring healthy corneal surfaces in patients with moderate or severe limbal stem-cell deficiency caused by burns as well as in improving their symptoms and vision" [107]. Holoclar™ is a cultured limbal epithelial transplant that consists of the patient's LESCs, which are removed and cultured on a substrate *ex vivo* prior to regrafting into the cornea to replace the damaged limbal stem cells.

Fibrin, which is isolated from human blood, has been used in the delivery of cultured LESCs for transplantation to re-surface the cornea. Human amniotic membrane (hAM), which provides a collagen-based scaffold that is enriched by a range of other bioresponsive proteins like fibronectin and laminin, as well as immune factors like IL-10, has also been successfully used as a substrate for delivery of LESCs (For review see [108]).

Corneal epithelial cells have also been differentiated from biopsies of patient oral mucosal tissue [109]. The process is called cultivated oral mucosal epithelial transplantation . The oral mucosal biopsy is seeded on hAM and cultured in the presence of mitomycin-C-treated 3T3 feeder cells prior to re-grafting. This process has been successfully used in Stevens-Johnson syndrome, aniridia, alkali and temperature burns [110–116].

In addition to *ex vivo* autologous transplants, a simple limbal epithelial stem cell transplant has been used to treat corneal epithelial defects. Simple limbal epithelial stem cell transplantation is a single surgical procedure where a biopsy of the patient's LESCs is removed, dissected into small pieces and placed on hAM during surgery to allow the LESCs to re-colonize the damaged corneal surface [117, 118]. Recent economic analysis of Simple limbal epithelial stem cell transplants vs. cultured limbal epithelial stem cell transplants has shown that simple limbal epithelial stem cell transplant procedures are 10% of the total cost of cultured limbal epithelial stem cell transplant procedures, as they do not require a cell processing facility and multiple surgeries [119]. However, despite the success in re-surfacing corneas, when the damage extends to the deeper layers of the cornea, the patients still require allografting with donor human corneas [120].

1.2.3.2. *Autologus Cell Therapies for Stroma*

CSKs can be successfully differentiated from limbal biopsies in culture. Basu *et al* reported the successful culture of CSKs derived from limbal biopsies [121]. Here, biomaterials have been used for cell cultures, to obtain expanded numbers of therapeutic cells. Limbal biopsies were cultured on FNC-coated plates. These cells formed spheres on poly(hydroxyethyl) methacrylate (pHEMA) coated plates. When transferred to collagen-coated plates, these cells differentiated into CSKs. The CSKs were then plated on poly(ϵ-caprolactone) aligned nanofiber inserts to generate constructs suitable for grafting. Mouse corneal epithelial wounds were generated using debridement. The wounds were then successively treated with thrombin and fibrinogen to attach the construct to the wound surface. The constructs prevented the formation of disorganized ECM causing haze and promoted collagen I and keratocan deposition in the central cornea at one month after surgery.

1.2.3.3. *Autologous Cell Therapies for Endothelium*

Corneal endothelial cells can be expanded in culture, but their fragility has traditionally limited their use in autologous transplants. In 2014, Okamura *et al.* reported a culture protocol using Rho-kinase inhibitors to allow for transplantation of endothelial cells in suspension [122]. Rho-kinase inhibitors can be co-injected with endothelial cells to improve the success rate of corneal endothelial cell transplants [123]. Economic analysis has shown that autologous endothelial transplants can be more cost effective than donor cornea-based transplants, despite the overhead costs for cell culture facilities [124].

1.3. Biomaterials in Regenerative Medicine for the Cornea

1.3.1. Naturally Derived Biomaterials

1.3.1.1. *Decellularized corneas*

The primary barrier to full integration of corneal allografts is the presence of cells from the donor (live or dead) which can produce an immune response that leads to graft rejection [125–127]. Decellularization aims to circumvent the inflammatory response by removing all of the cells and cell debris that can act as antigens. There are physical, chemical, and biological processes that are used alone, or in combination to fully decellularize animal or human corneas to prepare them for grafting (Table 1.1, 1.2, 1.3) [126]. The most common physical processes are freeze-thawing or submersion in hypertonic/hypotonic solutions to cause the cells to burst. Chemical processes use detergents like sodium dodecyl sulfate (SDS), sodium deoxycholate, or Triton X-100 to disrupt cellular membranes. Finally, enzymes like dispase or trypsin may be used to enzymatically degrade the ECM to release cells. DNAase and RNAase are used to remove DNA and RNA that may trigger innate immune responses to nucleic acid fragments. Phospholipase A2 has been used in place of dispase and trypsin to prevent ECM degradation, while enzymatically destroying cell membranes [128]. Decellularized tissues are often sterilized using γ irradiation to ensure that there are no bacterial or viral contaminants remaining in the matrix [128–135]. Decellularized ECM (dECM) has also been used to generate particles for corneal stromal repair (Table 1.4) and hydrogels for corneal epithelial and stromal repair (Table 1.5).

A single acellular graft cornea has been approved for use in clinical patients. The acellular graft cornea is cyrogenically decellularized and sterilized using 17 - 23 kGy of γ-irradiation [136–138]. Structural analysis of the aceullar graft cornea compared to HDC showed a similar Young's modulus (25.1 $\pm$ 5.8 kPa vs 24.4 $\pm$ 6.4 kPa), but a decrease in melting temperature ($T_{m)}$ (61.7 $\pm$ 1.1°C vs 65.7 $\pm$ 1.8°C), as measured by differential scanning calorimetry [138]. The acellular graft cornea supported greater CSK infiltration. A retrospective review of the fist 150 patients treated with the acellular graft cornea showed that it could be used as a glaucoma patch graft, corneal patch graft, anterior lamellar keratoplasty, or as the skirt for a KPro [137].

Decellularized tissues retain their native ECM composition, but are also subject to several negative factors. Tissue ECM many undergo a significant amount of damage during the decellularization process. This poses two potential problems: loss of structural integrity and the generation of damage-associated molecular patterns (DAMPs). dECM generally maintains a fraction of the structural stability of the tissue of origin. In addition, the γ-irradiation techniques commonly used to sterilize decellularized grafts crosslink the ECM resulting a in a more brittle, fragile material [139–141]. DAMPs are patterns recognized by the innate immune system as markers of tissue damage. They interact with pattern recognition receptors, including Toll-like receptors, C-type lectin receptors, NOD-like receptors, retinoic acid-inducible gene I-like receptors, and multiple intracellular DNA sensors [142]. DAMPs initiate an immune response in the absence of infection referred to as "sterile inflammation" [143]. Damage to the ECM, including collagen fragments, and remnants of DNA and RNA are all DAMPs that can initiate an innate immune response, potentially causing an inflammatory response in the host. Overall, decellularized corneas and dECM-based materials have seen limited use in human clinical trials due to their structural limitations.

Tab. 1.1. Decellularized Materials for Epithelial Repair

Decellularized Tissues for Epithelial Repair						
Identifier	**Source**	**Decellularization Method**	**Sterilization Technique**	**Model Species**	**Surgery**	**Ref**
Lin 2008	Porcine	trypsin freeze-thaw, sodium hydroxide, DNase, RNase, lyophilized	^{60}Co irradiation	Rabbit	Keratectomy wound	[129]
Wu 2009	Porcine	Sodium deoxycholate, Phospholipase A2	γ-irradiation (25 kGy)	Rabbit	Lamellar keratoplasty	[128]
Xiao 2011	Porcine	Sodium deoxycholate, phospholipase A_2, freezing, lyophilization.	γ-irradiation (25 kGy)	Rabbit	Interlamellar keratoplasty	[130]
Genicio 2015	Human	EDTA	-	-	-	[144]
Hashimoto 2015	Human	High hydrostatic pressure	-	-		[145]
Zhang 2015a	Porcine	NaCl, Triton X-100, glycerol	^{60}Co Irradiation	Human	Lamellar keratoplasty	[131]
Zhang 2015b	Human	Triton-X, ammonium hydroxide + DNase or NaCl + DNase	Antibiotics	-	-	[146]
Liu 2016	Ostrich	Hypertonic saline, trypsin/trypLE Express	γ-irradiation (25 kGy)	Rabbit	Lamellar keratoplasty	[132]

Decellularized Tissues for Epithelial Repair						
Identifier	**Donor species**	**Decellularization Method**	**Sterilization Technique**	**Model Species**	**Surgery**	**Ref**
Zheng 2019	Porcine	Sodium hypochlorite, hyper-hypotonic solution	^{60}Co irradiation	Human	Lamellar keratoplasty	[134]
Lin 2019	Porcine	Organic acids (formic, acetic, citric)	-	Rabbit	Deep Anterior Lamellar Keratoplasty	[147]
da Mata Martins 2020	Human	NaCl and nucleases	-	-		[148]
Wang 2020	- (dermal matrix)	-	-	Rabbit	Lamellar keratoplasty	[149]

Tab. 1.2. Decellularized Tissues for Stromal Repair

Decellularized Tissues for Stromal Repair						
Identifier	**Donor species**	**Decellularization Method**	**Sterilization Technique**	**Model Species**	**Surgery**	**Ref**
Proulx 2009	Human	Freeze-Thaw	-	Cat	Penetrating keratoplasty	[150]
Choi 2010	Human	Triton X-100	-	-	-	[151]
Du 2011	Porcine	SDS	-	-	Rabbit	[152]
Huang 2011	Porcine	sodium deoxycholate, Phospholipase A2	-	Rabbit	Subcutaneous	[153]
Shafiq 2014	Human	Sodium chloride, DNase, RNase	-	Rat	Limbal injury	[154]
Alio del Barrio 2015	Human	SDS and protease inhibitor under vacuum, DNase	Antibiotic/ antimycotic solution	Rabbit	-	[155]
Wilson 2016	Human	NaCl, SDS or Triton X-100 with DNase and RNase	-	-	-	[156]

Decellularized Tissues for Stromal Repair						
Identifier	**Donor species**	**Decellularization Method**	**Sterilization Technique**	**Model Species**	**Surgery**	**Ref**
He 2016	Human	Sonification, freeze/thaw, freezing/thawing in liquid nitrogen (LN) ; Freezing in LN and hypoxia; 1.5 M NaCl for 24 hours followed by 0.02% EDTA + 0.05%trypsin for 24 h; 0.1% SDS for 24 h; 1% SDS for 10 min (3 cycles); Cyclic 1% SDS and DNase	Ethanol	-	-	[157]
Yam 2016	Human	hyperosmotic, ionic detergent, non-ionic detergent, ionic and non-ionic detergent, Enzymatic, enzymatic and detergent,mid enzymatic, mid enxymatic and detergent, high enzymatic, high enzymatic and detergent	-	Rabbit	Small incision lenticule extraction	[158]
Yin 2016	Human	NaCl,DNase, RNase	-	Rabbit	small incision lenticule extraction	[159]

Decellularized Tissues for Stromal Repair						
Identifier	**Donor species**	**Decellularization Method**	**Sterilization Technique**	**Model Species**	**Surgery**	**Ref**
Xu 2017	Porcine	0.5% sodium deoxycholate and 0.04% sodium orthovanadate, DNase, RNase	Ionizing Radiation (25 kGy)	Dog	Lamellar keratoplasty	[133]
Guler 2017	Bovine	Supercritical CO2	Supercritical CO_2	-	-	[160]
Alio del Barrio 2018	Human	SDS	Antibiotic/ antimycotic solution	Human	Lamellar pocket	[161]
Huh 2018	Human	hypotonic trypsin-EDTA, DNase, RNase	-	Rabbit	Corneal pocket	[162]
Shi 2019	Porcine	HHP, sodium lauroylglutamate, endonuclease	hypochloric acid and Co60 irradiation (15 kGy)	Rabbit	Lamellar keratoplasty	[163]
Ahearne 2020		SDS, Tritox-X, DNase, RNase	-	-	-	[164]
Uyanıklar 2020	Bovine	SDS, GelMA photocrosslinking	-	-	-	[165]

Tab. 1.3. Decellularized Tissues for Endothelial Repair

Decellularized Tissues for Endothelial Repair						
Identifier	**Donor species**	**Decellularization Method**	**Sterilization Technique**	**Model Species**	**Surgery**	**Ref**
Amano 2008	Porcine	LN	LN	Rabbit	Stromal pocket	[166]
Lee 2014	Porcine, Primate	-	-	-	-	[167]
Bhogal 2017	Human	Freeze/Thaw	-	Rabbit	Endothelial Wound	[168]
Aslan 2018	Bovine	SDS	70% ethanol	-	-	[169]
Liu 2018	Porcine	SDS	-	Nonhuman primate	Intrastromal pocket	[170]
An 2020	Porcine	SDS	slightly acidic electrolyzed water	-	-	[171]
Chen 2020	Porcine	Sodium deoxycholate, Phospholipase A2	^{60}Co irradiation	Mouse	Subcutaneous	[135]

Tab. 1.4. Decellularized Tissue Particles for Stromal Repair

Decellularized Tissue Particles for Stromal Repair						
Identifier	**Donor species**	**Decellularization Method**	**Sterilization Technique**	**Model Species**	**Surgery**	**Ref**
Yin 2019a	Porcine	peracetic acid, Triton X-100 and EDTA, DNase, milling	UV at 253.7 nm	*Ex vivo* Rabbit	-	[172]
Yin 2019b	Porcine	peracetic acid, Triton X-100 and EDTA, DNase, milling	Sterile filtered (0.22 μm)	-	-	[173]
Chandru 2021	Human	NaCl, milling	Antibiotics	Guinea pigs/ Rabbits	Topical/lamellar keratoplasty	[174]

Tab. 1.5. Hydrogels Derived from Decellularized Tissues for Epithelial and Stromal Repair

Hydrogels Derived from Decellularized Tissues for Epithelial and Stromal Repair						
Identifier	**Donor species**	**Decellularization Method**	**Sterilization Technique**	**Model Species**	**Surgery**	**Ref**
Wang 2020	Porcine	HHP, dtergent, endonuclease, milling, CMC/NHS crosslinking	-	Rabbit	focal corneal defect	[175]
Ahearne 2015	Porcine	Freeze-thaw, nuclease	-	-	-	[176]
Hong 2018	Human	Trypsin, DNase, RNase, plastic compression collagen thermal gel	-	Rabbit	anterior lamellar keratoplasty	[177]
Kim 2019	Bovine	Ammonium hydroxide-Triton X-100,	Peracetic acid	Mouse/ Rabbit	Subcutaneous/ corneal pocket	[178]
Ahearne 2020	-	SDS, Triton X-100, DNase, RNase	-	-	-	[179]
Zhou 2021	Porcine	Freeze-dried, milled	-	Mouse	Corneal wound	[180]

1.3.1.2. *Culture-derived ECM matrices*

A number of full thickness tissue-engineered cornea models have been developed using cell culture systems (Table 1.7). These systems either grow CSF, CSK or CSSC on tissue culture plastic (TCP), transwell inserts, or a matrix in order to create a thick layer of corneal stroma. Once the CSKs or CSFs have proliferated into a layer of stroma, CEpCs are seeded on the top and/or CEnCs are seeded on the lower surface to develop a full thickness graft. The majority of these constructs are used to conduct experiments on the proliferative capacity and cell-cell interactions of the constructs *in vitro*. Models have been developed for type I and type II diabetes mellitus [181], keratoconus [182], and FCD [183].

Three studies of tissue engineered corneas have been evaluated in animal models. In 2017, Zhang *et al.* demonstrated the efficacy of a cultured CEnC for endothelial reconstruction in rabbits [184]. Syed-Picard *et al.* generated CSSC constructs on fibronectin that were successfully implanted in intrastromal pockets in mice [185]. Peh *et al.* used a similar model to demonstrate the efficacy of CEnCs cultured on a collagen matrix for endothelial keratoplasty [186]. Finally, Rico-Sànchez *et al.* demonstrated that a CSK and CEpC graft cultured on a fibrin-agarose substrate can be effectively used for anterior lamellar keratoplasty [187].

There has been a single report of a tissue engineered corneas used in a human clinical trial. Le-Bel *et al.* published a case report of a 72 -year old woman who received a cultured HCEpC graft for a spontaneous perforation caused by underlying Herpes Zoster Ophthalmicus neurotrophic keratitis [188]. Despite slow wound healing due to a *Stapholococcus epidermidis* infection, the HCEpC graft was successful at restoring the corneal surface so a successful penetrating keratoplasty could be performed with a HDC to restore the patient's corneal transparency.

Tab. 1.6. Decellularized Materials as Tissue Culture Substrates

Identifier	**Donor species**	**Decellularization Method**	**Sterilization Technique**	**Cell Type**	**Model Species**	**Surgery Performed**	**Ref**
Epithelium							
Zhang 2012	Canine	I mM Tris-HCl, 1% Triton X-100, 0.25% trypsin-EDTA, DNase and RNase, freeze dried	γ-irradiation	MSC, LESC			[189]
Luo 2013	Porcine	Hypotonic/hypertonic, 0.2% Triton X-10	15 K ^{60}Co	amniotic epithelial cells	Rabbit	Lamellar Keratoplasty	[190]
Zhao 2014	Porcine Conjunc-tiva	SDS	γ-irradiation (25 kGy)	CEpC	Rabbit	Intracorneal transplanta-tion	[191]
Wu 2014	Porcine	Hypotonic, Phospholipase A2 and 0.5% sodium deoxycholate, Phospholipase A2	γ-irradiation (25 kGy)	LESC	Rabbit	Lamellar Keratoplasty	[192]
Stroma							
Xiao 2011	Porcine	Phospholipase A2	γ-irradiation (25 kGy)	CSK	Rabbit	Lamellar Keratoplasty	[130]

Identifier	**Donor species**	**Decellularization Method**	**Sterilization Technique**	**Cell Type**	**Model Species**	**Surgery Performed**	**Ref**
Cen 2020	Canine	1.5 M NaOH	γ-irradiation	MSC	Rabbit	Lamellar Keratoplasty	[135]
Endothelium							
Proulx 2009	Human	freeze/thaw	-	CEnC	Cat	Penetrating Keratoplasty	[193]
Full Thickness							
Yoeruek 2012	Porcine	hypotonic tris buffer, ethylene diamine tetraacetic acid (EDTA, 0.1%), aprotinin (10 KIU/ ml) and 0.3% sodium dodecyl sulphate	-	CSK, CEpC, CEnC			[194]
Zhang 2017	Porcine	NaCl, DNase, RNase	Pen/Strep	LESC, CFC, CEnC	Rabbit	Penetrating Keratoplasty	
Xu 2017	Porcine	0.5% sodium deoxycholate and 0.04% sodium orthovanadate, DNase I and RNase A	γ-irradiation	non-tumor igenic CEpC, CSK	Dog	Lamellar Keratoplasty	[133]

Tab. 1.7. Cultured Tissue-Engineered Corneas

Identifier	**Matrix and/or Culture Surface**	**Cell Source**	**Cell Types**	**Model Species**	**Surgery**	**Ref**
Zieske 1994	Matrix deposited by fibroblasts	Rabbit	CSF, CEpC, CEnC	-	-	[195]
Guo 2007	Polyester or polycarbonate membrane	Human	CSK	-	-	[196]
Carrier 2008	Matrix deposited by fibroblasts	Human	CSK, CEpC, CEnC	-	-	[197]
Ren 2008	Disorganized pepsin extracted bovine dermal collagen	Human	CSF	-	-	[198]
Gonzàlez-Andrades 2009	Fibrin-agarose	Human	CSK, CEpC	-	-	[199]
Carrier 2009	Matrix deposited by fibroblasts	Human	CSF and CEpC, CSF and SEpC, SF and CEpC, SF and SEpC	-	-	[200]
Guillemette 2009	Microstructured thermoplastic elastomer	Human	CSF, CEpC	-	-	[201]

Identifier	**Matrix and/or Culture Surface**	**Cell Source**	**Cell Types**	**Model Species**	**Surgery**	**Ref**
Proulx 2010	Matrix deposited by fibroblasts	Human	CSF, CEpC, CEnC	-	-	[202]
Karamichos 2010	polycarbonate membrane	Human	CSK	-	-	[203]
Karamichos 2011	TCP	Human	CSF	-	-	[204]
Karamichos 2012	polycarbonate membrane	Human	CSF (Healthy and Keratoconus)	-	-	
Wu 2012	poly(ester urethane) urea	Human	CSSC	-	-	[205]
Lake 2013	Fibronectin or matrix deposited by fibroblasts	Rabbit	CSF, CEpC	-	-	[206]
Zaniolo 2013	Matrix deposited by fibroblasts	Human	CEpC, CSF,	-	-	[207]
Karamichos 2013	TCP	Human	CSF, CSK	-	-	[208]
Karamichos 2014	polycarbonate Transwell filters	Human	CSSC	-	-	[209]
Wu 2014	Silk fibroin patterned film functionalized with RGD	Human	CSSC, CSF	-	-	[210]

Identifier	**Matrix and/or Culture Surface**	**Cell Source**	**Cell Types**	**Model Species**	**Surgery**	**Ref**
Wu 2014b	poly(ester urethane) urea	Human	CSSC, CSF	-	-	[192]
Abidin 2015	Collagen	Human	CSK	-	-	[211]
Bourget 2016	Matrix deposited by fibroblasts	Human	CSK, CEnC	-	-	[212]
Couture 2016	Matrix deposited by fibroblasts	Human	CEpC, CSF,	-	-	[213]
Priyadarsini, 2016	polycarbonate membrane	Human	CSF (Healthy, Type I and Type II diabetes mellitus)	-	-	[181]
Zhang 2017	Collagen IV, hLaminin -511 or hLaminim -521	Human	CEnC	Rabbit	Endothelial keratoplasty	[184]
Ghezzi 2017	Silk fibroin patterned film functionalized with RGD	Human	CSF, CSSC	-	-	[214]
Couture 2018	Matrix deposited by fibroblasts	Human	CEpC, CSF,	-	-	[183]
Deardorff 2018	Silk fibroin patterned film functionalized with RGD	Human	CSSC, CEpC, induced neural stem cells	-	-	[215]

Identifier	**Matrix and/or Culture Surface**	**Cell Source**	**Cell Types**	**Model Species**	**Surgery**	**Ref**
Syed-Picard 2018	Fibronectin coated-polydimethylsiloxane (PDMS) vs Matrix deposited by fibroblasts	Human	CSSC	Mice	Intrastromal pocket	[185]
Thériault 2018	FNC	Human	CEnC (Healthy and FCD)	-	-	[183]
Peh 2019	Collagen	Human	CEnC	Rabbit	Endothelial keratoplasty	[186]
Rico-Sánchez 2019	Fibrin-agarose	Human	CSK, CEpC	Rabbit	Anterior lamellar keratoplasty	[186]
Le-Bel 2019	Fibrin	Human	CEpC	Human - Herpes Zoster Ophthalmic neurotrophic keratitis	Autologus epithelial transplant, PK	[188]
McKay 2019	polycarbonate membrane	Human	CSF, CEpC, CEnC	-	-	[216]

1.4. Keratoprostheses with Regenerative Properties

Traditional KPros are composed of an optical core and a skirt for attachment and integration to the cornea. The optic is made from a clear, but biologically inert, material such as PMMA which is attached to a biological skirt such as a piece of cornea, with the use of PMMA or titanium plates that hold them in place [217]. The devices do not contain bioactive ligands for cell adhesion. An incompletely adhered PMMA optic stem leaves a gap between the medical device and the tissue allowing for the passage of aqueous humour out of the anterior chamber, passage of infectious microorganisms into the anterior chamber, epithelial downgrowth, and potential loosening or extrusion of the device [218].

A number of strategies have been devised to improve the cell adhesion properties of KPros. The first strategy employed a coating of di-amino-PEG that was either conjugated to a peptide to promote adhesion or coated alone to prevent unwanted cell adhesion over the optics [218]. The second strategy uses hydroxyapatite, a primary component of bone, to improve collagen adhesion to the PMMA. Wang *et al* coated PMMA with hydroxyapatite using simulated body fluid (SBF) after treatment with either sodium hydroxide, dopamine, or dopamine and 11-mercaptoundecanoic acid (MUA) [219]. All three coating methods improved cell adhesion of stromal fibroblasts *in vitro*. The biointegration of the hydroxyapatite-coated PMMA was tested by incubating cylinders of the PMMA-dopamine-11-MUA-hydroxyapatite material in *ex vivo* porcine corneas for two weeks. The coating significantly increased the force required to remove the cylinder from the cornea by 14.7 times the force. Implantation into rabbit corneas revealed that the hydroxyapatite coating reduced the inflammatory foreign body response at one month post-operation compated to uncoated PMMA.

Riau *et al* compared plasma oxygen, dopamine and 11-MUA, and dopamine and 3-(aminopropyl)triethoxysilane pre-treatment before SBF incubation to adhere calcium phosphate to PMMA [220]. The coatings were tested by adhering collagen hydrogels to the surface. The plasma-calcium phosphate coating had the best interfacial adhesion, but the dopamine-calcium phosphate coating had longer lasting adhesion. The 3-(aminopropyl)triethoxysilane-calcium phosphate group was toxic to corneal fibroblasts. Overall the dopmaine-calcium phosphate coated PMMA provided the best surface for biointegration and cell adhesion. Riau *et al* also tested a hydroxyapatite and TiO_2 nanoparticle

(NP) coating of PMMA [221]. Chloroform was used to pit the PMMA surface to allow NP hydroxyapatite-TiO_2-NPs to adhere. The NP coating improved collagen and fibroblast adhesion on the PMMA surface. Chloroform dip-coating was then used to adhere hydroxyapatite NPs to PMMA to improve surface adhesion. After coating, the hydroxyapatite-NP coated surface was plasma treated to remove contaminants. The hydroxyapatite-NPs significantly improved collagen adhesion, demonstrated by a significant improvement of mean adhesion strength. The hydroxyapatite-NPs also supported corneal fibroblast proliferation *in vitro*.

PMMA has also been coated to improve the antibacterial properties of KPros. Radio frequency sputtering was used to coat PMMA with silver/silica NPs [222]. The coating resisted tape removal and was stable in liquid for one month. It inhibited the growth of *S. aureus* providing the potential to fight ocular bacterial infections. Behalu *et al* coated PMMA and titanium with N,N-hexyl,methyl-polyethylenimine (HMPEI) [223]. After coating, the materials were sterilized with ethylene oxide. HMPEI coating inhibited *S. aureus* clinical isolate and biofilm formation and promoted HCEnC proliferation *in vitro*. Intrastromal or anterior chamber implantation in rabbits was tolerated with decreased edema in the KPro front piece model and decreased mucous accumulation in the full implantation model compared to uncoated controls.

1.5. Biosynthetic-Based Implants

Biomaterial implants for the cornea have been designed from a number of naturally occurring proteins, polysaccharides and GAGs, including: collagen, gelatin, silk, agarose, chitin, cellulose and hyaluronic acid. For the purposes of this thesis, I will only review collagen-based or self-assembling, collagen-inspired materials.

1.5.1. Collagen-Based Biomaterials

Collagen is the primary structural component of the corneal ECM and one of the proteins best-positioned to serve as a scaffold for cellular infiltration in a wound. Collagen contains integrin-binding sites, used to anchor cells to the ECM, which allow for colonization of the scaffold with proliferating or migrating cells [224]. The cornea already has a regulatory mechanism for the production and degradation of collagen discussed in Section 1.1.1, which

means that the cells can remodel the surrounding matrix, replacing the scaffold collagen with newly secreted collagen they produce.

Collagen is abundant in mammalian tissue and it can be easily extracted from porcine, bovine and rat-based sources. Mature collagen isolated from tissues has been stabilized and crosslinked by the enzyme lysyl oxidase. In the process of crosslinking lysine, hydroxylysine and histidine are depleted [225]. Lysine particularly is a prime target for crosslinking and side group modification and is one of the most important moieties for the type of active ester chemistry used in all of the studies in this thesis. Naïve collagen is a very good starting material for this type of manufacture as it's very predictable in its make-up; it will have very close to 100% availability of non-modified lysines [226]. The high availability of carboxylic acids and amines also allows for modification of the material using non-collagen ECM components if needed. Collagen can be processed at a relatively wide range of pH without degradation of its quaternary structure, which allows for step-wise processing or combination of chemistries with different pH requirements [227]. The beneficial mechanical properties that come with collagen-based materials even at relatively low solid content allows for integration of interpenetrating networks that can carry additional functionality, such as modulation of cell adhesion, and infiltration speed, resistance to harmful chemical or biological processes, as well as osmotic regulation. When extracted using acidic processes, collagen can be purified as atelocollagen, with its triple-helix structure intact [228]. If a hydrolysis-based process is used, the triple-helix structure becomes unwound, producing gelatin [229]. This harsh processing increases the likelihood of contaminants from the tissue that can act as DAMPs. It is likely that xenogeneic collagens will always carry some small parts of partially degraded protein or ECM components that can trigger an innate immune response. While there is always a risk of partial degradation of proteins during isolation, this risk is far greater when using animal derived products compared to transgenic systems.

Collagen can be produced recombinantly using fermentation or plant-based methods [230, 231]. These methods have the benefit of producing the exact collagen type required for the scaffold and circumvents the risk of inflammatory reactions or infectious disease that accompany the use of xenogenic collagens in human medical applications. When collagens are produced in a transgenic system, the state of the collagen during extraction is that of a "young" tissue, it lacks the dense crosslinking and some of the types of crosslinks that are

found in more mature collagen. *Pichia pastoris* has been used to produce both recombinant human collagen type I and type III. This is a complex process because the yeast expression system must encode the collagen and the enzymes prolyl 4-hydroxylase and pepsin to hydroxylate the proline residues in the primary structure and cleave the telopeptides from the full-length collagen, respectively. Collagen type I has also been expressed in tobacco plants with prolyl 4-hydroxylase and lysyl hydroxylase 3 for post-translational modification [231]. The use of tobacco provides an opportunity for farmers to convert from the production of tobacco for cigarettes, an industry that will only continue to decrease in size due to the harms of tobacco smoking or other consumption, to the production of the raw material necessary for regenerative medicine applications.

There is an extremely diverse array of collagen-based hydrogels that have been designed to promote corneal wound healing. The primary types of collagen used in the literature are: rat collagen I (RCI), bovine collagen I (BCI), porcine collagen I (PCI), recombinant human collagen type I (RHCI), and recombinant human collagen, type III (RHCIII).

Xenogeneic collagens have been used extensively in corneal regenerative applications, with a diverse array of methods for producing collagen hydrogels, films and sponges (Table 1.8). Unfortunately, none of these biomaterials have progressed beyond efficacy studies in small animal models, such as rabbits.

Tab. 1.8. Xenogeneic Collagen-Based Biomaterials

Identifier	**Primary Scaffold Material**	**Method of Manufacture**	**Cell Culture Model**	**Surgical Model**	**Surgery**	**Ref**
Orwin 2000	Bovine Collagen I	Sponge	CEpC, CSK, CEnC			[232]
Orwin 2003	Bovine Collagen I		CSF			[233]
Mimura 2004	Bovine Collagen I	Dried	CEnC	Rabbit	Descemet Replacement	[234]
Borene 2004	Bovine Collagen I	lyophilized, dyhydrothermally crosslinked sponge	CSF			[235]
Crabb 2006	Bovine Collagen I	Sponge	CSF			[236]
Duan 2006	Bovine Collagen I	EDC/ Glutaraldehyde/ dendrimer	CEpC			[237]
Duan 2007	Bovine Collagen I	EDC-NHS- YIGSR Dendrimer	CEpC			[238]

Identifier	**Primary Scaffold Material**	**Method of Manufacture**	**Cell Culture Model**	**Surgical Model**	**Surgery**	**Ref**
Vrana 2008	Rat Collagen I - chondroitin sulfate	EDC/NHS, lyophilized, soaked in CS, EDC/NHS	CSK			[239]
Mi 2010	Rat Collagen I	Plastic compression	LESC			[240]
Builles 2010	Rat Collagen I	Magnetic Alignment and EDC/NHS	LESC/ CSK	Rabbits	anterior lamellar keratoplasty	[241]
Ahearne 2010	Rat Collagen I		CSF			[242]
Ahearne 2010	Rat Collagen I	Riboflavin/ UVA	CSF			[243]
Ke 2011	Rat Collagen I	Self-assembly	LESC			[244]
Kilic 2014	Rat Tail Collagen I w+w/o Elastin-like recombi-namer(YIGSR)	Solvent-film	CSK			[245]
Xiao 2014	Rat Collagen I	Plastic compression		Rabbit	Stromal Pocket	[246]
Chae 2015	Bovine Collagen I	Drying	LESC	Rabbit	Lamellar Keratectomy	[247]
Koulikovska 2015	Porcine Collagen I	EDC/NHS	HCEpC/ HCF	Rabbits	intrastromal keratoplasty	[248]

Identifier	**Primary Scaffold Material**	**Method of Manufacture**	**Cell Culture Model**	**Surgical Model**	**Surgery**	**Ref**
Kureshi 2015	Rat Collagen I	Thermal gel	CSSC, LESC			[249]
Palchesko 2016	Rat Collagen I	Plastic Compression, COL4-LAM surfce coating	CEnC			[250]
Rafat 2016	Porcine Collagen I-MPC	EDC/NHS/ APS/TEMED (Core/Skirt)	HCEpC	Rabbits	intrastromal keratoplasty	[251]
Vazquez 2016	Human Collagen I	Air drying, UV	CEnC	Rabbit	DMEK	[252]
Kishore 2016	Bovine Collagen I	Electrochemical compaction EDC/NHS	CSK			[253]
Kong 2017	Rat Collagen I/PLGA	electrospinning/ plastic compression	CEpC, CSK			[254]
Isaacson 2018	Bovine Collagen I - methacrylated	3D Printing	CSK			[255]
Cen 2018	Rat Collagen I	Plastic compression	CEnC			[256]

Identifier	**Primary Scaffold Material**	**Method of Manufacture**	**Cell Culture Model**	**Surgical Model**	**Surgery**	**Ref**
Shojaati 2018	Rat Collagen I	Film formation	CSSC	Mice	Superficial stromal wound	[257]
Mukhey 2018	Rat Collagen I	Thermal gels	CSSC			[258]
Miotto 2019	Rat Collagen I - peptide ampiphile	Plastic compression	CSMF			[259]
Gouveia 2019	Rat Collagen I	Plastic compression	CSK			[260]
Liu 2019	Bovine Collagen I	EDC/NHS - Lyophilization	-	Rabbits	anterior lamellar keratoplasty	[261]
Arabpour 2019	PLGA/collagen I	Electrospinning	Human endometrial stem cells			[262]

Identifier	**Primary Scaffold Material**	**Method of Manufacture**	**Cell Culture Model**	**Surgical Model**	**Surgery**	**Ref**
Xeroudaki 2020	Porcine Collagen I	EDC/NHS	CEpC	Rabbits / Rats	anterior lamellar keratoplasty or hybrid intrastromal LASIK flap combined with anterior lamellar keratoplasty	[263]
Chen 2020	Bovine Collagen I/Hyaluronate	HA-azido-PEG5-NHS, DBCO-sulfo-NHS w-ColI, click chemistry upon mixing	CEpC	Rabbits	Partial keratectomy	[264]
Fernandes-Cunha 2020	Bovine Collagen I	PEG-NHS	CEpC	Rabbits	Partial keratectomy	[265]

Identifier	**Primary Scaffold Material**	**Method of Manufacture**	**Cell Culture Model**	**Surgical Model**	**Surgery**	**Ref**
Wang 2020	Collagen/Vitrigel	Ammonium crosslinking, beta cyclodextric	CEnC, CSK			[266]
Islam 2021	Porcine Collagen I	EDC/ Glutaraldehyde	CEpC, CSK, CEnC			[267]
Na 2021	Bovine Collagen I	PEG-NHS encapsulation	MSC	*Ex vivo* / Organ Culture		[268]

Our group has been developing collagen based scaffolds for corneal regeneration for the last two decades. An initial comparison of RHCI vs. RHCIII indicated that performance of both recombinant collagens was similar. RHCIII fibrils were finer and allowed for a more tightly packed structure, as well as greater light transmission [269]. RHCIII corneal implants were designed using crosslinking with carbodiimide chemistry and moulded as 500 μm thick, 10 mm diameter corneal implants. A pilot study on the safety and efficacy of RHCIII implants was conducted in ten patients presenting with keratoconus or central scarring in the visual axis [270, 271]. Study participants received a central corneal graft of the RHCIII implant by anterior lamellar keratoplasty. Follow-ups at two- and four-years post-surgery indicated that the RHCIII grafts were well tolerated and successful in restoring the vision of the patients.

The RHCIII material was revised to add an interpenetrating network of polyphosphorylcholine [272]. Phosphorylcholine is an inflammation suppressing polymer that was added to increase the mechanical strength of the implants and prevent swelling and inflammation of the cornea in high-risk patients. An initial study of this material in a rabbit alkali burn model showed that the RHCIII-MPC material resulted in full epithelial coverage and growth of new stromal keratocytes, while resisting neovascularization [273]. The RHCIII-MPC implants were tested in a case series of high-risk participants with viral and fungal infection scars, alkali and thermal burns, and corneal ulcers [274]. In the participants with scarring, the RHCIII-MPC material improved central corneal transparency. Re-epithelialization was slowed in the participants with alkali and thermal burns due to LESC deficiency. In the participants with corneal ulcers, both of whom were neurologically blind, the regeneration of corneal tissue resulted in improved innervation and a cessation of corneal pain from the ulcers. Overall, the RHCIII-based materials represent the first human clinical trials of collagen-based biomaterials in the cornea and showed excellent safety and efficacy in both low and high-risk patients.

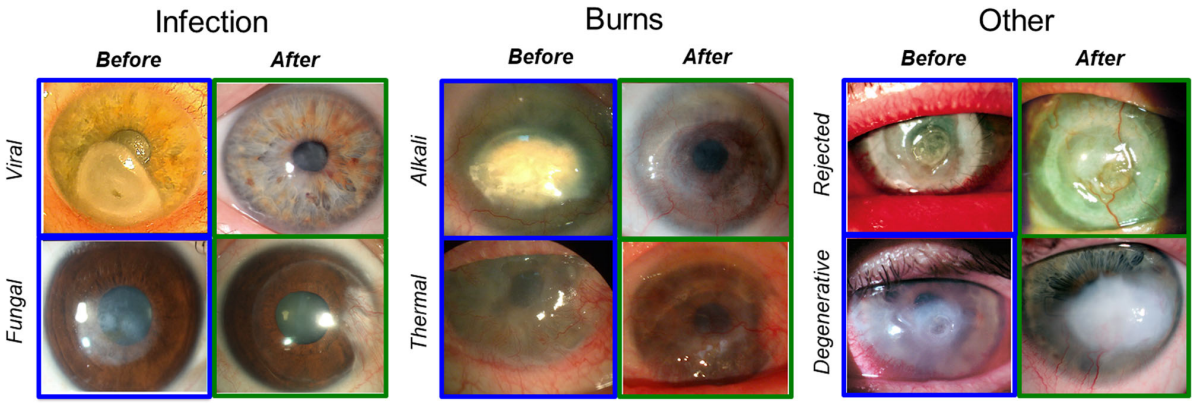

Fig. 1.3. Patients are divided into three groups based on their pre-operative diagnoses: infection (herpes simplex viral and fungal keratitis), burns (alkali and thermal) and other (failed graft and poststroke neurotrophic keratitis). Post-operation, regenerated neocorneas from Patients 1 and 2 are mostly clear. In Patients 3 and 4, where stem cell deficiency is present, some superficial vessels concurrent with conjunctival invasion are seen. Patient 5 has a mostly clear cornea encircled by blood vessels but has invaded in one quadrant, while Patient 6's cornea remains hazy. Patient 2 has an unrelated nasal pterygium. Reproduced from Islam *et al.* [274] under a Creative Commons Attribution 4.0 International License (CC BY 4.0).

1.5.2. Collagen Mimetic Peptide-Based Biomaterials

In 1998, Holmgren *et al* determined that the stability of the collagen helix was maintained by inductive interactions between the X_{aa}-Y_{aa}-Gly triple amino acid repeats in the collagen structure, not hydrogen bonds mediated by water bridges. Previous data had shown that $(Pro\text{-}Pro\text{-}Gly)_{10}$ and $(Pro\text{-}Hyp\text{-}Gly)_{10}$ peptides are stable in methanol or propane-1,2-diol in the absence of water [275]. In this study, peptides composed of $(Pro\text{-}Hyp\text{-}Gly)_{10}$, $(Pro\text{-}Pro\text{-}Gly)_{10}$ and $(Pro\text{-}Flp\text{-}Gly)_{10}$, where Flp is 4(R)-fluoroproline were compared for triple helix formation. Flp is unable to form hydrogen bonds due to the electronegativity of the fluorine. All three peptides showed similar stability using circular dichroism, indicating that hydrogen bonding is not the mechanism for collagen triple-helix, as previously thought. Based on this information about X_{aa}-Y_{aa}-Gly amino acid triplicates, O'Leary *et al.* designed a collagen mimicking peptide (CMP) or collagen-like peptide (CLP), designed to be a minimal unit for

self-assembled fibril formation [276]. This peptide monomer consists of (Pro-Lys-Gly)$_4$(Pro-Hyp-Gly)$_4$(Asp-Hyp-Gly)$_4$. It forms stable hydrogels based on fibrillar assembly at solid contents as low as 0.5% in water, Tris-buffer and PBS.

CLPs are an ideal functional substitute for full length collagen due to their synthetic origin and ease of processing. Peptides under approximately 40 amino acids can be synthesized by solid state synthesis, a readily commercially available service. Unlike animal collagens, which present concerns about infectious disease transmission, and recombinant collagens, whose manufacture is limited to select companies, CLPs can be affordably acquired from pharmaceutical-grade suppliers globally. CLPs are designed to be monomerized using high temperatures in order to undergo fibrillar assembly during thermal gelation. This means that unlike atelocollagens, CLPs can be processed using heat to reduce viscosity during moulding, instead of requiring high-pressure mixing (1 MPa) at 2-8°C due to the high viscosity of RHC solutions.

In 2016, the Griffith group modified the primary amino acid structure of the O'Leary CLP to add a thiol-containing cysteine with a glycine spacer to the N-terminus of the peptide [Cys-Gly-(Pro-Lys-Gly)$_4$(Pro-Hyp-Gly)$_4$(Asp-Hyp-Gly)$_4$] [278]. The thiol group was used to conjugate the peptide to an 8-arm polyethylene glycol (hexaglycerol core) (PEG) functionalized with malemide groups. The CLP-PEG conjugate was crosslinked into hydrogels using the carbodiimide chemistry employed in the predicate RHCIII materials. An *in vivo* study, conducted in Göttingen mini-pigs concluded that CLP-PEG performed equivalently to RHCIII-MPC in a deep anterior lamellar keratoplasty surgical model (Figure 1.4) [277, 278].

1.5.3. Peptide Ampiphile-Based Biomaterials

Peptide ampiphiles (PAs) were initially identified as substrates for corneal fibroblasts in 2013 [279]. Jones *et al.* demonstrated that the peptide ampiphile C_{16}–KTTKS increased corneal fibroblast collagen secretion in a dose dependant manner. In 2014, the peptide ampiphile A_6RGD was shown to form short fibrils in a concentration dependent-manner based on β-sheet assemblies [280]. A_6RGD films from 0.1-1.0% wt allowed for CSF attachment and proliferation. A subsequent study of $C_{16}G_3$RGD (RGD) and $C_{16}G_3$RGDS (RGDS) PAs mixed with C_{16}-ETTES demonstrated that both PAs formed successful cell culture

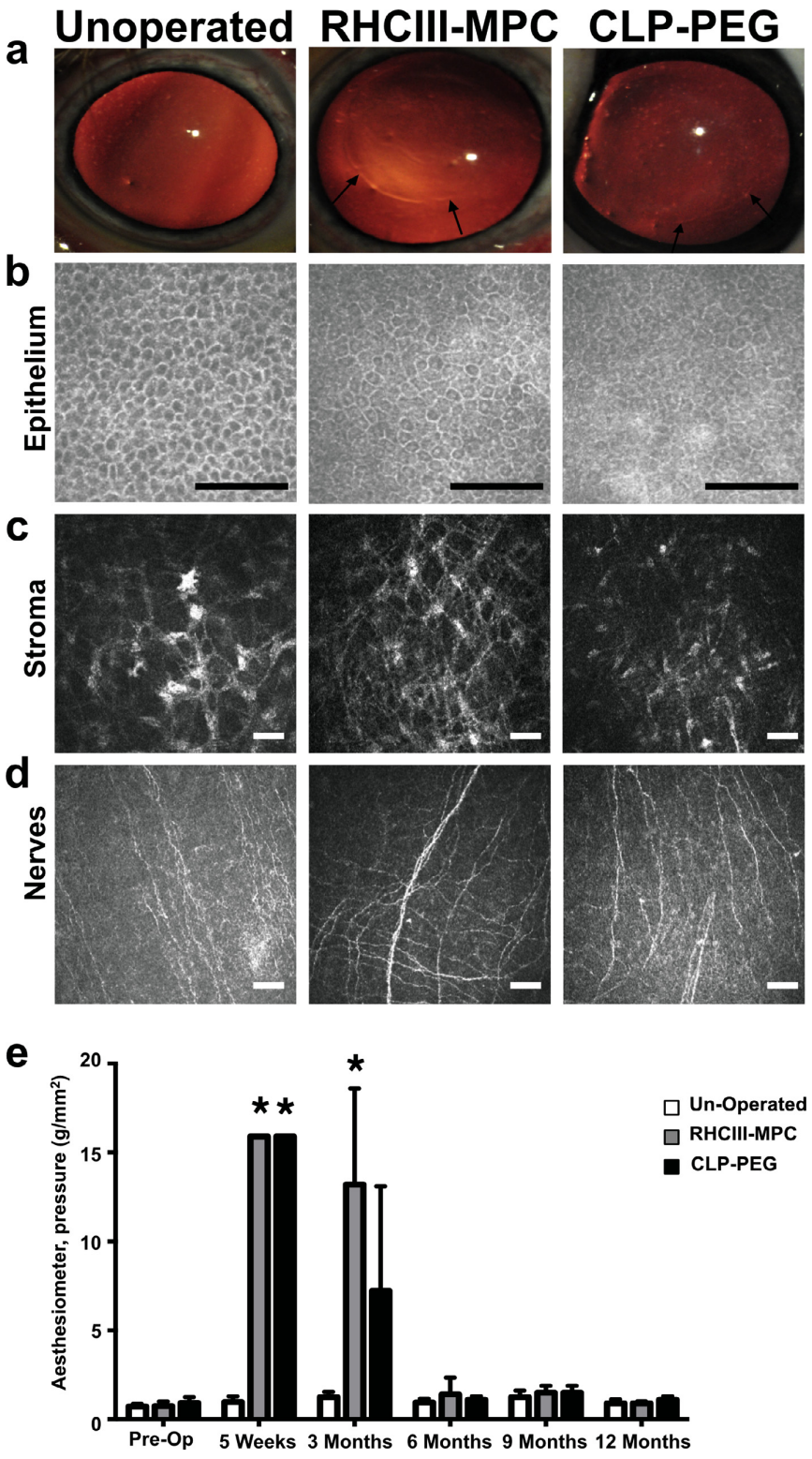

Fig. 1.4. RHCIII-MPC and CLP-PEG corneal implants and their performance in mini-pigs

Fig. 1.4. Examples of optically clear RHCIII-MPC and CLP-PEG hydrogel implants (a). After 12 months of implantation in corneas of mini-pigs, the implants remain clear like the unoperated cornea. Arrows indicate the boundaries of the implants. *In vivo* confocal microscopy shows that both RHCIII-MPC and CLP-PEG implanted corneas have regenerated their epithelium (b), stroma (c) and sub-epithelial nerve plexus (d) to resemble their counterparts in the normal, healthy cornea. Scale bars, 150 mm. Aesthesiometry measures the pressure needed to obtain a blink reaction, i.e. touch sensitivity, which is correlated to nerve function. Pre-operatively, all healthy corneas showed a response to light touch. At 5 weeks post-operation, the implanted corneas were non-responsive, even with maximal pressure exerted. At 3 months, touch sensitivity is returning so less pressure was needed for a response. By 6 months, sensitivity was back to normal levels. * – $p < .05$ as compared to un-operated eyes (Kruskal-Wallis test with Bonferroni post hoc test). Reproduced from Jangamreddy *et al.* [277] under a Creative Commons Attribution 4.0 International License (CC BY 4.0).

coatings on hydrophilic surfaces for the attachment and proliferation of CSFs [281]. The $C_{16}G_3RGD$ PA can also be used to generate self-curving tissue culture constructs in combination with a collagen-base [259]. The presence of PAs in the collagen material prevents contraction of the construct by myofibroblasts. The peptide ampiphile C_{16}-YEALRVANEVTL, derived from lumican, allowed for increased collagen production from CSFs, compared to TCP [282]. This PA aggregated into nanotapes and increased collagen secretion from CSFs two-fold in an activin receptor-like kinase receptor dependant process.

PAs have been developed to act as self-lifting auto-generated tissue equivalents (SLATEs) for CSFs. A self-releasing cell culture coating was designed based on the peptide ampiphile C_{16}-TPGPQGIAGQRGDS, which contains a MMP1 cleavage site [283, 284]. This self-assembling peptide-ampiphile supported CSF attachment and proliferation. After the removal of retinoic acid (RA) from the cell culture media, MMPs released the tissue sheet from the cell culture plate. A new coating of C_{16}-TPGPQGIAGQRGDS allowed for re-attachment of the sheet. A subsequent study was conducted of a PA film using a 15:85 ratio of C_{16}-TPGPQGIAGQRGDS and C_{16}-ETTES, respectively [284]. The PA coating was deposited on a microrubbed polytetrafluoroethylene (PTFE) coated glass slide to produce aligned materials and directly onto a silica glass coverslip to produce non-aligned materials.

CSFs were seeded on the two surfaces and cultured until a multi-layered tissue was formed. Removal of retinoic acid from the culture media allowed MMP cleavage of the tissue sheet in three days. In 2017, this culture methodology was combined with the seeding of CEpCs on the CSF tissue substrate to form SLATEs [285]. CSFs were originally cultured on aligned or random SLATEs for analysis. The aligned SLATE (aSLATE) has a greater elastic modulus than the random SLATE and increased expression of collagen, proteglycan, enzyme mRNA, as well as reduced fibrotic markers. IHC confirmed significantly more collagen type I, collagen type V and decorin depostion on the aSLATE. The aSLATE also supported greater cytokeratin 3 and β-integrin expression in CEpC seeded on the tissue. Both CSF-only SLATEs were implanted into peripheral intrastromal pockets in the same eye of rabbits. At 9 month follow-up both constructs were well tolerated with minimal haze and edema. IHC analysis one and nine months after implantation showed that the the aSLATE had reduced vimentin and α-SMA expression than the rSLATE. Overall, the aSLATE generated successful corneal stromal grafts.

1.6. Fabricating Biomaterials for Delivery

1.6.1. Molding

The vast majority of the biomaterials discussed in sections 1.3.1.1, 1.5.1 and 1.5.2 are manufactured by molding, either as films, flat sheets, or in the form of semi-spherical corneal implants. Molding is advantageous because it allows for the production of biomaterials with identical physical dimensions. It is a fast and efficient manufacturing method and can easily be adapted for future automation for commercial manufacturing. The Griffith lab's corneal implants are molded using a sandwich of two identical polypropylene molds, designed to match the curvature of the human eye. These molds produce implants that are 10 mm in diameter and 500 μm thick, so they are appropriate for deep anterior lamellar keratoplasty procedures. The group also has thinner molds designed for use in rabbits (350 μm) and rodents (200 μm) to facilitate pre-clinical trials.

1.6.2. 3D Printing

3D printing of corneas is usually bioprinting that contains cells. 3D printers are unable to generate smooth, high resolution curves due to their linear application of bioink. Their

advantage is the ability to print corneal cells directly into the hydrogel matrix to allow the CSKs to immediate repopulate the graft, instead of migrating into the graft from the periphery. The first report of a 3D printed corneal tissue was published by Isaacson *et al* in 2018 [255]. CSK keratocytes were 3D printed in a bioink composed of alginate and collagen I-methacrylate (ColMA) and solidified using $CaCl_2$. The CSKs in the 3D printed structure were viable after seven days in culture. Duarte-Campos *et al.* reported a CSK-containing corneal stromal graft 3D printed using a 0.5% agarose with 0.2% collagen hydrogel [286]. After seven days in culture, the CSKs expressed keratocan and lumican, but not the α-SMA indicative of myofibroblasts. In 2019, Park *et al.* reported the successful transplantation of CSKs 3D printed in a bioink composed of dECM [287]. Four weeks post-surgery the CSKs were visible in H&E analysis of the tissue. Inflammatory cells, but not T-cells, were observed in the immediate vicinity of the grafts, suggesting a moderate immune repsonse to the grafted tissue. Kutlehria *et al* also reported a 3D printed corneal stroma using an alginate, collagen I, and gelatin bioink [288]. After 2 weeks of culture, the CSKs had >95% cell viability and expressed fibrin and actin.

Gelatin-methacrylate (GelMA) has also been used to 3D print corneal stromal tissue. Bektas *et al* report CSKs that were 3D printed in GelMA containing Irgacure 2959, which was subsequently photocrosslinked using UV light [289]. After 21 days of culture, 98% of the CSKs were viable. Mahdavi *et al* also used 12.5% GelMA bioink to print a corneal stromal equivalent [290]. After 28 days in culture the printed CSKs expressed collagen I and lumican.

There is a single report of an acellular 3D printed corneal implant. Gibney *et al* reported an aerosol jet printed collagen III corneal implant crosslinked using carbodiimide chemistry [291]. The material was optically clear and had an elastic modulus of 506 $\pm$ 173 kPa.They did not perform cell compatibility studies.

1.6.3. Injectable Hydrogels

Injectable hydrogels are designed to be applied as a liquid and solidify in the wound. These biomaterials can be designed to gel using physical methods such as ionic crosslinking [292, 293], hydrophobic interactions [294, 295], host-guest interactions [296–298], $\pi-\pi$ stacking [299], or hydrogen bonding [300]. Alternatively, they can employ chemical crosslinking like click reactions [301–310], Michael addition [311, 312], photo-polymerization [313–316],

Schiff's base reaction [317, 318], or enzymatic crosslinking [319, 320]. Injectable hydrogels have been designed using a wide variety of biomolymers including, but not limited to, gelatin-methacrylate, PEGs, chitosan, alginate, and hyaluronic acid [321]. For a complete review of *injectable hydrogels* please see Appendix A.

1.7. Anti-infective Additives for Corneal Implants

Fabricated biomaterials-based corneal implant present a unique opportunity to add functional molecules, enzymes or NPs to expand the wound healing or anti-infective properties of the material. The additives can be directly conjugated to the hydrogel matrix or entrapped in the porous structure of the hydrogel material. Several iterations of antibacterial solid and *in situ* corneal implants have been developed. Anumolu *et al* developed an *in situ* gelling doxycycline (DOX) loaded PEG hydrogel that released the DOX in a biphasic pattern over seven days [322]. *Ex vivo* rabbit corneal organ cultures showed that the DOX had improved corneal penetrance. When wounded with CEES (half mustard, 2-chloroethyl ethyl sulfide), the DOX hydrogels improved corneal wound healing with a flattened epithelial-stromal border compared to wounded corneas treated with DOX eye drops. The DOX hydrogel also reduced MMP-9 in the corneal epithelium. Unas Daza *et al* developed a polyvinyl alcohol (PVA)/anionic collagen membranes containing ciprofloxacin or tobramycin [323]. These membranes were effective in preventing *E. coli* and *S. aureus* proliferation *in vitro*. Chang *et al* developed a collagen/gelatin/alginate hydrogel containing liposomal dexamethasone-moxifloaxin NPs to promote corneal wound healing in corneal infections [324]. In an *ex vivo* central corneal epithelial debridement mouse model, the NP-hydrogel material promoted corneal wound healing and decreased leukocyte infiltration and corneal edema. Khalil *et al* developed an *in situ* gelatin methacrylate (GelMA) hydrogel containing ciprofloxacin micelles [325]. The GelMA-ciprofloxacin micelle hydrogels inhibited the proliferation of *S. aureus* and *P. aeruginosa in vitro*. The GelMA-ciprofloxacin micelle hydrogels also inhibited *P. aeruginosa* in an *ex vivo* porcine corneal culture model. Overall, hydrogel materials provide an opportunity to expand their functionality beyond wound healing, into the prevention and control of corneal infections.

Chapter 2

Thesis Research Summary

2.1. Rationale

There is an urgent need for corneal therapies that are accessible in regions where HDCs are not available, or contraindicated for use in patients at high-risk for graft rejection. These therapies need to have a long-shelf life, thermostability for deployment and biocompatibility in high-risk patients. There are two types of biomaterials products that can meet this need. Solid corneal implants are intended for the grafting of large corneal opacities (3-6 mm) and use by ophthalmic surgeons. *In situ* gelling hydrogels provide the opportunity to seal small corneal perforations (1-3 mm) and to fill large superficial corneal wounds. This thesis explores biomaterials formulations for solid and *in situ* gelling corneal biomaterials, their performance as composite devices, the addition of terminal sterilization to the manufacture of solid corneal implants, and the development of future collagen mimetic proteins for hydrogel formulations.

2.2. Objectives and Hypotheses

Objective 1. Develop a solid corneal implant suitable for implantation in high-risk corneal patients

Hypotheses

A. Phosphorylcholine will reduce inflammation and improve corneal regeneration in alkali burns

B. Peptide-capped silver nanoparticles coated on collagen hydrogels can inhibit bacteria.

C. Electron-beam is an effective sterilization method for RHCIII-MPC corneal implants

Objective 2. Design a hydrogel that will solidify *in situ* to seal corneal perforations

Hypotheses

A. Fibrinogen can be added to a CLP-PEG hydrogel to seal it to a corneal wound bed using thrombin

B. A CLP-PEG-fibrin(ogen) hydrogel can regenerate corneal tissue

Objective 3. Improve the design and performance of collagen mimetic proteins for future corneal biomaterials

Hypotheses

A. Collagen mimetic proteins can be produced using a low-endotoxin *E. coli* expression system and purified for use in biomaterial manufacture

2.3. Summary of Research Papers and Contributions

Article 1. Collagen analogs with phosphorylcholine as inflammation-suppressing scaffolds for corneal regeneration in high-risk alkali burns

Reproduction of: **Simpson, FC***, McTiernan C*, Islam MM, Buznyk O, Lewis PN, Meek KM, Haagdorens M, Audiger C, Lesage S, Gueriot FX, Brunette I, Robert MC, Olsen D, Koivusalo L, Liszka A, Fagerholm P*, Gonzalez-Andrades M*, Griffith M*. Collagen analogs with phosphorylcholine as inflammation-suppressing scaffolds for corneal regeneration in high-risk alkali burns. *Commun Biol.* 2021;4:608. (* Equivalent contributions) Reproduced under a Creative Commons Attribution 4.0 International Public License (CC BY).

Contributions

I helped plan the study logistics and collect the samples from the pig study, performed the dendritic cell assays and immunohistochemistry, and analysed the clinical results from the pig study. I wrote the primary draft of the manuscript with CDM and MG, and assembled all the figures. I contributed to revisions and approved the final version of the manuscript.

Article 2. Nanoengineering the surface of corneal implants: Towards functional anti-microbial and biofilm materials

Reproduction of: Khatoon Z, Guzman I, McTiernan CD, Lazurko C, **Simpson F**, Zhang L, Cortes D, Mah T, Griffith M and Alarcon EI. Nanoengineering the surface of corneal implants: Towards functional anti-microbial and biofilm materials. *RSC Adv.* 2020;10:23675-23681.Reproduced under a Creative Commons Attribution-Non Commercial 4.0 International Public License (CC BY-NC).

Contributions

I performed the bone-marrow dendritic cell assays which showed that the peptide-capped silver nanoparticles were not immunogenic. This is important for a medical device that will go into the eye of a patient who may have a compromised cornea that the device does not trigger any adverse immune reactions. I also contributed to the writing up the sections pertaining to these assays in the draft, and approved the final manuscript.

Article 3. Electron-Beam Irradiated Recombinant Human Collagen-Phosphorylcholine Corneal Implants Retain Pro-Regeneration Capacity

Simpson FC, Islam MM, Buznyk O, Edin E, Ljunggren MK, Liszka A, Fagerholm P, Griffith M. Electron-Beam Irradiated Recombinant Human Collagen-Phosphorylcholine Corneal Implants Retain Pro-Regeneration Capacity. (In Preparation)

Contributions

I manufactured the biomaterials for microbial and mechanical testing. I performed the statistical analyses for manuscript. I drafted the initial version of the manuscript with MMI, EE and MG.

Article 4. LiQD Cornea: Pro-Regeneration Collagen Mimetics as Patches and Alternatives to Corneal Transplantation

Reproduction of: LiQD Cornea: Pro-regeneration collagen mimetics as patches and alternatives to corneal transplantation. Christopher D. Mctiernan†, Fiona C. Simpson†, Michel Haagdorens, Chameen Samarawickrama, Damien Hunter, Oleksiy Buznyk, Per Fagerholm, Monika K. Ljunggren, Philip Lewis, Isabel Pintelon, David Olsen, Elle Edin, Marc Groleau, Bruce D. Allan*, May Griffith*. Science Advances 17 JUN 2020 : EABA2187. DOI: 10.1126/sciadv.aba2187. Reproduced under a Creative Commons Attribution-Non Commercial 4.0 International Public License (CC BY-NC).

Contributions

I performed the dendritic assays, immunohistochemistry and analyses of the clinical results from the pig study. I wrote the primary draft of the manuscript with CDM and MG. I participated in all revisions and approved the final version of the manuscript.

Article 5. Synthesis and application of collagens for assembling a corneal implant

Reproduction of: Edin E, **Simpson F**, Griffith M. Synthesis and application of collagens for assembling a corneal implant. In: Methods in Molecular Biology. 2020;2145:169-183. Reproduced with permission of Springer Nature Customer Service Centre GmbH.

Contributions I validated the methods in described in this paper to produce a recombinant collagen mimetic program. I drafted the initial version of the manuscript with EE and MG. I contributed to revisions and approved the final version of the manuscript.

Appendix A. *In situ* Tissue Regeneration in the Cornea from Bench-to-Bedside.

Reproduction of: Poudel BK, Robert MC, **Simpson FC**, Malhotra K, Jacques L, LaBarre P, Griffith M. *In situ* Tissue Regeneration in the Cornea from Bench-to-Bedside. *Cells Tissues Organs*. 2021. doi: 10.1159/000514690. Reproduced with the permission of S. Karger AG, Basel.

Contributions

I contributed the sections on Extracellular Vesicles, Exosomes, and *in situ* Tissue Regeneration; Exosomes in Corneal Wound Healing; and Regeneration, and Regulatory Considerations. I contributed to revisions and approved the final version of the manuscript.

Appendix B. Plant Recombinant Human Collagen Type I Hydrogels for Corneal Regeneration

Reproduction of: Haagdorens M*, Edin E*, Fagerholm P, Groleau M, Shtein Z, Ulčinas U, Yaari A, Samanta A, Cepla V, Liszka A, Tassignon MJ, **Simpson FC**, Shoseyoy O, Valiokas R, Pintelon I, Ljunggren MK, Griffith M. Plant Recombinant Human Collagen Type I Hydrogels for Corneal Regeneration. *Regen Eng Transl Med.* 2021. https://doi.org/10.1007/s40883-021-00220-3. (* Equivalent contributions) Reproduced under a Creative Commons Attribution 4.0 International Public License (CC BY).

Contributions

I performed the immunohistochemistry with Marc Groleau. I also contributed the primary draft of the manuscript, revisions and approved the final version of the manuscript.

Chapter 3

Collagen analogs with phosphorylcholine as inflammation-suppressing scaffolds for corneal regeneration in high-risk alkali burns

Fiona C. Simpson[1,4,†], Christopher D. McTiernan[5, †], Mohammad Mirazul Islam[6], Oleksiy Buznyk[7,8], Philip N. Lewis[9], Keith M. Meek[9], Michel Haagdorens[10], Cindy Audiger[1,11], Sylvie Lesage[1,11], François-Xavier Gueriot[1,12], Isabelle Brunette[1,2], Marie-Claude Robert[1,4], David Olsen[13], Laura Koivusalo[14], Aneta Liszka[7], Per Fagerholm[7,*], Miguel Gonzalez-Andrades[6, 15,*], May Griffith[1-4, *]

[1]Centre de recherche, Hôpital Maisonneuve-Rosemont, Montréal, QC, Canada

[2]Départment d'Ophtalmologie, Université de Montréal, Montréal, QC, Canada

[3]Institut du Génie Biomédicale, Université de Montréal, Montréal, QC, Canada

[4]Centre de recherche du Centre hospitalier de l'Université de Montréal, Montréal, QC, Canada

[5]Division of Cardiac Surgery, University of Ottawa Heart Institute, Ottawa, ON, Canada

[6]Disruptive Technology Laboratory, Massachusetts Eye and Ear and Schepens Eye Research Institute, Department of Ophthalmology, Harvard Medical School, Boston, MA, USA

[7]Institute for Clinical and Experimental Medicine, Linköping University, Linköping, Sweden

[8]Filatov Institute of Eye Diseases and Tissue Therapy of the NAMS of Ukraine, Odessa, Ukraine

[9]School of Optometry and Vision Sciences, Cardiff University, Cardiff, UK

[10]Department of Ophthalmology, Visual Optics and Visual Rehabilitation, University of Antwerp, Antwerp, Belgium

[11]Département de microbiologie, infectiologie et immunologie, Université de Montréal, Montréal, QC, Canada

[12]Department of Ophthalmology, Valence Hospital, France

[13]FibroGen Inc., San Francisco, CA, USA

[14]Faculty of Medicine and Health Technology, Tampere University, Tampere, Finland

[15]Maimonides Biomedical Research Institute of Cordoba (IMIBIC), Department of Ophthalmology, Reina Sofia University Hospital and University of Cordoba, Cordoba, Spain

[†]These authors contributed equally. *These authors jointly supervised this work.

[*]To Whom Correspondence Should be Addressed:

May.Griffith@umontreal.ca, Per.Fagerholm@liu.se, miguel.gonzalez@imibic.org

Abstract

The long-term survival of biomaterial implants is often hampered by surgery-induced inflammation that can lead to graft failure. Considering that most corneas receiving grafts are either pathological or inflamed before implantation, the risk of rejection is heightened. Here, we show that bioengineered, fully-synthetic, and robust corneal implants can be manufactured from a collagen analog (collagen-like peptide-polyethylene glycol hybrid, CLP-PEG) and inflammation suppressing polymeric 2-methacryloyloxyethyl phosphorylcholine (MPC) when stabilized with the triazine-based crosslinker 4-(4,6-Dimethoxy-1,3,5-triazin-2-yl)-4-methylmorpholinium chloride. The resulting CLP-PEG-MPC implants led to reduced corneal swelling, haze, and neovascularization in comparison to CLP-PEG only implants when grafted into a mini-pig cornea alkali burn model of inflammation over 12 months. Implants incorporating MPC allowed for faster nerve regeneration and recovery of corneal sensation. CLP-PEG-MPC implants appear to be at a more advanced stage of regeneration than the CLP-PEG only implants, as evidenced by the presence of higher amounts of cornea-specific type V collagen, and a corresponding decrease in the presence of extracellular vesicles and exosomes in the corneal stroma, in keeping with the amounts present in healthy, unoperated corneas.

Introduction

Biomaterial implants, like organ transplants, suffer inflammation that can result in immune rejection and graft failure.[1] This is a consideration when developing corneal implants for treating patients not amenable to conventional human donor transplantation.

Globally, approximately 23 million people have unilateral corneal blindness and 4.6 million are bilaterally blind.[2] For the past century, the only widely accepted treatment for corneal blindness has been human donor corneal transplantation. First-time, low-risk grafts are over 90% successful for the first two years post-operation.[3] However, this declines to 55% by 15 years due to chronic inflammation.[4] A severe worldwide human donor cornea shortage leaves 12.7 million patients awaiting transplantation, with only one in 70 patients being treated.[5] Patients with inflammation and severe pathologies have risks of up to 70% for rejecting donor allografts.[3] So, they often remain untreated, with valuable tissues allocated to patients with better chances of success.[6]

Artificial corneas or keratoprostheses (KPros) were developed to treat high-risk patients, but most have failed due to adverse biomaterial-induced host reactions. The most successful design currently in clinical application, the Boston KPro, has a poly(methyl methacrylate)(PMMA) optic cylinder that allows light transmission into the eye for vision. However, human corneal tissue is needed as a carrier for implantation. The graft-host tissue interface has been implicated in the formation of retroprosthetic membrane,[7] corneal tissue melt (keratolysis) and tractional retinal detachment. Further, the issues of PMMA-induced inflammation remain[8] and potentially contribute to periprosthetic keratolysis and KPro extrusion.[9] In a mouse model, it was shown that inflammatory cytokines, TNF-α and IL-1, elicited by Boston KPro implantation can result in optic nerve damage.[10] Hence, KPros are only used for end-stage eyes.

Diverse anti-inflammatory approaches have been developed to improve biocompatibility and integration of biomaterial implants. Many of these involve surface modification of the biomaterials.[11] Introduction of topographical features on surfaces were reported to reduce adherence of macrophages,[12] and alter the profile of cytokines produced *in vivo* in rats. Other strategies involve converting hydrophobic surfaces that promote inflammatory

reactions (e.g., increased leukocyte adhesion, macrophage fusion, and pro-inflammatory cytokine release[13,14]) to more tolerogenic hydrophilic ones by modifying surface chemistries.[11,13] Hydrophilic terminal groups (NH_2, OH, COOH) were shown to temper macrophage conversion into foreign body giant cells that characterize adverse reactions, and decrease expression of proinflammatory cytokines.[11] Inflammation-decreasing surface coatings include anti-fouling molecules such as polyethylene glycol (PEG) that prevent non-specific cell adhesion, and anti-inflammatory molecules like glycosaminoglycans, steroids (e.g., dexamethasone), α-melanocyte-stimulating hormone, and interleukin-1 receptor antagonists.[11]

Corneal transplantation, particularly in high-risk cases, can trigger allogenic sensitization against foreign cells, releasing inflammatory chemokines/cytokines that mediate the recruitment and activation of immune cells including antigen-presenting dendritic cells to the graft.[15,16] Host dendritic cells are exposed to shed donor antigen as they migrate into the graft. As the dendritic cells process the alloantigens, they drain via the lymphatic system to local lymph nodes where they activate naive T-cells that are involved in rejection.[15] The inflammatory cycle triggered by dendritic cell activation also results in lymphangiogenesis and angiogenesis, which in turn enhances the sensitization to alloantigens.[17] Implants that do not activate dendritic cells at the outset would therefore be optimal.

To address corneal donor shortage and circumvent immune problems, Fagerholm *et al.* developed corneal implants made from carbodiimide-crosslinked recombinant human collagen type III (RHCIII) and grafted 500 μm thick implants into 10 patients.[18,19] Being cell-free, the implants were immune compatible, did not activate dendritic cells, and supported the stable regeneration of corneal epithelium, stroma and nerves.[19,20] Polymeric 2-methacryloyloxyethyl phosphorylcholine (MPC) was incorporated into implants to modulate the inflammation in corneas of patients at high-risk of graft rejection and therefore not prioritized for donor corneal transplantation.[21] Partial-thickness RHCIII-MPC grafted into high-risk corneas after removing active ulcers or scars promoted stable corneal epithelium and stromal regeneration over the averaged 24-month observational period.21 It was subsequently shown that MPC-containing RHCIII hydrogels do not activate dendritic cells, but instead induce dendritic cell apoptosis.[20]

While RHCIII-based implants performed well in clinical trials, RHCIII is a large macromolecule with manufacturing challenges. Replicating full-length native collagen, RHCIII contains numerous 4-hydroxyproline amino acids for stable triple helix formation. Therefore, to produce RHCIII, it is not only necessary to produce the collagen but also prolyl 4-hydroxylase, the enzyme that catalyses 4-hydroxyproline formation from proline.[22] In addition, recombinant pepsin is needed to cleave the telopeptides from the full-length protein prior to use.[23] This means expression of three different complex proteins is required to produce RHCIII. Short, self-assembling collagen-like peptides (CLPs) have been developed by several groups as alternatives to native collagen.[24] As short peptides, they can be produced synthetically, are easy to purify and also easy to manipulate and customize for different applications.[24,25] A 36 amino-acid CLP was developed by the Hartgerink group as a collagen analog,[26] and performed well as a hemostat.[27] When conjugated to a multi-arm polyethylene glycol (PEG) through a short peptide and thiol-maleimide, the resulting CLP-PEG hydrogel could be fabricated into corneal implants that promoted regeneration in the corneas of mini-pigs.[28,29] However, the N-(3- dimethylaminopropyl)-N'-ethylcarbodiimide hydrochloride (EDC) used for stabilizing the hydrogels was possibly pro-inflammatory.[20,30]

As mentioned above there are currently no or limited treatment options for patients awaiting corneal transplantation that are at high-risk of graft rejection. Our goal was thus to bioengineer fully-synthetic, robust and easy to manufacture corneal implants, as alternatives to human donor corneas or prostheses. In addition to a simple manufacturing process, the implants must promote tolerogenic properties or limit inflammation while stimulating stable regeneration of corneal tissues and nerves, to be amenable for use in high-risk patients. Hence, we improved on CLP-PEG implants by stabilizing with 4-(4,6-Dimethoxy-1,3,5-triazin-2-yl)-4-methylmorpholinium chloride (DMTMM) a triazine based crosslinker, as opposed to using the pro-inflammatory EDC stabilizer. Indeed, DMTMM has a much lower toxicity compared to EDC and its commonly used co-reactant, N-hydroxy-succinimide (NHS).[31] We further modified the CLP-PEG implants by including inflammation-suppressing MPC. The novel CLP-PEG-MPC implants were characterized and compared to those without MPC *in vitro* and after grafting into the corneas of mini-pigs. Inflammation and severe pathological conditions were simulated by a standard alkali burn cornea model.

Results

Hydrogel Manufacture and Characterization

Infrared spectroscopy (Fig. 1a) and ^{31}P NMR spectroscopy (Fig. 1b) confirmed the incorporation of MPC into DMTMM-crosslinked CLP-PEG hydrogels that were fabricated into cornea-shaped implants, 10 mm in diameter and 500 μm thick. In particular, the CLP-PEG-MPC hydrogels showed a peak at approximately 0 ppm on ^{31}P NMR, which was indicative of the ring opening generated by the addition of trimethylamine to the 2-hydroxyethyl methacrylate (HEMA) and ethylene chlorophosphate intermediary during MPC synthesis (Fig. 1b).[32] Both hydrogels were highly transparent in visible light (%T400 nm – 700 nm $>$ 80%) (Fig 1 c). However, CLP-PEG-MPC (Fig. 1c), but not CLP-PEG, hydrogels blocked up to 60% transmission of UV-A (300-400 nm wavelength).

Table 1 summarizes the implant properties and how they compare with RHCIII implants that were tested clinically, and to human corneas. Neither hydrogels nor the RHCIII comparator were as tough as the human cornea, although they were optically slightly superior. As the hydrogels contained over 90% water, their refractive indices approximated that of water (1.33). CLP-PEG hydrogels were stiffer (Young's modulus of 0.150 $\pm$ 0.015 MPa) and less elastic (elongation at break 49.96 $\pm$ 8.10 %) than those incorporating MPC. CLP-PEG-MPC implants displayed a lower Young's modulus (0.044 $\pm$ 0.010 MPa) and higher elongation at break (59.50 $\pm$ 7.70 %). Furthermore, rheology showed that the CLP-PEG hydrogels had a higher storage modulus (G') (22.36 $\pm$ 1.489 kPa) than the CLP-PEG-MPC (15.15 $\pm$ 1.086 kPa) indicating an increased amount of structure present in the CLP-PEG only implants. However, considering the loss modulus of both gels was lower than the storage modulus, both hydrogels were considered ductile. Apparent and cumulative permeability measurements of the implants (Fig. 1d,e) showed no significant difference in the apparent or cumulative permeability amongst CLP-PEG-MPC, CLP-PEG, or the human amniotic membrane (hAM) control, which is the current gold standard for ocular surface reconstruction. Both CLP-PEG-MPC and CLP-PEG implants were highly resistant to bacterial collagenase degradation *in vitro* (Fig. 1f).

In vitro biocompatibility and immune compatibility

Initial growth (1-6 days) of immortalized human corneal epithelial cells (HCECs) expressing green fluorescent protein (GFP) on CLP-PEG-MPC was slower than on CLP-PEG and tissue culture plastic controls (Fig. 2a-c), but at seven days in culture, cells on both hydrogels were confluent (Fig 2d,e). Live-dead staining showed very few dead cells, confirming that the hydrogels were non-cytotoxic (Fig. 2g,h). These observations were confirmed by an Alamar Blue proliferation study carried out with non-GFP tagged HCECs (Fig. 2j).

Bone-marrow-derived dendritic cell (BMDC) activation assays were conducted for the individual hydrogel components (Fig. 2k) and the completed hydrogels (Fig. 2l). The crosslinker EDC-NHS was compared to equimolar concentrations of DMTMM. However, EDC-NHS was cytotoxic and resulted in such low absolute cell counts of $CD11c^+$ cells, that it was excluded from subsequent analysis. Of the structural hydrogel components, only conjugated CLP-PEG activated CD40 (Fig. 2k). Both hydrogels upregulated CD40 to levels above that of the untreated controls, but significantly lower than the lipopolysaccharide positive control level ($F= 40.03$, $p<0.0001$) (Fig. 2l).

In vivo clinical evaluation of implants

In compliance with the Swedish Animal Welfare Ordinance and the Animal Welfare Act, the mini-pig study was approved by the animal ethics committee in Stockholm (N209/15). One cornea each of eight Göttingen mini-pigs was subjected to an alkali burn, while the contralateral untreated corneas served as controls. Alkali burns caused swelling of the ocular surface and lids, tearing for two weeks, squinting for up to one month, and corneal opacity (Fig. 3a,b, 4a). At 15 weeks post-burn, inflammation had resolved but the corneal haze remained (Fig. 3c,d, 4a, Supplementary Table 2). There were no changes to the pigs' body weights and overall health status due to the burns or implantation of CLP-PEG-MPC and CLP-PEG hydrogels.

All cell-free implants epithelialized by the seven-week post-operative examination when the sutures used to stabilize the implants were removed. Between seven weeks and three-months post-operation, corneal haze increased (Fig. 3e-h, Fig. 4a, Supplementary Table 2) as stromal cells began migrating into the implants as visualized by *in vivo* confocal microscopy (IVCM). The Cochet-Bonnet aesthesiometer measures the pressure needed to produce a blink

response by progressive shortening of a retractable nylon monofilament. Aesthesiometry showed decreased touch sensitivity that was most prominent at the seven-week and three-month follow-ups, correlating to the corneal nerves being damaged during the surgery (Fig. 4b, Supplementary Table 3).

From three to six months post-operation, corneal haze decreased (Fig. 3g-j, 4a, Supplementary Table 2) while touch sensitivity increased as the newly remodelled areas became re-innervated (Fig. 4b, Supplementary Table 3). At nine and twelve months post-operation, corneal haze was reduced to a light haze with a clinical score of 1 (Fig. 3k,l, 4a, Supplementary Table 2) while aesthesiometry showed touch sensitivity equivalent to that in unoperated corneas (Fig. 4b, Supplementary Table 3). IVCM confirmed the presence of a fully regenerated corneal epithelium (Fig. 3m,n), and regenerating sub-basal nerve plexus (Fig. 3p, q) and stroma (Fig. 3s,t) comparable to the controls (Figs. 3o,r,u). The endothelium which was untouched during the surgery, remained intact (Fig. 3v,w) like the control (Fig. 3x).

The CLP-PEG-MPC implanted corneas maintained a thickness of 745 $\pm$ 83 μm (mean $\pm$ SEM) at three months post-op to 773 $\pm$ 60 μm at 12 months post-operation, comparable to that of unoperated contralateral corneas which were 789 $\pm$ 18 at three months and 801 $\pm$ 16 at 12 months (Fig. 4c, Supplementary Table 4). CLP-PEG only implanted corneas, however, showed a significant thickness increase of approximately 200 μm that was most pronounced at three months post-operation, persisting and remaining significant compared to the unoperated control ($p = 0.0365$) at 12 months post-operation.

Schirmer's tear test showed that the alkali burn decreased tear production (Fig. 4d, Supplementary Table 5). However, tear production recovered and remained within normal values thereafter. Intraocular pressure was unaffected by the burn or hydrogel implantation, remaining within normal ranges of 8 to 20 mmHg over the entire study (Fig. 4e, Supplementary Table 6).

Implants were also grafted into the corneal stroma of a cat after ethical permission from the Maisonneuve-Rosemont Hospital Committee for Animal Protection and in accordance to the Association for Research in Vision and Ophthalmology Statement for the Use of Animals in Ophthalmic and Vision (Supplementary Note 1). The implants were grafted

using limbal incisions at a depth of 350 μm (centre of the stroma). Unlike the mini-pigs, the cat cornea was healthy and the implants served as inlays of 4 mm in diameter and 200 μm thickness. In the absence of alkali burns, both CLP-PEG-MPC and CLP-PEG implants remained optically transparent over the 14-month follow-up period (Supplementary Figs. 1,2). Optical coherence tomography (OCT) showed the presence of clear implants at 14 months post-operation (Supplementary Fig. 3). The edges of the implants showed haziness on both OCT and slit-lamp imaging, which could be edge artefacts or cells that have migrated to the implants.

Histopathology of implanted mini-pig corneas

Histopathology on the mini-pig eyes was performed by a certified, 3rd party veterinary pathologist (vivo Science GmbH, Gronau, Germany). The alkali burned corneal samples excised during implantation showed morphologically detectable corneal tissue damage characterized by focal epithelial erosion, multi-focal epithelial hyperplasia, and stromal hypercellularity together with dissociation and irregularity of the collagen fibres. The pathology observed was in accordance with established descriptions of post-burn healing.[40]

At 12-months post-grafting, both regenerated CLP-PEG and CLP-PEG-MPC implanted corneas resembled healthy unoperated corneas (Fig. 5a-c, Fig. 6a). Although hyperplasia was more noticeable in CLP-PEG regenerated corneas than CLP-PEG-MPC, there were no significant difference (p=0.981, Supplementary Table 7). There was no difference in neovascularization either (p=1.000). Descemet's membrane, which delineates the stroma from the underlying endothelium was intact, showing that neither the burns nor implants extended through to the endothelial compartment.

Immunohistochemistry on regenerated mini-pig neo-corneas

Immunohistochemistry showed the regeneration of a tear film (Fig. 5d-f), terminally differentiated corneal epithelium (Fig. 5g-i), and cornea-specific collagen V in the stroma (Fig. 5j-l). Immunohistochemical staining for α-smooth muscle actin and CD31 as markers of blood vessels, lymphatic vessel endothelial hyaluronan receptor 1 (LYVE1) as markers of lymphatic vessels and CD172a as a marker of myeloid cells showed a trend towards higher

expression in CLP-PEG implanted corneas (Fig. 6b, Supplementary Fig. 4, Supplementary Table 8). Expression of cathelicidin peptide, LL37, a host defence peptide showed no marked differences (Supplementary Fig. 5).

Biochemical analyses on regenerated mini-pig neo-corneas

Proteins extracted from regenerated neo-corneas contained significant levels of type I and type V collagens, the main corneal collagens (Fig 6c). These results suggest that host cells had synthesized a collagenous matrix enriched in the same collagen types as are found in the normal cornea. Overall, there were differences in the amounts of individual α chains, β-dimers and γ trimers of collagen between CLP-PEG-MPC and CLP-PEG only implants. CLP-PEG-MPC has equivalent amounts of covalently crosslinked high molecular weight collagen to unoperated corneas, but showed decreased amounts of individual α chains, β-dimers and γ trimers compared to the CLP-PEG and unoperated groups. CLP-PEG implants had significantly less cornea-specific type V (α1(V)) collagen than CLP-PEG-MPC or untreated corneas (Fig. 6c, Supplementary Table 9).

Electron microscopy on regenerated mini-pig neo-corneas

Serial block-face scanning electron microscopy (SBF-SEM) (Fig. 7a-f) and transmission electron microscopy (Fig. 7g-i) showed that both neo-corneas resembled naïve corneas, except that the basal aspect of their basal epithelial cells showed numerous invaginations. SBF-SEM also revealed a more regular lamellar keratocyte arrangement in CLP-PEG-MPC neo-corneas (Fig. 7a,d) resembling that of the healthy, unoperated controls (Fig. 7c,f). However, the CLP-PEG neo-corneas had more unevenly spaced stromal keratocytes with fewer cell layers (Fig. 7b,e), suggesting a still-evolving morphology.

Extracellular Vesicles and Exosomes

Intense staining for Tsg101-positive extracellular vesicles (EVs) was seen in CLP-PEG neo-corneas (Fig. 8b) compared to unoperated controls (Fig. 8c). Colocalization of Tsg101 and the exosomal surface marker CD9, showed that many of the EVs were exosomes (Fig. 8e). The CLP-PEG-MPC implants showed a slightly higher amount of both EVs (Fig. 8a) and exosomes (Fig. 8d) compared to the unoperated control corneas (Fig. 8c, f). TEM of

the corneal basement membrane showed the presence of exosomes in both grafted materials (Fig. 8g, h, j, k) but observably more copious amounts in the CLP-PEG neo-corneas.

Discussion

Our aim was to develop a full-synthetic peptide-based corneal implant with inflammation suppressing properties. We showed that CLP-PEG-MPC implants, like previously described CLP-PEG ones, were readily and reliably mouldable.[29] Both implants had refractive indices of 1.34, in keeping with their high water content. However, while both implants were highly transparent in visible light, CLP-PEG-MPC but not CLP-PEG implants filtered up to 60% of potentially damaging UV-A, which is essential for lens and retina protection (from cataract and macular degeneration). CLP-PEG hydrogels were stiffer and less elastic than those containing MPC. Interestingly, a similar trend was previously observed upon incorporation of MPC within RHCIII implants.[39] Although the CLP-PEG-MPC implants had lower overall tensile strength, their elasticity made them sufficiently robust for surgical handling and implantation with overlying sutures. Neither hydrogel was as tough as the human cornea, but they had properties close to those of RHCIII corneal implants successfully tested in a clinical trial for over four years.[18,19] Here, as in Fagerholm *et al.*,[19] the original implant was remodelled during corneal regeneration. Furthermore, Jangamreddy *et al.*[29] showed that the weaker, cell-free CLP-PEG hydrogels implanted into rabbit corneas transformed into regenerated neo-corneas with mechanical properties approximating those of healthy, unoperated corneas, the desired end-points. Here, the objective was to synthesize a decreased-cost, peptide-based implant with the immunosuppressive qualities of MPC.

Both hydrogels supported HCEC proliferation *in vitro*, with the slower initial growth on the MPC-containing gels attributed to the non-adherent “slippery" nature of phosphorylcholine-derived hydrogel surfaces.[34,35] When evaluating the effect of crosslinking agents on the activation of dendritic cells, EDC-NHS was cytotoxic and killed the cells at levels where DMTMM yielded live cells with minimal activation compared to positive LPS controls. These observations correlate with Samarawickrama *et al.* (2018)[31], who showed that 0.5% (w/v) EDC-NHS was more toxic than 1% (w/v) DMTMM. The components and prepared CLP-PEG and CLP-PEG-MPC hydrogels had significantly lower capacity to

activate dendritic cells compared to LPS. Hence, the hydrogels would be well-tolerated as implants.

The alkali burn cornea model is a well-established ophthalmology model of severe pathology in rodents and rabbits, resulting in marked inflammation and often neovascularization. In a study by Rehany and Waissman, 20 rabbits with alkali burns required intramuscular injections of 25 mg/kg cyclosporin A daily for 30 days post-operation to allow allograft tolerance.[36] Rabbits that did not receive an intensive steroid regimen uniformly rejected the allografts following severe vascularization. Here, we adapted the alkali burn model to Gottingen mini-pig corneas. A certified veterinary pathologist confirmed the resulting burn pathology of stromal disruption and hypercellularity in the excised scarred corneal tissue.[33]

Both CLP-PEG-MPC and CLP-PEG implants showed healing and regeneration over the 12-month post-operation period, in the absence of steroids or immunosuppressive drugs. The presence of terminally differentiated epithelial cells, regenerated tear film and host-defence peptide, LL37, showed that both hydrogels promoted functional epithelial regeneration. However, CLP-PEG-MPC implants had significantly reduced corneal epithelial hyperplasia and stromal thickening, supporting the contention that MPC suppresses corneal inflammation. While not apparent in H&E histopathology sections, immunohistochemistry revealed that CLP-PEG-MPC implanted corneas also showed a trend towards reduced blood and lymphatic vessels and fewer myeloid cells in the graft site. The phosphorylcholine network appeared to decrease corneal haze and improve the rate of nerve regeneration to restore the corneal blink response. Unfortunately, although CLP-PEG-MPC showed a trend towards improved performance, the small number of pigs in each experimental group used due to cost constraints of performing a certified GLP study in a large animal model, did not allow sufficient power to discriminate and show statistical significance.

CLP-PEG-MPC corneas expressed lower amounts of monomeric (α), dimeric (β), and trimeric (γ) collagen than CLP-PEG implanted ones, although they expressed similar amounts of crosslinked collagen fibrils (HMW) to unoperated controls. More interestingly, the CLP-PEG-MPC implanted corneas had higher amounts of type V collagen, which is a collagen that is present in the corneas in enhanced amounts and shown to be involved in the maintenance of corneal transparency.[37] CLP-PEG-MPC implants also had a lower amount of

EVs and exosomes than CLP-PEG implanted corneas. CLP-PEG has previously been shown to stimulate regenerating corneal cells to produce large amounts of cornea-specific type V collagen associated exosomes.[29] Taken together, these results strongly suggest that regenerated CLP-PEG-MPC neo-corneas were at a more advanced stage of corneal regeneration than the CLP-PEG ones, with more type V collagen in its extracellular matrix, possibly due to the modulation of inflammation in the former.

The CLP-PEG biomaterial in the alkali burned corneas resulted in low-grade haze throughout the 12-month follow-up period with blood vessels in three of four pigs. Incorporation of MPC decreased the haze in the regenerated neo-tissues but they did not reach full optical clarity. There were also residual traces of neovascularisation. However, when CLP-PEG-MPC and CLP-PEG hydrogels were implanted within the stroma of a healthy, non-burned cat cornea, both implants remained optically transparent over 14 months. Both hydrogels performed equivalently as low-risk implants, with the presence of MPC only noticeable under high-risk grafting conditions.

The CLP-PEG-MPC implants were therefore able to restore the alkali burned corneal environment to one that resembled an uninflamed state, allowing regeneration of corneal epithelium, stroma and nerves. The presence of MPC circumvented the increased thickness seen in the non-MPC-containing implants. These results coupled with previous observations of MPC incorporated into full-length recombinant human collagen as hydrogels implants decreased neovascularization in rabbits[38] and allowed stable regeneration in a clinical trial of six high-risk patients with active ulcers and scarring[21], show that MPC is an effective inflammation suppressing polymer that also imparts elasticity to the overall hydrogel. These results confirm the decreased neovascularization observed in rabbits[38] and the stable regeneration of six high-risk patients with active ulcers and scarring in a clinical trial using full-length RHCIII-MPC implants.[21] Combined, these studies show that MPC is an effective inflammation suppressing polymer that also imparts elasticity to the overall hydrogel. The novelty of the present study is that CLP-PEG-MPC implants combine inflammation suppression with a fully synthetic collagen analog comprising CLP and PEG. The short, synthetically produced CLPs are readily manufactured without the need for co-expression of

several full-length proteins needed to produce recombinant human collagen and avoids possible xenogeneic-origin allergy[39] or zoonotic transmission of pathogens such as viruses that may result from animal-derived materials.[40] Furthermore, the use of synthetic analogs allows for future modification and customization of implants for personalized medicine, which is difficult with more chemically inert full-length collagens. The results indicate that evaluation of CLP-PEG-MPC implants in a clinical trial is merited.

Outlook

With a formidable 12.7 million patients on waiting lists worldwide for corneal transplantation and a severe shortage of human donor corneas, CLP-PEG-MPC implants may in the near future be an alternative treatment and further address the unmet need of patients with inflammation and severe conditions who are not amenable to standard donor corneal tissue transplantation.

Methods

Fabrication

Collagen-like peptide ($CG(PKG)_4(POG)_4(DOG)_4$) (AmbioPharm, SC, USA) was conjugated to an 8-arm poly(ethylene glycol) with a hexaglycerol core (Sinopeg Biotech Co. Ltd., Beijing, China).[28] In brief, CLP was conjugated to PEG at pH 4.5, sterile filtered and dialyzed using a 12-14 kDa membrane to remove unreacted CLP. The product was lyophilized and re-dissolved at 12% (w/w). CLP-PEG hydrogels were produced using 4-(4,6-dimethoxy-1,3,5-triazin-2-yl)-4-methylmorpholinium chloride (DMTMM) at molar ratio of 1:2 CLP-PEG:DMTMM. CLP-PEG-PC implants were manufactured using an additional phosphorylcholine network based on the interpenetrating network from our previous recombinant human collagen type III-phosphorylcholine implants.[21] The phosphorylcholine network is composed of 2-methacryloyloxyethyl phosphorylcholine (MPC) (Paramount Fine Chemicals, Beijing, China) and polyethylene glycol diacrylate (PEGDA) (Sigma-Aldrich, St. Louis, MO) The ratio of CLP-PEG:MPC was 2:1 (w/w) and MPC:PEGDA was 3:1 (w/w). Ammonium persulfate and N,N,N',N'-tetramethylethylenediamine (Sigma-Aldrich, St. Louis, MO) were both used as polymerization initiators at a ratio of MPC:APS of 1:0.03

and APS:TEMED of 1:0.77 (Supplementary Table 1). Corneal implants were cast as 10 mm dimeter, 500 μm thick curved hydrogel molds (custom manufactured by Formteknik, Anderstorp, Sweden). Dogbone shaped hydrogels of the same thickness were used for physical, mechanical and *in vitro* testing. The CLP-PEG-MPC and CLP-PEG hydrogel implants used in the *in vivo* mini-pig study and supplemental cat study were custom manufactured by UAB Ferentis (Vilnius, Lithuania) and stored in PBS containing 1% chloroform.

NMR Spectroscopy

Incorporation of MPC into the CLP-PEG-MPC hydrogels was assessed with ^{13}C and ^{31}P Cross Polarization Magic-Angle Spinning (CPMAS) nuclear magnetic resonance (NMR) spectroscopy on a Bruker AVANCE 400 MHz spectrometer at room temperature. CLP-PEG only hydrogels served as negative controls. ^{13}C NMR produced convoluted spectra in the region between 55 and 70 ppm that made it difficult to interpret, but ^{31}P NMR gave definitive peaks. Peak analysis was performed using Mnova (Mestrelab Research, Santiago de Compostela, Spain).

Young's Modulus and Mechanical Strength

Dogbone-shaped hydrogels (500 μm thick) were evaluated using an Instron electromechanical universal tester (Model 3342, Instron, Norwood, MA) equipped with Series IX/S software. The hydrogels were washed in 1X PBS for 1 hour before testing and blotted to remove excess water. The elongation tests were performed using a crosshead speed of 10 mm min^{-1}.

Rheology

Circular hydrogels, 8 mm in diameter and 500 μm thick, were tested using a Discovery Hybrid-2 rheometer (TA Instruments, New Castle, DE, USA) fitted with an 8 mm circular geometry. After blotting to remove excess water, the hydrogels were compressed to an approximate pressure of 1 N of axial force. An amplitude sweep was run from 0.1 to 500% using an angular frequency of 10 rad/s. Analysis was conducted using Trios v5.1.1.46572 (TA Instruments, New Castle, DE, USA).

Light Transmission of Hydrogels

Flat hydrogel sheets of 500 μm thickness and 5 mm x 10 mm dimensions were evaluated for light transmission between 250 nm and 800 nm. Each hydrogel was placed on the inside wall of a quartz cuvette filled with PBS. The absorption was read using a Spectramax M2e series plate/cuvette spectrophotometer (Molecular Devices, San Jose, CA, USA). A cuvette filled with PBS was used as the baseline reference. The percent transmission was calculated from the measured absorbances.

Refractive Index

The refractive index of the hydrogels was measured at RT on an Abbemat 300 (Anton Parr) refractometer.

Water content of hydrogels

A baseline measurement of a blotted hydrogel was obtained as the starting "wet weight" (W_0) of the hydrogel. The hydrogels were then dried until a stable "dry weight" (W) was obtained. The percent water content of the hydrogels (W_t) was calculated according to the equation: W_t % = (W - W_0) / W %.

Collagenase Degradation

Samples were equilibrated in Tris-HCl buffer (0.1 M, pH 7.4) overnight. Hydrogels were then incubated in 5 mL 5 U/mL type I bacterial collagenase dissolved in Tris-HCl at 37°C. The undigested mass was weighed at time 0 (W'_0) and every 8 hours (W'_t) for 2 days (48 hours). At every interval, surface water was blotted away, and samples were weighed using an ultra-microbalance (SE2, Sartorius, Göttingen, Germany). At every weighing occasion, the collagenase solution was replaced with a fresh collagenase mixture. The percentage of mass remaining after digestion was calculated according following equation: Residual mass (%) = (W'_t/W'_0) x 100%.

Permeability

Permeability studies were conducted for two concentrations of CLP-PEG hydrogels (12% and 8%) and one concentration of CLP-PEG-MPC hydrogel (9%).[41] Hydrogels or human amniotic membrane (hAM) were clamped in an Ussing Chamber system (Physiologic instruments, San Diego, CA) with P2300 EasyMount Diffusion Chambers and P2307 sliders. A 700 Da Alexa Fluor® 568 hydrazide sodium salt (10 μM) was placed in aqueous solution in the donor chamber and PBS was placed in the recipient chamber. Samples were drawn at multiple time points and fluorescence was quantified using a at 590 nm excitation wavelength and a 642 nm emission wavelength by a Wallac Viktor2 1420 Multilabel counter (PerkinElmer, Waltham, MA, USA). The apparent permeability coefficient (P_{app}, cm s^{-1}) was calculated using the equation $P_{app} = (dC/dt)/(60C_0A)$ [dC/dt is the slope, C_0 the initial concentration of the donor chamber and A the exposed surface area of the sample in the slider (0.031 cm^2)]. Cumulative permeability was calculated as the percentage of diffused fluorescent marker from the donor chamber to the receiving chamber during the experiment.

Human Corneal Epithelial Cell Culture

A stable GFP-HCEC cell line was established by the transfection of SV40 immortalized HCEC cells (Gift of H Handa, Division of Ophthalmology, Kinki Central Hospital, Hyogo, Japan) with a vector containing a puromycin-resistant gene together with GFP, using the Lipofectamine 2000 Transfection Reagent (Life Technologies, California, USA).[42,43] Selection of puromycin-resistant cells with 2 μg ml^{-1} of puromycin added to the medium was performed to obtain stable GFP-expressing lines. The initial immortalized HCEC line was characterized using the expression of keratin and large T antigen.[42] GFP-HCECs were subsequently characterized by morphology, and expression of Integrin β1 and focal adhesion kinase cell proliferation rate.[43] These cells were not checked for mycoplasma contamination.

To conduct proliferation studies, CLP-PEG and CLP-PEG-MPC hydrogels were punched using a 5mm biopsy punch and placed in a 96 well plate. GFP-HCECs were seeded into the control wells and onto the materials at a density of 5,000 cells/well. GFP-HCECs were supplemented with keratinocyte serum-free medium (KSFM; Gibco, ThermoFisher, Waltham, MA, USA) containing 0.05 mg/mL bovine pituitary extract, 5 ng/mL epidermal growth factor, and 1 mg/mL penicillin/streptomycin and their growth monitored for 7 days in a

humidified incubator at 37°C and 5% CO_2. Growth was assessed by photographing the cultured cells and examining the % coverage of the culture dishes.

For the Alamar Blue and live dead studies, the hydrogels were cut into 6-mm-diameter and overnight immersed in the cell culture media. 5,000 HCECs were seeded on top of each hydrogel for culturing with keratinocyte serum free medium (KSFM) supplemented with 50 μg/ml bovine pituitary extract and 5 ng/ml epidermal growth factor (EGF) (Gibco, California, USA) in a 37°C and 5% CO_2 incubator. Media was changed every alternative day. Cells seeded on tissue culture plate (TCP) were used as control. The Alamar Blue study was performed at day 1, day 4 and day 6 after cell seeding.[44] At each time point, resazurin sodium salt were added to the cell culture wells to obtain the final concentration of 0.004% (w/ v) and incubated for 3 hours. Afterwards, the media was transferred to a new 96 well plate and read on a BioTek plate reader (Synergy 2, BioTek Instruments; Winooski, VT) at 530/25 nm for excitation and 590/35 nm for emission. At day 6, live/dead staining was performed with a staining kit (Life Technologies Corporation, Oregon, USA), where cells were double-stained by calcein acetoxymethyl (Calcein AM) and ethidium homodimer-1 (EthD-1). Images were taken by using a fluorescence microscope (Zeiss Axio Observer Z1, Carl Zeiss Microimaging GmbH, Jena, Germany).

Bone Marrow-Derived Dendritic Cell (BMDC) Activation Assay

Bone marrow was isolated from the femur and tibia of 6 to 12-week-old, male C57BL/6J mice (*Mus musculus*). Cells ($1x10^6$/well) were seeded onto 6-well suspension culture plates in RPMI 1640 containing 10% (v/v) fetal bovine serum (Wisent, Saint-Jean-Baptiste, QC), 0.5 mg/mL penicillin-streptomycin-glutamine, 10 mM HEPES, 1 mM sodium pyruvate, 55 μm β-mercaptoethanol and 2.5 ng/mL granulocyte-macrophage colony-stimulating factor (GM-CSF) (Gibco, Waltham, MA). Complete RPMI, containing 5.0 ng/mL GM-CSF, was exchanged for half of the media on days two and three of culture. Cultures were maintained for six days, then collected and subject to density gradient centrifugation using Histodenz™ (Sigma-Aldrich, St. Louis, MO) to separate the enlarged BMDCs. The selected cells were seeded at a density of $1x10^6$ cells/well on a 24 well plate for materials testing.

Hydrogel components (EDC/NHS, DMTMM, CLP, CLP-PEG, and MPC) were applied to the BMDCs at an equivalent total mass to a 10 mm, 500 μm thick hydrogel disk, to simulate the total amount present in a complete corneal implant. Hydrogels disks (6 mm diameter, 500 μm thick) were incubated with BMDCs for 24 hours. Lipopolysaccharide (LPS) was used as a positive control. BMDCs were collected and labelled with direct-conjugate antibodies for CD11c, CD40, CD80 and CD86 (Supplementary Table 10) and Zombie Aqua™ Fixable Viability Kit (BioLegend, San Diego, CA). Flow cytometry was performed using a BD LSR II and analyzed using FlowJo software (Becton, Dickinson & Company). The cells were gated for size and granularity using a FSC/SSC gate (Supplementary Fig. 6a), followed by a gate to remove dead cells, based on low Zombie-Aqua (Fig. S6b). The live cells were gated for CD11c high, autofluorescence low (Supplementary Fig. 6c) and this is the gate that was subject to subsequent analysis. Mature dendritic cells composed 50-99% of the live gate, as there was significant cell death in BMDCs exposed to the toxic crosslinker EDC-NHS.

In Vivo Study in Göttingen Mini-Pigs

A study to evaluate the safety and biocompatibility of CLP-PEG-MPC and CLP-PEG implants in mini-pigs was performed in compliance with the Swedish Animal Welfare Ordinance and the Animal Welfare Act, with ethical permission from the local ethical committee in Stockholm (N209/15), and in accordance with OECD Principles of Good Laboratory Practices (GLP), ENV/MC/CHEM (98) 17, 1997, by Adlego Biomedical AB (Stockholm, Sweden). All animals were examined prior to alkali burn, and after alkali burn prior to surgical implantation of CLP-PEG or CLP-PEG-MPC hydrogels. The pig samples size is based on the standard amount for safety and toxicology testing (n=4 per group). The pigs were randomly allocated to the two biomaterials groups by the veterinary team at Adlego AB (Solna, Sweden). The corneal surgeons were blinded as to which of the CLP-PEG or CLP-PEG-MPC implants were implanted in each pig cornea. No data was excluded from this study and this study has not been replicated. The full GLP study report by Adlego AB is available on Figshare.[45]

Eight female Göttingen mini-pigs (*Sus scrofa domesticus*) were placed under general anesthesia and pre-treated with tetracaine 1% eye drops (Chauvin Pharmaceuticals Ltd,

UK). Alkali burns were created in the right corneas of each pig. A 5 mm, circular piece of filter paper soaked in 1M NaOH was placed on the right cornea of each animal for 60 seconds, followed by a thorough rinse in 0.9% saline, by flooding the treated cornea to remove excess NaOH. Buprenorphine (0.05 mg/kg, Vetergesic, Orion Parma, Finland) was administered at the end of the procedure and when signs of pain and discomfort were observed during recovery. The injured eyes received chloramphenicol eye drops (5 mg/mL, Santen), twice daily for eight days post-procedure. The alkali burns were evaluated by slit lamp under sedation, six weeks after the procedure. A full clinical exam was performed at 13 weeks, immediately prior to surgery.

Each alkali burned cornea underwent an anterior lamellar keratoplasty (ALK) procedure to replace the anterior 2/3s of each scarred cornea. Under general anesthesia, each alkali burned cornea (average thickness 750 μm) was trephined to a depth of 500 μm using a 6.5 mm diameter Barron Hessberg trephine. A corneal diamond knife was used to complete the lamellar dissection. A 500 μm thick CLP-PEG-MPC or CLP-PEG only implant, purchased from UAB Ferentis (Vilnius, LT) was trephined to a diameter of 6.75 mm, placed in the wound bed and sutured in place using 10-0 nylon (MANI Ophthalmic). Six interrupted sutures were used to retain the implants where possible; otherwise overlying mattress sutures were used. Each operated eye received a single dose of 3 mg/mL dexamethasone and 1 mg/mL tobramycin eye drops (Tobrasone, Alcon, Sweden) at the end of surgery.

After surgery, the animals were examined daily for 10 days and then weekly. The operated eye received one drop of Tobrasone three times daily for five weeks. Suture removal was performed under general anesthesia at postoperative 7 weeks. Full eye examinations under general anesthesia were performed at 7 weeks as well as 3, 6, 9 and 12 months post-operation. Restrained, fully conscious pigs were assessed for central corneal touch sensitivity in using a Cochet-Bonnet aesthesiometer (Handaya Co, Tokyo, Japan). After topical anesthesia and confirmation of the extinction of the corneal blink response, the eyes were also tested for tear production using Schirmer's tear test (TearFlo, Hub Pharmaceuticals USA), under sedation and prior to general anaesthesia. For the remaining examinations, animals were examined under general anaesthesia. Examinations include measurements of intraocular pressure (TonoVet Tonometer, Icare Finland Oy, Finland), and pachymetry (Handy

Pachymeter SP-100, Tomey, AZ, USA). A full slit lamp evaluation (Kowa SL-15 Portable Slot Lamp, Kowa Company, Ltd., Aichi, Japan) was conducted in the presence of fluorescein eye drops (Lidocaine-fluorescein 4% + 0.25%, Chauvin Pharmaceuticals Ltd.) using the McDonald-Shadduck scoring system to quantify anterior segment findings. Each eye was scored from 0 to +4 on conjunctiva congestion, swelling and discharge, aqueous flare, iris involvement and percent corneal haze. Full thickness IVCM was performed at peripheral and central portions of the implant and similar positions in the unoperated corneas (Heidelberg HRT3 with Rostock Cornea Module with HEYEX software, Heidelberg, Germany).

The pigs were euthanized at 12 months post-operation with an overdose of pentobarbitol (100 mg/mL, Allfatal Vet, Omnidea, Sweden) and corneas were dissected out with a 2 mm rim of surrounding conjunctiva. The center 2 mm of each cornea was excised with a biopsy punch and snap frozen in isopentane chilled with dry ice for collagen content analysis. The remaining cornea was then quartered for further processing.

Histopathology of Mini-Pig Corneas

One quarter of the cornea was fixed in 4% paraformaldehyde in phosphate buffer for Haematoxylin and Eosin (H&E) staining and histopathological analysis under GLP by a certified veterinary pathologist at *in vivo* Science GmbH (Gronau, Germany). Standard H&E stained research sections were imaged using a Zeiss AxioObserver Z1 inverted light microscope using the tiling function in Zen Blue v2.3 at 20x magnification (Carl Zeiss Microscopy, Göttingen, Germany).

Collagen Analysis of Mini-Pig Central Cornea

Frozen biopsied corneal samples from within the surgical areas of both implanted and control corneas were thawed and re-suspended in 10 mM HCI at a wet weight to volume ratio of 1:35. Pepsin (Roche, catalog# 200911, lot#93100120) was added to a final concentration of 1 mg/ml from a 10 mg/ml stock solution prepared just before use. The samples were digested with pepsin at 2 - 8°C for 96 hours and the soluble fraction was recovered by centrifugation in a microfuge at 16,000 x g for 30 minutes at 2 - 4°C. An aliquot of the pepsin soluble fraction was mixed with NuPAGE 4× LDS sample buffer (Life Technologies)

denatured at 75 °C for 8 minutes and analyzed on 3 - 8 % Tris-acetate gels under non-reducing conditions. Proteins were visualized by staining with Gelcode Blue (Pierce). Prestained broad range marker (New England Biolabs, catalog# P7712) and porcine skin type I collagen (Koken Co. Ltd., Japan) were used as molecular weight standards. To quantitate the amounts of type I and type V collagens in control and operated corneas, densitometric scans of the stained gels were made to obtain relative numerical units using a GE Healthcare Image Quant 350. ANOVA was performed to determine statistical differences using GraphPad Prism 5 on a DELL Latitude E6420 computer using Windows 7 OS.

Immunohistochemistry of Mini-Pig Corneas

One quarter of each cornea was fixed in 4% paraformaldehyde in phosphate buffer containing 5% sucrose. The corneas were processed through a sucrose gradient prior to embedding in OCT. Immunohistochemical staining was conducted using antibodies against cytokeratin, CD172a, smooth muscle actin, LYVE-1, CD31, collagen V (Supplementary Table 11). Corneal sections (7 μm) were fixed in cold 4% PFA followed by ice-cold methanol, air-dried, washed in PBS and then blocked with 5% normal goat serum (NGS) in PBS. All primary antibodies were incubated overnight at 4°C. Slides were washed in PBS with 1% Tween 20 and then incubated with secondary antibodies diluted 1:1000 in blocking solution. After washing the slides were dehydrated and mounted in Vectashield Antifade Mounting Medium with DAPI (Vector Laboratories, Burlingame, CA, USA). Slides stained using lectin were washed in PBS, stained with lectin overnight at 4°C, washed and counterstained with DAPI, before mounting in Vectashield Antifade Mounting Medium. Fluorescent images were obtained with a confocal laser-scanning microscope (LSM800, Carl Zeiss Microscopy, Göttingen, Germany). Immunohistochemical staining of exosomes was conducted using dual staining with CD9 and TSG101, per the ISEV positive staining requirement for one transmembrane protein and one cytosolic protein associated with exosomes.[46] Corneal sections were air dried, washed in PBS, and permeabilized in PBS with 0.3% Triton-X. The sections were washed and incubated in Tris-buffered saline (TBS) containing 50 mM ammonium chloride. The samples were blocked in PBS with 5% NGS and 0.01 g/mL saponin at room temperature prior to incubation in primary antibodies overnight. Slides were washed in PBS containing 5% FBS and 0.01 g/mL saponin and incubated in secondary antibodies diluted in blocking at room

temperature. The samples were quenched for autofluorescence using Vector® TrueVIEW™ Autofluorescence Quenching Kit (Vector Laboratories, Burlingame, CA, USA). Slides were stained with DAPI (5 μg/mL) for 10 minutes prior to mounting in Vectashield Antifade Mounting Medium (Vector Laboratories, Burlingame, CA, USA). Fluorescent images were obtained with a confocal laser-scanning microscope (LSM880, Carl Zeiss Microscopy, Göttingen, Germany). Images were denoised using Zen Blue v2.3. Three-dimensional reconstructions of the slices were generated in Imaris v9.2.1 (Bitplane Inc., Concord, MA, USA). Surfaces were reconstructed for Tsg101 using a manual threshold value of 5. A co-localization channel was constructed for CD9 and Tsg101 and surfaces were reconstructed using a manual threshold value of 1.5. All surfaces used a minimum voxel threshold of 10 and surface grain threshold of 0.141 μm. Immunohistochemistry for LL37 was performed as described above for exosomes. Three-dimensional reconstructions of the slices were generated in Imaris v9.2.1 (Bitplane Inc., Concord, MA, USA). Ten 700 μm^3 regions of interest (ROIs), five in the epithelium and five in the stroma, were generated for each slice. LL37 staining in each ROI was reconstructed as spots with an intensity threshold of 7.57 and a minimum voxel threshold of 10. The number of spots and sum intensity of each ROI was analyzed by the total volume of the ROIs. A one-way Kruskal Wallis test was performed using a Dunn's multiple comparisons test (GraphPad Prism v9.0.2, GraphPad Software, LLC., San Diego, CA, USA).

Electron Microscopy of Mini-Pig Corneas

The mini pig corneal/construct samples were fixed using 2.5% glutaraldehyde/2% paraformaldehyde in 100 mM cacodylate buffer pH 7.2 at room temperature (RT) for 12 hours after dissection and placed in 100 mM cacodylate storage buffer pH 7.2. The samples were processed for TEM and SBF-SEM using a method for the generation of high backscatter electron contrast for serial block face scanning (SBF SEM).[51] After the fixation, the sample quadrants were cut into thin <1 mm slices to preserve the positioning of the implant in relation to host cornea. Each sample slice was transferred to 1.5% potassium ferricyanide/1% osmium tetroxide in cacodylate buffer for 1 hr and then washed in distilled water. The samples were then placed sequentially in 1% aqueous thiocarbohydrazide, 1%

osmium tetroxide and 1% aqueous uranyl acetate, each for 1 hour. All the staining steps were followed by 30 mins distilled water washing steps.

The samples were then incubated for 1 hr in a solution of lead aspartate at 60°C and then washed in two changes of distilled water for 30 mins. They were dehydrated in an ethanol series from 70% through to 100% and, following via propylene oxide infiltration, they were embedded in CY212 (TAAB) epoxy resin and polymerised for 24 hr at 60°C. The surfaces of polymerized resin blocks were then trimmed and attached to Gatan (PEP6590) specimen pins. The pins were gold coated and transferred to a Zeiss Sigma VP FEG SEM equipped with a Gatan 3View2 system, where data sets of up to 1000 images were acquired of the block surface every 100 nm through automated sectioning. Each image was acquired at 4K $\times$ 4K pixels, at a pixel resolution of between 6.5-21 nm and a pixel dwell time of 8 μs, using an SEM accelerating voltage of 3.5 keV in low vacuum variable pressure mode (28-30 Pa). Imaging data was acquired from a 26.5 μm $\times$ 26.5 μm region of interest. Selected serial image sequences were extracted from the image data and 3D reconstructions were generated using Amira 6.1 software (FEI). For TEM ultrathin 90nm sections were taken from the SBF-SEM TEM prepared specimen pins using a Leica UC6 ultramicrotome. TEM sections were collected on TEM 300hex grids and examined on a JEOL 1010 TEM at an accelerating voltage of 80Kv.

Statistics and Reproducibility

The Alamar Blue proliferation assay of HCEC on the hydrogels was analyzed using a two-way ANOVA (n=5 technical replicates (TR) per group). BMDC activation assays was performed using a one-way ANOVA with a Brown-Forsythe test and Tukey's multiple comparisons test with a confidence interval of 95% for each marker (GraphPad Prism 8.4.2, GraphPad Software, LLC., San Diego, CA, USA). The unit of analysis was the mouse (n=6, per group). The unit of analysis for the clinical statistics was the eye. The clinical statistics were conducted on uneven population sizes (CLP-PEG n=4; CLP-PEG-MPC n=4; unoperated n=8). For variables with repeated measures over time, a mixed-effects analysis with Geisser-Greenhouse's correction was performed (α=0.05) with a Tukey multiple comparison test for treatment effects by time point (GraphPad Prism 8.4.2). Post-mortem collagen content analysis was performed using the two-way ANOVA with Tukey's multiple

comparisons test. (α=0.05) (IMB® SPSS® Statistics Version 25, IMB Corp., Armonk, NY, USA). Ordinal data for histopathological assessments of corneal epithelial hyperplasia and neovascularization were analyzed by Mann-Whitney U. Statistical significance was set at $p \leq 0.05$.

All graphs for were prepared using GraphPad Prism. Data is displayed as mean with individual data points or mean ± standard error of the mean.

Data Availability

The quantitative datasets and full GLP mini-pig report generated during the current study are available in the Figshare repository, https://doi.org/10.6084/m9.figshare.14251088.v1. The image datasets generated during the current study are available from the corresponding author on reasonable request.

Acknowledgements

The GLP mini-pig study (AB16-07) was funded by a DBT-Vinnova Indo-Swedish strategic cooperative grant DNR 2013-04645, and conducted by Adlego AB. Funding for dendritic cell studies, data analyses was from CIHR grant 391487 to MG and IB, Fonds de recherche en ophtalmologie de l'Université de Montréal (FROUM) to MG and SL, and a Caroline Durand Foundation Research Chair for Cellular Therapy in the Eye to MG. FCS acknowledges support for her doctoral studies from the Natural Sciences and Engineering Research Council of Canada (NSERC). KMM and PL are funded by Programme Grant MR/S037829/1 from the Medical Research Council. MG-A acknowledges funding from ISCIII (ICI19/00006), co-funded by ERDF/ESF, "A way to make Europe"/"Investing in your future"). MC holds the Tier 1 Canada Research Chair for Biomaterials and Stem Cells in Ophthalmology. We thank Dr. Virender Sangwan, PI on the DBT-Vinnova grant for his tremendous leadership throughout the whole project, Dr. Ayan Samanta, Uppsala University for assistance with the HCEC assays, and Prof. Heli Skottman, Tampere University for assistance with the permeability assays. We also thank Drs. Malcolm Latorre and Elle Edin, Linköping University for assistance with *in vivo* confocal microscopy, Dr. Christopher R. McLaughlin and Marc

Groleau, Université de Montréal respectively for assistance with the mini-pig final examinations and assistance with the LL37 immunostaining and imaging, and Dr. Emilio Alarcon, University of Ottawa Heart Institute for help with NMR.

Author Contributions

MG designed the overall study and drafted the MS together with FCS and CDM, MG and MG-A were responsible for the revised MS. FCS, CDM, MMI, MH did the *in vitro* studies, analyses. FCS, CA, SL designed and performed the dendritic cell analyses. OB, PF and AL performed the surgeries and follow-ups; FS and AL performed immunohistochemistry; PL and KMM performed the electron microscopy; DO performed biochemical analyses; FCS, CDM, MH, MMI, MG-A and LK characterized hydrogels. MCR and MG-A interpreted the surgical findings in the GLP animal study report. FXG and IB performed feline studies in the supplemental material. All authors contributed to writing and revision of the MS and approved the final version for submission.

Competing Interests

MG is a named inventor on PCT patents WO2007/028258 A2 Interpenetrating networks, and related methods and compositions, assigned to the Ottawa Hospital Research Institute and University of Ottawa; PCT/IB2017/056342 Collagen and collagen like peptide-based hydrogels, corneal implants, filler glue and uses thereof, which was assigned to the Hyderabad Eye Research Foundation, and then subsequently assigned to North Grove Investments, Inc. wherein PCT national phase applications have been filed in the USA, EU, India, China, and Canada. CDM and MG are named inventors on a US provisional patent application no. 62916765, subsequent to a disclosure to Univalor, technology transfer agent to Maisonneuve-Rosemont Hospital and Université de Montréal. There are no other competing interests from other co-authors.

References

(1) Mori, D. N., Kreisel, D., Fullerton, J. N., Gilroy, D. W. & Goldstein, D. R. Inflammatory triggers of acute rejection of organ allografts. *Immunol. Rev.* **258**, 132–144 (2014).

(2) Oliva, M. S., Schottman, T. & Gulati, M. Turning the tide of corneal blindness. *Indian J. Ophthalmol.* **60**, 423–427 (2012).

(3) Qazi, Y. & Hamrah, P. Corneal Allograft Rejection: Immunopathogenesis to Therapeutics. *J. Clin. Cell. Immunol.* **2013**, 6 (2013).

(4) Williams, K. A. *et al.* How effective is penetrating corneal transplantation? Factors influencing long-term outcome in multivariate analysis. *Transplantation.* **81**, 896–901 (2006).

(5) Gain, P. *et al.* Global Survey of Corneal Transplantation and Eye Banking. *JAMA Ophthalmol.* **134**, 167–173 (2016).

(6) Yorston, D. & Garg, P. Corneal grafting: What eye care workers need to know. *Community Eye Heal. J.* **22**, 44–45 (2009).

(7) Stacy, R. C., Jakobiec, F. A., Michaud, N. A., Dohlman, C. H. & Colby, K. A. Characterization of retrokeratoprosthetic membranes in the Boston type 1 keratoprosthesis. *Arch. Ophthalmol.* **129**, 310–316 (2011).

(8) Frick, C., Dietz, A. C., Merritt, K., Umbreit, T. H. & Tomazic-Jezic, V. J. Effects of prosthetic materials on the host immune response: Evaluation of polymethylmethacrylate (PMMA), polyethylene (PE), and polystyrene (PS) particles. *J. Long-Term Eff. Med. Implant.* **16**, 423–433 (2006).

(9) Robert, M. C. & Dohlman, C. H. A review of corneal melting after Boston Keratoprosthesis. *Semin. Ophthalmol.* **29**, 349–357 (2014).

(10) Črnej, A. *et al.* Effect of penetrating keratoplasty and keratoprosthesis implantation on the posterior segment of the eye. *Investig. Ophthalmol. Vis. Sci.* **57**, 1643–1648 (2016).

(11) Zhou, G. & Groth, T. Host Responses to Biomaterials and Anti-Inflammatory Design—a Brief Review. *Macromol. Biosci.* **18**, (2018).

(12) Chen, S. *et al.* Characterization of topographical effects on macrophage behavior in a foreign body response model. *Biomaterials.* **31**, 3479–3491 (2010).

(13) Brodbeck, W. *et al.* Influence of Biomaterial Surface Chemistry on the Apoptosis of Adherent Cells. *J. Biomed. Mater. Res.* **55**, (2001).

(14) Brodbeck, W. G. *et al.* Biomaterial surface chemistry dictates adherent monocyte/macrophage cytokine expression *in vitro*. *Cytokine* **18**, 311–319 (2002).

(15) Coster, D. J., Jessup, C. F. & Williams, K. A. Mechanisms of corneal allograft rejection and regional immunosuppression. *Eye* **23**, 1894–1897 (2009).

(16) Di Zazzo, A., Kheirkhah, A., Abud, T. B., Goyal, S. & Dana, R. Management of high-risk corneal transplantation. *Surv. Ophthalmol.* **62**, 816–827 (2017).

(17) Niederkorn, J. Y. High-risk corneal allografts and why they lose their immune privilege. *Curr. Opin. Allergy Clin. Immunol.* **10**, 493–7 (2010).

(18) Fagerholm, P. *et al.* A Biosynthetic Alternative to Human Donor Tissue for Inducing Corneal Regeneration: 24-Month Follow-Up of a Phase 1 Clinical Study. *Sci. Transl. Med.* **2**, 46ra61 (2010).

(19) Fagerholm, P. *et al.* Stable corneal regeneration four years after implantation of a cell-free recombinant human collagen scaffold. *Biomaterials* **35**, 2420–2427 (2014).

(20) Mölzer, C. *et al.* Activation of dendritic cells by crosslinked collagen hydrogels (artificial corneas) varies with their composition. *J Tiss Eng Regen Med* **13**, 1528–1543 (2019).

(21) Islam, M. M. *et al.* Biomaterials-enabled cornea regeneration in patients at high risk for rejection of donor tissue transplantation. *NJP Regen. Med.* **3**, 2 (2018).

(22) Vuorela, A., Myllyharju, J., Nissi, R., Pihlajaniemi, T. & Kivirikko, K. I. Assembly of human prolyl 4-hydroxylase and type III collagen in the yeast Pichia pastoris: formation of a stable enzyme tetramer requires coexpression with collagen and assembly of a stable collagen requires coexpression with prolyl 4-hydroxylase. *EMBO J.* **16**, 6702–12 (1997).

(23) Yang, C. *et al.* Development of a Recombinant Human Collagen-Type III Based Hemostat. J. *Biomed. Mater. Res. - Part B Appl. Biomater.* **69**, 18–24 (2004).

(24) Sewald, N. & Jakubke, H.-D. Peptides: Chemistry and Biology. (Wiley-VCH, 2015).

(25) Collier, J. H. & Segura, T. Evolving the use of peptides as components of biomaterials. *Biomaterials.* **32**, 4198–4204 (2011).

(26) O'Leary, L. E. R., Fallas, J. A., Bakota, E. L., Kang, M. K. & Hartgerink, J. D. Multi-hierarchical self-assembly of a collagen mimetic peptide from triple helix to nanofibre and hydrogel. *Nat. Chem.* **3**, 821–828 (2011).

(27) Kumar, V. A. *et al.* A nanostructured synthetic collagen mimic for hemostasis. *Biomacromolecules.* **15**, 1484–1490 (2014).

(28) Islam, M. M. *et al.* Self-assembled collagen-like-peptide implants as alternatives to human donor corneal transplantation. *RSC Adv.* **6**, 55745–55749 (2016).

(29) Jangamreddy, J. R. *et al.* Short peptide analogs as alternatives to collagen in pro-regenerative corneal implants. *Acta Biomater.* **69**, 120–130 (2018). 30. Delgado, L. *et al.* Collagen cross-linking increases scaffold stability while modulates pro-inflammatory macrophage response. *Front. Bioeng. Biotechnol.* **4**, (2016).

(30) Samarawickrama, C. *et al.* Collagen-Based Fillers as Alternatives to Cyanoacrylate Glue for the Sealing of Large Corneal Perforations. *Cornea.* **37**, 609–616 (2018).

(31) Cho, H. K. *et al.* Preparation and characterization of MRI-active gadolinium nanocomposite particles for neutron capture therapy. *J. Mater. Chem.* **21**, 15486–15493 (2011).

(32) Pahlitzsch, T. & Sinha, P. The alkali burned cornea: electron microscopical, enzyme histochemical, and biochemical observations. *Graefe's Arch. Clin. Exp. Ophthalmol.* **223**, 278–286 (1985).

(33) Ishihara, K., Ishikawa, E., Iwasaki, Y. & Nakabayashi, N. Inhibition of fibroblast cell adhesion on substrate by coating with 2-methacryloyloxyethyl phosphorylcholine polymers. *J. Biomater. Sci. Polym. Ed.* **10**, 1047–1061 (1999).

(34) McRae Page, S. *et al.* Promoting cell adhesion on slippery phosphorylcholine hydrogel surfaces. *J. Mater. Chem. B* **2**, 620–624 (2014).

(35) Rehany, U. & Waisman, M. Suppression of corneal allograft rejection by systemic cyclosporine-A in heavily vascularized rabbit corneas following alkali burns. Cornea. 13, 447–453 (1994).

(36) Sun, M. *et al.* Collagen V is a dominant regulator of collagen fibrillogenesis: Dysfunctional regulation of structure and function in a corneal-stroma-specific Col5a1-null mouse model. J. Cell Sci. 124, 4096–4105 (2011).

(37) Hackett, J. M. *et al.* Biosynthetic Corneal Implants for Replacement of Pathologic Corneal Tissue: Performance in a Controlled Rabbit Alkali Burn Model. Invest. Ophthalmol. Vis. Sci. 52, 651–657 (2011).

(38) Wong, M. L. & Griffiths, L. G. Immunogenicity in xenogeneic scaffold generation: Antigen removal vs. decellularization. Acta Biomaterialia vol. 10 1806–1816 (2014).

(39) Food and Drug Administration, C. for B. E. and R. Source Animal, Product, Preclinical, and Clinical Issues Concerning the Use of Xenotransplantation Products in Humans; Guidance for Industry. http://www.fda.gov/BiologicsBloodVaccines/GuidanceComplianceRegulatoryInformation/Guidances/default.htm. (2003).

(40) Haagdorens, M. *et al.* In vitro cultivation of limbal epithelial stem cells on surface-modified crosslinked collagen scaffolds. Stem Cells Int. 2019, (2019).

(41) Araki-Sasaki, K. *et al.* An SV40-immortalized human corneal epithelial cell line and its characterization. Invest. Ophthalmol. Vis. Sci. 36, 614–621 (1995).

(42) Islam, M. M. *et al.* Functional fabrication of recombinant human collagen-phosphorylcholine hydrogels for regenerative medicine applications. *Acta Biomater.* **12**, 70–80 (2015).

(43) Islam, M. M. *et al.* Effects of gamma radiation sterilization on the structural and biological properties of decellularized corneal xenografts. *Acta Biomater.* **96**, 330–344 (2019).

(44) Simpson, F. C. *et al.* Collagen analogs with phosphorylcholine serve as inflammation-suppressing scaffolds for corneal regeneration from burns in mini-pigs : Raw Data. figshare, Dataset (2021) https://doi.org/10.6084/m9.figshare.14251088.v1

(45) Deerinck, T. *et al.* Enhancing Serial Block-Face Scanning Electron Microscopy to Enable High Resolution 3-D Nanohistology of Cells and Tissues. *Microsc. Microanal.* **16**, 1138–1139 (2010).

(46) Zeng, Y., Yang, J., Huang, K., Lee, Z. & Lee, X. A comparison of biomechanical properties between human and porcine cornea. *J. Biomech.* **34**, 533–537 (2001).

(47) Crabb, R. A. B., Chau, E. P., Evans, M. C., Barocas, V. H. & Hubel, A. Biomechanical and microstructural characteristics of a collagen film-based corneal stroma equivalent. *Tissue Eng.* **12**, 1565–1575 (2006).

(48) Jue, B. & Maurice, D. M. The mechanical properties of the rabbit and human cornea. *J. Biomech.* **19**, 847–853 (1986).

(49) Doutch, J., Quantock, A. J., Smith, V. A. & Meek, K. M. Light transmission in the human cornea as a function of position across the ocular surface: Theoretical and experimental aspects. *Biophys. J.* **95**, 5092–5099 (2008).

(50) Liu, W. *et al.* Collagen-phosphorylcholine interpenetrating network hydrogels as corneal substitutes. *Biomaterials.* **30**, 1551–1559 (2009).

(51) Patel, S. & Tutchenko, L. The refractive index of the human cornea: A review. *Contact Lens Anterior Eye.* **42**, 575–580 (2019).

(52) Maurice, D. M. IV. Limiting Layers. in The Eye (ed. Davson, H.) 525 (Elsevier Science, 1984).

Figure Legends

Figure 1. Chemical and optical analyses of CLP-PEG-MPC and CLP-PEG hydrogels. (a) Fourier transformed infra-red spectroscopy shows the incorporation of the CLP-PEG monomer (lavender line) into the CLP-PEG hydrogel (black line) the CLP-PEG monomer and MPC monomer (purple line) into the CLP-PEG-MPC hydrogel (pink line). (b) ^{31}P NMR spectroscopy with peaks that show the incorporation of phosphorylcholine (purple line) into CLP-PEG-MPC hydrogels (pink line) (n=1, per group). (c) Both CLP-PEG (black line) and CLP-PEG-MPC (pink line) hydrogels transmit the full spectrum of visible light, but CLP-PEG-MPC blocks short UV wavelengths (n=1, per group). (d-e) Apparent and cumulative permeability of 700 Da Alexa Fluor® 568 hydrazide sodium salt through CLP-PEG-MPC hydrogels (pink squares, n=4 technical replicates (TR)) in comparison to 12 and 8% CLP-PEG (black circles, n=4; light blue triangles, n=3 TR, respectively) hydrogels and hAM (grey inverted triangles, n=3 TR). (f) Both CLP-PEG-MPC (pink squares) and CLP-PEG hydrogels (black circles) remained stable and minimally degraded when exposed to collagenase enzyme (n=3 TR per group).

Figure 2. *In vitro* analyses of CLP-PEG-MPC and CLP-PEG hydrogels. (a-f) GFP-tagged human corneal epithelial cells proliferated on both CLP-PEG-MPC and CLP-PEG hydrogels over seven days (n=4 per group). White scale bars, 1 mm. (g-i) Live/dead pictures of human corneal epithelial cells proliferated on both CLP-PEG-MPC and CLP-PEG hydrogels over six days (green represents live cells and red represents dead cells) (n=5 per group). Red scale bars, 200 μm. (j) Alamar Blue proliferation study of human corneal epithelial cells proliferated on CLP-PEG-MPC hydrogels (pink squares), CLP-PEG hydrogels (black circles) and tissue culture plate controls (aqua triangles) at different time points (n=5 TR per group). Analysis by one-way ANOVA with Tukey's multiple comparisons test within each time point. (k) Culture of BMDCs on monomeric hydrogel components and crosslinkers showed no activation as determined by the significantly lower expression of co-stimulatory receptors CD40-APC (blue squares), CD80-PE (orange triangles) and CD86-FITC (yellow inverted triangles) compared to lipopolysaccharide (LPS) stimulation, a positive control for dendritic cell activation. Analysis by one-way ANOVA with Dunnett's multiple comparisons test (n=6 biological replicates (BR) per group). *LPS vs component, $p<0.0001$, †CLP-PEG

vs component, $p<0.05$. (l) CLP-PEG-MPC and CLP-PEG hydrogels do not upregulate CD40-APC (blue squares), CD80-PE (orange triangles) or CD86-FITC (yellow inverted triangles). One-way ANOVA with Tukey's multiple comparisons test. *LPS vs hydrogel, $p<0.0001$.

Figure 3. CLP-PEG-MPC implants in alkali burned mini-pig corneas compared to CLP-PEG only implants. (a-l) Surgical progression of CLP-PEG-MPC hydrogels compared to CLP-PEG hydrogels implanted in mini-pig corneas following alkali burns. Corneal haze was seen immediately after the alkali burn to the central cornea (a-b) and is still present just before surgery (c-d). After surgery, haze is present up to 6 months (e-j) and is decreased by 12 months post-operation (k-l). (m-u) In vivo confocal microscopy of the regenerated CLP-PEG-MPC and CLP-PEG neo-corneas at 12 months post-operation in comparison to unoperated corneas, showing regeneration of corneal epithelium, subepithelial nerves (arrowheads) and stroma. The unoperated endothelium (v-x) remains intact. White scale bars, 100 μm.

Figure 4. Clinical follow-up of regenerating neo-corneas after CLP-PEG and CLP-PEG-MPC implantation into post-alkali burned mini-pig corneas. (a) Corneal haze increased in response to alkali burn and surgery in CLP-PEG (black circles) and CLP-PEG-MPC (pink squares) but diminished over the 12-month follow-up period. (b) Corneal blink response measured by Cochet-Bonnet aesthesiometry showing immediate decrease post-surgery in CLP-PEG-MPC (pink squares) and CLP-PEG (black circles) with recovery to pre-operative levels by twelve months. Unoperated eyes (aqua triangles) do not show changes in the blink response. (c) CLP-PEG-MPC (pink squares) grafts resulted in a corneal thickness comparable to the unoperated eye (aqua triangles), but CLP-PEG (black circles) resulted in significant increases in corneal thickness. (d) Schirmer's tear tests showing a decrease in tear production immediately post-burn due to trauma, followed by a normal tear production in CLP-PEG-MPC (pink squares) and CLP-PEG (black circles) compared to unoperated controls (aqua triangles). (e) Intraocular pressure was maintained within normal parameters CLP-PEG-MPC (pink squares), CLP-PEG (black circles) and unoperated (aqua triangles) corneas throughout all stages of follow-up. Data displayed as mean $\pm$ SEM. Statistical analyses by two-way repeat measures ANOVA with Geisser's Greenhouse correction and a

Tukey's or Sidak multiple comparison test. *Unoperated vs CLP-PEG, $p<0.05$. †Unoperated vs. CLP-PEG-MPC, $p<0.05$. ‡ CLP-PEG vs. CLP-PEG-MPC, $p<0.05$. For all charts the unit of analysis is the eye: CLP-PEG n=4, CLP-PEG-MPC n=4, unoperated n=8.

Figure 5. Regenerated mini-pig neo-corneas at 12-month after post-CLP-PEG-MPC implantation compared to CLP-PEG and controls. (a-c) Hematoxylin and eosin staining of the implanted corneas shows morphological similarity of the regenerated epithelium (rE) and stroma (rS) to the epithelium (E) and stroma (S) of an unoperated, healthy control cornea. The unoperated endothelium (arrowheads) remained intact in all samples. (d-f) Positive Ulex Europaeus Agglutinin lectin staining shows the presence of a tear film in both regenerated corneas and the control. (g-i) Terminally differentiated corneal cells were cytokeratin 3/76-positive in both regenerated neo-corneas. (j-l) Collagen V staining of the neo-cornea stromas shows the regeneration of corneal specific ECM components. Black scale bars, 500 μm; white scale bars, 200 μm.

Fig. 6. Histopathological, immunohistochemical and biochemical characteristics of regenerated neo-corneas at 12 months post-implantation with CLP-PEG-MPC implants compared to CLP-PEG implants. (a) Corneal epithelial hyperplasia was noticeably higher in the CLP-PEG only implants (black circles) compared to CLP-PEG-MPC implants (pink squares), while neovascularization was not markedly different. However, neither was statistically significant by the Mann-Whitney U test. (b) Mean cell counts normalized to the contralateral control eye for myofibroblast α-smooth muscle actin, blood vessel marker CD31, lymphatic vessel marker LYVE1, and the myeloid cell marker CD172a show no significant differences between CLP-PEG-MPC (pink squares) and CLP-PEG (black circles). Statistical analysis by unpaired, two-way t-test were performed with statistical significance set at $p\leq0.05$. (c) Collagen content analysis of the central cornea in CLP-PEG-MPC (pink squares), CLP-PEG (black circles) and unoperated (aqua triangles) corneas. Statistical analysis of collagen by two-way ANOVA with Tukey's multiple comparisons test. Data is displayed using the mean. *Unoperated vs CLP-PEG, $p<0.05$. †Unoperated vs. CLP-PEG-MPC, $p\leq0.05$. ‡CLP-PEG vs. CLP-PEG-MPC, $p\leq0.05$. For all charts the unit of analysis is the eye: CLP-PEG n=4, CLP-PEG-MPC n=4, unoperated n=8.

Figure 7. Electron micrographs of regenerated neo-corneas after CLP-PEG and CLP-PEG-MPC implantation. Serial block face scanning electron microscope overview scans show comparable epithelial and stromal compartments (a-c). 3D reconstructions (d-f) of the neo-corneas after digital removal of the extracellular matrix show that keratocytes within the stroma are arranged in interconnected lamellae. The lamellae in the CLP-PEG only implanted corneas are less organized than in the other two groups. (g-i) Transmission electron microscopy of the corneas indicates that both operated groups (g, h) have invaginated basal epithelia. E, epithelium; S, stroma; r, regenerated.

Figure 8. Extracellular vesicles and exosome secretion by regenerating CLP-PEG-MPC and CLP-PEG implanted corneas. (a-c) Greater amounts of Tsg101+ EVs (red staining) were present in the grafted regions, with the highest level of secretion in the CLP-PEG implants compared to CLP-PEG-MPC implants and unoperated controls. DAPI (blue staining) was used to identify the cell nuclei. (d-f) CLP-PEG implants also had the highest amount of Tsg101+, CD9+ exosomes represented by yellow staining. White scale bars, 200 μm. (g-i) High resolution TEM of the basement membrane confirms the increased release of exosomes from the epithelium into the stroma. Black scale bars, 2 μm. (j-l) High magnification of the inset yellow-boxed areas showing the presence of exosomes (white arrowheads) in the stroma. Yellow scale bars, 500 nm.

Supplementary Figure Legends

Supplementary Figure 1. Monthly (M1 to M12) slit-lamp follow-up of the implants in the feline model over a 12-month observation period. At 1-month post-operation, the implants remained transparent as shown in the gross morphology (a1,b1) and corresponding slit lamp images (a2, b2). Maximum haze and neovascularization was seen between M3-6, corresponding to in-growth of stromal cells (c-g). After 6 months, both haze and neovascularization regressed so that both implants are transparent at 9 months (i, j) and 12 months (k, l) post-operation. The vessel seen in the slit lamp image (g2 – arrowed) was no longer present at 9 or 12 months.

Supplementary Figure 2. Corneal transparency at 14 months post-operation, allowing visualization of the fine details of the iris through the implants (a, b). Surface mapping of

corneal front surface curvature showed stable flattening induced by the implants (c) while preserving central pachymetry (d).

Supplementary Figure 3. Optical coherence tomography (OCT) of the CLP-PEG-MPC (Top) and CLP-PEG (Bottom) implants one year after implantation in feline model showing retention of shape and transparency.

Supplementary Figure 4. Vascular and inflammatory markers in the regenerated mini-pig neo-corneas at 12-month after CLP-PEG-MPC implantation compared to CLP-PEG and controls. One out of four CLP-PEG-MPC pigs showed positive staining for α-SMA (a), CD31 (f) and LYVE 1 (k). Three of four CLP-PEG pigs showed positive vascular staining for α-SMA (b-d), CD31 (g-i) and LYVE 1 (l-n). Unoperated corneas express no vascular markers. (e,j,o). Both the regenerated corneas (p-s) and unoperated cornea (t) contain CD172a positive mononuclear cells.

Supplementary Figure 5. Quantification of LL37 in CLP-PEG and CLP-PEG-MPC grafts. (a-c) 3D reconstructions of confocal images of LL37 counterstained with DAPI. (d-e) Quantification of the intensity sum of spots constructed using LL37 fluorescence by area. (f-g) Quantification of the total number of spots by area.

Supplementary Figure 6. Sample flow cytometry gating strategy for bone marrow-derived dendritic cells (BMDCs). The cells were gated for size and granularity using a FSC/SSC gate (a). The cells were gated to remove dead cells, based on low Zombie-Aqua fluorescence in live cells that were impermeable to the dye (b). The live cells were gated for CD11c high, autofluorescence low (c) and this is the gate that was subject to subsequent analysis.

Figures

Figure 1.

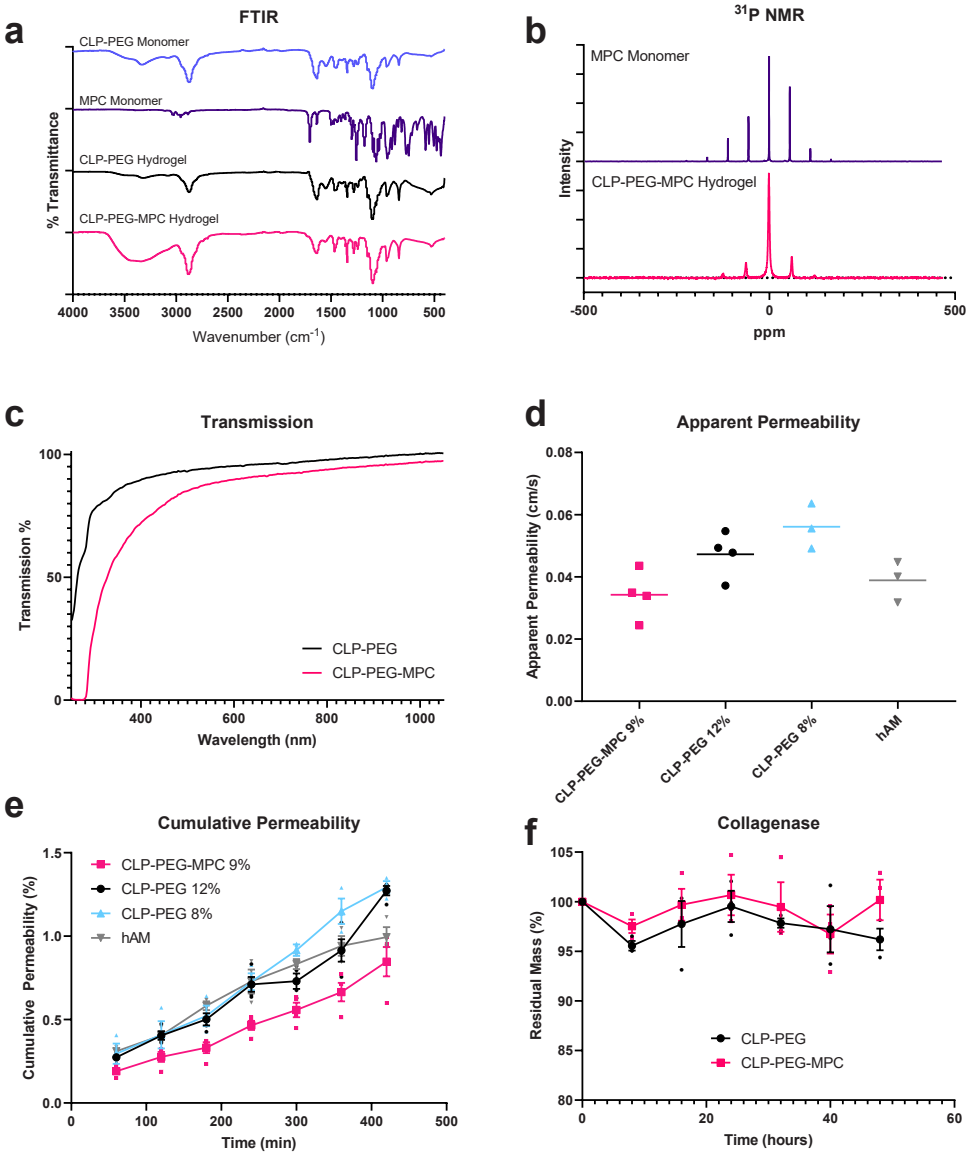

Figure 2.

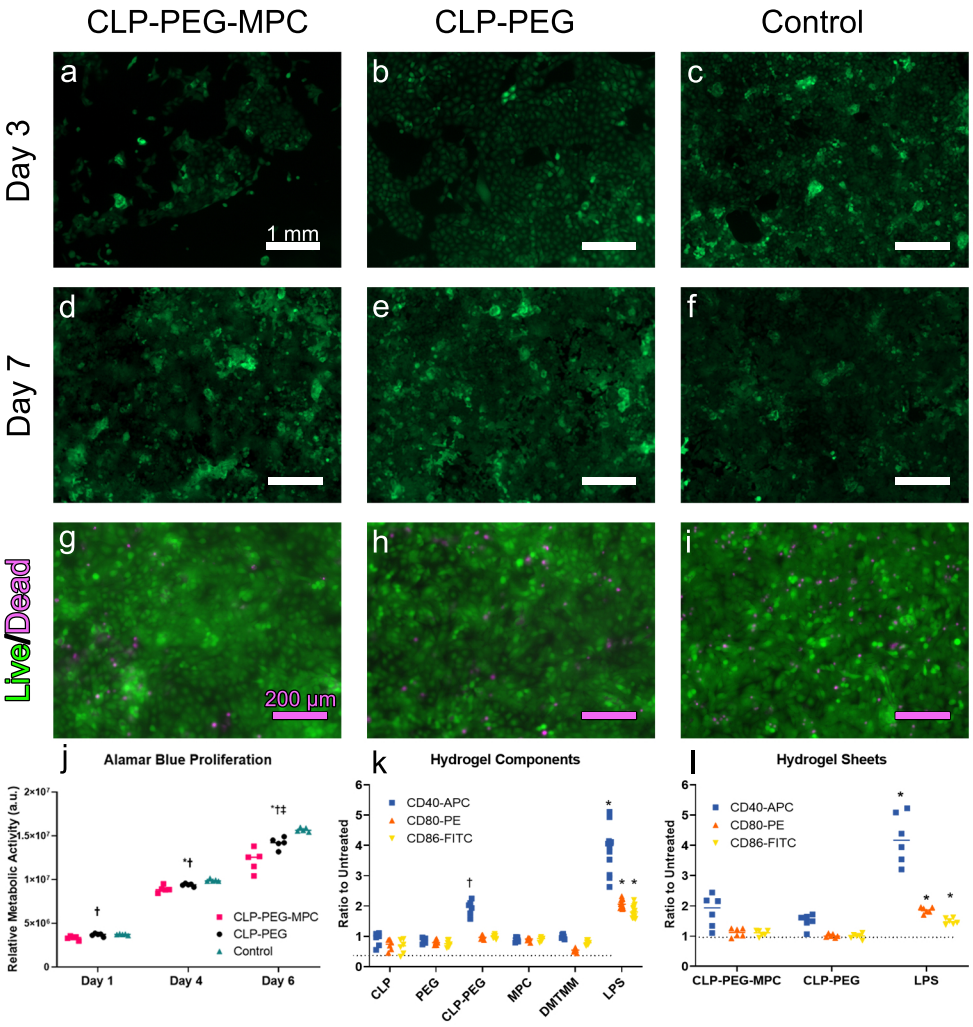
CLP-PEG-MPC
CLP-PEG
Control
Day 3
Day 7
Live/Dead
a
b
c
d
e
f
g
h
i
1 mm
200 µm
j
Alamar Blue Proliferation
Relative Metabolic Activity (a.u.)
CLP-PEG-MPC
CLP-PEG
Control
Day 1
Day 4
Day 6
k
Hydrogel Components
CD40-APC
CD80-PE
CD86-FITC
Ratio to Untreated
CLP
PEG
CLP-PEG
MPC
DMTMM
LPS
l
Hydrogel Sheets
CD40-APC
CD80-PE
CD86-FITC
Ratio to Untreated
CLP-PEG-MPC
CLP-PEG
LPS

Figure 3.

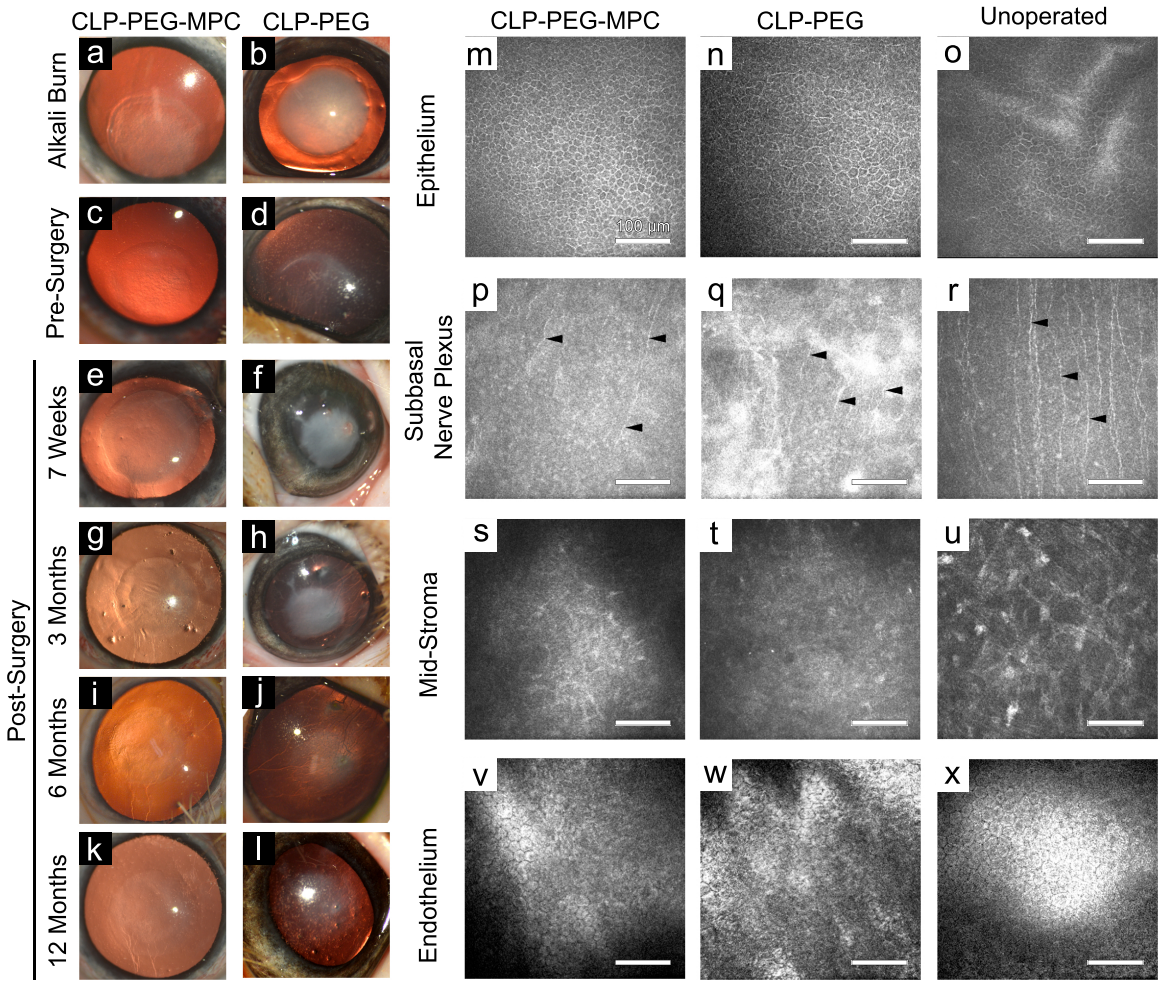
CLP-PEG-MPC
CLP-PEG
Alkali Burn
Pre-Surgery
Post-Surgery
7 Weeks
3 Months
6 Months
12 Months
a
b
c
d
e
f
g
h
i
j
k
l
CLP-PEG-MPC
CLP-PEG
Unoperated
Epithelium
Subbasal Nerve Plexus
Mid-Stroma
Endothelium
m
n
o
p
q
r
s
t
u
v
w
x
100 µm

Figure 4.

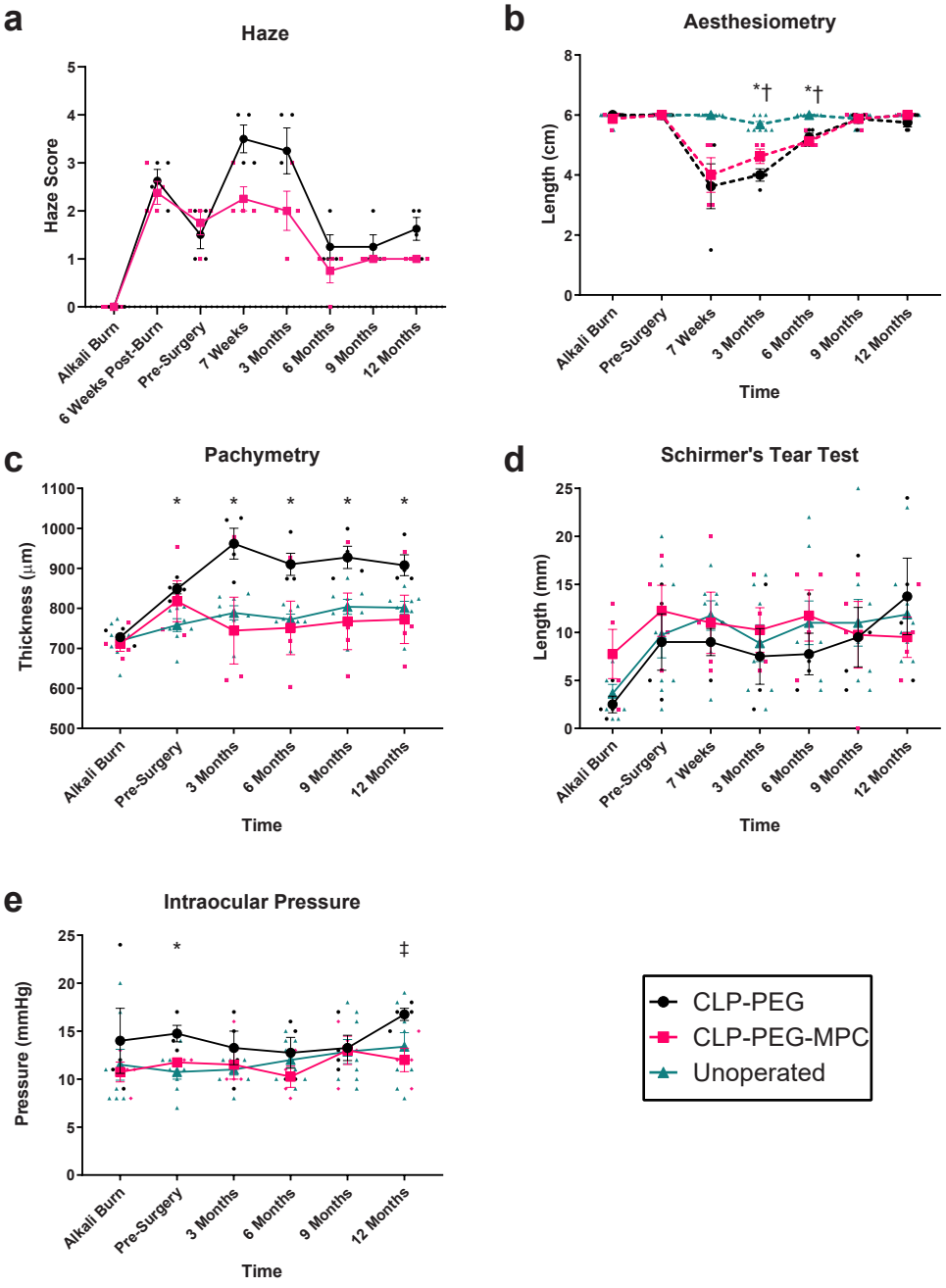
a
Haze
Haze Score
Alkali Burn
6 Weeks Post-Burn
Pre-Surgery
7 Weeks
3 Months
6 Months
9 Months
12 Months
b
Aesthesiometry
Length (cm)
*†
*†
Time
c
Pachymetry
Thickness (μm)
Time
d
Schirmer's Tear Test
Length (mm)
Time
e
Intraocular Pressure
Pressure (mmHg)
‡
Time
CLP-PEG
CLP-PEG-MPC
Unoperated

Figure 5.

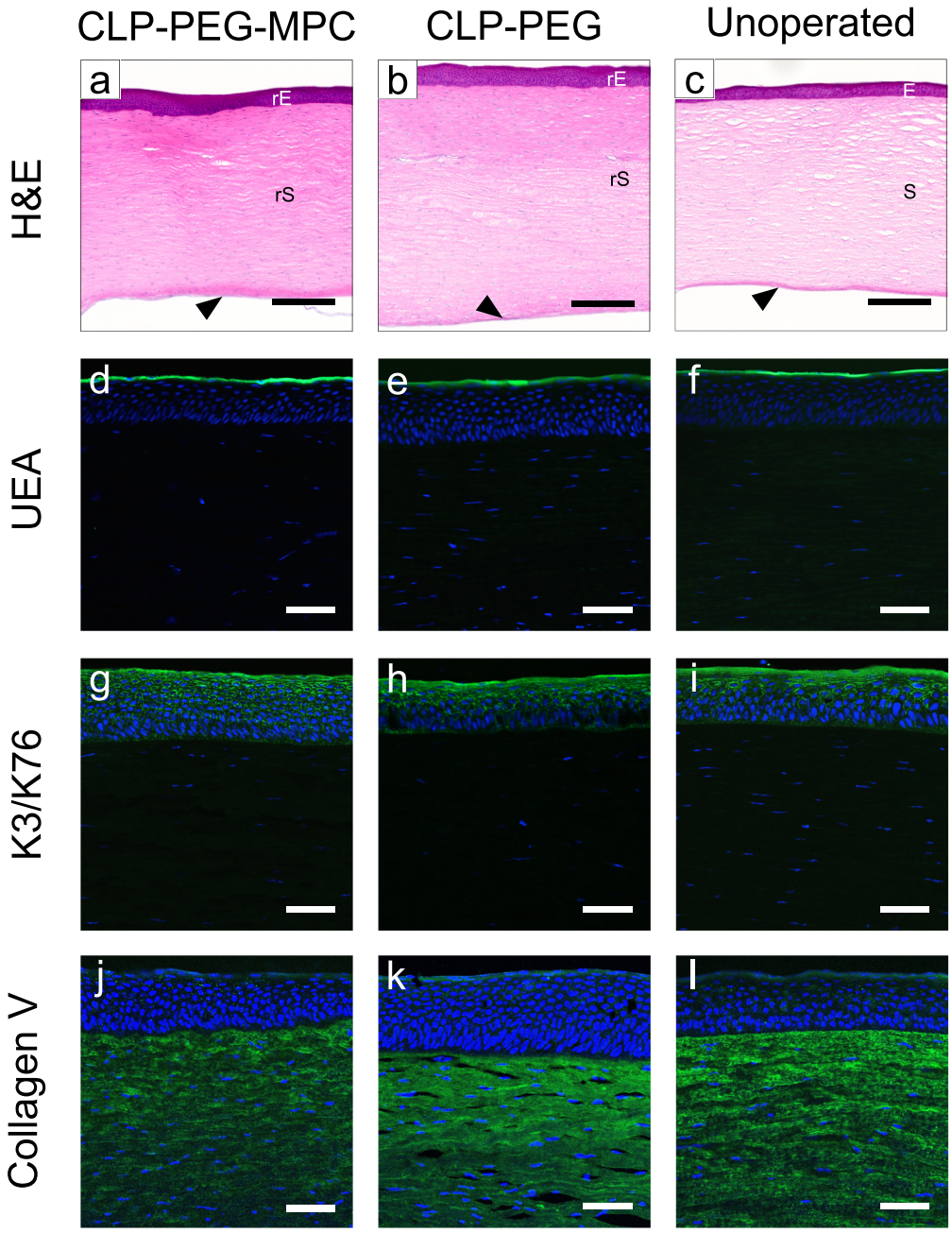
CLP-PEG-MPC
CLP-PEG
Unoperated
H&E
UEA
K3/K76
Collagen V
a
b
c
d
e
f
g
h
i
j
k
l
rE
rS
E
S

Figure 6.

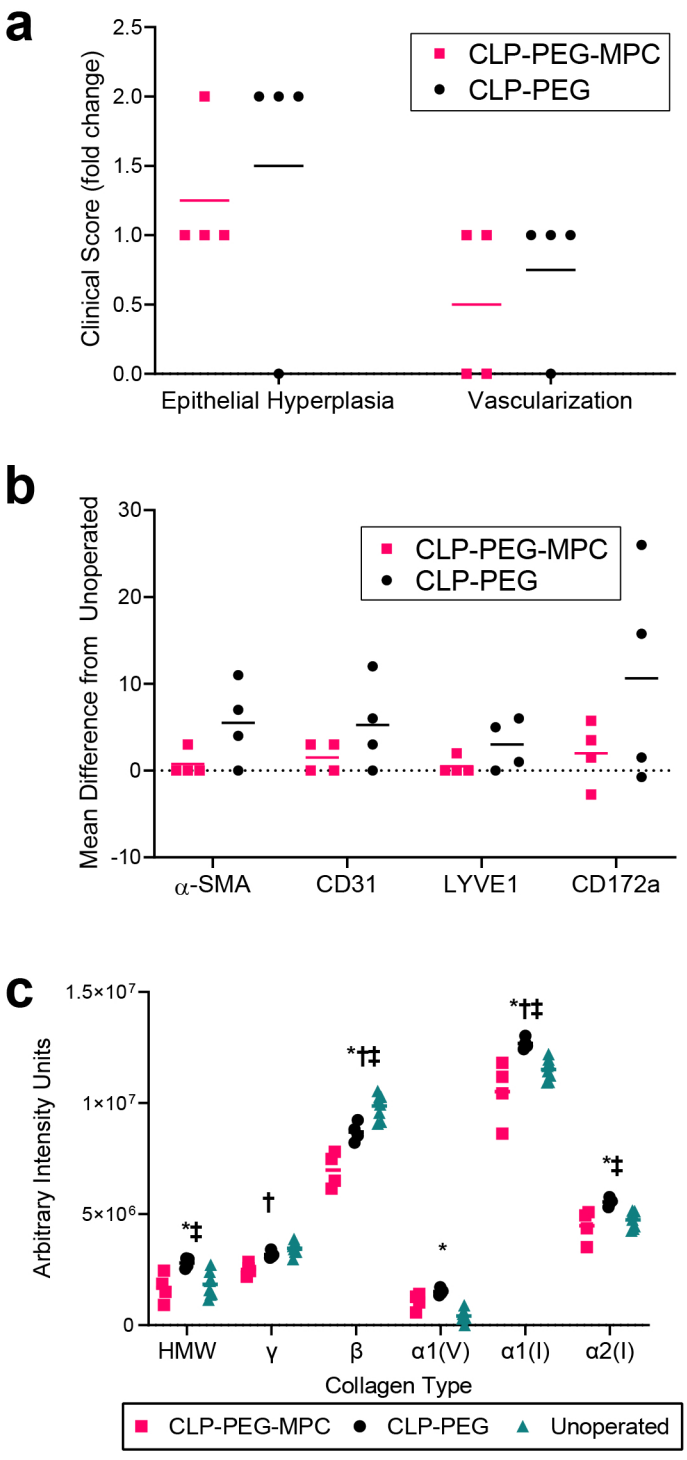
a
Clinical Score (fold change)
2.5
2.0
1.5
1.0
0.5
0.0
CLP-PEG-MPC
CLP-PEG
Epithelial Hyperplasia
Vascularization
b
Mean Difference from Unoperated
30
20
10
0
-10
CLP-PEG-MPC
CLP-PEG
α-SMA
CD31
LYVE1
CD172a
c
Arbitrary Intensity Units
1.5×10^7
1×10^7
5×10^6
0
*‡
†
*†‡
*
*†‡
*‡
HMW
γ
β
α1(V)
α1(I)
α2(I)
Collagen Type
CLP-PEG-MPC
CLP-PEG
Unoperated

Figure 7.

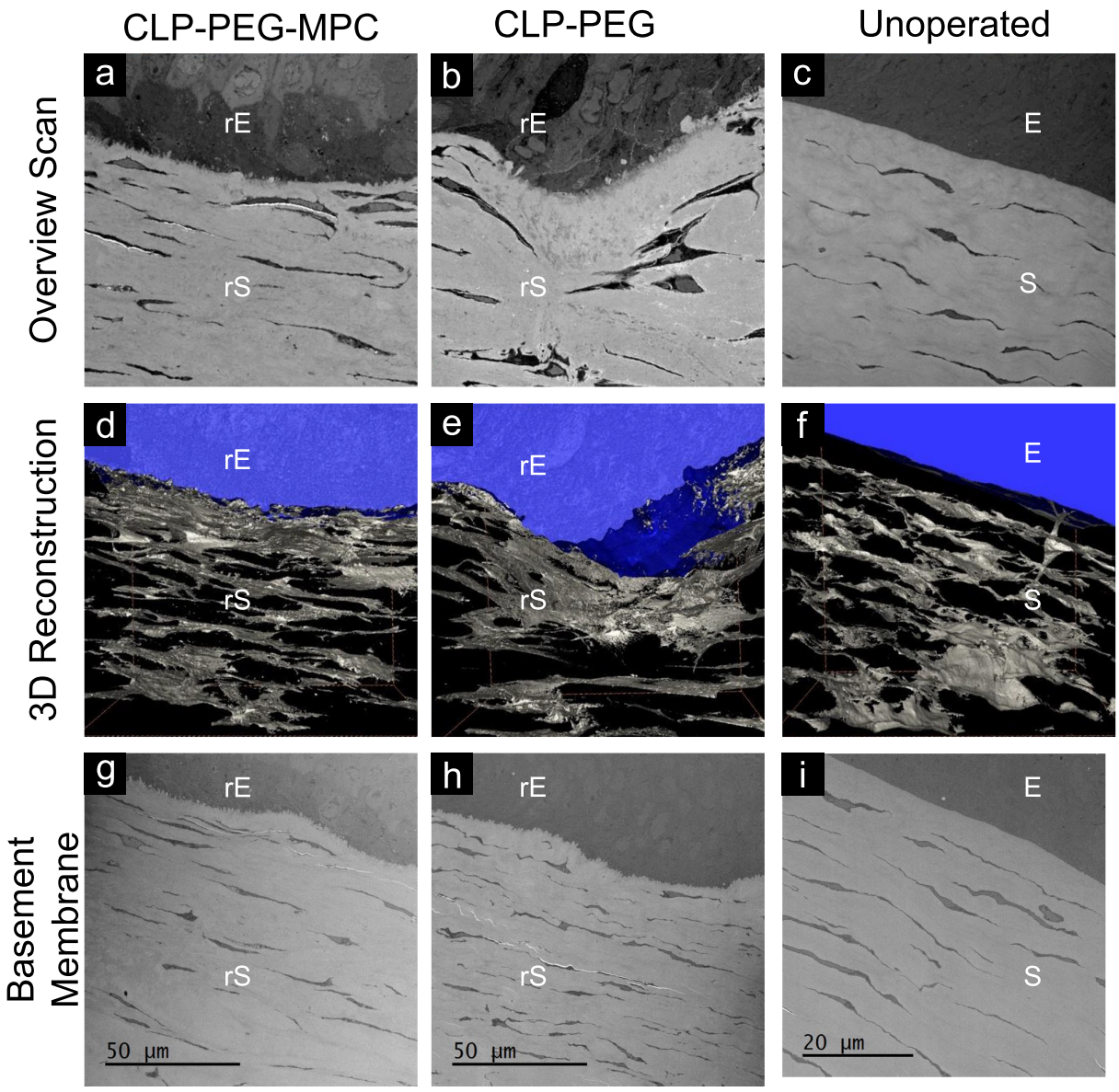
CLP-PEG-MPC
CLP-PEG
Unoperated
Overview Scan
3D Reconstruction
Basement Membrane
a
b
c
d
e
f
g
h
i
rE
rS
E
S
50 µm
20 µm

Figure 8.

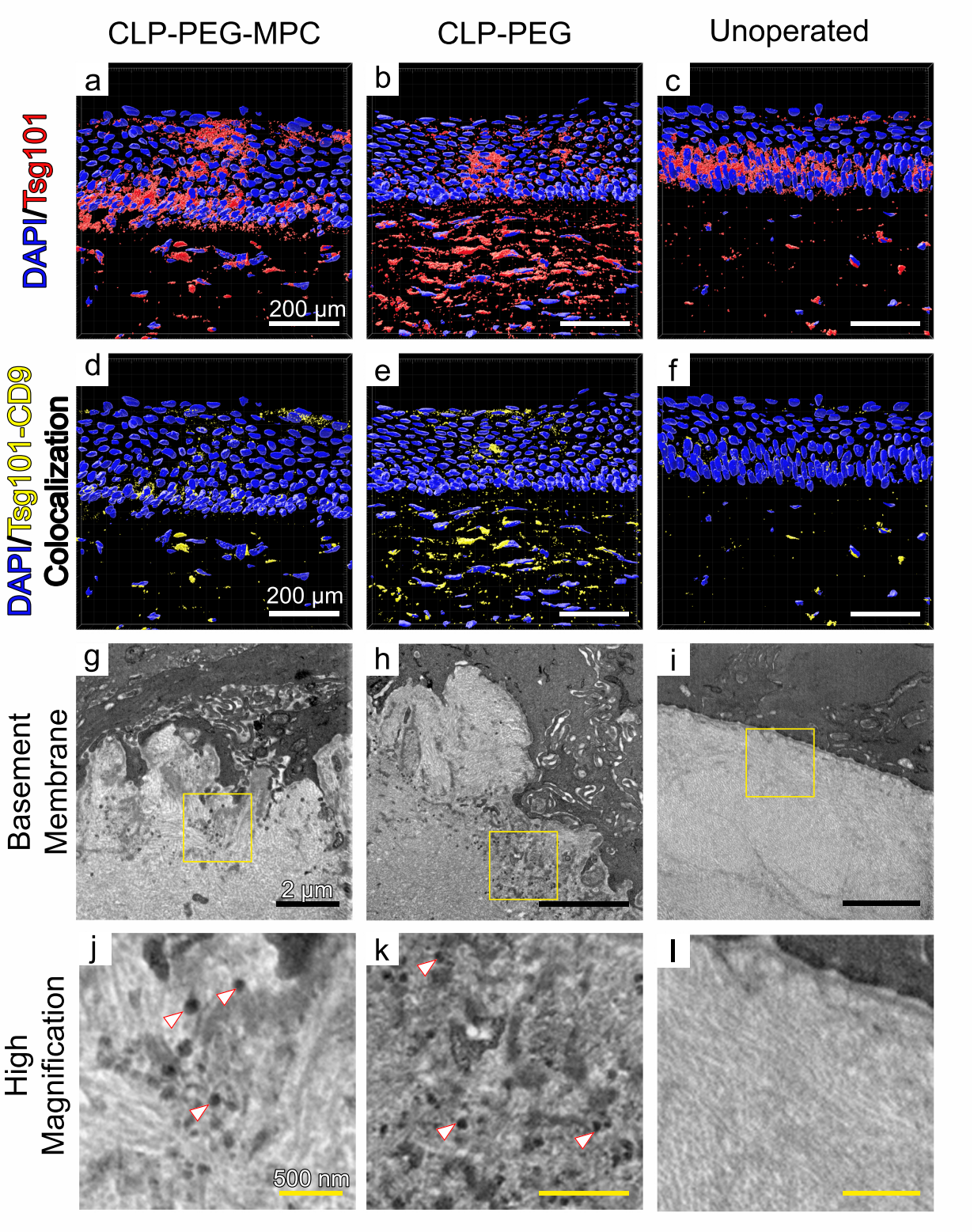
CLP-PEG-MPC
CLP-PEG
Unoperated
a
b
c
DAPI/Tsg101
200 μm
d
e
f
DAPI/Tsg101-CD9
Colocalization
200 μm
g
h
i
Basement
Membrane
2 μm
j
k
l
High
Magnification
500 nm

Supplementary Figures

Supplementary Figure 1.

[h]

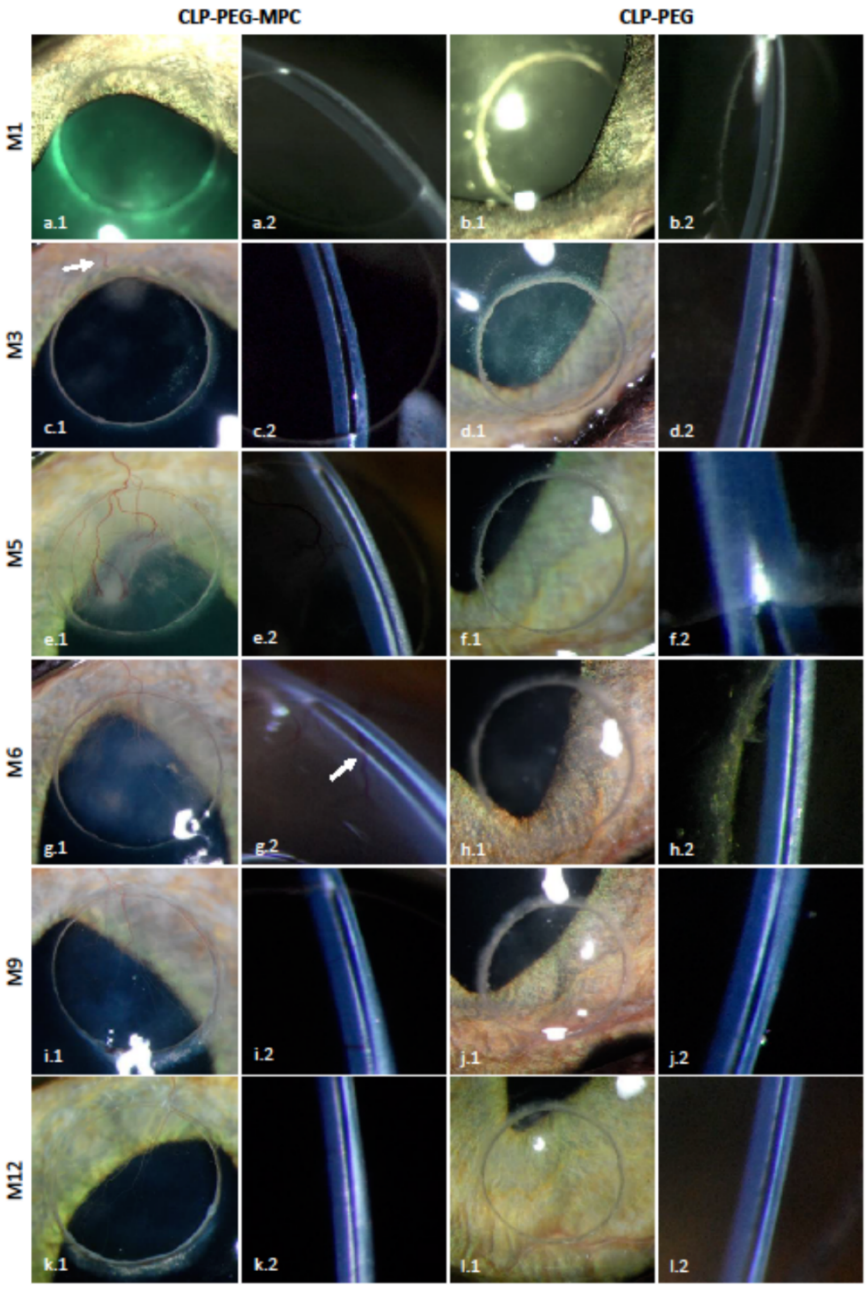

Supplementary Figure 2.

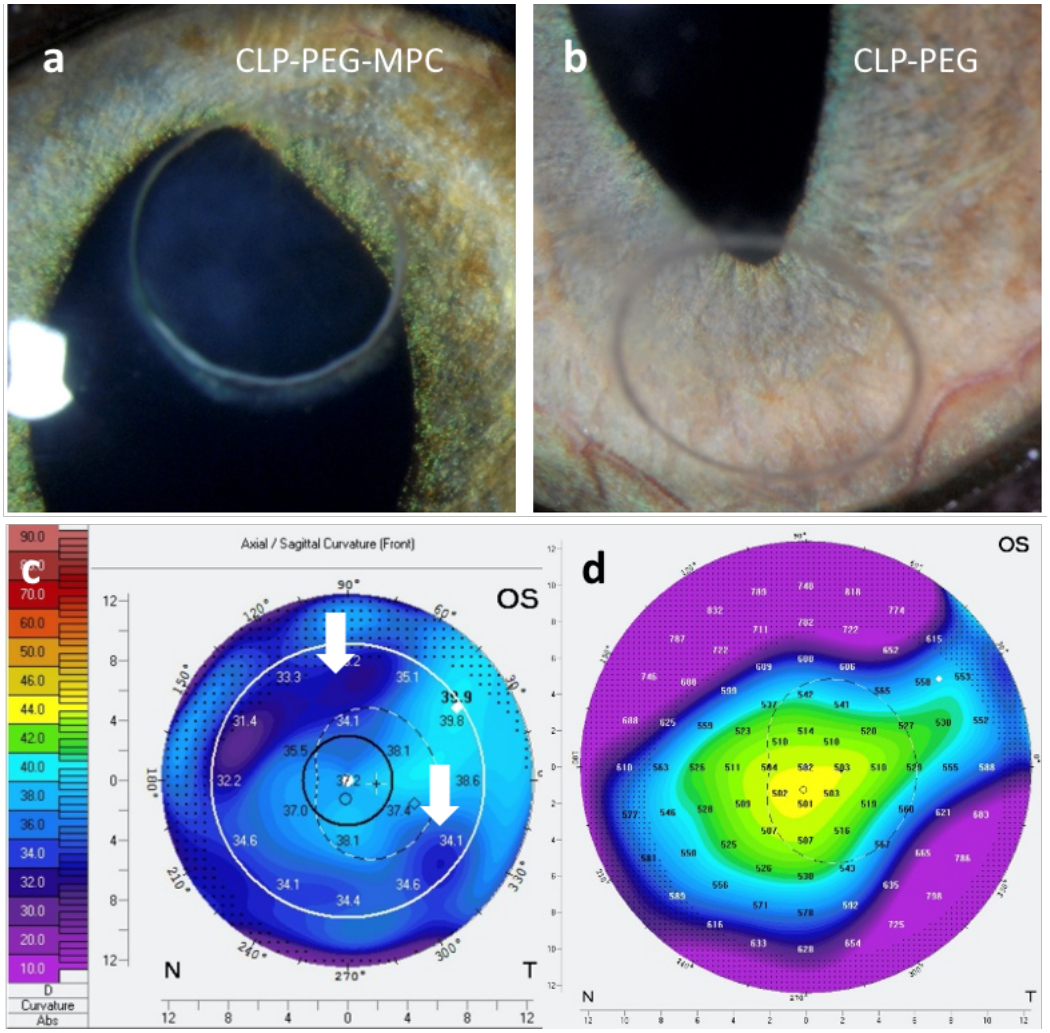

Supplementary Figure 3.

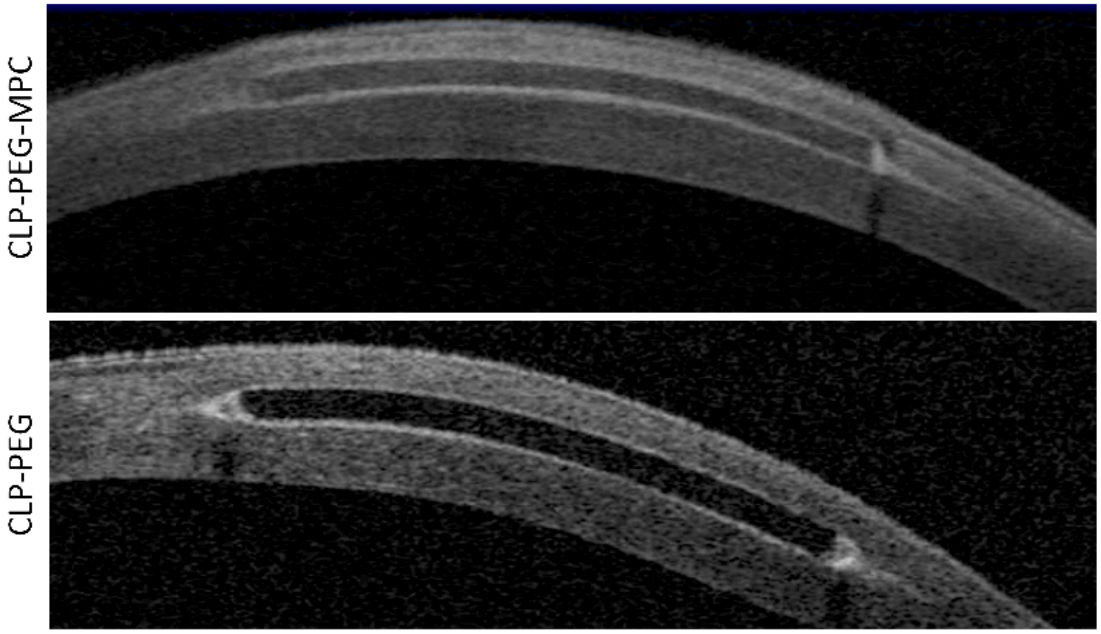

Supplementary Figure 4.

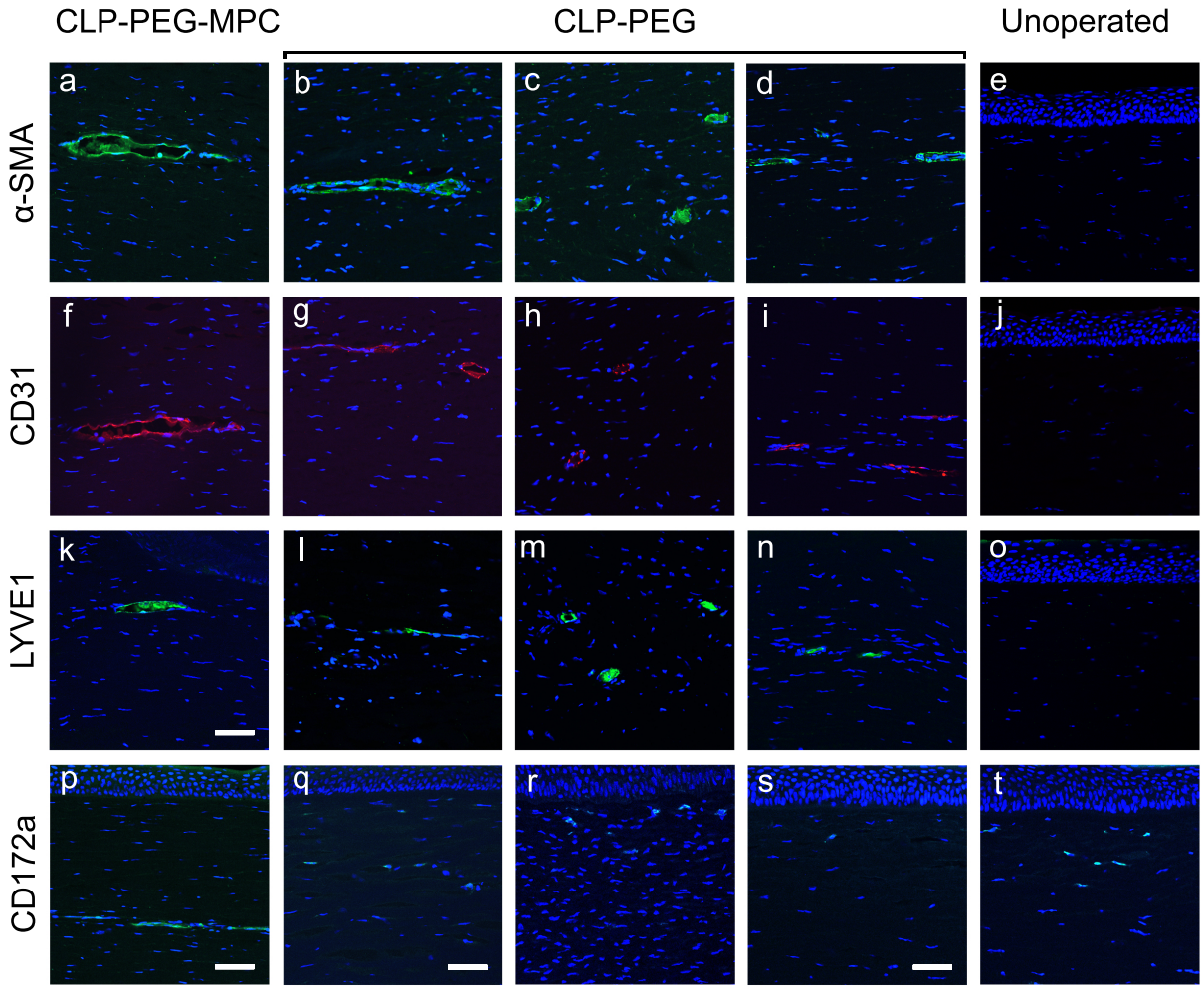

Supplementary Figure 5.

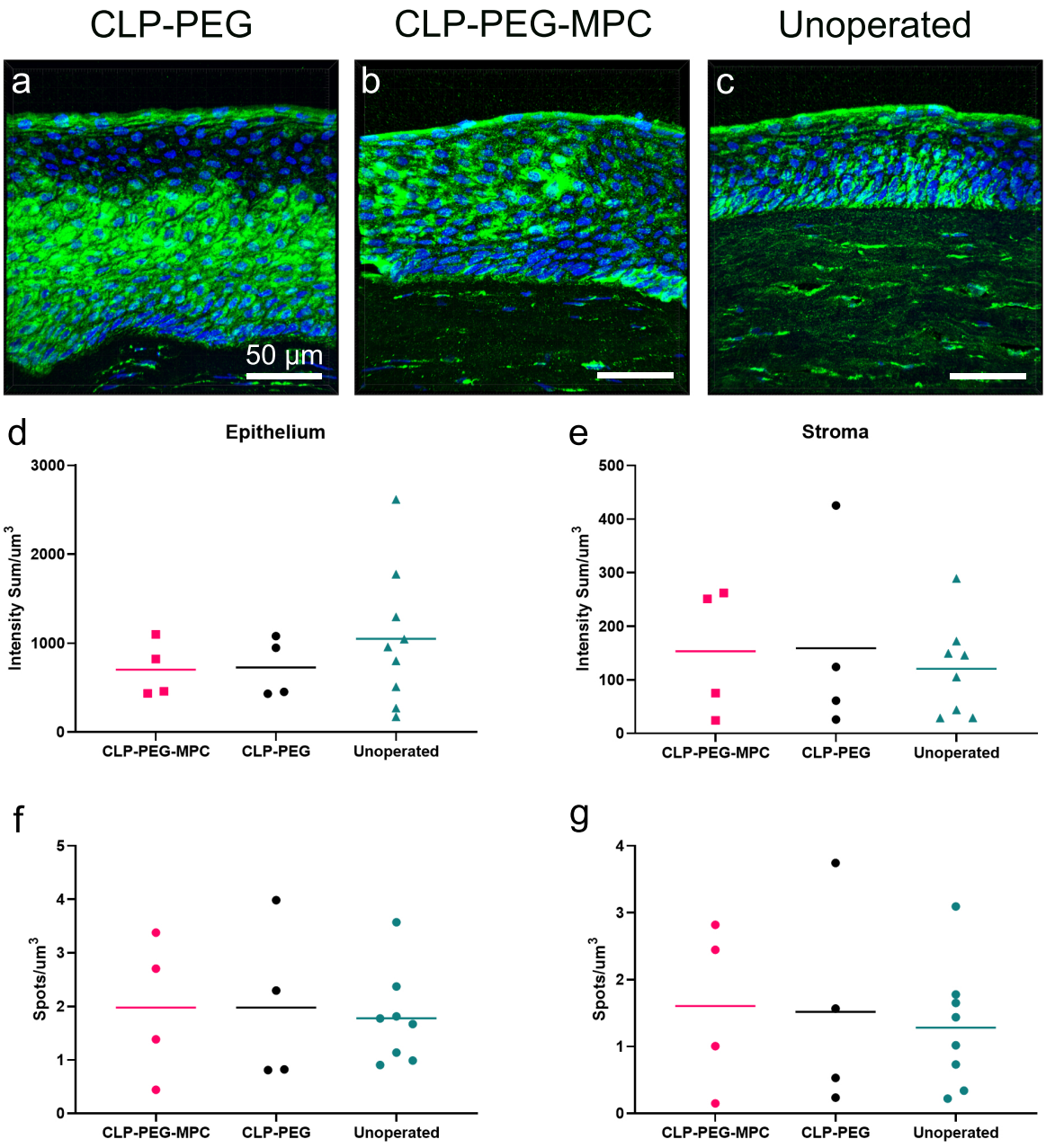

Supplementary Figure 6.

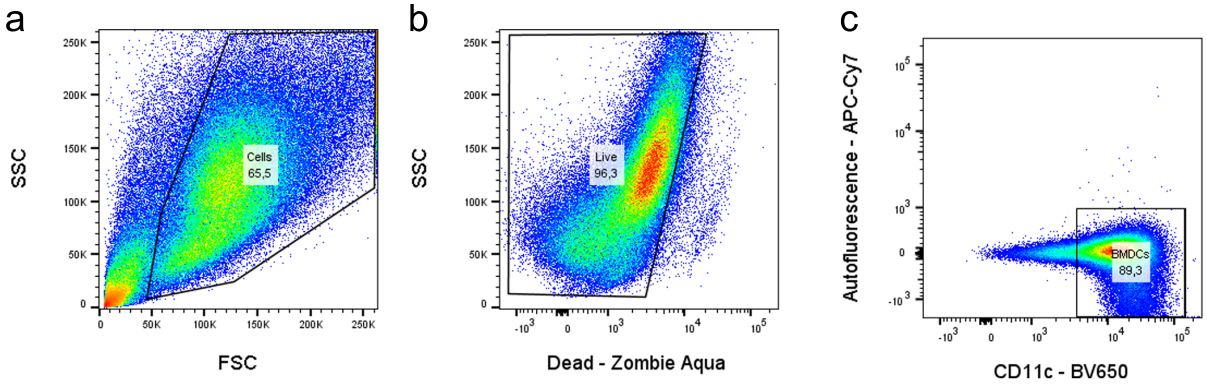

Tables

Table 1. Characterization of CLP-PEG-MPC hydrogels compared to CLP-PEG only hydrogels, biosynthetic implants currently in patients and the human cornea

	CLP-PEG-MPC	CLP-PEG	Biosynthetic implants*	Human cornea
Tensile Strength (MPa)	0.022 ± 0.004	0.56 ± 0.21	0.286 ± 0.06[19]	3.81 ± 0.40[33]
Elongation (%)	59.50 ± 7.70	49.96 ± 8.10	20.149 ± 7.614[19]	N/A
Young's Modulus (MPa)	0.044 ± 0.010	0.150 ± 0.015	1.749 ± 0.782[19]	3-13[34,35]
Storage Modulus (G') (kPa)	15.15 ± 1.086	22.36 ± 1.489	-	-
Loss Modulus (G") (kPa)	0.1522 ± 0.0569	0.0433 ± 0.006	-	-
Transmission (%)	29-80(UV) 80-97(Vis)	32-92(UV) 92-99(Vis)	95.1 ± 0.05[19]	87.1 ± 2.0 (at 500 nm)[36]
Refractive Index	1.340 ± 0.005	1.338 ± 0.004	1.3507 ± 0.0011[37]	1.423 - 1.436[38]
Water Content (%)	90.94 ± 0.78	92.67 ± 0.85	91.5 ± 0.9[19]	78[39]
Residual Mass (%) from Collagenase Degradation at 48h	100.17 ± 3.54	96.19 ± 1.89	<10%[37]	-

*RHCIII implants that have been stably grafted into 10 patients and showed regeneration at 4 years post-operation as reported in Fagerholm et al., 2014 [19].

Supplementary Tables

Supplementary Table 1. Two-Way ANOVA of Alamar blue proliferation study

ANOVA table	SS	DF	MS	F (DFn, DFd)	P value
Time x Treatment	1.37E+13	4	3.42E+12	F (4, 24) = 14.28	P<0.0001
Time	8.22E+14	2	4.11E+14	F (1.163, 13.96) = 1713	P<0.0001
Treatment	2.02E+13	2	1.01E+13	F (2, 12) = 31.96	P<0.0001
Subject	3.8E+12	12	3.17E+11	F (12, 24) = 1.320	P=0.2706
Residual	5.76E+12	24	2.4E+11		
Source of Variation		% of total variation		P value	GGϵ
Time x Treatment		1.584		<0.0001	
Time		94.97		<0.0001	0.5815
Treatment		2.339		<0.0001	
Subject		0.4392		0.2706	
Tukey's multiple comparisons test		Mean Diff.		95.00% CI of diff.	Adjusted P Value
Day 1					
CLP-PEG vs. CLP-PEG-MPC		355174		-7340 to 717688	0.0544
CLP-PEG vs. Control		-42545		-311772 to 226681	0.8751
CLP-PEG-MPC vs. Control		-397719		-737139 to -58299	0.0281
Day 4					
CLP-PEG vs. CLP-PEG-MPC		482553		-108848 to 1073954	0.0991
CLP-PEG vs. Control		-521052		-798324 to -243779	0.0018
CLP-PEG-MPC vs. Control		-1003604		-1596622 to -410587	0.0062
Day 6					
CLP-PEG vs. CLP-PEG-MPC		2002578		20439 to 3984717	0.0481
CLP-PEG vs. Control		-1503370		-2490533 to -516208	0.0098
CLP-PEG-MPC vs. Control		-3505949		-5529979 to -1481919	0.0071

Supplementary Table 2. Two-Way ANOVA of Haze

ANOVA table	SS	DF	MS	F (DFn, DFd)	P value
Time x Treatment	4.152	7	0.5932	F (7, 42) = 3.075	P=0.0104
Time	53.65	7	7.665	F (3.082, 18.49) = 39.73	P<0.0001
Treatment	3.754	1	3.754	F (1, 6) = 5.049	P=0.0657
Subject	4.461	6	0.7435	F (6, 42) = 3.854	P=0.0038
Residual	8.102	42	0.1929		
Source of Variation		% of total variation		P value	Geisser-Greenhouse's ϵ
Time x Treatment		0.0657		0.0657	
Time		0.0038		0.0038	0.4403
Treatment		0.0657		0.0657	
Subject		0.0038		0.0038	
Sidak's multiple comparisons test		Mean Diff.		95.00% CI of diff.	Adjusted P Value
CLP-PEG vs. CLP-PEG-MPC					
Alkali Burn		0			
6 Weeks Post-Burn		0.25		-1.136 to 1.636	0.9953
Pre-Surgery		-0.25		-1.829 to 1.329	0.9979
7 Weeks		1.25		-0.3288 to 2.829	0.1315
3 Months		1.25		-1.356 to 3.856	0.5513
6 Months		0.5		-0.9479 to 1.948	0.8437
9 Months		0.25		-1.460 to 1.960	0.9811
12 Months		0.625		-1.013 to 2.263	0.4850

Supplementary Table 3. Two-Way ANOVA of Aesthesiometry

ANOVA table	SS	DF	MS	F (DFn, DFd)	P value
Time x Treatment	18.8	12	1.567	F (12, 78) = 10.72	P<0.0001
Time	31.79	6	5.298	F (1.622, 21.09) = 36.24	P<0.0001
Treatment	11.86	2	5.929	F (2, 13) = 27.67	P<0.0001
Subject	2.786	13	0.2143	F (13, 78) = 1.466	P=0.1496
Residual	11.4	78	0.1462		
Source of Variation		% of total variation		P value	GG ϵ
Time x Treatment		28.61		<0.0001	
Time		48.37		<0.0001	0.2703
Treatment		18.04		<0.0001	
Subject		4.239		0.1496	
Tukey's multiple comparisons test		Mean Diff.		95.00% CI of diff.	Adjusted P Value
Alkali Burn					
CLP-PEG vs. CLP-PEG-MPC		0.125		-0.3973 to 0.6473	0.6259
CLP-PEG vs. Unoperated		0.0625		-0.1216 to 0.2466	0.6000
CLP-PEG-MPC vs. Unoperated		-0.0625		-0.5331 to 0.4081	0.8980
7 Weeks					
CLP-PEG vs. CLP-PEG-MPC		-0.375		-3.324 to 2.574	0.9179
CLP-PEG vs. Unoperated		-2.375		-5.495 to 0.7445	0.0983
CLP-PEG-MPC vs. Unoperated		-2		-4.413 to 0.4126	0.0802
3 Months					
CLP-PEG vs. CLP-PEG-MPC		-0.625		-1.597 to 0.3472	0.1980
CLP-PEG vs. Unoperated		-1.688		-2.463 to -0.9118	0.0029
CLP-PEG-MPC vs. Unoperated		-1.063		-1.986 to -0.1389	0.0322
6 Months					
CLP-PEG vs. CLP-PEG-MPC		0.125		-0.4643 to 0.7143	0.7969
CLP-PEG vs. Unoperated		-0.75		-1.353 to -0.1468	0.0280
CLP-PEG-MPC vs. Unoperated		-0.875		-1.397 to -0.3527	0.0122
9 Months					

CLP-PEG vs. CLP-PEG-MPC	0	-0.5424 to 0.5424	>0.9999
CLP-PEG vs. Unoperated	0	-0.4661 to 0.4661	>0.9999
CLP-PEG-MPC vs. Unoperated	0	-0.4661 to 0.4661	>0.9999
12 Months			
CLP-PEG vs. CLP-PEG-MPC	-0.25	-0.8532 to 0.3532	0.3292
CLP-PEG vs. Unoperated	-0.25	-0.8532 to 0.3532	0.3292
CLP-PEG-MPC vs. Unoperated	0		

Supplementary Table 4. Two-Way ANOVA of Pachymetry

ANOVA table	SS	DF	MS	F (DFn, DFd)	P value
Time x Treatment	0.7125	4	0.1781	F (4, 24) = 0.4597	P=0.7645
Time	27.59	4	6.897	F (1.280, 7.682) = 17.80	P=0.0023
Treatment	0.5062	1	0.5062	F (1, 6) = 0.8351	P=0.3961
Subject	3.638	6	0.6063	F (6, 24) = 1.565	P=0.2006
Residual	9.3	24	0.3875		
Source of Variation		% of total variation		P value	GGϵ
Time x Treatment		9.078		<0.0001	
Time		15.95		<0.0001	0.4514
Treatment		26.69		0.0351	
Subject		39.57		<0.0001	
Tukey's multiple comparisons test		Mean Diff.		95.00% CI of diff.	Adjusted P Value
Pre-Surgery					
CLP-PEG vs. CLP-PEG-MPC		31		-173.7 to 235.7	0.8332
CLP-PEG vs. Unoperated		90.5		34.61 to 146.4	0.0033
CLP-PEG-MPC vs. Unoperated		59.5		-140.5 to 259.5	0.5607
3 Months					
CLP-PEG vs. CLP-PEG-MPC		217.3		-102.1 to 536.6	0.1504
CLP-PEG vs. Unoperated		172.9		27.21 to 318.5	0.0281
CLP-PEG-MPC vs. Unoperated		-44.38		-381.7 to 292.9	0.8668
6 Months					
CLP-PEG vs. CLP-PEG-MPC		159		-98.86 to 416.9	0.1854
CLP-PEG vs. Unoperated		137.8		32.88 to 242.6	0.0194
CLP-PEG-MPC vs. Unoperated		-21.25		-293.0 to 250.5	0.9486
9 Months					
CLP-PEG vs. CLP-PEG-MPC		160		-113.8 to 433.8	0.2060
CLP-PEG vs. Unoperated		123.5		20.17 to 226.8	0.0247
CLP-PEG-MPC vs. Unoperated		-36.5		-318.5 to 245.5	0.8762
12 Months					

CLP-PEG vs. CLP-PEG-MPC	135.3	-96.61 to 367.1	0.2120
CLP-PEG vs. Unoperated	106.1	8.618 to 203.6	0.0365
CLP-PEG-MPC vs. Unoperated	-29.13	-269.3 to 211.1	0.8905

Supplementary Table 5. Two-Way ANOVA of Schirmer's Tear Test

ANOVA table	SS	DF	MS	F (DFn, DFd)	P value
Time x Treatment	152.9	12	12.75	F (12, 78) = 0.4649	P=0.9292
Time	456.2	6	76.04	F (4.508, 58.60) = 2.774	P=0.0300
Treatment	53.05	2	26.53	F (2, 13) = 0.5568	P=0.5861
Subject	619.4	13	47.64	F (13, 78) = 1.738	P=0.0693
Residual	2139	78	27.42		
Source of Variation		% of total variation		P value	GGϵ
Time x Treatment		4.33		0.9292	
Time		12.92		0.03	0.7513
Treatment		1.502		0.5861	
Subject		17.54		0.0693	
Tukey's multiple comparisons test		Mean Diff.		95.00% CI of diff.	Adjusted P Value
Alkali Burn					
CLP-PEG vs. CLP-PEG-MPC		-5.250		-15.29 to 4.792	0.2503
CLP-PEG vs. Unoperated		-1.125		-4.735 to 2.485	0.6720
CLP-PEG-MPC vs. Unoperated		4.125		-5.777 to 14.03	0.3818
Pre-Surgery					
CLP-PEG vs. CLP-PEG-MPC		-3.250		-15.46 to 8.956	0.7058
CLP-PEG vs. Unoperated		-0.750		-11.94 to 10.44	0.9788
CLP-PEG-MPC vs. Unoperated		2.500		-7.821 to 12.82	0.7717
7 Weeks					
CLP-PEG vs. CLP-PEG-MPC		-2.000		-14.24 to 10.24	0.8406
CLP-PEG vs. Unoperated		-2.750		-8.582 to 3.082	0.4208
CLP-PEG-MPC vs. Unoperated		-0.750		-12.79 to 11.29	0.9757
3 Months					
CLP-PEG vs. CLP-PEG-MPC		-2.750		-14.31 to 8.813	0.7508
CLP-PEG vs. Unoperated		-1.375		-12.19 to 9.444	0.9185
CLP-PEG-MPC vs. Unoperated		1.375		-7.469 to 10.22	0.8930
6 Months					

CLP-PEG vs. CLP-PEG-MPC	-4.000	-14.66 to 6.657	0.5151
CLP-PEG vs. Unoperated	-3.250	-12.08 to 5.583	0.5759
CLP-PEG-MPC vs. Unoperated	0.750	-9.436 to 10.94	0.9750
9 Months			
CLP-PEG vs. CLP-PEG-MPC	160.000	-14.58 to 14.08	0.9984
CLP-PEG vs. Unoperated	123.500	-13.20 to 10.20	0.9239
CLP-PEG-MPC vs. Unoperated	-36.500	-14.23 to 11.73	0.9535
12 Months			
CLP-PEG vs. CLP-PEG-MPC	4.250	-10.95 to 19.45	0.6421
CLP-PEG vs. Unoperated	1.875	-13.22 to 16.97	0.9069
CLP-PEG-MPC vs. Unoperated	-2.375	-10.50 to 5.750	0.6879

Supplementary Table 6. Two-Way ANOVA of Intraocular Pressure

ANOVA table	SS	DF	MS	F (DFn, DFd)	P value
Time x Treatment	43.63	10	4.363	F (10, 65) = 0.4729	P=0.9016
Time	55.88	5	11.18	F (2.416, 31.40) = 1.211	P=0.3169
Treatment	100.3	2	50.13	F (2, 13) = 3.589	P=0.0574
Subject	181.6	13	13.97	F (13, 65) = 1.514	P=0.1363
Residual	599.7	65	9.226		

Source of Variation	% of total variation	P value	GGϵ
Time x Treatment	4.422	0.9016	
Time	5.665	0.3169	0.4831
Treatment	10.16	0.0574	
Subject	18.41	0.1363	

Tukey's multiple comparisons test	Mean Diff.	95.00% CI of diff.	Adjusted P Value
Alkali Burn			
CLP-PEG vs. CLP-PEG-MPC	3.25	-10.16 to 16.66	0.6630
CLP-PEG vs. Unoperated	2.5	-10.32 to 15.32	0.7934
CLP-PEG-MPC vs. Unoperated	-0.75	-6.002 to 4.502	0.9196
Pre-Surgery			
CLP-PEG vs. CLP-PEG-MPC	3	-0.3856 to 6.386	0.0702
CLP-PEG vs. Unoperated	4	0.7067 to 7.293	0.021
CLP-PEG-MPC vs. Unoperated	1	-1.237 to 3.237	0.4501
3 Months			
CLP-PEG vs. CLP-PEG-MPC	1.75	-5.370 to 8.870	0.7398
CLP-PEG vs. Unoperated	2.25	-4.611 to 9.111	0.5073
CLP-PEG-MPC vs. Unoperated	0.5	-5.295 to 6.295	0.9485
6 Months			
CLP-PEG vs. CLP-PEG-MPC	2.5	-3.694 to 8.694	0.4585
CLP-PEG vs. Unoperated	0.75	-5.276 to 6.776	0.9096
CLP-PEG-MPC vs. Unoperated	-1.75	-5.904 to 2.404	0.454
9 Months			

CLP-PEG vs. CLP-PEG-MPC	0.25	-5.828 to 6.328	0.9912
CLP-PEG vs. Unoperated	0.375	-4.814 to 5.564	0.977
CLP-PEG-MPC vs. Unoperated	0.125	-5.520 to 5.770	0.9977
12 Months			
CLP-PEG vs. CLP-PEG-MPC	4.75	0.07843 to 9.422	0.0473
CLP-PEG vs. Unoperated	3.375	-1.096 to 7.846	0.1434
CLP-PEG-MPC vs. Unoperated	-1.375	-6.679 to 3.929	0.7595

Supplementary Table 7. Mann-Whitney U tests of Histopathology Data

	P value	Mean rank of CLP-PEG	Mean rank of CLP-PEG-MPC	Mean rank diff.	Mann-Whitney U	q value
Epithelial Hyperplasia	0.485714	5.125	3.875	1.25	5.5	0.981143
Vascularization	>0.999999	5	4	1	6	>0.999999

Supplementary Table 8. Multiple unpaired t-tests of IHC Quantification

	α-SMA	CD31	LYVE1	CD172a
P value	0.131512	0.243655	0.18914	0.267544
Mean of CLP-PEG	5.5	5.25	3	10.63
Mean of CLP-PEG-MPC	0.75	1.5	0.5	2
Difference	4.75	3.75	2.5	8.625
SE of difference	2.445	2.704	1.555	6.548
t ratio	1.943	1.387	1.608	1.317
df	3.616	3.677	3.683	3.491
q value	0.270219	0.270219	0.270219	0.270219

Supplementary Table 9. Collagen Content Two-Way ANOVA with Tukey's multiple comparisons test

ANOVA table	SS (Type III)	DF	MS	F (DFn, DFd)	P value
Interaction	2.55E+13	10	2.55E+12	F (10, 78) = 10.07	P<0.0001
Collagen Type	1.20E+15	5	2.41E+14	F (5, 78) = 950.0	P<0.0001
Treatment	1.79E+13	2	8.93E+12	F (2, 78) = 35.28	P<0.0001
Residual	1.97E+13	78	2.53E+11		

Source of Variation	% of total variation	P value
Interaction	1.753	<0.0001
Collagen Type	82.69	<0.0001
Treatment	1.228	<0.0001

Tukey's multiple comparisons test	Predicted (LS) mean diff.	95.00% CI of diff.	Adjusted P Value
HMW			
CLP-PEG vs. CLP-PEG-MPC	1116880	266844 to 1966916	0.0067
CLP-PEG vs. Unoperated	966473	230320 to 1702625	0.0067
CLP-PEG-MPC vs. Unoperated	-150407	-886560 to 585746	0.8771
γ			
CLP-PEG vs. CLP-PEG-MPC	664016	-186020 to 1514052	0.1553
CLP-PEG vs. Unoperated	-284861	-1021014 to 451291	0.6265
CLP-PEG-MPC vs. Unoperated	-948877	-1685030 to -212725	0.008
β			
CLP-PEG vs. CLP-PEG-MPC	1718101	868065 to 2568136	<0.0001
CLP-PEG vs. Unoperated	-1166399	-1902551 to -430246	0.0009
CLP-PEG-MPC vs. Unoperated	-2884499	-3620652 to -2148347	<0.0001
α1(V)			
CLP-PEG vs. CLP-PEG-MPC	436061	-413975 to 1286097	0.4417
CLP-PEG vs. Unoperated	1092919	356767 to 1829072	0.0019
CLP-PEG-MPC vs. Unoperated	656859	-79294 to 1393011	0.09
α1(I)			
CLP-PEG vs. CLP-PEG-MPC	2167571	1317535 to 3017607	<0.0001
CLP-PEG vs. Unoperated	1169005	432853 to 1905158	0.0008

CLP-PEG-MPC vs. Unoperated	-998566	-1734719 to -262413	0.0049
α2(I)			
CLP-PEG vs. CLP-PEG-MPC	1077958	227922 to 1927994	0.0092
CLP-PEG vs. Unoperated	807574	71422 to 1543727	0.0281
CLP-PEG-MPC vs. Unoperated	-270384	-1006536 to 465769	0.656

Supplementary Table 10. Antibodies used for flow cytometry

Target	Antibody	Dilution Factor
CD11c	Brilliant Violet 650™ anti-mouse CD11c, (Clone: N418),(IsoType: Armenian Hamster IgG), (Reactivity: Mouse), (Format: BV650), (APP: FC), (Species: Hamster), Biolegend, 117339	1:1600
IA-IE (MHC Class II)	PerCP/Cy5.5 anti-mouse I-A/I-E,(Clone: M5/114.15.2),(IsoType: Rat IgG2b, κ),(Reactivity: Mouse),(Format: PerCP/Cy5.5),(APP: FC),(Species: Rat), Biolegend, 107626	1:3200
CD40	CD40, APC, clone: 1C10, eBioscience™, 501129392	1:400
CD80	PE anti-mouse CD80,(Clone: 16-10A1),(IsoType: Armenian Hamster IgG),(Reactivity: Mouse, Cross-Reactivity: Dog (Canine)),(Format: PE),(APP: FC),(Species: Hamster), Biolegend, 104708	1:100
CD86	FITC anti-mouse CD86,(Clone: GL-1),(IsoType: Rat IgG2a, κ),(Reactivity: Mouse),(Format: FITC),(APP: FC),(Species: Rat), Biolegend, 105006	1:50

Supplementary Table 11. Antibodies used for immunohistochemistry

Target	Antibody (or Lectin)	1:500
Mucin	Lectin from *Ulex europaeus* (gorse, furze) FITC conjugate, Sigma-Aldrich, L9006	1:50
Cytokeratin K3/K76	Anti-Keratin K3/K76 Antibody, clone AE5, Millipore, CBL218	1:500
α-SMA	Anti-alpha smooth muscle Actin antibody [1A4], AbCam, ab7817	1:100
LYVE1	Anti-LYVE1 antibody, AbCam, ab33682	1:100
CD172a	Mouse Anti Pig CD172a, Nordic BioSite, ST-MCA2312GA	1:100
Collagen V	Anti-Collagen V antibody, AbCam, ab134800	1:500
CD31	Anti-CD31 antibody, AbCam, ab28364	1:50
LL37	Anti-LL37/Cathelicidin antibody, LSBio, LS-B6696	1:100
Mouse IgG	Alexa Fluor® 488 AffiniPure Goat Anti-Mouse IgG (H+L), Jackson Immuno Labs, 115-545-146	1:1000
Rabbit IgG	Alexa Fluor® 488 AffiniPure Goat Anti-Rabbit IgG (H+L), Jackson ImmunoResearch Laboratories, 111-545-144	1:1000
CD9	CD9 Mouse anti-Bovine, Canine, Equine, Feline, Human, Mink, Mustelid, Non-human primate, Porcine, Rabbit, Clone: MM2/57, Invitrogen™, MA180307	1:100
Tsg101	Recombinant Anti-TSG101 antibody [EPR7130(B)], AbCam, ab125011	1:100
Rabbit IgG	IgG (H+L) Highly Cross-Adsorbed Goat anti-Rabbit, Alexa Fluor® 594, Invitrogen, A11037	1:1000
Mouse IgG	IgG (H+L) Highly Cross-Adsorbed Goat anti-Mouse, Alexa Fluor® Plus 647, Invitrogen™, PIA32728	1:1000

Chapter 4

Nanoengineering the surface of corneal implants: Towards functional anti-microbial and biofilm materials

Zohra Khatoon,[a] Irene Guzmán-Soto,[a] Christopher D. McTiernan,[a] Caitlin Lazurko,[a] Fiona Simpson,[b] Li Zhang,[c] David Cortes,[a] Thien-Fah Man,[c], May Griffith,[*bd] and Emilio I. Alarcon,[*ac]

[a] Division of Cardiac Surgery, University of Ottawa Heart Institute, 40 Ruskin Street, Ottawa, Canada. E-mail: Ealarcon@ottawaheart.ca

[b]Centre de Recherche Hôpital Maisonneuve-Rosemont, Montréal, QC, Canada. E-mail: May.Griffith@umontreal.ca

[c]Department of Biochemistry, Microbiology, and Immunology, Faculty of Medicine, University of Ottawa, Ottawa, Canada

[d]Département d'ophtalmologie, Université de Montréal, Montréal, QC, Canada

Abstract

We report the development and use of a light-mediated *in situ* grafting technology for the surface modification of biosynthetic corneal implants with peptide-capped nanoparticles (15–65 nm). The resulting materials have antimicrobial properties in bacterial suspension and also reduced the extent of biofilm formation. Our *in situ* grafting technology offers a rapid route for the introduction of antimicrobial properties to premoulded corneal implants, and potentially other soft implant targets.

Introduction

Bacterial infection of the cornea is a serious problem as it is the most frequent cause of infectious keratitis, often resulting in ulceration of the corneal surface and even blindness if the resulting damage is permanent.[1–6] While the most common cause of bacterial keratitis is contact lens wear,[7] other causes include physical trauma (introduction of foreign bodies due to mechanical injury or ocular surgery), burns (chemical, thermal), changes in the corneal surface (from dry eye, eyelid misdirection, and exposure), altered ocular defense mechanisms (from topical and systemic immune suppression), loose sutures with adjacent infections (blepharitis and viral keratitis), and corneal edema.[8,9]

Although antibiotic eyedrops are the current mainstay treatment, they have intrinsic limitations which relate to the ease at which they can be washed from the surface by tears[10–12] and the emergence of antibiotic resistance. As such, there has been a push to develop new treatments and antimicrobial agents that circumvent these limitations. A well-documented, but rarely employed agent displaying antibacterial activity is silver. While ionic silver (Ag^+) in the form of silver nitrate, silver sulfadiazine, and other ionic silver compounds have been historically used as topical antibacterial agent, more recently silver nanoparticles (AgNP) have been explored as the next iteration of the active component of these formulations by various groups including our team.[13–15] Furthermore, through careful consideration of the size, shape, and capping agent of the employed AgNP it has been observed that one can also limit the cytotoxicity usually observed upon use of ionic Ag agents.[16] Recently, the incorporation of antimicrobial structures, such as nanoparticles, in wearable devices, including contact lenses, has been explored as an option for imparting anti-infective properties.[17–19] While interesting, many of these materials and devices rely on impregnation or multistep chemical modifications of the implant to tether the antimicrobial component.[20,21] As such, potential clinical use of the devices can become limited due to modifications that change key physical properties of the implants or render the manufacturing process too difficult or costly.

Herein, we have developed a unique approach that allows for temporal and spatial control of the *in situ* incorporation of anti-infective AgNP onto corneal implants. The flexibility of our technology allows for surface grafting of premade implants in only minutes without the need for complex procedures or manufacturing protocols. Through evaluation of the safety and efficacy of our proposed surface modifications, we aim to highlight the promise our method holds over the more conventional approaches to the incorporation of anti-infective properties.

Results and discussion

A schematic depiction of the strategy employed for *in situ* grafting of peptide (CLKRS)-capped AgNP is presented in Fig. 1A. In our protocol, we have kept constant the ionic silver and precursor concentration within a range we have demonstrated high silver reduction with minimal side effects.[13,22] Our photo-grafting technique allows grafting of nanosilver onto biosynthetic premade corneal implants with only 5 min of irradiation. When comparing the plasmonic absorption for the grafted AgNP after 5 min of irradiation to that measured in colloidal solutions, see Fig. 1B left and middle; one can see a shift in the plasmonic absorption from 430 to z500 nm. Increasing the concentration of the peptide, however, does not change the kinetic profile for the surface plasmon band, see Fig. S1.†Further, upon *in situ* grafting the characteristic yellow colour of nanosilver is macroscopically observable in the implants as shown in Fig. 1B right. No opacity was observed in the surface modified corneal implants, which suggests that silver was fully stabilized in its nanometric form.

Preparation of the particles in the absence of the implants resulted in colloidal solutions in which increasing concentrations of CLKRS peptide resulted in AgNP with narrow size distributions and smaller diameters see Fig. 1C. This is reminiscent to recent findings reported by our group for the formation of colloidal CLKRS-capped spherical nanosilver via a two-step method involving capping agent exchange.23 Measurements for the nanoparticle sizes on the biosynthetic corneal implants did not indicate significant size differences between the different experimental groups (187 $\pm$ 29 nm, 181 $\pm$ 26 nm, and 192 $\pm$ 35 nm for 15, 20, and 100 mM CLKRS, respectively). The lack of significant differences should be cautiously considered as it is limited by the CRYO-SEM imaging resolution of the system used for imaging the gels.

When measuring the loading of total silver in the implants upon photo-grafting, we also found no trend in the total silver concentration as a function of increasing peptide loading (Fig. 1D). These results are in good agreement, and almost mirror, the relative abundance of silver nanostructures which were grafted onto the surface of the various implants (Fig. 1E), as semi-quantitatively illustrated in Fig. 1E right. Furthermore, grafting of the nanoparticles onto the corneal implants does not modify the mechanical properties of the implants as depicted in Fig. S2†. Fig. 2A shows the results of a proliferation assay for human corneal epithelial cells seeded onto implants without and with a grafted layer of peptide protected nanosilver. At day 1 postseeding, cell proliferation on nanosilver grafted surfaces prepared in the presence of 100 mM peptide was slower than that of the

other tested groups. However, by day 3, cell growth on all of the nanosilver grafted groups had surpassed that of the uncoated implant. A dendritic cell assay performed (n = 3 mice) showed that the AgNP did not activate dendritic cells. This illustrates that the AgNP grafted onto the implants are not likely to cause inflammation, as immature dendritic cells are tolerogenic (Fig. S3†). This agrees well with the multiplex cytokine analysis carried out on the tissue surrounding the area in which the various corneas were subcutaneously implanted in a murine model, see Fig. S4.†Analysis of proliferation and polarization of mononuclear derived bone marrow macrophages, Fig. 2B, showed that in the first three days post seeding there is very little proliferation observed in either the unmodified control implant or any of the three CLKRS–AgNP modified implants. However, at 7 days post-seeding there is a marked increase in the extent of proliferation. The lag in growth may have been caused by macrophage polarization, as it has been previously documented that these cells do not proliferate well during polarization.[24] In all cases, the tendency for monocytes to remain undifferentiated or polarized towards an anti-inflammatory or tolerogenic M2 macrophage phenotype was greater than the polarization towards pro-inflammatory M1 cells (n = 3) (Fig. 2C). In particular, the number of M1 macrophages was significantly reduced for the 100 mM peptide group when compared to the unmodified control. These findings are in line with the non-inflammatory activity of collagen-based biomimetic implants previously developed by our team members.[13,25]

Next, we assessed the antimicrobial potency of our *in situ* grafted implants, Fig. 3. First, we analyzed the extent to which the implants could eradicate bacteria in suspension. The data in Fig. 3A shows that upon *in situ* grafting of CLKRS–AgNP onto the implants, no surviving bacterial colonies (colony forming units per ml; CFU ml^{-1}) were detectable for any of the three bacterial strains assessed (*Pseudomonas aeruginosa* (PA), *Staphylococcus aureus* (SA), and *Staphylococcus epidermidis*). We next evaluated the ability of the surface grafted nanoparticles to delay biofilm formation, see Fig. 3B. Our results for air-liquid biofilms of PA and SA indicate that grafting of the surface with 100 mM CLKRS-capped nanosilver produced implants with reduced biofilm bacteria when compared to the unmodified control implant. Further experimentation was carried out using a human cornea-like model with a custom designed 3D printed artificial corneal chamber. The corneal implants were perfused with saline solution to form a "dome" with a geometry similar to that in the human eye, bacteria were then inoculated on the surface and then capped with a CLKRS–AgNP grafted implant. The entire system was then cultured overnight in a humidity chamber. The schematics for the 3D printed devices are shown in Fig. 3C (stl files are available from the authors upon request). Our mimetic model cornea system allows us to account for factors such as curvature and contact angle between the biofilm and the antimicrobial layer. Evaluation of

the number of surviving bacterial colonies was carried out using two standard techniques namely swabbing and sonication. For both sampling techniques, quantification of the number of surviving bacterial colonies after 17 h of incubation show that the AgNP grafted corneal implants have a significant lower number of colonies when compared to the unmodified control group (Fig. 3C right).

Conclusions

We have developed a simple and effective *in situ* method for the grafting of peptide-capped nanosilver, that within 5 minutes is capable to generating corneal implants with antimicrobial properties that were effective at eradicating *P. aeruginosa, S. aureus*, and *S. epidermidis*. Upon grafting with the CLKRS– AgNPs the implants were also shown to reduce the extent of biofilm formation for both *P. aeruginosa* and *S. aureus* bacteria. Future studies will look at incorporating multiarmed and multifunctional peptides for chemical tethering to other types of corneal implants; our *in situ* grafting approach presents an integrative technology that allows for excellent spatial control of nanosilver formation and could be expanded to antimicrobial grafting of other functional implants such as skin.

Experimental section

Chemicals and reagents

Silver nitrate ($AgNO_3$), 2-hydroxy-40-(2-hydroxyethoxy)-2-methylpropiophenone (I-2959), glycine, 25% glutaraldehyde solution, sodium hydroxide (NaOH), phosphate buffered saline (PBS), sodium citrate, sodium chloride (NaCl), 40,6-diamidino-2- phenylindole dihydrochloride (DAPI), 1,4-butanediol diglycidyl ether (BDDGE), lysogeny broth (LB) and tryptic soy broth (TSB) were purchased from Sigma-Aldrich and used without further purification. The pentapeptide CLKRS was purchased from CanPeptide. Theracol porcine type I collagen solution was purchased from Sewon Cellontech Co Ltd. Solutions were prepared with Milli-Q water, unless otherwise noted. Other cell culture media and reagents such as Dulbecco's modified Eagle Medium (DMEM), keratinocyte media, fetal bovine serum etc. were purchased from Thermo Fisher Scientific unless otherwise specified.

Collagen based cornea-like hydrogel synthesis

Hydrogels of 500 mm or 200 mm thicknesses were prepared using type I medical grade porcine collagen solution. Briefly, 10% w/v collagen solutions were crosslinked using 1,4-butanediol diglycidyl ether (BDDGE) after neutralization of the collagen solution. Gels were cast into hemispherical moulds or between two glass plates and allowed to cure in a humidity chamber at 4°C for 18–20 h. Once solidified, gels were stored in sterile PBS at 4°C.

in situ synthesis of CLKRS capped AgNP

in situ formation of CLKRS capped AgNP was performed using 3 formulations. Briefly, collagen-based cornea like gels were washed with Milli-Q water and then dried. 2 mL of selected formulation containing 15, 20 or 100 mMof the peptide (mixture of CLKRS peptide, silver nitrate and Irgacure-2959) was then added to a weighing boat containing the gel to be modified. The solution was then irradiated in a UVA photoreactor (Luzchem) for 5 minutes. Gels were then washed with Milli-Q water and sterile PBS three times.

Surface plasmon band spectra

Surface plasmon band spectra were recorded using a SpectraMax M2 (Molecular Devices) microplate reader. Samples were prepared and kept in a 96 well plate which was then measured directly in the plate reader from 350–700 nm. Scanning electron microscopy (SEM) Cryo-SEM images were taken at -50°C using a Tescan (Model: Vega II-XMU) equipped with a cold stage sample holder, a backscatter electron detector (BSE) and a secondary electron detector (SED).

Transmission electron microscopy (TEM)

TEM images of the CLKRS–AgNP solutions were prepared from 10× diluted samples. 10 mL of each of the formulations was dropped onto carbon mesh copper grids and allowed to rest for 10 min. The solution was removed, and grids were dried in a vacuum desiccator for 2–3 days. Images were obtained using a FEI Tecnai G2 F20 TEM operating at 75 kV. All samples were measured in triplicate.

Dynamic light scattering (DLS)

Hydrodynamic size and zeta potential of the CLKRS–AgNP was measured using a Malvern Zetasizer Nano ZS at room temperature in 1.0 cm path-length disposable plastic cuvettes. Samples were measured in triplicate and values correspond to the average of three measurements.

Young's modulus

Cornea-like gels with and without surface functionalization with CLKRS–AgNP were prepared as sheets and cut into strips of 3 cm length and 5 mm width. Using an Instron 3342 instrument the gels were then extended until fracture. The Young's modulus was calculated from the resulting stress–strain curve.

Microbiology assays

Bacteria cultures. Bacteria cultures were prepared using 10 mL of the bacterial suspension, initially stored in -80°C, streaked on a LB agar plate in a 2-phase streaking pattern and incubated for 16 h at 37°C. After single colonies had grown on the agar plate, a single colony was resuspended in 2mL of 100
LB agar broth and incubated in an orbital shaker incubator for 16–18 h at 225 rpm and 37°C. The treated cornea gels (500 mm thickness, 5 mm diameter) were placed in a 24-well plate and 1.5 mL of 10^5 CFU mL^{-1} of *P. aeruginosa* PA14, *S. aureus* (ATCC 25923) and *S. epidermidis* (ATCC 35984), were added in each well and incubated for 16 h. They were then plated on LB agar and quantified by CFU counting.

Biofilm assays. Biofilms of *P. aeruginosa* PA14, *S. aureus* and *S. epidermidis* were grown on the control and treated gels and quantified by counting CFU. *P. aeruginosa* cells were cultured in 5 mL LB medium whereas *S. aureus* and *S. epidermidis* were cultured in 5 mL TSB medium overnight at 37°C. The cultures of PA14 were then diluted with M63 medium whereas *S. aureus* and *S. epidermidis* cultures were diluted with TSB + 0.5% glucose. *P. aeruginosa* biofilms were grown for 6 h and staphylococci biofilms were grown for 22 h. The biofilms were cultured in a 12-well microtiter plate using an air–liquid interface at 37°C and then plated on LB agar plates.

Bacteria cornea like-system test. 3D printed artificial anterior chambers were used in this part of our work. Cornea-like gels (synthetic cornea) were prepared as cornea-like and flat sheets (500 mm thickness, cut into circular discs with 10 mm diameter). This biosynthetic corneas were inoculated with bacteria and then small circular disc shaped gels functionalized with CLKRS–AgNP were mounted into the cornea holders. After 17 h the upper discs were removed and abundantly washed with PBS. Using an inoculation loop the surface of the corneas was swabbed and plated on LB agar to ensure there was no prior contamination on the surface. These corneas were then inoculated with 1×10^7 CFU mL^{-1} of *P. aeruginosa* PAO1 and incubated in a humidity chamber for 17 h at 37°C. Control and treated gels were swabbed and plated on LB agar or sonicated for 15 min in sterile saline and plated on a LB agar plate.

Cell assays

Human cornea derived epithelial cells. The *in vitro* compatibility of CLKRS-capped AgNP grafted corneas were tested using green fluorescence protein (GFP) transfected immortalized human corneal epithelial cells (HCECs).26,27 Briefly, CLKRScapped nanosilver corneas and unmodified control gels were fitted into a 96 well plate. The gels were washed with sterile 1× PBS for 12 h, followed by 3 h in keratinocyte serum free media (K-SFM). 2500 cells per well were then seeded into each well in K-SFM media. The cells were cultured for 3 days, with half the media being exchanged every second day. Images were captured on a NanoEntek Juli Br&Fl microscope and quantified using ImageJ.

Murine bone marrow derived macrophages and polarization assay. Macrophages were isolated as previously described28 with ethical permission from the Animal Care and Use Committee of the Ottawa Heart Research Institute. Briefly, bone marrowderived macrophages (BMDMs) were generated from the tibial bones of C57BL/6 female mice (8–10 weeks old). BMDMs were maintained for 1 week in DMEM with 10% FBS, 15% L929 media containing macrophage colony-stimulating factor and penicillin–streptomycin.

For the assay, BMDM precursors from female C57BL/6 mice (8–10 weeks old) were used. The wells of a 24-well culture plate were fitted with the modified and unmodified corneal implants. The hydrogel was washed 3 times with 1mL of 1× PBS, followed by two additional 1 mL rinses with media before the seeding of cells. The BMDMs were seeded into the control wells and onto the material at a density of 20 000 cells per well in a 48-well plate. The plate was then placed in a humidified incubator at 37°C and 5% CO2 with the media in each well being exchanged every 48 h up to 7 days. Images were captured and quantified at day 0, 1, 3, and 7. On day 7 the wells were processed for immunofluorescence analysis to determine their polarization towards either an M1 or M2 phenotype. Briefly, media was removed, wells were washed 2× with Hank's buffer, and then cells were fixed with a solution of 4% PFA in 1× PBS at 4°C in the dark. Fixative was removed and wells were washed 2× with NH4Cl in PBS, waiting 7 minutes between washes. The samples were then washed 3× with 1× PBS. On the final wash 0.2% NaN3 was added from a 2% NaN3 stock (10 mL/1 mL). When ready for staining, samples were washed with PBS and then blocked and permeabilized using a 2% BSA in PBS solution containing 0.5% Triton X-100 for 1.5 h at RT. Primary antibodies for CD206 and CD86 were then diluted appropriately and added to the well plate to incubate overnight covered in foil at 4°C. The next day wells were washed with 1× PBS. Secondary antibodies were diluted and added to the plate and incubated at RT covered in foil for 1

h. After 1 h of incubation with the secondary antibodies, the wells were washed 3× with 1× PBS. The coverslips were removed from the wells and mounted onto a glass slide using Prolong^{TM} Gold antifade reagent with DAPI (Invitrogen, P36931). Cells were imaged with a Zeiss Axiovert 200M Fluorescence microscope equipped with an AxioCam MR camera using 63× oil immersion objective. The filters employed were DAPI blue filter (Ex: 352–402 nm/Em: 417–477 nm), GFP green filter (Ex: 457–487 nm/Em: 502–538 nm), Texas Red filter (Ex: 542–582 nm/Em: 604–644 nm). For quantification, 4 random microscopic images were obtained from each well and the number of M2 and M1 macrophages was quantified using ImageJ software.

Dendritic cells. Ethical permission for this assay was obtained from the Animal Care and Use Committee of Maisonneuve-Rosemont Hospital. The tibia and femur of male, 6–12 week old, C57BL/6J mice were removed and the bone marrow was isolated.[29] Red blood cells in the marrow were lysed using ammonium chloride solution (155 mM NH4Cl, 10 mM KHCO3). Cells (1×10^6 cells per well) were seeded onto suspension culture plates in complete RPMI 1640 (RPMI-C) containing 10% containing 10% (v/v) fetal bovine serum (Wisent), 0.5 mg mL^{-1} penicillin–streptomycin–glutamine, 10 mM HEPES, 1 mM sodium pyruvate, 55 mM b-mercaptoethanol with 25 ng mL^{-1} granulocyte-macrophage colonystimulating factor (GM-CSF) (all Gibco, ThermoFisher, Waltham, MA, USA). The cells were maintained in culture for six days and half of the media was exchanged for fresh RPMI-C containing 50 ng mL^{-1} GM-CSF on days two and three. The hydrogels (9 mm diameter, 200 mm thick) were pre-incubated overnight in 2 mL of RPMI-C before being transferred into 1 mL of fresh RPMI-C on a 24-well plate. The cells were selected using a Histodenz^{TM} density gradient (Sigma-Aldrich, St. Louis, MO) and seeded on the hydrogels at a density of 1×10^6 cells per well in a total volume of 2 mL for materials testing. Lipopolysaccharide (1 mg mL^{-1}) was used as a positive control for BMDC activation and untreated cells were used as a negative control. The cells were labelled with direct-conjugate antibodies for CD11c, IA/IE CD40, CD80 and CD86 (Table S1†) and Zombie Aqua^{TM} Fixable Viability Kit (BioLegend, San Diego, CA). Flow cytometry was performed with a BD LSR II and analyzed using FlowJo v10.6.1 (Becton, Dickinson & Company, Franklin Lakes, NJ, USA). The cells were gated using Zombie Aqua and CD11c as markers of a live, dendritic cell phenotype (see Fig. S5†for a gating example). A histogram of the fluorescent intensity of CD40, CD80 and CD86 was obtained and the mean fluorescent intensity was transformed into a ratio over the untreated BMDC control for analysis. The *in vitro* statistical analysis for BMDCs was performed using a one-way ANOVA with Holm–Sidak multiple comparison test (GraphPad Prism 8.4.1, GraphPad Software, LLC., San Diego, CA, USA). The unit of analysis was the mouse (n = 3, per group).

Animal surgery

All *in vivo* studies were conducted with ethical approval from the University of Ottawa Animal Care Committee and in compliance with the National Institutes of Health Guide for the Use of Laboratory Animals. Female C57BL/6J mice 8 weeks, each weighing 20–25 g, were chosen to assess the cytokine activation to the implanted hydrogels. The materials were prepared under sterile conditions and 6 mmc ircular pieces were cut. During the surgical procedure, mice were anesthetized with 3% isflurane through a nose cone inhaler and their backs shaved and washed with betadine/70% ethanol. Paravertebral incisions were made 1.0 cm away from the vertebral column to create subcutaneous pockets by blunt dissection using hemostats. Then, the pieces of the materials were implanted (n = 4 per group, 4 animals for 72 h) and the incision closed with a 5.0 silk suture. Sham group underwent the surgical procedure but without the implant insertion (n = 3). All animals were observed for signs of inflammation and pain was managed by Buprenorphine administered post-surgery. Mice were euthanized after 72 h. Implants and skin surrounding pocket were collected to run cytokine array.

Cytokine assay

After collection at 72 h post-implantation, surrounding tissue and implant samples were homogenized and processed for protein analysis. Multiplex analysis of protein concentrations for 14 growth factors/cytokines [granulocyte-macrophage colony-stimulating factor (GM-CSF), macrophage colonystimulating factor (M-CSF), tumor necrosis factor alpha (TNFα), EMMPRIN, vascular endothelial growth factor (VEGF), epidermal growth factor receptor (EGF-R), interleukin 3 (IL3), interleukin 6 (IL6), interleukin 1 alpha (IL1-α), interferon gamma (IFN-γ), matrix metallopeptidase 2 (MMP2), matrix metallopeptidase 9 (MMP9), matrix metallopeptidase 12 (MMP12) and basic fibroblast growth factor (FGF-basic)] was performed with the Luminex 200 platform built on xMAP technology (Luminex Corp.) using specific magnetic beads, according to the manufacturer's instructions. All the treated samples were normalized to control which was plotted and compared amongst the treatment groups.

Silver content quantification

Silver content of treated cornea-like gels and the silver content in each of the mice organs collected were measured by inductively coupled plasma-mass spectroscopy. For the gels, samples were prepared and synthetized with CLKRS–AgNP and then freeze-dried for seven days. Similarly, the organs from mice were harvested, frozen, and freeze-dried for seven days. The samples were

digested in a DigiPREP MS system (SCP Science) and silver concentration was determined by inductively coupled plasma-mass spectroscopy (ICP-MS; Agilent 7700x) by monitoring the 107 m/z signal (100 ms integration), using Argon as a carrier gas (0.85 mL min^{-1}, Ar plasma gas flow: 15 L min^{-1}). The final concentration of silver in each sample tissue were measured in mg kg^{-1} and plotted.

Statistical analysis

All tests mentioned above were repeated a minimum of 3 times in batches of 3 or 4. All data are presented as mean ± standard deviation. The statistical analysis was performed using one-way ANOVA with Holm's post-hoc in Kaleida graph or Holm-Sidak multiple comparison GraphPad.

Conflicts of interest

The authors state there are no conflicts to declare.

Acknowledgements

This work was funded by the Canadian Institutes of Health Research (CIHR) to MG & EIA. EIA thanks the support of the Ministry of Economic Development, Job Creation and Trade for an Early Researcher Award and to the Natural Sciences and Engineering Research Council of Canada for a Discovery Grant. The authors thank Dr Francois Xavier Gueriot for providing insights on the design of the 3D holder.

References

(1) L. Ung, P. J. M. Bispo, S. S. Shanbhag, M. S. Gilmore and J. Chodosh, *Surv. Ophthalmol.*, 2019, 64, 255–271.

(2) S. Watson, M. Cabrera-Aguas and P. Khoo, *Aust. Prescr.*, 2018, 41, 67–72.

(3) A. Shah, A. Sachdev, D. Coggon and P. Hossain, *Br. J. Ophthalmol.*, 2011, 95, 762–767.

(4) J. C. Hernandez-Camarena, E. O. Graue-Hernandez, M. Ortiz- Casas, A. Ramirez-Miranda, A. Navas, L. Pedro-Aguilar, N. L. Lopez-Espinosa, C. Gaona-Juarez, L. A. Bautista- Hernandez and V. M. Bautista-de Lucio, *Cornea*, 2015, 34, 778–785.

(5) G. Varaprasathan, K. Miller, T. Lietman, J. P. Whitcher, V. Cevallos, M. Okumoto, T. P. Margolis, M. Yinghui and E. T. Cunningham Jr, *Cornea*, 2004, 23, 360–364.

(6) R. Farias, L. Pinho and R. Santos, *Rev. Bras. Oftalmol.*, 2017, 76, 116–120.

(7) A. Lin, M. K. Rhee, E. K. Akpek, G. Amescua, M. Farid, F. J. Garcia-Ferrer, D. M. Varu, D. C. Musch, S. P. Dunn and F. S. Mah, *Ophthalmology*, 2019, 126, P1–P55.

(8) T. Bourcier, F. Thomas, V. Borderie, C. Chaumeil and L. Laroche, *Br. J. Ophthalmol.*, 2003, 87, 834–838.

(9) S. Egrilmez and S. Yildirim-Theveny, *Clin. Ophthalmol.*, 2020, 14, 287–297.

(10) V. Agrahari, A. Mandal, V. Agrahari, H. M. Trinh, M. Joseph, A. Ray, H. Hadji, R. Mitra, D. Pal and A. K. Mitra, *Drug Delivery Transl. Res.*, 2016, 6, 735–754.

(11) N. M. Davies, *Clin. Exp. Pharmacol. Physiol.*, 2000, 27, 558– 562.

(12) S. S. Chrai, T. F. Patton, A. Mehta and J. R. Robinson, *J. Pharm. Sci.*, 1973, 62, 1112–1121.

(13) E. I. Alarcon, B. Vulesevic, A. Argawal, A. Ross, P. Bejjani, J. Podrebarac, R. Ravichandran, J. Phopase, E. J. Suuronen and M. Griffith, *Nanoscale*, 2016, 8, 6484–6489.

(14) L. J. Luo, T. Y. Lin, C. H. Yao, P. Y. Kuo, M. Matsusaki, S. G. Harroun, C. C. Huang and J. Y. Lai, *J. Colloid Interface Sci.*, 2019, 536, 112–126.

(15) T. Mokabber, H. T. Cao, N. Norouzi, P. van Rijn and Y. T. Pei, *ACS Appl. Mater. Interfaces*, 2020, 12, 5531–5541.

(16) M. Vignoni, H. de Alwis Weerasekera, M. J. Simpson, J. Phopase, T.-F. Mah, M. Griffith, E. I. Alarcon and J. C. Scaiano, *Nanoscale*, 2014, 6, 5725–5728.

(17) X. W. Tan, T. W. Goh, P. Saraswathi, C. L. Nyein, M. Setiawan, A. Riau, R. Lakshminarayanan, S. Liu, D. Tan, R. W. Beuerman and J. S. Mehta, Antimicrob. *Agents Chemother.*, 2014, 58, 5229–5238.

(18) D. Dutta, A. K. Vijay, N. Kumar and M. D. Willcox, *Invest. Ophthalmol. Visual Sci.*, 2016, 57, 5616–5624.

(19) D. Dutta, B. Kamphuis, B. Ozcelik, H. Thissen, R. Pinarbasi, N. Kumar and M. D. P. Willcox, *Optom. Vis. Sci.*, 2018, 95, 937–946.

(20) O. Gherasim, A. M. Grumezescu, V. Grumezescu, F. Iordache, B. S. Vasile and A. M. Holban, *Materials*, 2020, 13, 768.

(21) A. Besinis, S. D. Hadi, H. R. Le, C. Tredwin and R. D. Handy, *Nanotoxicology*, 2017, 11, 327–338.

(22) E. I. Alarcon, K. Udekwu, M. Skog, N. L. Pacioni, K. G. Stamplecoskie, M. Gonz´alez-B´ejar, N. Polisetti, A. Wickham, A. Richter-Dahlfors, M. Griffith and J. C. Scaiano, *Biomaterials*, 2012, 33, 4947–4956.

(23) H. Poblete, A. Agarwal, S. S. Thomas, C. Bohne, R. Ravichandran, J. Phopase, J. Comer and E. I. Alarcon, *Langmuir*, 2016, 32, 265–273.

(24) L. Liu, Y. Lu, J. Martinez, Y. Bi, G. Lian, T. Wang, S. Milasta, J. Wang, M. Yang, G. Liu, D. R. Green and R. Wang, *Proc. Natl. Acad. Sci. U.S.A.*, 2016, 113, 1564–1569.

(25) S. McLaughlin, B. McNeill, J. Podrebarac, K. Hosoyama, V. Sedlakova, G. Cron, D. Smyth, R. Seymour, K. Goel, W. Liang, K. J. Rayner, M. Ruel, E. J. Suuronen and E. I. Alarcon, *Nat. Commun.*, 2019, 10, 4866.

(26) K. Araki-Sasaki, Y. Ohashi, T. Sasabe, K. Hayashi, H. Watanabe, Y. Tano and H. Handa, *Invest. Ophthalmol. Visual Sci.*, 1995, 36, 614–621.

(27) P. Bedford, J. Jy, L. Collins and S. Keizer, *Front. Med.*, 2018, 5, 118.

(28) J. Weischenfeldt and B. Porse, *Cold Spring Harb. Protoc.*, 2008, 2008, pdb.prot5080.

(29) A. Madaan, R. Verma, A. T. Singh, S. K. Jain and M. Jaggi, J. *Biol. Methods*, 2014, 1, e1.

Figure Legends

Fig. 1 Synthesis and characterization of CLKRS–AgNP grafted collagen-based corneal implants. (A) Schematic depiction for the in situ grafting of CLKRS–AgNP to the surface of collagen implants. The nanoparticle precursors used in the study correspond to: Irgacure- 2959 (I-2959), silver nitrate ($AgNO_3$), and the CLKRS peptide. (B) Left: Surface plasmon absorption for the AgNP prepared using three different nanoparticle concentrations of the CLKRS peptide measured in colloidal solution. Middle: Surface plasmon absorption of the CLKRS capped AgNP grafted *in situ* onto the surface of the implant. Right: Representative images of the *in situ* CLKRS–AgNP grafted implants. Scale bar in all images correspond to 5 mm. (C) Average size of colloidal AgNP prepared in the presence of different concentrations of the CLKRS peptide. Diameters were calculated from measuring >100 individual particles. (D) Total silver content per g of dried implants whose surfaces were modified with nanosilver in the presence of increasing concentration of CLKRS. n = 3–4 samples per group, analysis was conducted using ICP-MS, see experimental. (E) Left: Representative CRYO-SEM images of the implant surface without and with *in situ* grafted nanosilver prepared using different CLKRS concentrations. Scale bars correspond to 5 mm in all cases. Right: Number of nanoparticles per field of view (FOV) counted on the surfaces of implants prepared using the three different CLKRS concentrations employed in this study. Counting was carried out in 3 randomly selected regions of the implants. Values in plots C and D are represented as box plots. The bars extending from the top and bottom of each box mark the minimum and maximum values with the data set that fall within an acceptable range. p values were calculated using one-way ANOVA followed by Holms post hoc analysis.

Fig. 2 *in vitro* cell compatibility assays for CLKRS–AgNP grafted corneal implants. (A) Number of human dermal epithelial cells (GFP+) per field of view (FOV) counted at 1- and 3 days post-seeding. (B) Number of macrophages per FOV counted at different time points, up to 7 days, post-seeding of bone marrow derived mouse macrophages. (C) Number of positive stained M1 or M2 macrophages per FOV counted after 7 days post-seeding on the corneal implants prepared with different concentrations of the CLKRS peptide. Values in plots are represented as box plots. The bars extending from the top and bottom of each box mark the minimum and maximum values with the data set that fall within an acceptable range. p values were calculated using one-way ANOVA followed by Holms post hoc analysis. Sample sizes were n = 4, n = 3, n = 4, and n = 4 for A, B, C and D, respectively.Fig. 2 *in vitro* cell compatibility assays for CLKRS–AgNP grafted corneal implants. (A) Number of human dermal epithelial cells (GFP+) per field of view (FOV) counted at 1- and 3 days post-seeding. (B) Number of macrophages per FOV counted at different time points,

up to 7 days, post-seeding of bone marrow derived mouse macrophages. (C) Number of positive stained M1 or M2 macrophages per FOV counted after 7 days post-seeding on the corneal implants prepared with different concentrations of the CLKRS peptide. Values in plots are represented as box plots. The bars extending from the top and bottom of each box mark the minimum and maximum values with the data set that fall within an acceptable range. p values were calculated using one-way ANOVA followed by Holms post hoc analysis. Sample sizes were n = 4, n = 3, n = 4, and n = 4 for A, B, C and D, respectively.

Fig. 3 Biomimetic assays for the antimicrobial properties of the CLKRS–AgNP grafted corneal implants. (A) Number of surviving colonies in solution for different bacterial strains. Colonies were counted after 16 h of incubation in LB media. Initial seeding inoculum was 1×10^5 CFU mL^{-1} from an overnight culture. (B) Number of surviving colonies. Overnight cultures of Pseudomonas aeruginosa were diluted with M63 medium whereas Staphylococcus aureus overnight cultures were diluted with TSB + 0.5% glucose. *P. aeruginosa* biofilms were grown for 6 h and staphylococci biofilms were grown for 22 h. The biofilms were cultured using an air–liquid interface at 37°C and plated on LB agar plates. (C) Left: 3D render of the chamber used for the ex vivo testing of the antimicrobial corneal implants. The numbers in the figure correspond the different parts of the chamber: (1) securing cap, (2) perfusion chamber, (3) inflow channel (4) outflow channel. Middle: Photograph of an assembled chamber. The corneal implant is positioned at the centre of the chamber (5) and the fluid is pressurized to form a cornea-like curvature. Right: Number of colonies recovered from the implants (initial seeding inoculum 1×10^7 CFU mL^{-1}) after 17 h at 37°C. Samples from the corneas were collected through swabbing or upon 15 min of sonication in sterile saline and plated on LB agar plates. In all the plots, the bars extending from the top and bottom of each box mark the minimum and maximum values with the data set that fall within an acceptable range. p values were calculated using one-way ANOVA followed by Holms post hoc analysis The 0 mM CLKRS groups correspond to non-grafted corneal implants. Sample sizes were n = 4, n = 3, and n = 4 for A, B, and C, respectively.

Supplementary Figure Legends

Figure S1. Changes in the surface plasmon band (SPB) absorption as a function of the irradiation time for nanoparticles prepared at different peptide concentrations prepared onto the corneal implants. Samples were measured at their respective SPB maximun. Error bars correspond to standard deviation from the mean (n=4), measured at room temperature.

Figure S2. Young modulus for corneal implants before and after nanosilver-peptide grafting. Error bars correspond to standard deviation from the mean (n=5-7), measured at room temperature.

Figure S3. Expression of CD40, CD80, or CD86 relative to untreated BMDCs for the different experimental groups. Cells were precultured on the corneal implants with and without the peptide-nanosilver prepared at different peptide concentration.

Figure S4. Relative to control cytokine levels measured by multiplex sample analysis (n=3). Samples were measured after 72h post-subcutanous implantation (see experimental). In all cases, but for MMP12 (20 vs 100 μM CLKRS) there were no significant differences.

Figure S5. A representative example of the gating strategy used in the dendritic cell experiments.

Figures

Figure 1.

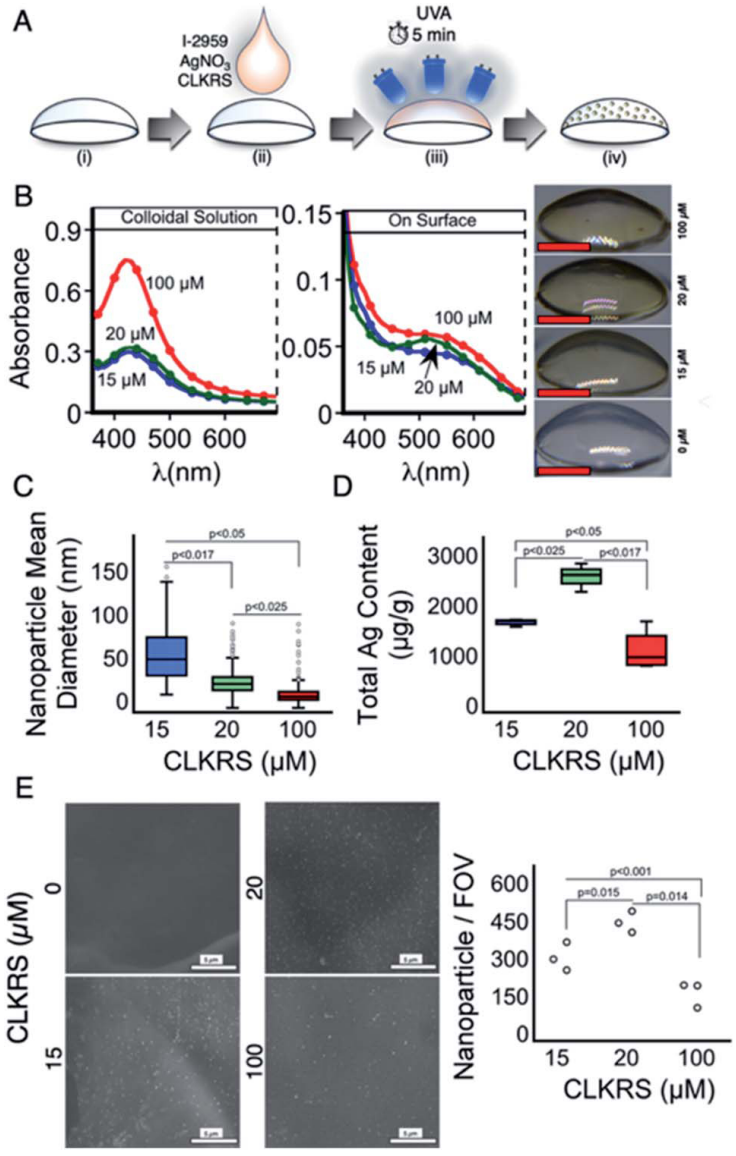

Figure 2.

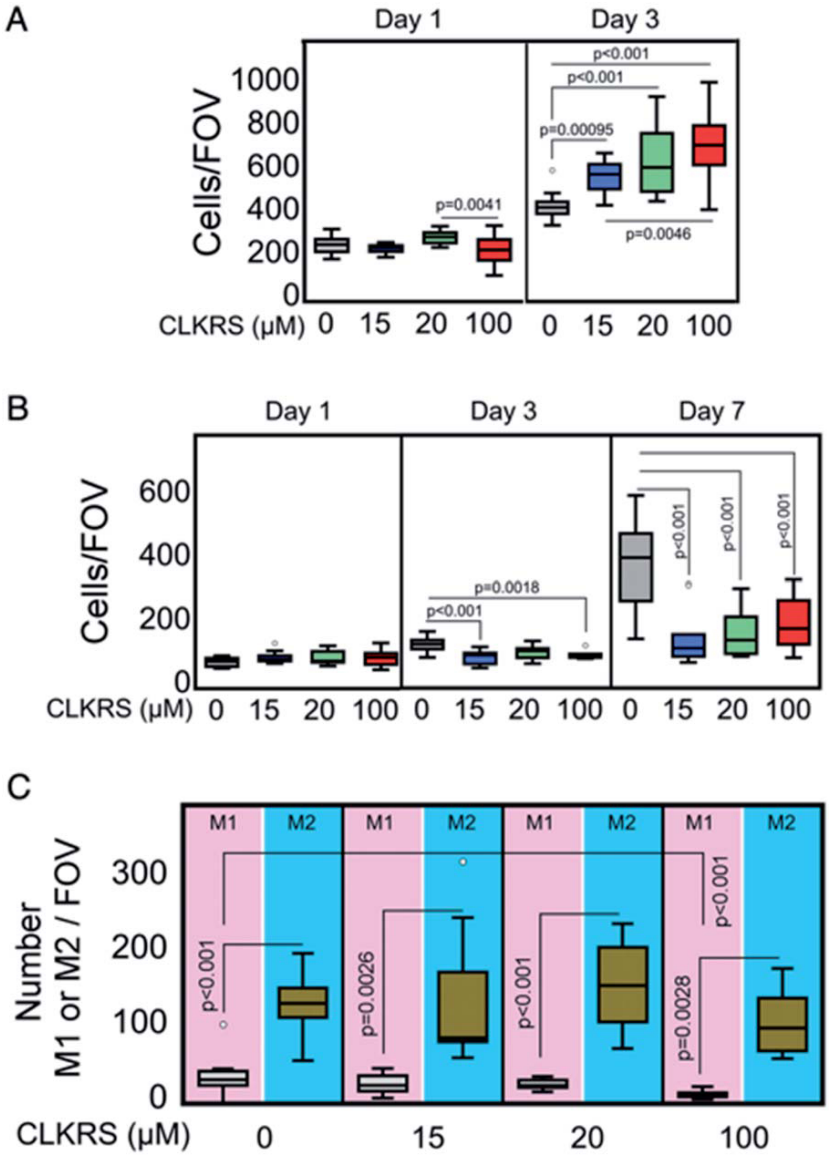
A
Day 1
Day 3
Cells/FOV
1000
800
600
400
200
0
p<0.001
p<0.001
p=0.00095
p=0.0041
p=0.0046
CLKRS (μM) 0 15 20 100 0 15 20 100
B
Day 1
Day 3
Day 7
Cells/FOV
600
400
200
0
p=0.0018
p<0.001
p<0.001
p<0.001
p<0.001
CLKRS (μM) 0 15 20 100 0 15 20 100 0 15 20 100
C
M1
M2
Number
M1 or M2 / FOV
300
200
100
0
p<0.001
p=0.0026
p<0.001
p<0.001
p=0.0028
CLKRS (μM) 0 15 20 100

Figure 3.

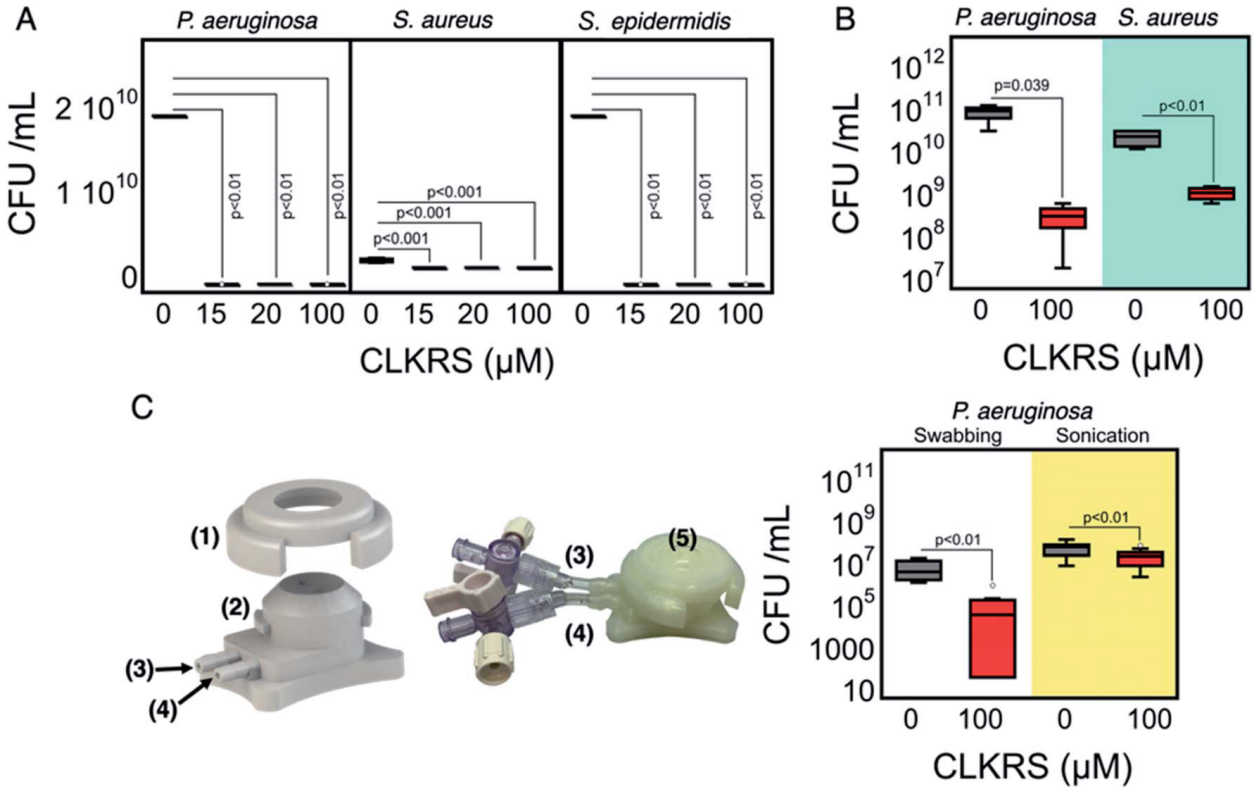
A
P. aeruginosa
S. aureus
S. epidermidis
CFU /mL
2 10^10
1 10^10
0
p<0.01
p<0.001
0 15 20 100 0 15 20 100 0 15 20 100
CLKRS (µM)
B
P. aeruginosa
S. aureus
CFU /mL
10^12
10^11
10^10
10^9
10^8
10^7
p=0.039
p<0.01
0 100 0 100
CLKRS (µM)
C
(1)
(2)
(3)
(4)
(5)
P. aeruginosa
Swabbing
Sonication
CFU /mL
10^11
10^9
10^7
10^5
1000
10
p<0.01
0 100 0 100
CLKRS (µM)

Supplementary Figures

Figure S1.

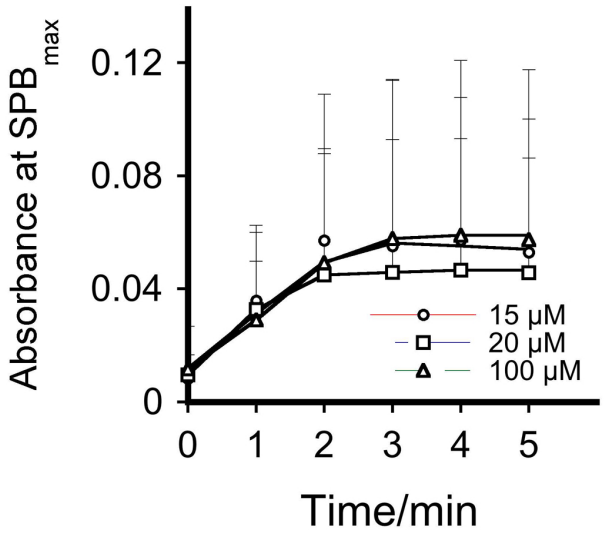

Figure S2.

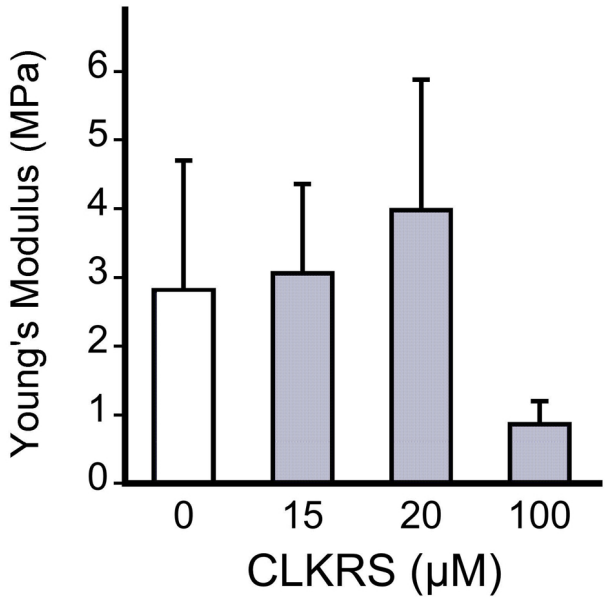

Figure S3.

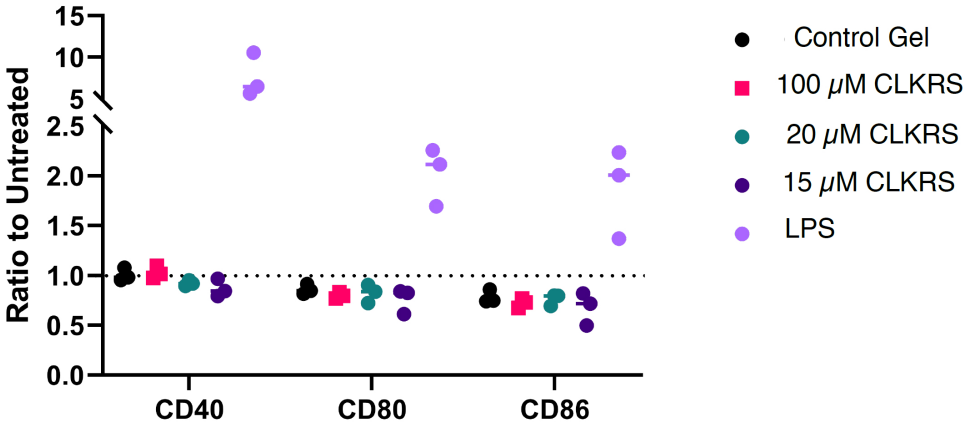
Ratio to Untreated
15
10
5
2.5
2.0
1.5
1.0
0.5
0.0
CD40
CD80
CD86
Control Gel
100 μM CLKRS
20 μM CLKRS
15 μM CLKRS
LPS

Figure S4.

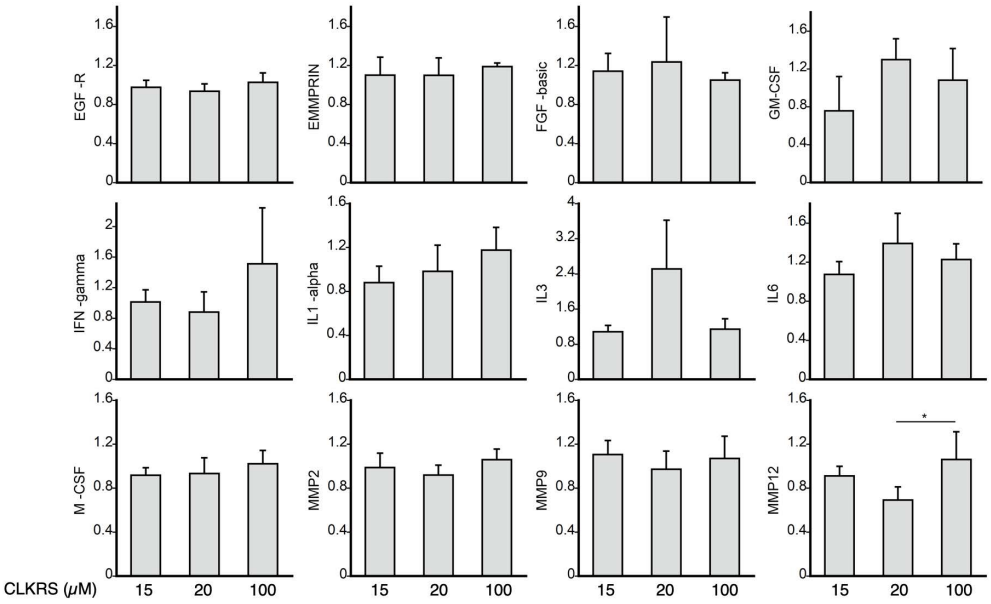
EGF -R
EMMPRIN
FGF -basic
GM-CSF
IFN -gamma
IL1 -alpha
IL3
IL6
M -CSF
MMP2
MMP9
MMP12
*
CLKRS (μM)
15
20
100

Figure S5.

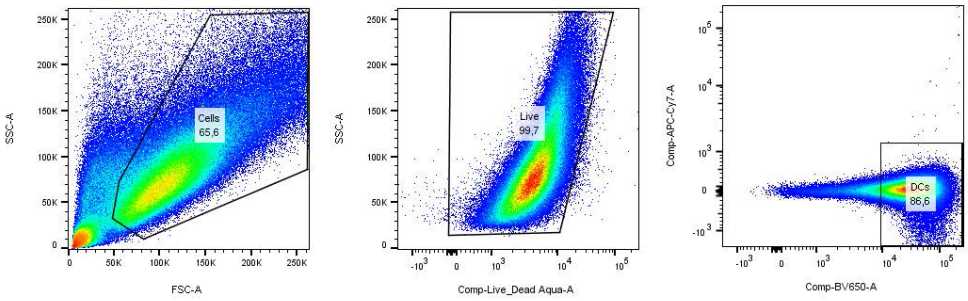
SSC-A
FSC-A
Cells
65,6
SSC-A
Comp-Live_Dead Aqua-A
Live
99,7
Comp-APC-Cy7-A
Comp-BV650-A
DCs
86,6

Supplementary Table

Table S1. Antibodies for Flow Cytometry

Target	**Antibody**	**Dilution Factor**
CD11c	Brilliant Violet 650^{TM} anti-mouse CD11c,(Clone: N418),(IsoType: Armenian Hamster IgG),(Reactivity: Mouse),(Format: BV650),(APP: FC),(Species: Hamster), Biolegend, 117339	1/1600
IA-IE (MHC Class II)	PerCP/Cy5.5 anti-mouse I-A/I-E,(Clone: M5/114.15.2), (IsoType: Rat IgG2b, κ), (Reactivity: Mouse),(Format: PerCP/Cy5.5), (APP: FC), (Species: Rat), Biolegend, 107626	1/3200
CD40	CD40, APC, clone: 1C10, eBioscience^{TM}, 501129392	1/400
CD80	PE anti-mouse CD80,(Clone: 16-10A1),(IsoType: Armenian Hamster IgG),(Reactivity: Mouse, Cross-Reactivity: Dog (Canine)),(Format: PE),(APP: FC),(Species: Hamster), Biolegend, 104708	1/100
CD86	FITC anti-mouse CD86,(Clone: GL-1),(IsoType: Rat IgG2a, κ),(Reactivity: Mouse),(Format: FITC),(APP: FC),(Species: Rat), Biolegend, 105006	1/50

Chapter 5

Electron-Beam Irradiated Recombinant Human Collagen-Phosphorylcholine Corneal Implants Retain Pro-Regeneration Capacity

Fiona Simpson[1,2,3,†], M. Mirazul Islam[1,5,†], Oleksiy Buznyk[1,6,†], Elle Edin[1,2,3,7], Monika Kozak-Ljunggren[1], Federica M. Magrelli[8], Dina B. AbuSamra[5], Palbo Argüeso[5], James Chodosh[5], Aneta Liszka[1], Per Fagerholm[1,†], May Griffith[1,2,3*]

[1]Department of Clinical and Experimental Medicine, Linköping University, Linköping, Sweden

[2]Maisonneuve-Rosemont Hospital Research Centre, Montréal, Québec, Canada

[3]Department of Ophthalmology, and Institute of Biomedical Engineering, Université de Montréal, Montréal, Quebec, Canada

[4] Centre de Recherche - Centre hospitalier de l'Université de Montréal, Montréal, Quebec, Canada

[5] Disruptive Technology Laboratory, Massachusetts Eye and Ear and Schepens Eye Research Institute, Department of Ophthalmology, Harvard Medical School, Boston, MA, USA.

[6]Filatov Institute of Eye Diseases and Tissue Therapy of the NAMS of Ukraine, Odessa 65061, Ukraine.

[7]Department of Polymer Chemistry, Uppsala University, Uppsala, Sweden.

[8]Interdepartmental Centre for Regenerative Medicine "Stefano Ferrari", University of Modena and Reggio Emilia, Modena, Italy.

[†]Equivalent contribution

* Correspondence:

May Griffith

May.Griffith@umontreal.ca

Keywords: collagen, implant, e-beam, irradiation, rabbits, cornea

Abstract

Sterilization of biodegradable, protein-based implants is challenging as conventional terminal sterilization methods can impact their performance in clinical use. Electron beam (e-beam) irradiation is a terminal sterilization method that has been used for biologically-derived implants. Here, e-beam doses of 17 kGy, 19 kGy or 21 kGy were examined for their effects on recombinant human collagen, type III-phosphorylcholine (RHCIII-MPC) hydrogels and their subsequent biocompatibility and ability to promote regeneration in rabbit corneas. Controls comprised unirradiated hydrogels stored in 1% chloroform in phosphate-buffered saline (C-PBS). There were no significant differences between irradiated and non-irradiated samples in optical properties, physical properties (tensile strength, modulus, elasticity) or the ability to support cell growth. However, irradiated implants were more sensitive to high levels of collagenase than unirradiated controls. When implanted into rabbit corneas, corneal implants e-beamed at 17 kGy when implanted into rabbit corneas showed no adverse biological effects of the irradiation. Both e-beamed and C-PBS corneas had epithelial coverage at one-week post-operation. Both showed mild neovascularization that resolved by six months, so all regenerated neo-corneas were clear at six months post-operation. In vivo confocal microscopy identified newly regenerated nerves in the sub-basal nerve plexus. Histology showed that the regenerated corneas were morphologically normal. Immunohistochemistry indicated the presence of a differentiated corneal epithelium and functional tear film. In conclusion, e-beamed corneal implants performed as well as control implants, resulting in fully regenerated neo-corneas with new nerves, and without blood vessels or inflammation that may impede vision or corneal function. Therefore, a complete validation study to establish e-beam irradiation as an effective means for corneal implant sterilization prior to clinical application is necessary.

INTRODUCTION

Biomaterials are increasingly used as implants, but post-operative infections associated with the materials remain a significant complication. Implants are sterilized to minimize the risk of infection. However, those made from biodegradable, biologically-derived materials are often sensitive to conventional sterilization techniques and therefore sterilization remains problematic (Zhang et al., 2006; Dai et al., 2016). We developed and successfully tested in clinical trials pro-regeneration, biosynthetic corneas made from recombinant human collagen type III (RHCIII) as prospective alternatives to human donor corneas for the treatment of corneal blindness. Our implants successfully and stably stimulated regeneration of the corneal epithelium, stroma, and associated nerves, after lamellar keratoplasty, without the need for sustained immunosuppression in a first-in-human study (Fagerholm et al., 2010, 2014). For use in patients with severe pathologies that put them at high risk of rejecting conventional donor transplantation, RHCIII implants incorporating a synthetic lipid polymer, 2-methacryloyloxyethyl phosphorylcholine (MPC) that suppresses inflammation, were successfully tested in high-risk patients with ulcerated and badly scarred corneas (Hackett et al., 2011; Islam et al., 2013, 2015; Kakinoki et al., 2014). In these early clinical studies, RHCIII-MPC implants were manufactured aseptically under Class 100 or ISO 5 conditions and stored in phosphate-buffered saline (0.1 M) containing 1% chloroform (C-PBS) to maintain sterility (Fagerholm et al., 2010, 2014; Hackett et al., 2011; Islam et al., 2013, 2015; Buznyk et al., 2015). However, this storage solution requires an extensive washing procedure to remove the chloroform before surgery. The implants are then further washed in antibiotics before use to ensure their sterility.

For expanded clinical testing and future clinical application, an effective terminal sterilization procedure that allows the surgeon to open the vial to use the implants simply is needed. However, like most complex proteins, collagen responds to heat or irradiation by changing its physical or biological properties due to alterations in chemical and morphological structures. With these, its associated biointeractive properties (Hoburg et al., 2010; Stoppel et al., 2014). Electron beam (e-beam) sterilization uses high-energy electrons that produces beams with a lower depth of penetration and high dose rate and is less stressful to materials than gamma irradiation, which has a low dose rate and high penetrability. It has been shown that e-beam is preferable to gamma irradiation for tissue grafts (Hoburg et al., 2011). For collagen sponges in particular, gamma irradiation has been shown to cause significant shrinkage (Noah et al., 2002) and hence loss of implant weight (Grimes et al., 2005). Nevertheless, low irradiation doses have been successfully used to sterilize biological materials such as collagen scaffolds and decellularized porcine dermis (Dearth et al., 2016;

Herbert et al., 2017; Monaco et al., 2017). The VisionGraft® is an acellular graft cornea gamma-irradiated at 17 - 23 kGy (CorneaGen; Daoud et al., 2011; Chae et al., 2013). This process causes a decrease in the corneal melting temperature indicative of free-radical damage to the peptide backbone, which could affect the RHCIII fibrils present in RHCIII-MPC. In contrast, e-beam has been successfully used to irradiate a number of different biomaterials. Kajii et al. e-beam irradiated at 15 and 40 kGy an octacalcium phosphate and collagen composite (OCP/Col) designed to promote bone regeneration as bioburden-spiked samples. They found that while both doses sterilized the composites, the 15 kGy dose permitted more effective bone regeneration (Kajii et al., 2018). In Proffen et al., extracellular matrix proteins containing collagen were aseptically manufactured into scaffolds for improving anterior cruciate ligament repair (Proffen et al., 2015). Subsequently, samples that were e-beam irradiated at 15 kGy maintained their sterility while non-irradiated scaffolds became contaminated with bacteria and fungi. These reports are in keeping with the industrial standard (ISO 11137-2) indicating that a 15 kGy irradiation dose can result in a log reduction of 10^{-6} colony-forming units of bacteria and fungi when used on a material with a low initial bioburden (International Standards Organization, 2012).

The use of e-beam irradiation for the sterilization of medical devices requires process validation following ISO 11137-2:2012 (International Standards Organization, 2012). Prior to pursuing a very costly full process validation, here, we conducted an evaluation on the ability of low doses of e-beam irradiation to maintain the sterility of RHCIII-MPC corneal implants manufactured under low initial bioburden conditions, as an alternative to C-PBS. We also examined the effects of 17, 19 and 21 kGy of e-beam irradiation on the physical properties of the implants, and, most importantly, biocompatibility and performance as corneal implants in rabbit models.

METHODS

Implant fabrication and packaging

RHCIII-MPC implants were fabricated under aseptic conditions, as previously described (Islam et al., 2015). Briefly, 500 mg of 18% (w/w) aqueous solution of recombinant human collagen-III (Fibrogen Inc., San Francisco, CA) was buffered with 150 μl of 0.625 M 2-(N-morpholino)ethanesulfonic acid (MES; Sigma-Aldrich, Steinheim, Germany) buffer in a syringe mixing system. N-hydroxylsuccinimide (NHS; Sigma-Aldrich, Steinheim, Germany), 2-methacryloyloxyethyl phosphorylcholine (MPC; Paramount Fine Chemicals Co. Ltd, China), poly(ethylene glycol) diacrylate (PEGDA; Sigma-Aldrich, Steinheim, Germany), ammonium persulphate (APS; Sigma-Aldrich, Steinheim,

Germany), N,N,N',N'-tetramethylethylenediamine (TEMED; Sigma-Aldrich, Steinheim, Germany) and 1-ethyl-3-(3-dimethylaminopropyl) carbodiimide (EDC; Sigma-Aldrich, Steinheim, Germany) were sequentially added into the syringe mixing system followed by mixing at 0°C. The collagen primary amine:NHS:EDC molar ratio was 1:0.35:0.7 while the MPC:collagen ratio (w/w) was 1:2. PEG-DA:MPC ratio (w/w) equaled 1:3, APS:MPC ratio was 0.03:1 and APS:TEMED equaled 1:0.77. After demoulding, the hydrogels were washed thoroughly in a phosphate bath and bottled in 0.1M sterile phosphate-buffered saline (PBS). Implants were packaged in 10 mL of either 0.1M PBS or in PBS containing 1% chloroform (C-PBS) in 10 mL sized vials. The vials were sealed with "tear-off' aluminum crimp caps with 3 mm butyl/PTFE septa, sealed using a hand-crimper. After sealing, the vials were placed in double autoclave bags for irradiation. For the in vitro e-beam dose-response study, implants were cast in dogbone-shaped molds, 0.5 mm thick, with a central test section with the dimensions 14 x 6 mm, and a grip area at each end of 6 x10 mm. For the third-party sterility testing and rabbit study, implants were cast as 12 mm wide, 350 μm thick corneal-shaped implants with 3 mm concave curvature.

E-beam irradiation and ability to retain sterility

To determine an optimal e-beam dose, 3 implants per group were sent for e-beam sterilization at 17, 19 and 21 kGy (Sterigenics, Espergarde, Denmark). A dosimeter packet was placed with each vial during irradiation to measure the absorbed dose. The applied radiation dose was very precisely controlled with an acceptable dose deviation of $\pm$ 0.1 kGy. Another 3 control implants were stored in C-PBS.

The ability of the 17 kGy dose irradiated implants to maintain sterility was assessed by the sterilization provider following DS/EN ISO 11737-2 (Sterigenics, Espergaerde, Denmark). Sterility and endotoxin levels were assessed for the 17 kGy dose following DS/EN ISO 11737-2 by a second independent third party (APL, Stockholm, Sweden). The sterility test was conducted following Ph.Eur. 2.6.1 Sterility, using the direct inoculation method [22]. Human cornea-shaped and sized implants (10 mm diameter, 500 μm thick curved hydrogels) were irradiated at 17kGy. Irradiated implant samples were then immersed directly into tryptone broth and incubated at 28-32°C for 14 days. During this time, the contents of the containers were examined for evidence of microbial growth. If turbidity were observed, confirmation of growth or no growth was done by sub-culturing on tryptone soya agar (TSA) plates at 30-35°C for an additional 7 days. The amount of bacterial endotoxin in the irradiated hydrogels was tested following Ph.Eur. 2.6.14 Bacterial endotoxins, using the gel clot method that detects and quantifies the amount of toxin present by the clotting of

an amoebocyte lysate from the horseshoe crab (European Directorate for the Quality of Medicines & HealthCare, 2014).

Sterility of Controlled Bioburden Corneal Samples

The initial e-beam samples weren't carrying sufficient bioburden to establish the efficacy of the dose. Corneal samples were manufactured and intentionally inoculated with known bioburden. The efficiency of sterilization methods was evaluated against gram (+) and gram (-) bacteria, *Staphylococcus aureus* and *Pseudomonas aeruginosa*, respectively. The individual implant was placed in a 10 mL PBS containing vial. *Staphylococcus aureus* (400 CFU) was added to half of the vials (n=6) and the rest of the vials were treated with *Pseudomonas aeruginosa* (400 CFU) (Fig 1A,F). From each bacteria group, half of the vials (n=3) were sent for e-beam irradiation (Nutek Bravo, Hayward, CA 94545, USA) and to the rest of the vials (n=3) 1% chloroform was added. After irradiation, the vials were returned to the lab and tested for bacterial viability. For double conformation of the sterility, two sets of studies were performed with the irradiated and chloroform treated vials. In one study set, a 100 μL of the vial storage solution were streaked over Tryptic soy agar plates and monitored for bacterial growth. In the other study set, the implants from the vials were transferred to another sterilized vial containing 2 mL Tryptic soy broth (TSB) media (Teknova Inc., Hollister, CA 95023, USA) media. These vials were incubated overnight with shaking (80rpm). Then the TSB media from the vials were streaked over Tryptic soy agar plates and monitored for bacterial growth. After 24h, the total CFU for both bacteria were counted.

Materials Testing

Mechanical and Thermal Properties

Three 3 dogbone-shaped hydrogels receiving 17, 19 or 21 kGy of irradiation or C-PBS stored controls were examined. Tensile strength, Young's modulus and elongation at break were measured using an Instron Universal test machine (Biopuls 3343, High Wycombe, UK). These measurements were carried out under water immersion at 37°C. The crosshead speed was 10 mm•min-1 and the lead cell was 50 N. All the samples broke at the waist of the dogbone-shaped sample. The thermal properties of the hydrogels were measured using differential scanning calorimetry (DSC). The denaturing temperature was determined using a Cellbase DSC (Instrument Specialists Inc, Twin Lakes, USA), measured in the heating range of 8 to 80°C at a scan rate of 8°C min^{-1}. Approximately 5-10mg of the hydrogels were weighed after removing the surface water and hermetically sealed in

an aluminum pan to prevent material dehydration. Tmax of the curve of heat flow (W/g) versus temperature (°C) gives the denaturing temperature.

Optical Properties

Light transmission and backscattering measurements of e-beam irradiated and C-PBS treated implants (n=3 per group) were carried out at room temperature using a custom-built instrument, as previously reported (Liu et al., 2008).

Biodegradation Study

Collagenase from *Clostridium histolyticum* (Sigma-Aldrich, MO, USA) was used to evaluate the biodegradation of irradiated and unirradiated hydrogels. Approximately 15 mg of each hydrogel (n=3 per group) were cut out and placed into 0.1M Tris-HCl buffer (tris(hydroxymethyl)aminomethane hydrochloride (Merck KGaA Darmstadt, Germany) containing 5 mM calcium chloride and 5 U/mL collagenase. The collagenase solution was refreshed every eight hours. At different time points (Fig. 1) each sample was weighed after blotting off surface water. The percentage of residual weight was calculated using the following equation: Residual mass % = W_t / W_o %, where W_t is the weight of hydrogel at a particular time point and W_o is the initial weight of the hydrogel.

In vitro biocompatibility

To evaluate the effect of e-beam irradiation on cell growth, green fluorescence protein (GFP) transfected immortalized human corneal epithelial cells (GFP-HCECs) were seeded onto hydrogels that were e-beam irradiated at doses of 17, 19 and 21 kGy (Islam et al., 2015). Controls consisted of C-PBS incubated hydrogels. All the hydrogels were trephined into 6 mm discs to fit into the wells of a 96-well plate. Five thousand GFP-HCECs were seeded onto each hydrogel sample and maintained in Keratinocyte Serum-Free Medium (KSFM; Life Technologies, Invitrogen, Paisley, UK) containing 50 μg/ml bovine pituitary extract and 5 ng/ml epidermal growth factor in a 37°C incubator. The medium was changed on every alternative day. Images of cultured cells were taken at different time points using a fluorescence microscope (AxioVert A1, Carl Zeiss, Göttingen, Germany).

Primary HCECs were cultured on 5 mm discs of 17 kGy and C-PBS treated hydrogels in a 96 well plate with a seeding density of 1000 cells/well. The cells were maintained in KSFM in a 37°C incubator for 5 days. The cells were fixed with 4% paraformaldehyde and stained with cytokeratin 3 (1:100, NBP1-69045, Novus Biologicals, USA or ab77869, AbCam, UK) with Goat anti-Rabbit,

Alexa Fluor® 488 secondary (1:1000, A11034, Invitrogen, USA). The hydrogels were removed from the wells and mounted on slides with coverslips for visualization using a fluorescent microscope (Zeiss AxioImager Z2, Carl Zeiss, Göttingen, German).

***In vivo* evaluation in rabbit corneas**

This study was conducted in compliance with the Swedish Animal Welfare Ordinance and the Animal Welfare Act, and with ethical permission from the local ethical committee (Linköpings Djurförsöksetiska Nämnd). Three groups of curved RHCIII-MPC implants 6 mm in diameter and 350 μm thick were tested. These were e-beam irradiated at 17 kGy, irradiated and then frozen at -80°C after PBS removal, or maintained sterile in C-PBS. An implant from one group was grafted into each New Zealand rabbit's right cornea (weight 3.5-4 kg) by deep anterior lamellar keratoplasty (DALK), n=4 per group. Rabbits were anesthetized with xylazine (Rompun; Bayer, Gothenburg, Sweden) and ketamine (Ketalar; Parke-Davis, Taby, Sweden). Each rabbit cornea was cut centrally with a 6 mm diameter Baron Hessberg trephine set to a depth of 300 μm. The corneal tissue was then dissected lamellarly with a diamond knife and removed. A 6.25 mm diameter implant was placed into the wound bed and anchored with three 10/0 nylon overlying sutures. Animals were given antibiotics in the form of 1% fucithalmic ointment (Fucithalmic; Leo Pharma AB, Malmö, Sweden) topically 2 times daily during the first week after the surgery. No immunosuppression was used. Sutures were removed at one-month post-operation. Clinical examinations were performed daily on each animal for up to 7 days post-operation, and then at 1, 3 and 6-months post-operation. Slit-lamp biomicroscopy was used to evaluate the implants for optical clarity/haze and any inflammation (as indicated by excessive conjunctival redness, swelling compared to the unoperated contralateral control eye) or neovascularization using a modified MacDonald-Shadduck scoring system (Altmann et al., 2010). Other tests included intraocular pressure (IOP) measurements, Schirmer's strip test for tear production, fluorescein staining to access epithelial integrity, ultrasound pachymetry (Tomey SP 3000, Tomey, Inc., Japan) to check corneal thickness and aesthesiometry to assess corneal touch sensitivity (Cochet-Bonnet aesthesiometer, Luneau Oftalmologie, France).

Pre-operatively and at the 6-month follow-up, both corneas of each rabbit were examined by *in vivo* confocal microscopy (IVCM) (ConfoScan3, Nidek, Japan) to image epithelial coverage, in-growth of stromal cells, nerves and any blood vessels or immune infiltrate into the implants. A total of 2106 IVCM images were analyzed from 16 eyes of 8 rabbits. Nerve count analysis was performed according to Lagali et al. (Lagali et al., 2007). All images with nerves or nerve fiber bundles (referred to collectively as nerves) were identified. For identification purposes, nerves were

defined as bright, slender, straight, or branching structures; as substantially uniform in intensity along their length and width, and as having a marked contrast difference from the background intensity level. The following parameters were noted for each image: corneal depth location and the number of nerves present. A total of 302 images with nerves were analyzed from all the groups. To describe the location of corneal nerves, four corneal zones were defined: 20-50 μm below the epithelial surface, representing the nerves of the subbasal nerve plexus at the basal epithelial and subepithelial regions; sixty to 100 μm below the epithelial surface, representing the most anterior stromal region; 110 to 150 μm below the epithelial surface, representing the deep anterior stroma; 160 μm and deeper – mid and deep corneal stroma. The outcome measures used in this study consisted of the total number of nerve branches compiled within each depth zone and the total number of nerves per each cornea.

Histopathology and Immunohistochemistry

Rabbit corneas were excised with a 3-4 mm rim of sclera around them, rinsed in 0.1M phosphate-buffered saline (PBS) and then fixed in 4% paraformaldehyde in PBS. They were either processed for paraffin embedding or frozen in optimal cutting temperature (OCT) compound. Routine hematoxylin-eosin staining was performed on paraffin-embedded samples for histopathological examination.

Frozen sections were prepared for immunohistochemical staining with antibodies against Cytokeratin 3 and Cytokeratin 12 (2Q1040, ab68260, Abcam, UK) at a 1/50 dilution. FITC-conjugated Ulex europaeus agglutinin (UEA, Sigma-Aldrich) was used for mucin detection. Seven-micron frozen sections irradiated, irradiated and frozen and non-irradiated, implanted corneas as well as their corresponding unoperated contralateral controls were used and mounted on glass slides. Samples were fixed with cold acetone (10 min, -20°C), air dried, immersed in PBS and then blocked with 5% goat serum in PBS with 0.1% Tween 20 (blocking solution) for 60 min at room temperature. All slides were washed in PBS with 1% Tween 20 (PBS-T) and then incubated with the secondary antibodies (goat anti-rabbit Alexa 488 or goat anti-mouse Alexa 488; Jackson Immuno Research Laboratories, Inc., West Grove, PA) diluted 1:1000 with the blocking solution for 60 min at room temperature. After washing in PBS-T, the slides were dehydrated and mounted with Vectashield mounting medium with DAPI (Vector Laboratories, Inc., Burlingame, CA). An LSM-700 Zeiss upright confocal microscope (LSM700, Carl Zeiss, Oberkochen, Germany) with a 20X objective was used for capturing images. Images were captured with a light microscope (Axio Lab.A1, Carl Zeiss,

Oberkochen, Germany), with a color camera (AxioCam ICc5) with a 20X objective connected to the camera.

Statistical analyses

Statistical analyses were conducted using GraphPad Prism 8 (GraphPad Software Inc., La Jolla, CA, USA). Data are presented as mean ± standard deviation, unless otherwise indicated. For all tests within this study, a $P \leq 0.05$ was considered statistically significant. Data were checked for normality using a Shapiro-Wilkes test where appropriate ($n<50$). One- and two-way ANOVA with Tukey/Tamhane's T2 post-hoc analyses was used to check between-group differences for data with a normal distribution, including optical, mechanical, and thermal data. Collagenase degradation was analyzed using non-linear regression to determine if the rate of degradation differed between the irradiated and unirradiated samples. A one-phase exponential decay model was compared to a sigmoidal curve to determine best fit based on graphical analysis of the raw data. The comparison resulted in a sigmoidal curve being preferred for all data sets. The data were fitted with a sigmoidal curve and tested to determine if one curve fit all data and if the best-fit values of selected unshared data points differed between data sets. Clinical data were analyzed using a Kruskal-Wallis test with Dunn's multiple comparison test for post-hoc tests.

Corneal IVCM images were sorted according to eye, depth zone, and whether exposed to e-beam or not. Paired sample t-tests were used to determine significant differences between nerve numbers, corneal thickness and corneal aesthesiometry in control versus surgical corneas in each depth zone. Student's t-tests were used for comparisons between irradiated and non-irradiated samples.

RESULTS

E-beam Irradiation and Sterility

Sterigenics confirmed the irradiation of the dog-bone-shaped hydrogels at 17 ± 0.1 kGy, 19 ± 0.1 kGy and 21 ± 0.1 kGy, and cornea-shaped samples at 17 ± 0.1 kGy. Independent analyses showed that after the 14-day sample immersion in broth, the 17 kGy-irradiated implants showed no microbial growth, indicating that the samples maintained their sterility (Sterigenics; APL, Stockholm, Sweden). The endotoxin test results showed that the implants were compliant with the <0.5 EU/ml cut-off requirement for implantable medical devices (U.S. Department of Health and Human Services Food and Drug Administration, 2012).

For the controlled bioburden samples, e-beam was shown to be effective against both gram + and – bacteria (Fig. 1H-I). Zero CFU was observed from storage media of *Staphylococcus aureus* added vials, irrespective of sterilization methods (Fig 1H-I). Two *Pseudomonas aeruginosa* treated vials showed 1 CFU each when irradiated (Fig. S1), whereas only one vial from chloroform sterilized group of *Pseudomonas aeruginosa* showed 1 CFU (Fig S1). Implants soaked in TSB confirmed the sterility of the implants (Fig S1). One chloroform treated *Staphylococcus aureus* vial showed 2 CFU (Fig S1). Vials that were not explicitly mentionedcarried zero observed CFU.

Materials Properties

A summary of the mechanical, optical and thermal stability testing is given in Table 1. There were no significant between group differences for any mechanical or optical properties between the C-PBS and e-beam doses. One-way ANOVA of the thermal stability measurements obtained using DSC showed an overall significant difference ($p=0.02$). There were significant differences between 17 kGy and 21 kGy ($p=0.02$), as well as 19 kGy and 21 kGy ($p=0.03$); however, no between group differences were observed between the unirradiated and irradiated groups ($p=0.8$).

The collagenase biodegradation study was conducted to compare the stability of the hydrogels in response to enzymatic degradation (Fig. 1A). Each data set was fitted with a sigmoidal curve with a top value constrained at 100% to account for the total solid content mass at the beginning of the assay (Table 1B). A test for one curve for all data sets was rejected ($p<0.0001$) indicating that each curve was different. The hill slope of the irradiated implants was steeper than the C-PBS implants, demonstrating an initial increased rate of degradation in the presence of collagenase within the first 24 hours, before levelling out.

In vitro cell biocompatibility

Both unirradiated and irradiated RHCIII-MPC hydrogels at all three doses supported the attachment and proliferation of GFP-HCEC cultured on them (Fig. . 1A-F). Cultures of GFP-HCEC reached confluence at day four on all hydrogels (Fig 1A-D). Cytokeratin 3 staining of primary HCECs cultured on the 17 kGy and C-PBS materials showed that both hydrogels support terminally differentiated corneal epithelial cells (Fig 1E-F).

Clinical Evaluation

No immune-suppressive eye drops were used to determine the effects of any free radical or hydroperoxide accumulation in post-irradiated implants that could cause irritation and inflammation. Post-surgical slit lamp examination of the implanted corneas showed no excessive redness or swelling in irradiated implants compared to non-irradiated control samples. All implants were stably incorporated over the surgical period without the use of immune suppressive eye drops.

Full epithelial coverage of the implants was completed within the first week post-surgery, as demonstrated by the exclusion of sodium fluorescein, when the dye was applied. The healing process was accompanied by mild neovascularization in all implanted animals. However, the neovessels gradually resolved. At 6 months post-implantation, no or very few ghost vessels remained. Mild subepithelial haze (grade 0.5-1) was observed in all rabbits throughout the follow-up period regardless of the sterilization method (Table 2), but all implanted grafts remained transparent (Fig. 2A-C). One rabbit in the irradiated group experienced significant subepithelial fibrosis and haze in both the operated and unoperated eyes, leading to a significant outlier in the statistical analysis (Fig. 3). Measurement of corneal thickness in the central zone at 6 months after surgery by pachymetry revealed that the corneas implanted with unirradiated implants were thinner than unoperated corneas. Still, the irradiated implants were not significantly different from either group (Table 3).

In Vivo Confocal Microscopy

In vivo confocal microscopy performed at 6 months post-surgery showed that the epithelial and stromal layers had regenerated as in all previous RHCIII-MPC grafts in various species. The morphology of epithelial and stromal cells in irradiated, C-PBS and control untreated corneas were similar. Both e-beamed and C-PBS and hydrogel implanted corneas were re-innervated (Fig. 2I-L, 3A). Nerve counts made from IVCM images revealed that sterilization with e-beam and or 1% chloroform solution did not influence the rate of nerve regeneration (Fig. 3A). Cochet-Bonnet aesthesiometry showed no differences between nerve sensitivity in the corneas (Fig. 3B).

Histopathology and immunohistochemistry

Histopathological examination of H&E sections of the regenerated neo-corneas shows that e-beam irradiated and C-PBS samples had stratified epithelia and lamellate stroma with flattened cells, similar to that of the untreated, healthy contralateral corneas (Fig. 4 A-C). No significant differences in epithelial thickness were noted. The sections were also free from any infiltrating immune cells.

Immunohistochemistry showed that like healthy control corneas, the regenerated neocorneas from both irradiated and unirradiated corneal samples stained positively for epithelial cytokeratins 3 and 12, and mucin (Fig. 4 D-I). No significant differences in the thickness of cytokeratin and mucin layer or intensity of the staining were observed.

DISCUSSION

E-beam, like gamma irradiation, is a widely accepted method for sterilization, and has been effectively used for terminal sterilization to eliminate any microbial, fungal or viral contamination that may have been introduced during the manufacturing process. E-beam sterilization is governed by the ISO standards 11137 and 13409 and uses very high-energy electrons that directly destroy bioburden. The high-energy electrons also collide with other local electrons, generating secondary electrons with sufficient energy to destroy bioburden.

While RHCIII-MPC implants have been manufactured aseptically and stored with 1% chloroform to maintain sterility in clinical trials with small cohorts of patients, for routine clinical use, a more repeatable and controlled process that gives a high assurance of sterility is needed. Here, we showed that while e-beam irradiation at 17, 19 and 21 kGy resulted in changes in the degradation profile of RHCIII-MPC implants under high concentrations of collagenase, no significant differences in optical or mechanical properties were observed for all irradiation doses when compared to unirradiated controls. The lack of observed changes may be attributed the EDC crosslinking, as it has been reported that EDC crosslinked materials are subject to radioprotective effects during e-beam irradiation (Seto et al., 2008).

The dose range study established that the minimum e-beam dose tested, 17 kGy, was effective at maintaining the sterility of the aseptically fabricated implants. There was no bacterial growth on the irradiated hydrogel samples after 14 days of immersion into bacterial growth medium, confirming the ability of the samples to retain sterility.

The irradiated hydrogels did not show significantly different optical or mechanical properties from unirradiated controls. The irradiated samples showed a difference in the rate of collagenase degradation, suggesting that these implants could have an altered rate of remodeling within the body after implantation. These observations are in keeping with the findings of Grimes et al. that e-beam increases percent weight loss in ECM-based substrates (Grimes et al., 2005). The specific biological effects of significant changes in collagenase degradation on the regeneration of the human cornea grafted with an RHCIII-MPC matrix are unknown. As the goal of these implants is to act as

a substrate for the complete remodeling of the cornea during the regenerative process, an irradiation dose that may increase the rate of degradation of the RHCIII-MPC matrix may be unsuitable to promote the formation of a cornea of appropriate thickness and mechanical strength; therefore, the higher 19 and 21 kGy doses were excluded from further study.

The clinical study in rabbits using implants sterilized with 17 kGy established that there were no significant differences in the long-term performance between irradiated and unirradiated implants for any of the outcome measures studied. The differences in thickness between the implanted, regenerated neo-corneas observed were non-significant and most likely due to growth of the un-operated corneal as rabbits matured, compared to the catching-up required in the operated eyes. Both classes of implants resulted in successful re-epithelialization, demonstrating that the irradiated RHCIII-MPC matrix retained the critical biochemical or structural properties required to support the attachment and migration of limbal epithelial stem cells from the periphery of the cornea over the implant, and their subsequent stratification to re-establish a multilayered epithelium. The presence of differentiation markers, cytokeratins 3 and 12, plus mucin in the corneal explants, without changes in intensity and thickness, indicates that the regenerated epithelium was fully differentiated and could secrete mucin, i.e., was fully functional. Hence, the observed changes in collagenase degradation profiles between the C-PBS and 17 kGy implants did not have a biological effect on the ability of the implants to stimulate regeneration of a morphologically accurate and functional epithelium.

Equivalent nerve counts confirmed functional innervation of the regenerated neo-corneas and blink response in both grafts compared to unoperated controls. We also found that freezing of e-beamed samples at -80°C did not result in a loss in the ability of RHCIII-MPC hydrogels to promote regeneration of corneal epithelium, stroma and nerves.

E-beam irradiation has been used in the sterilization of commercially available ECM-based biomaterials in clinical applications; including the artificial skin, Integra®, which is made from collagen and glycosaminoglycans (Mattern et al., 2001). A dose of 20 kGy was used, but the matrices were irradiated dry. A lower dose such as ISO 11137-2:2015 Method VDmax15, however, is a validated dose that has been used for e-beam sterilization (International Standards Organization, 2012). In this study, a slightly higher dose of 17 kGy irradiation of RHCIII-MPC in PBS maintained sterility of the implants whole preserving their ability to promote regeneration. In the future, the verification of the safety and efficacy of this dose will allow for sterility validation following ISO 11137-2:2015 Method $VD_{max}15$.

In conclusion, we have shown that an e-beam dose of 17 kGy can be used to maintain the sterility of aseptically fabricated RHCIII-MPC implants while preserving their critical optical, mechanical and chemical properties. Most importantly, the full regeneration-enabling functionality of the implants was preserved. A full validation study of e-beam sterilization as a terminal sterilization technique for RHCIII-MPC implants for clinical use is therefore merited.

CONFLICT OF INTEREST

A patent for RHCIII-MPC has been filed by the Ottawa Hospital Research Institute and University of Ottawa, where MG was previously employed. MG has no commercial nor financial relationship to licensees of the technology. Other authors have no commercial or financial relationships that could be construed as a potential conflict of interest.

AUTHOR CONTRIBUTIONS

FS, MMI, FMM, AL, DA and PA did the experiments. OB, MKL and PF performed the surgeries. EE performed the IVCM and statistical analyses. MG was responsible for designing and supervising the study. FS, MMI and MG wrote up the first draft of the manuscript. All authors contributed to the editing, revisions and final approval of the manuscript.

FUNDING

Support for this study was from a Vinnova, Sweden grant DNR 2013-04645, CIHR grant PJT - 155924, and NSERC RGPIN-2017-05410. FCS is supported by an NSERC doctoral studentship. MMI is an NIH K99/R00 (K99EY031373) fellow at MEEI-Harvard Medical School. MG acknowledges support from her Tier 1 Canada Research Chair and Caroline Durand Foundation research chair.

ACKNOWLEDGMENTS

We thank Dr. C-J Lee for production of the GFP-transfected human corneal epithelial cells and Ms. Kimberley Merrett for assistance in mechanical properties measurements. The authors would also like to thank Dr. Graziella Pellegrini for her supervision of Federica M. Magrelli during this project.

REFERENCES

Altmann, S., Emanuel, A., Toomey, M., McIntyre, K., Covert, J., Dubielzig, R. R., et al. (2010). A Quantitative Rabbit Model of Vaccinia Keratitis. *Invest. Ophthalmol. Vis. Sci.* 51, 4531–4540. doi:10.1167/IOVS.09-5106.

Buznyk, O., Pasyechnikova, N., Islam, M. M., Iakymenko, S., Fagerholm, P., and Griffith, M. (2015). Bioengineered Corneas Grafted as Alternatives to Human Donor Corneas in Three High-Risk Patients. *Clin. Transl. Sci.* 8, 558–562. doi:10.1111/cts.12293.

Chae, J., Choi, J., Stark, W., and Elisseeff, J. (2013). Extracellular matrix characterization of the acellular gamma-irradiated cornea. Poster Presented at the Association for Research in Vision and Ophthalmology Annual Meeting May 5-9, Seattle Washington. *Invest. Ophthalmol. Vis. Sci.* 54, 5257. Available at: https://iovs.arvojournals.org/article.aspx?articleid=2150200 [Accessed September 30, 2021].

CorneaGen VisionGraft® THE CLEAR CHOICE® . Available at: https://corneagen.com/wp-content/uploads/2021/01/VG100-Cornea_2-Page_2020-01.pdf [Accessed September 30, 2021].

Dai, Z., Ronholm, J., Tian, Y., Sethi, B., and Cao, X. (2016). Sterilization techniques for biodegradable scaffolds in tissue engineering applications. *J. Tissue Eng.* 7. doi:10.1177/2041731416648810.

Daoud, Y. J., Smith, R., Smith, T., Akpek, E. K., Ward, D. E., and Stark, W. J. (2011). The intraoperative impression and postoperative outcomes of gamma-irradiated corneas in corneal and glaucoma patch surgery. *Cornea* 30, 1387–1391. doi:10.1097/ICO.0B013E31821C9C09.

Dearth, C. L., Keane, T. J., Carruthers, C. A., Reing, J. E., Huleihel, L., Ranallo, C. A., et al. (2016). The effect of terminal sterilization on the material properties and in vivo remodeling of a porcine dermal biologic scaffold. *Acta Biomater.* 33, 78–87. doi:10.1016/J.ACTBIO.2016.01.038.

European Directorate for the Quality of Medicines & HealthCare (2014). "2.6.14. Bacterial endotoxins," in European Pharmacopoeia 8.0, 161–168.

Fagerholm, P., Lagali, N. S., Merrett, K., Jackson, W. B., Munger, R., Liu, Y., et al. (2010). A Biosynthetic Alternative to Human Donor Tissue for Inducing Corneal Regeneration: 24-Month Follow-Up of a Phase 1 Clinical Study. *Sci. Transl. Med.* 2, 46ra61. doi:10.1126/scitranslmed.3001022.

Fagerholm, P., Lagali, N. S., Ong, J. A., Merrett, K., Jackson, W. B., Polarek, J. W., et al. (2014). Stable corneal regeneration four years after implantation of a cell-free recombinant human collagen scaffold. *Biomaterials* 35, 2420–2427. doi:https://doi.org/10.1016/j.biomaterials.2013.11.079.

Grimes, M., Pembroke, J. T., and McGloughlin, T. (2005). The effect of choice of sterilisation method on the biocompatibility and biodegradability of SIS (small intestinal submucosa). *Biomed Mater Eng* 15, 65–71.

Hackett, J. M., Lagali, N., Merrett, K., Edelhauser, H., Sun, Y., Gan, L., et al. (2011). Biosynthetic Corneal Implants for Replacement of Pathologic Corneal Tissue: Performance in a Controlled Rabbit Alkali Burn Model. *Invest. Ophthalmol. Vis. Sci.* 52, 651–657. doi:10.1167/iovs.10-5224.

Herbert, A., Edwards, J. H., Jones, G. L., Ingham, E., and Fisher, J. (2017). The effects of irradiation dose and storage time following treatment on the viscoelastic properties of decellularised porcine super flexor tendon. *J. Biomech.* 57, 157–160. doi:10.1016/J.JBIOMECH.2017.04.005.

Hoburg, A., Keshlaf, S., Schmidt, T., Smith, M., Gohs, U., Perka, C., et al. (2011). Fractionation of high-dose electron beam irradiation of BPTB grafts provides significantly improved viscoelastic and structural properties compared to standard gamma irradiation. *Knee Surgery, Sport. Traumatol. Arthrosc.* 19, 1955–1961. doi:10.1007/s00167-011-1518-9.

Hoburg, A. T., Keshlaf, S., Schmidt, T., Smith, M., Gohs, U., Perka, C., et al. (2010). Effect of electron beam irradiation on biomechanical properties of patellar tendon allografts in anterior cruciate ligament reconstruction. *Am. J. Sports Med.* 38, 1134–1140. doi:10.1177/0363546509361161.

International Standards Organization (2012). ISO 11137-2:2012 Sterilization of health care products – Radiation – Part 2: Establishing the sterilization dose.

Islam, M. M., Cepla, V., He, C., Edin, J., Rakickas, T., Kobuch, K., et al. (2015). Functional fabrication of recombinant human collagen-phosphorylcholine hydrogels for regenerative medicine applications. *Acta Biomater.* 12, 70–80. doi:10.1016/j.actbio.2014.10.035.

Islam, M. M., Griffith, M., and Merrett, K. (2013). Fabrication of a human recombinant collagen-based corneal substitute using carbodiimide chemistry. *Methods Mol Biol* 1014, 157–164. doi:10.1007/978-1-62703-432-6_10.

Kajii, F., Iwai, A., Tanaka, H., Matsui, K., Kawai, T., and Kamakura, S. (2018). Influence of electron beam irradiation doses on bone regeneration by octacalcium phosphate collagen composites. *J. Tissue Eng. Regen. Med.* 12, e1186–e1194. doi:10.1002/TERM.2505.

Kakinoki, S., Sakai, Y., Takemura, T., Hanagata, N., Fujisato, T., Ishihara, K., et al. (2014). Gene chip/PCR-array analysis of tissue response to 2-methacryloyloxyethyl phosphorylcholine (MPC) polymer surfaces in a mouse subcutaneous transplantation system. http://dx.doi.org/10.1080/09205063.2014.939917 25, 1658–1672. doi:10.1080/09205063.2014.939917.

Lagali, N. S., Griffith, M., Shinozaki, N., Fagerholm, P., and Munger, R. (2007). Innervation of tissue-engineered corneal implants in a porcine model: A 1-year in vivo confocal microscopy study. *Invest. Ophthalmol. Vis. Sci.* 48, 3537–3544. doi:10.1167/iovs.06-1483.

Liu, W., Merrett, K., Griffith, M., Fagerholm, P., Dravida, S., Heyne, B., et al. (2008). Recombinant human collagen for tissue engineered corneal substitutes. *Biomaterials* 29, 1147–1158. doi:10.1016/j.biomaterials.2007.11.011.

Mattern, R.-H., Pierschbacher, M. D., Cahn, F., Tschopp, J. F., and Malaney, T. I. (2001). Collagen/glycosaminoglycan matrix stable to sterilizing by electron beam radiation. Available at: https://patents.google.com/patent/US6969523B1/en [Accessed July 26, 2021].

Monaco, G., Cholas, R., Salvatore, L., Madaghiele, M., and Sannino, A. (2017). Sterilization of collagen scaffolds designed for peripheral nerve regeneration: Effect on microstructure, degradation and cellular colonization. *Mater. Sci. Eng.* C 71, 335–344. doi:10.1016/J.MSEC.2016.10.030.

Noah, E. M., Chen, J., Jiao, X., Heschel, I., and Pallua, N. (2002). Impact of sterilization on the porous design and cell behavior in collagen sponges prepared for tissue engineering. *Biomaterials* 23, 2855–2861. doi:10.1016/S0142-9612(01)00412-4.

Proffen, B. L., Perrone, G. S., Fleming, B. C., Sieker, J. T., Kramer, J., Hawes, M. L., et al. (2015). Electron beam sterilization does not have a detrimental effect on the ability of extracellular matrix scaffolds to support in vivo ligament healing. *J. Orthop. Res.* 33, 1015–1023. doi:10.1002/JOR.22855.

Seto, A., Gatt, C. J., and Dunn, M. G. (2008). Radioprotection of Tendon Tissue via Crosslinking and Free Radical Scavenging. *Clin. Orthop. Relat. Res.* 2008 4668 466, 1788–1795. doi:10.1007/S11999-008-0301-9.

Shetty, R., Kumar, N. R., Pahuja, N., Deshmukh, R., Vunnava, K., Abilash, V. G., et al. (2018). Outcomes of Corneal Cross-Linking Correlate with Cone-Specific Lysyl Oxidase Expression in Patients with Keratoconus. *Cornea* 37, 369–374. doi:10.1097/ICO.0000000000001478.

Stoppel, W. L., White, J. C., Horava, S. D., Henry, A. C., Roberts, S. C., and Bhatia, S. R. (2014). Terminal sterilization of alginate hydrogels: Efficacy and impact on mechanical properties. *J. Biomed. Mater. Res. Part B Appl. Biomater.* 102, 877–884. doi:10.1002/JBM.B.33070.

U.S. Department of Health and Human Services Food and Drug Administration (2012). Guidance for Industry. Pyrogen and Endotoxins Testing:Questions and Answers. 240–276.

US Pharmacopeia (USP) (2011). Transfusion and Infusion Assemblies and Similar Medical Devices. *US Pharmacop.*

Zhang, J., Davis, T. A., Matthews, M. A., Drews, M. J., LaBerge, M., and An, Y. H. (2006). Sterilization using high-pressure carbon dioxide. *J. Supercrit. Fluids* 38, 354–372.

FIGURE LEGENDS

Figure 1. A-D) GFP-HCEC cells at day 4 of proliferation on irradiated and unirradiated implants show confluence in all cultures. A) 17 kGy, B) 19 kGy, C) 21 kGy, D) Unirradiated (C-PBS). E-F) Cytokeratin 3 staining of primary HCECs cultures on 17 kGy and C-PBS treated hydrogels. G) Collagenase degradation of the e-beamed materials demonstrating that E-beam changes the rate but not the extend of collagenase degradation of E-beamed RHCIII-MPC. H-I) Post-e-beam bioburden measured in the storage media in the implants (H) and direct culture of the corneal implants (I).

Figure 2. RHCIII-MPC implants that had been sterilized with e-beam at 17 kGy irradiation in phosphate-buffered saline (n=4) (A,E,I), irradiated and then stored frozen at -80^{circ}C after withdrawal of saline (n=4) (B,F,J) or in phosphate buffered saline (PBS) containing 1% chloroform (n=4) (C,G,K) after grafting into rabbit corneas in comparison to unoperated eyes (n=12) (D,H,L). Slit lamp images at 6 months post-operation (E-H) and corresponding in vivo confocal microscopy (IVCM) images at these times (I-L). The IVCM images were captured at a depth of 60 to 100 μm, showing the regenerated neo-cornea stroma keratocytes and nerves (arrowheads).

Figure 3. Innervation, thickness and microscopy of the regenerated cornea. A) Number of nerve fibers per central IVCM corneal scan in RHCIII-MPC implanted corneas at 6 months post-implantation. B) Results of Cochet-Bonnet corneal aesthesiometry at 6 months after surgery. C) Corneal thickness at 6 months post-implantation. D) Composite McDonald-Shadduck clinical score at 6 months post-implantation.

Figure 4. Microscopy of sections from unoperated (n=12), unirradiated (n=4), and irradiated eyes (n=4). (A-C) Hematoxylin- eosin staining; (D-F) Cytokeratin 3+12 (green); (G-I)) FITC-conjugated Ulex europaeus agglutinin (green), DAPI was used to stain the cell nuclei (pseudo-colored blue).

SUPPLEMENTARY FIGURE LEGENDS

Figure S1. Bioburden reduction study of RHCIII-MPC implants irradiated at 17 kGy or stored in C-PBS. (A,F) Initial bioburden of *P. aeruginosa* and *S. aureus* used to spike the implants. (B, C) Storage media of implants spiked with P. aeruginosa resulted in the persistence of a single CFU. (D,E) No growth was observed from the implants cultured in TSB. (G-J) No colonies of *S. aureus* persisted after the two methods of sterilization.

FIGURES

Figure 1.

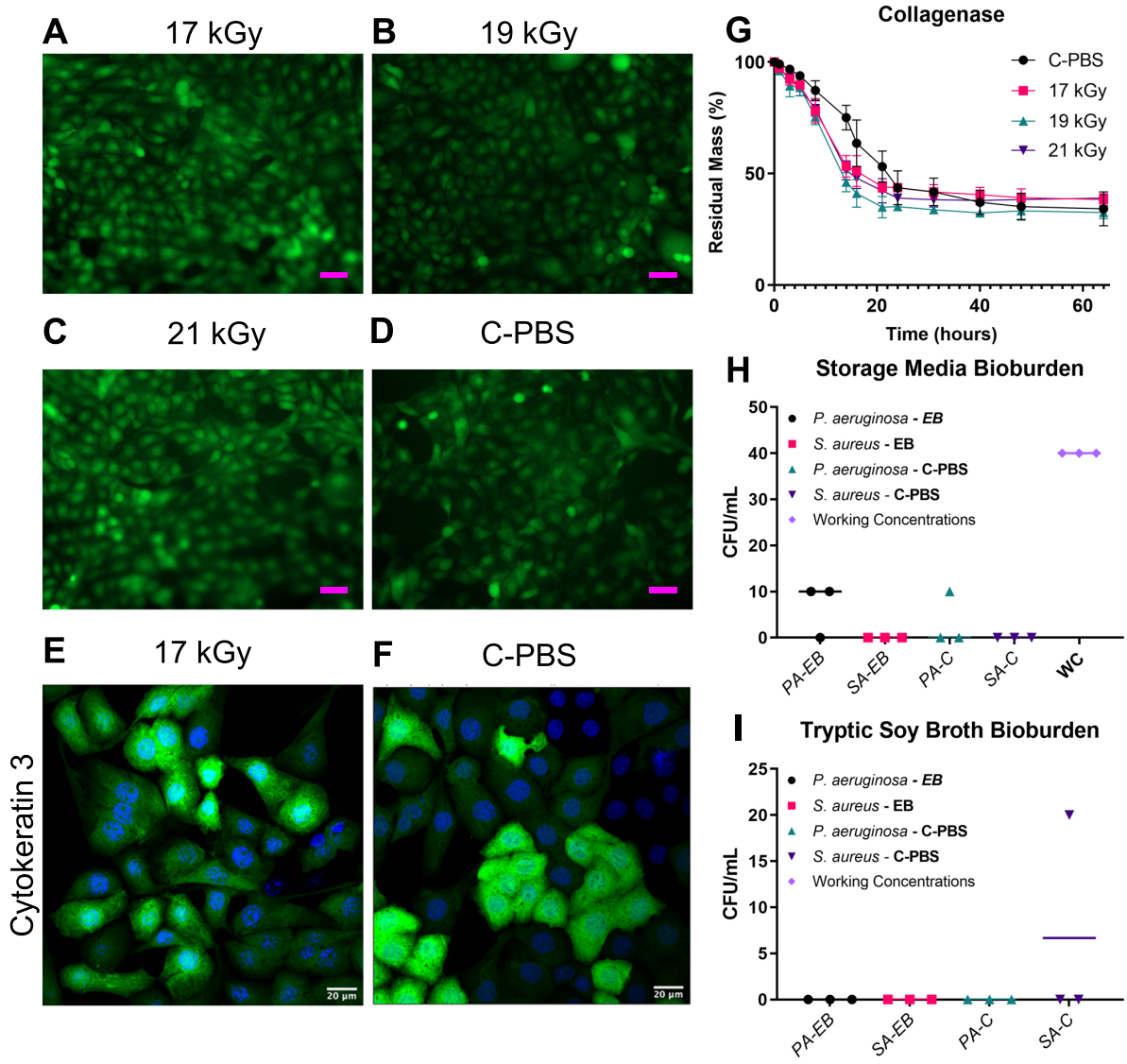

Figure 2.

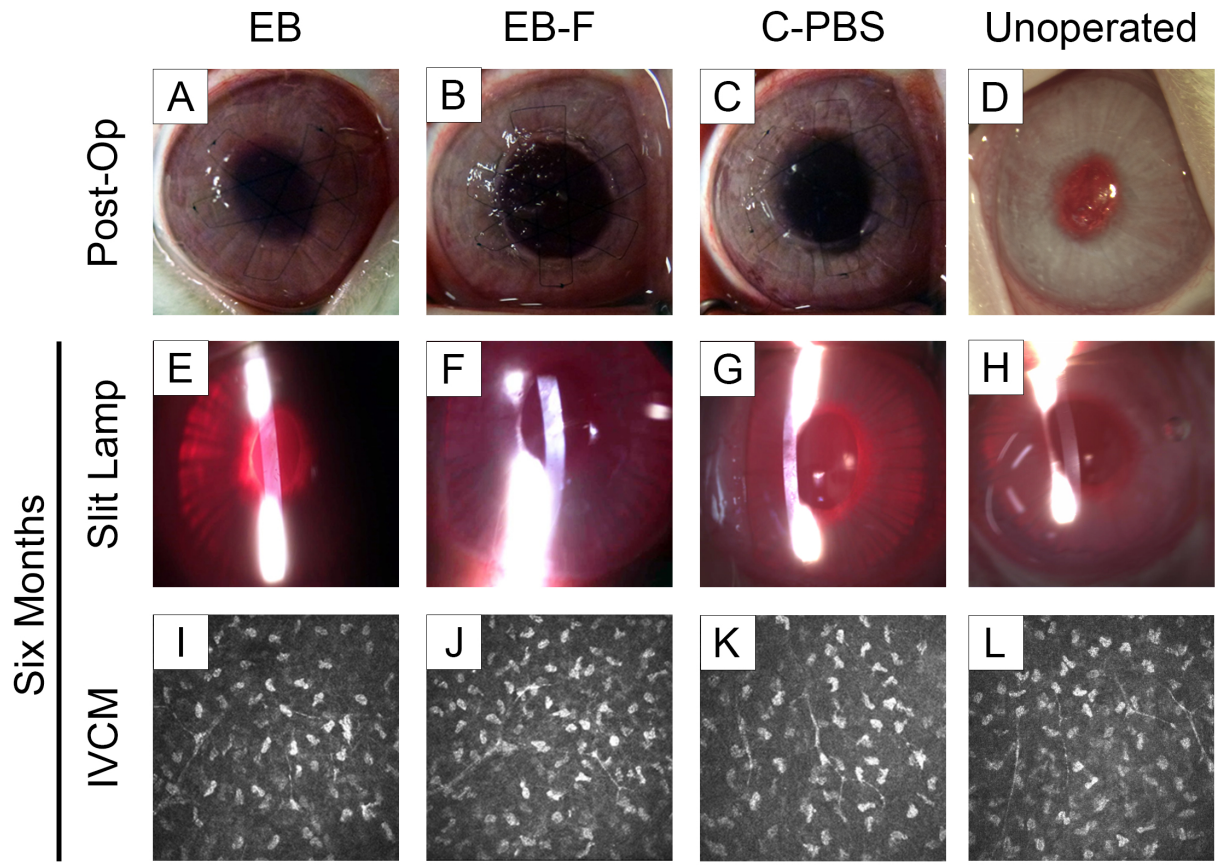
EB
EB-F
C-PBS
Unoperated
Post-Op
Six Months
Slit Lamp
IVCM
A
B
C
D
E
F
G
H
I
J
K
L

Figure 3.

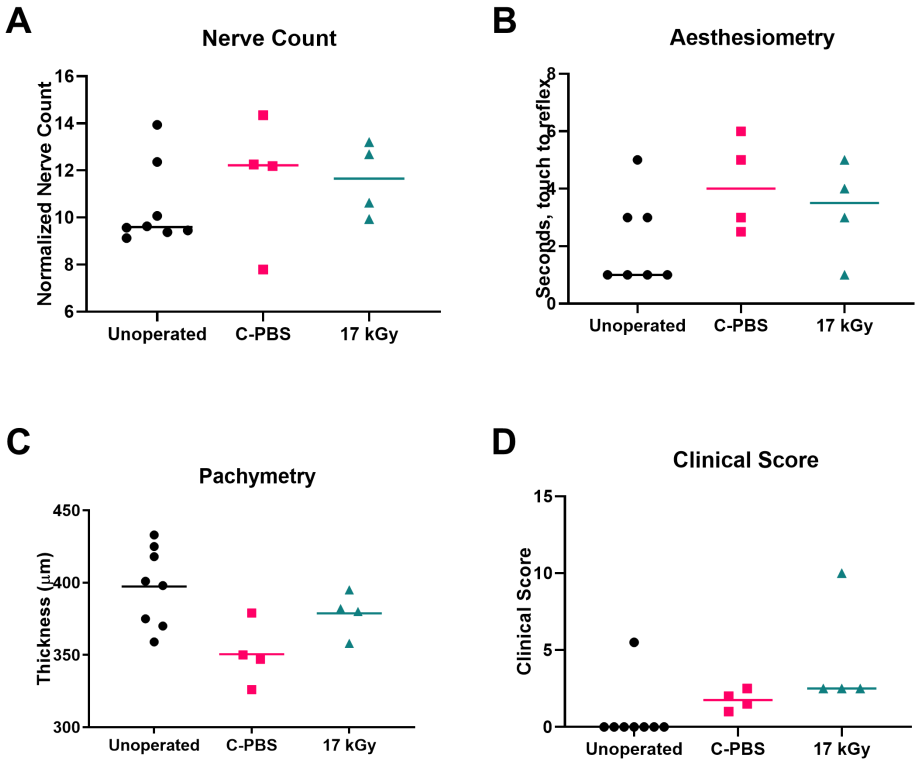
A
Nerve Count
Normalized Nerve Count
16
14
12
10
8
6
Unoperated
C-PBS
17 kGy
B
Aesthesiometry
Seconds, touch to reflex
0
Unoperated
C-PBS
17 kGy
C
Pachymetry
Thickness (μm)
450
400
350
300
Unoperated
C-PBS
17 kGy
D
Clinical Score
Clinical Score
15
10
5
0
Unoperated
C-PBS
17 kGy

Figure 4.

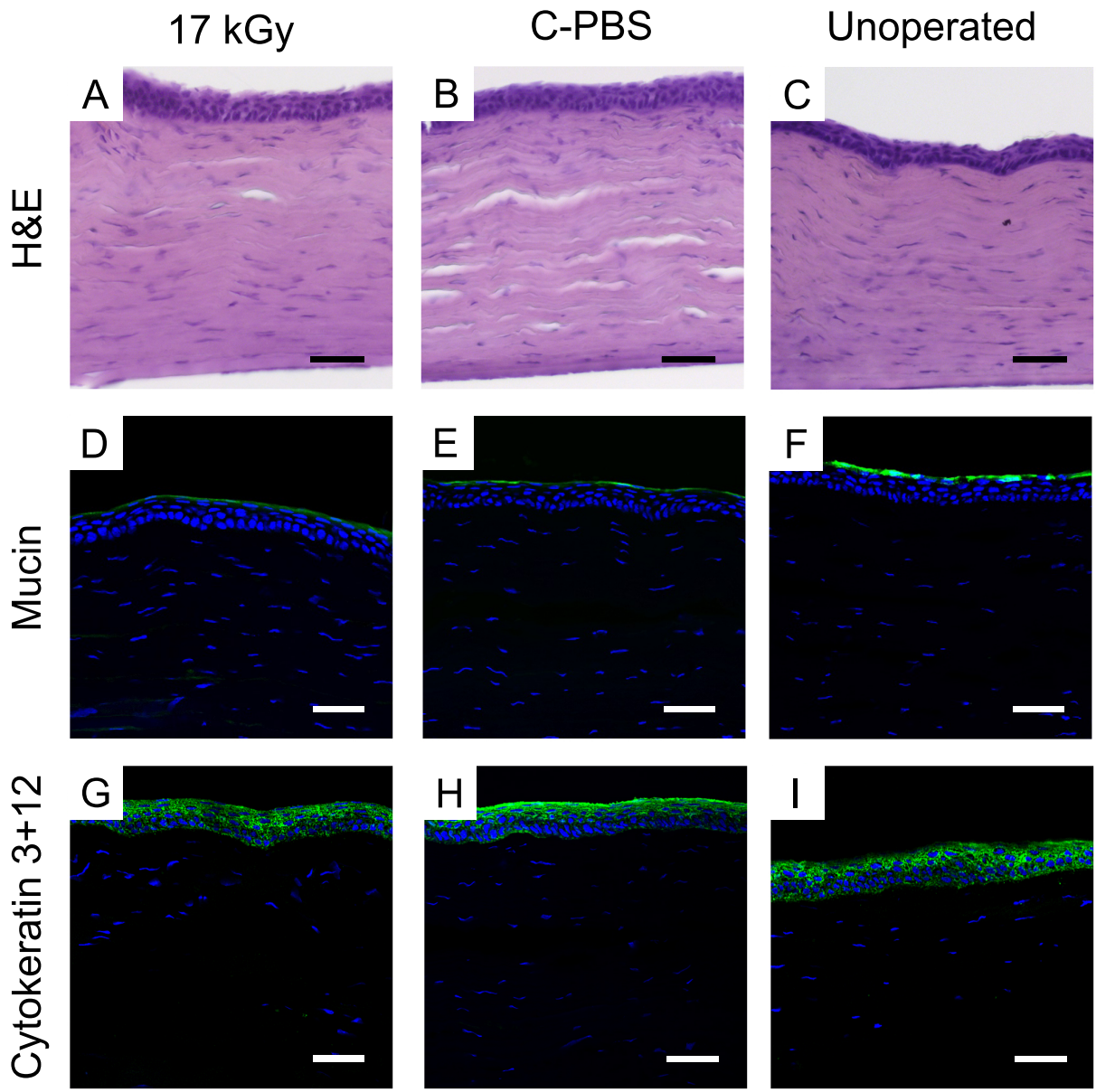

TABLES

Table 1. Comparison of physical properties of e-beam irradiated and unirradiated corneal implants.

	C-PBS	**17 kGy**	**19 kGy**	**21 kGy**	**p-Value**
Optical Properties					
Transmission (%)	88 ± 1.9	84 ± 3.8	88 ± 4.6	88 ± 7.8	0.704
Backscatter (%)	1.6 ± 0.4	1.2 ± 0.7	0.03 ± 0.06	1.2 ± 1.4	0.2
Mechanical Properties					
Tensile Strength (MPa)	0.3 ± 0.1	0.3 ± 0.04	0.2 ± 0.1	0.3 ± 0.3	0.7
Elongation at break (%)	12 ± 0.8	12 ± 0.4	10 ± 2.3	11 ± 4.4	0.8
Young's modulus (MPa)	3.6 ± 0.8	3.7 ± 0.6	2.9 ± 0.5	4.1 ± 3.2	0.9
Thermal Stability					
Denaturation Temperature (°C)	54 ± 1.7	51 ± 2.3	51 ± 2.0	56 ± 0.5	0.02

Data is reported as mean ± SE. Top value was constrained to 100.

Table 2. Slit lamp evaluation performed at six months post-operative.

Outcome	**Unoperated**	**C-PBS**	**17 kGy**	**K-W**
Corneal Opacity Severity	0	1 [-5.6, ns]	1 [-6.9, *]	8.4, p=0.003
Corneal Opacity (Area)	0	1 [-5.6, ns]	1 [-6.9, *]	8.4, p=0.003
Corneal Vascularization	0	0 [-2.0, ns]	0 [-2.0, ns]	3.0, p=0.5
Conjunctival Congestion	0	0	0	N/A
Conjunctiva Chemosis and Swelling	0	0	0	N/A
Corneal Staining	0	0	0	N/A

The exam was performed by two independent raters with an inter-rater reliability score of κ=0.6, so the median score, rounded up, was used for all comparative analysis. Clinical score is reported as the median group score. Groups were compared using a Kruskal-Wallis test, with a Dunn's multiple comparison correction for between group analyses. Data is reported as (Median, [Mean Rank Diff. to UO, Significance])

Table 3. Corneal thickness measurements of the implantation area of operated and non-operated eyes at 6 months post-operation by pachymetry.

Group	Corneal thickness M ± SD	Mean Rank Difference to Unoperated
EB	378 ± 15.4	2.50
EB-F	379 ± 37.3	3.9
C-PBS	351 ± 21.8	7.50*
Unoperated	407 ± 35.9	-

Statistical significance ($P \leq 0.05$) of operated eyes from healthy, unoperated control eyes was determined using a Kruskal-Wallis test (6.6, $p=0.03$) with a Dunn's multiple comparison between experimental and unoperated corneas.

SUPPLEMENTARY TABLES

Supplementary Table 1. Sigmoidal Regression of Collagenase Assay

Sigmoidal regression of irradiated and unirradiated implants after collagenase treatment					
	C-PBS	**17 kGy**	**19 kGy**	**21 kGy**	**p-Value**
Top	100	100	100	100	N/A
Bottom	36 ± 1.6	41 ± 0.9	33 ± 0.8	39 ± 0.7	<0.0001
IC50	15 ± 0.6	10 ± 0.4	10 ± 0.3	10 ± 0.3	<0.0001
Hill Slope	-0.09 ± 0.01	-0.13 ± 0.01	-0.14 ± 0.01	-0.13 ± 0.01	0.0016
Span	64	59	67	61	N/A
R square	0.96	0.98	0.99	0.99	N/A

Figure S1.

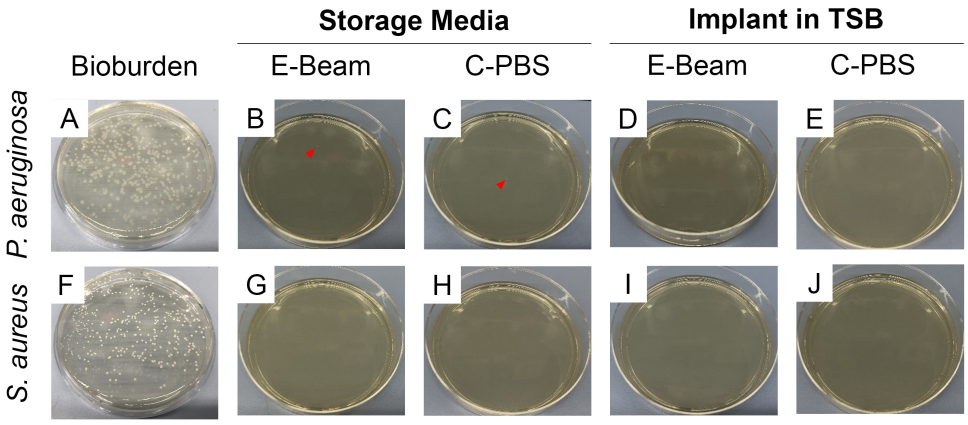
Storage Media
Implant in TSB
Bioburden
E-Beam
C-PBS
E-Beam
C-PBS
P. aeruginosa
S. aureus
A
B
C
D
E
F
G
H
I
J

Chapter 6

LiQD Cornea: Pro-Regeneration Collagen Mimetics as Patches and Alternatives to Corneal Transplantation

Christopher D. McTiernan[1,2,3†], Fiona C. Simpson[1,2†], Michel Haagdorens[4], Chameen Samarawickrama[5,6], Damien Hunter[5], Oleksiy Buznyk[6], Per Fagerholm[6], Monika K. Ljunggren[6], Philip Lewis[7], Isabel Pintelon[8], David Olsen[9], Elle Edin[1,2], Marc Groleau[1], Bruce D. Allan[10*], May Griffith[1,2*]

Affiliations:

[1]Centre de recherche Hôpital Maisonneuve-Rosemont, Montréal, QC, Canada.

[2]Department of Ophthalmology and Institute of Biomedical Engineering, Université de Montréal, Montréal, QC, Canada

[3]Division of Cardiac Surgery, University of Ottawa Heart Institute, Ottawa, ON, Canada

[4]Department of Ophthalmology, Visual Optics and Visual Rehabilitation, University of Antwerp, Antwerp, Belgium

[5]Centre for Vision Research, The Westmead Institute for Medical Research, and Faculty of Medicine and Health, University of Sydney, Sydney, Australia

[6]Institute for Clinical and Experimental Medicine, Linköping University, Linköping, Sweden

[7]School of Optometry and Vision Sciences, Cardiff University, Cardiff UK

[8]Laboratory of Cell Biology and Histology, University of Antwerp, Antwerp, Belgium

[9]FibroGen Inc., San Francisco, CA, USA

[10]NIHR Biomedical Research Centre at Moorfields Eye Hospital NHS Foundation Trust and UCL Institute of Ophthalmology, London, United Kingdom

†Denotes equivalent contributions.

*To Whom Correspondence Should be Addressed:

May.Griffith@umontreal.ca; bruce.allan@ucl.ac.uk

One Sentence Summary: LiQD Cornea is an injectable pro-regeneration alternative to corneal transplantation for treating corneal blindness and repair perforations.

Abstract: Transplantation with donor corneas is the mainstay for treating corneal blindness, but a severe worldwide shortage necessitates the development of other treatment options. Corneal perforation from infection or inflammation is sealed with cyanoacrylate glue. However, the resulting cytotoxicity requires transplantation. LiQD Cornea is an alternative to conventional corneal transplantation and sealants. It is a cell-free, liquid hydrogel matrix for corneal regeneration, comprising short collagen-like peptides conjugated with polyethylene glycol and mixed with fibrinogen to promote adhesion within tissue defects. Gelation occurs spontaneously at body temperature within five minutes. Light exposure is not required - particularly advantageous since patients with corneal inflammation are typically photophobic. The self-assembling, fully-defined, synthetic collagen analog is much less costly than human recombinant collagen and reduces any risk of immune rejection associated with xenogeneic materials. *In situ* gelation potentially allows for clinical application in outpatient clinics instead of operating theatres, maximizing practicality, and minimizing healthcare costs.

Introduction

The cornea is the transparent front surface of the eye that provides about two-thirds of the focusing power of the eye. Any permanent transparency loss from injury or disease can result in blindness. Currently, 23 million people globally have unilateral corneal blindness, while 4.9 million are bilaterally blind (1). Transplantation with human donor corneas has been the mainstay for treating corneal blindness for a century. However, a global donor cornea shortage leaves 12.7 million on waiting lists, with only 1 in 70 patients treated (2).

Conditions requiring corneal transplantation include persistent ulceration leading to scarring or perforation after corneal infection, burns, auto-immune diseases, and physical trauma. Corneal perforations are an emergency, and in many centers, the cornea is temporarily sealed using cyanoacrylate glue to maintain integrity and avoid losing the eye (3). However, cyanoacrylate glue is toxic and can cause local irritation and inflammation. Its incomplete polymerization leaves behind toxic cyanoacrylate monomers, while its hydrolysis releases potentially toxic compounds like formaldehyde and alkyl cyanoacrylate (4). These induce corneal scarring and vascularization. Patients generally require follow-up corneal transplantation. Despite these clear limitations, the use of cyanoacrylate glue to seal corneal perforations has remained the established emergency treatment for over 50 years (5). Other interventions include corneal suturing (6), tectonic corneal grafts (7), conjunctival flaps (8), multilayered amniotic membrane transplantation (9), soft 'bandage' contact lenses (10), and tissue sealants.

Sealants examined include a variety of natural adhesives like fibrin, gelatin, chitosan, and alginate (11), as well as a number of synthetic polyethylene glycol (PEG) derivatives (12). Most of these interventions, however, work only in a limited range of cases or require invasive surgery with possible limitations for future visual rehabilitation (13).

PEG based sealants have shown promise in sealing perforating microincisions, but to the best of our knowledge there is no study which has looked at their efficacy in sealing macroperforations. Furthermore, PEG based sealants typically require multicomponent mixing and suffer from short application windows. For example, ReSure (Ocular Therapeutic) which requires two component mixing of PEG and a trilysine acetate solution allows only a 20 second window for application upon initiation of polymerization (14).

A new bioadhesive, GelCORE, was recently reported as an alternative to cyanoacrylate glue for corneal tissue repair in partial-thickness corneal defects and corneal perforations. The authors used white light, with Eosin Y, triethanolamine (TEA), and N-vinylcaprolactam (VC) as initiators to gel a mixture of methacryloyl functionalized gelatin *in situ* (11). The GelCORE report included a 14-day rabbit study in which a 50% thickness wound was repaired. However, due to the short duration of the study, long-term effects could not be evaluated. The use of animal-derived gelatin has an associated risk of zoonotic disease transfer and severe allergic reactions to both bovine and porcine gelatin in vaccines have been reported (15). Photocrosslinking may also be problematic in the clinical setting. Patients with corneal inflammation are photophobic (light-sensitive) and may not be able to tolerate intense visible light application over four minutes without retrobulbar or general anaesthesia. In a mechanism analogous to corneal crosslinking for keratoconus, the creation of free-radicals in photocrosslinking may also be toxic to the corneal endothelium in thinned or perforated corneas (16). Hyaluronic acid-based materials have also been tested as alternative bioadhesives in an *in vitro* organ setting using excised porcine eyes (17). This solution relied on hydrazone crosslinking of dopamine-modified hyaluronic acid (HA-DOPA), where dopamine supplied the tissue adhesive properties. While successful *in vitro*, this material has not been evaluated in animal models. Neither GelCORE nor HA-DOPA was tested for repair of full-thickness corneal perforations, nor have they been examined as alternatives to donor corneal tissue for transplantation.

Over 10 years ago, our team members conducted a first-in-human clinical trial on cell-free, biosynthetic hydrogels made from recombinant human collagen type III (RHCIII). These hydrogels promoted stable corneal tissue and nerve regeneration, showing that they were immune-compatible alternatives to donor cornea transplantation in anterior lamellar keratoplasty (ALK) (18, 19). Recently, we demonstrated that hydrogel implants derived from a short collagen-like peptide (CLP) conjugated to an inert, but mechanically robust, multifunctional polyethylene glycol (PEG) are functionally equivalent to the RHCIII-based implants when tested under pre-clinical conditions in mini-pigs (20). The use of fully-defined short synthetic peptides provides homogeneous materials that are easily modified and scaled up in comparison to their full-length analogs. In addition to being fully synthetic, the use of CLP-PEG collagen analogs circumvents the batch-to-batch heterogeneity seen with extracted proteins, as well as potential allergic reactions to xenogeneic proteins (21) and possible zoonotic disease transmission (22). Despite being able to promote regeneration, these solid implants require an operating theatre for implantation, involving costs for a full surgical team. Realistically, to reach the enormous numbers of patients awaiting transplantation, most of them living in low to middle income countries, a drastic paradigm change is needed.

To date, vaccines have been vastly successful both in cost and delivery, with every person receiving a vaccine delivered in a syringe. By analogy, in dentistry, when someone has a cavity in a tooth, the pathologic tissue is removed, and the tooth is filled. A similar paradigm is likely needed to tackle this significant global issue, where the pathologic tissue is replaced by a regeneration-stimulating liquid corneal replacement, LiQD Cornea, in a syringe that gels *in situ*. Previously, we reported that CLP-PEG polymerizes *in situ* and can form a seal in experimental *in vitro* models of corneal perforation when supported by an ab interno patch (23). In this study, we introduce the LiQD Cornea, a new injectable hydrogel matrix with adhesive properties. We examined the potential efficacy of our LiQD Cornea comprising CLP-PEG-fibrinogen as a sealant/filler of full-thickness corneal perforations and an alternative to lamellar corneal transplantation that potentially allow treatments to be carried out in an ophthalmologist's office.

Results

Physical and Mechanical Characterization

The CLP-PEG-fibrinogen LiQD Cornea formed a porous hydrogel upon gelation in the presence of thrombin and a non-toxic crosslinker, 4-(4,6-Dimethoxy-1,3,5-triazin-2-yl)-4-methylmorpholinium chloride (DMTMM) (Fig. S1). LiQD Cornea hydrogel samples showed a refractive index of 1.354 ± 0.037, consistent with human corneas and physical and chemical properties consistent with previous generations of RHCIII and CLP-PEG hydrogels (Table 1) (18, 20). In the visible spectrum (400-800 nm), LiQD Cornea samples transmitted between 93% and 99% of incident light. The transmission of light in the UV region decreased to a low value of 19% in the UVC spectral region. Bursting pressure testing using *ex vivo* porcine corneas showed that the LiQD Cornea formulation, although less robust than cyanoacrylate or fibrin sealant, nevertheless withstood 170 mmHg of pressure. This was a 7.7 fold increase over the average 11 – 21 mmHg intraocular pressure within the human eyeball (Table 1).

In vitro Characterization

Human corneal epithelial cells from an immortalized line (24) adhered to and spread readily on *in vitro* gelled matrices, indicating that the LiQD Cornea supports epithelial growth (Fig. 1A). The materials were also found to be immune compatible. Precursors of murine bone marrow-derived macrophages (BMDM) cells seeded on LiQD Cornea hydrogels in the presence of macrophage differentiation media showed higher levels of expression of CD 206 (anti-inflammatory M2 marker) in comparison to CD 86 (pro-inflammatory M1 marker) at the time points examined (Fig. 1B).

This showed a polarization of the mononuclear macrophage precursors into anti-inflammatory or tolerizing phenotypes. Exposure of bone marrow-derived dendritic cells (BMDC) to the LiQD Cornea hydrogel and its components resulted in low expression of CD 40, CD80, and CD86, which are markers of activated, antigen-presenting dendritic cells. This showed that overall, the LiQD Cornea formulation did not activate dendritic cells, which are the main cells associated with triggering graft rejection (25). By comparison, dendritic cells showed significant activation marker expression when exposed to the positive lipopolysaccharide (LPS) controls (Fig. 1C).

In Vivo Rabbit Perforation Study

In accordance with the Association for Research in Vision and Ophthalmology (ARVO) Statement for the Use of Animals in Ophthalmic and Visual Research and with ethical permission from the Western Sydney Local Health District Animal Ethics Committee (Australia), conical perforations were made in one cornea each in three New Zealand white rabbits. The perforations measured 3 mm in diameter on the external epithelial surface tapering to 1 mm on the internal endothelial surface. To seal the wound gape, thrombin solution was first applied to the wound margins. Then a mixture of CLP-PEG-fibrinogen and DMTMM crosslinker was applied. As the gel sets, the thrombin which was applied to the wound surface converted the fibrinogen at the interface of the gel to fibrin, adhering the gel firmly to the wound. DMTMM then crosslinks the entire mixture. The surgically-created perforations were completely sealed with the LiQD Cornea hydrogel, as indicated by the retention of an air bubble placed within the anterior chamber (Fig. 1E). Two rabbits had a complete seal with the first application, while the third cornea required additional material for an air-tight seal. All animals received antibiotic (chloramphenicol), and anti-inflammatory (dexamethasone) eye drops three times daily for three days. There was no incidence of leakage or infection of the perforation sites in any animal, and by seven days post-surgery, all normal peri-surgical inflammation had subsided. The hydrogels initially showed haze that began to recede one day after surgery. At 28 days follow-up, two out of three rabbits had transparent corneas (Fig. 1E) and normal slit lamp exams. In the third rabbit, the gel remained visible as a slight haze in the cornea. Histopathology of the cornea showed epithelial hyperplasia and reduced corneal stroma in the perforation site, indicating that the perforation site of each cornea had undergone re-epithelialization. There was also keratocyte infiltration, indicating the onset of corneal stromal regeneration, and partial regeneration of Descemet's membrane. Furthermore, when LiQD cornea was applied to the perforated corneas of the rabbits the gel remained cohesive with itself and generally did not leak into the anterior chamber. While there was small degree of post-operative anterior chamber inflammation on Day 1, this subsided by day 3 and remained that way for the duration of the study.

In Vivo Study in Göttingen Mini-Pigs

Genetically uniform Göttingen mini-pigs were used (26) in compliance with the Swedish Animal Welfare Ordinance and the Animal Welfare Act, and with ethical permission from the local ethical committee (Linköpings Djurförsöksetiska Nämnd). Anterior lamellar keratoplasty wound beds, 6.5 mm in diameter, 500 μm deep (i.e., over 70% depth) were made in one cornea each of four mini-pigs by trephination followed by dissection with a blade. LiQD cornea was applied as for the rabbits. Fig. S2A shows the progress of repair and regeneration of all pigs receiving the LiQD Cornea compared to syngeneic grafts and healthy unoperated controls. At 12 months, the application of LiQD Cornea was successful in all pigs (Fig 1F), although in all cases the surgeon applied the LiQD Cornea at least twice, removing the first material before reapplication to achieve the desired curvature. One pig, who received four attempts at LiQD Cornea application, underwent full corneal perforation and was given a suture to bridge the unintended gape. Post-surgical OCT of the LiQD cornea application (Fig. S2B) showed that although the initial LiQD Cornea fills were imperfect, the anterior corneal surfaces of all four pigs were smooth and followed the contours of the host tissue by three months post-operation. These results also show that an easy-to-use point-of-care delivery device (Fig. S3) is merited for future clinical application.

Clinical follow-up showed that at one-month follow-up, all pigs had successfully re-epithelialized. At three months post-surgery, pachymetric analyses showed that the standard corneal thickness was restored in LiQD Cornea animals. (Fig. 3A, S2B). Intraocular pressure was normal at all post-surgical exams, indicating that the LiQD cornea successfully sealed the surgical site (Fig. 2B). The LiQD cornea pigs showed more significant haze and neovascularization than syngeneic grafts at all post-surgical time points, but haze was reduced in three out of four animals at 12 months post-operation (Fig. 2C-D). The fourth pig had poor surgical results with iritis and formation of peripheral anterior synechiae (attachment of the iris to the cornea) and infiltration of a large blood vessel into the surgical site, resulting in a hazy cornea at 12 months post-operation. This pig had inadvertently received a full-thickness corneal perforation that was reattached with a suture that trekked in a large blood vessel. This pig nevertheless showed full regeneration of corneal tissue and nerves. Aesthesiometry performed to determine touch sensitivity showed the restoration of the corneal blink response in all operated corneas, indicating the presence of regenerated nerves within the graft site (Fig. 2E). Analysis of the density of corneal nerves over time showed that by 12 months post-operation, there was no statistically significant differences in the nerve density (Fig. 2F) between the LiQD Cornea (3012.8 $\pm$ 1613.7 μm/mm^2), syngeneic (2205.3 $\pm$ 1162.4 μm/mm^2), and unoperated control (4800.4 $\pm$ 1964.9 μm/mm^2). However, it is clear that the unoperated

controls had a higher nerve density. There were no marked differences in tear production in the three treatment groups at any time point, as indicated by Schirmer's test (Fig. 2G). Collagen content analysis of the central cornea demonstrated significantly lower levels of high molecular weight, γ, β, α1(V) and α1(I) type collagen in the LiQD Cornea pigs, as compared to the syngeneic grafts and unoperated eyes (Fig. 2H, Table S5).

H&E sections of mini-pig corneas at 12-months post-surgery showed that LiQD Cornea-treated corneas had regenerated their epithelia and stroma (Fig. 3A) and resembled corneas in the syngeneic graft (Fig. 3B) and untreated control groups (Fig. 3C). The unoperated endothelia remained healthy. Transmission electron microscopy (TEM) confirmed the presence of healthy electron-lucent epithelial cells in all three samples (Fig. 3D-F). There were no cells with condensed cytoplasm or pyknotic, shrunken nuclei that are characteristic of apoptotic cells. TEM also revealed that the basal epithelial cells in all samples had desmosomes between them (Fig. 3G-I)), showing that regenerated cells in the LiQD Cornea had tight junctions and were functional as a barrier. Immunohistochemical analysis showed the presence of mucin, indicating a functional tear film in all samples (Fig. 3J-L), and epithelial cytokeratin 12, indicating terminal differentiation of regenerated epithelium (Fig. 3M-O). All samples contained very few CD163-positive cells from the monocyte/macrophage lineage (Fig. 3P-R). Immunohistochemical staining for smooth muscle actin (α-SMA) (Fig. S4A-C) and the lymph vessel marker, lymphatic vessel endothelial hyaluronan receptor 1(LYVE1) (Fig. S4D-F) respectively showed no increase in staining for myofibroblasts or lymphatics in the LiQD Cornea, as compared to allografts.

TEM images of the epithelial-stromal junction shows the presence of small vesicles in the epithelial cells in all three samples (Fig. 4A-C). Immunohistochemical staining showed the presence of large numbers of Tsg101 positive vesicles in the epithelium and stroma of LiQD Cornea treated samples (Fig. 4D). Tsg101 is an established marker for extracellular vesicles (EVs), forming part of the Endosomal Sorting Complex Required for Transport-I (ESCART-I) which is necessary for exosome-dependent intercellular signaling and vesicular trafficking (27). The staining is more diffuse in the syngeneic grafts (Fig. 4E) and minimal in the untreated controls (Fig. 4F). The samples were also stained for the tetraspanin, CD9, another established extracellular vesicle marker that more specifically marks exosomes (28). Co-localization of Tsg 101 with CD9 showed that exosomes were present in the basal epithelium and upper stroma in the LiQD cornea pigs (Fig 4G), to a lesser extent in syngeneic grafts (Fig 4H) and only minimally in the untreated corneas (Fig. 4I).

In vivo confocal microscopy (IVCM) showed that the epithelium in the LiQD Cornea was fully regenerated at the three-month examination time point and remained stable at the 12-month end-point (Fig. 5A), resembling that of the syngeneic (Fig. 5B) and untreated corneas (Fig. 5C). Regenerated nerves were found within the sub-basal epithelium of the LiQD cornea starting at three to six months post-surgery. At 12 months post-operation, the nerves present were in distinct parallel bundles (Fig. 5D), characteristic of the sub-epithelial nerve plexus, similar to those found in the healthy unoperated control corneas (Fig. 5F). Nerves in the syngeneic grafts were not as well-defined in their configuration (Fig. 5E). From three to nine months, reflective keratocytes indicative of in-growing cells were seen within the matrix. The presence of reflective cells corresponded with the increased haze seen by slit lamp biomicroscopy (Fig. 2C). At 12 months, keratocytes grew into the cell-free matrix to reconstitute the stroma (Fig. 5G). The majority of these keratocytes were not reflective and resemble keratocytes in the syngeneic grafts (Fig. 5H) and untreated controls (Fig. 5I). The decrease in reflectivity likely corresponds to the decrease in haze in Fig. 2C.

Discussion

In order to address the severe shortfall of donor tissue in the treatment of corneal blindness, it is imperative that novel alternatives to corneal transplantation and perforation repair are developed. While a number of techniques and materials are currently available to treat corneal defects and perforations, many of them involve complex procedures and employ materials with poor biocompatibility, mechanical mismatch, and an inability to support regeneration. Ideally, any newly developed method should be easy to apply in a clinical setting, readily fill corneal defects and seal perforations. At the same time, it should support tissue regeneration, limiting the need for further surgical intervention and follow-up corneal transplantation.

Our results showed that LiQD Cornea behaved as an injectable liquid at temperatures above 37°C, gelling as it cools down. *in situ* gelation of the LiQD Cornea in animal corneas took five minutes at body temperature, after initiation with DMTMM, a non-toxic crosslinker (23). Most patients with corneal perforations have inflamed eyes and are photophobic. Unlike light activated systems, LiQD Cornea did not require a dedicated light source for curing. Without the requirement for light activation, no anaesthetic will be needed in future clinical application to render the exposure to an intense light source for crosslinking tolerable. In addition, photoinitiated crosslinking has been reported to have possible phototoxic effects on the corneal endothelial cells (16). Considering that the initial perforation in pathologic corneas would also impact the health of the endothelium, it would be prudent not to further deplete the local population of endothelial cells.

The incorporation of an approved surgical fibrin sealant permitted adhesion of the LiQD cornea during *in situ* gelation. Corneal perforations in *ex vivo* corneas were completely sealed *in situ* with a bursting pressure of 170 mmHg, which is several-fold higher than normal intraocular pressures of 11 to 21 mm Hg (29). HCECs grew readily on the LiQD Cornea hydrogels. The BMDC study indicated that the LiQD Cornea did not activate dendritic cells unlike the positive control, LPS, which is a well-established activator of dendritic cells. As the LiQD Cornea formulation does not activate dendritic cells, the risk of graft rejection due to activation of CD4+ and CD8+ T-cells is reduced (30). The BMDM assay indicated that naïve BMDMs cultured in the presence of LiQD Cornea hydrogels primarily matured into a M2 phenotype that is associated with tolerogenic activity (31). These results taken together demonstrated that the LiQD Cornea formed a seal that will withstand the pressures encountered within the eye and will be fully biocompatible and immune compatible.

Injection of the LiQD Cornea into full-thickness corneal perforations in rabbits confirmed the ability to seal the wound gape. The completeness of the seal was validated by the addition of a post-surgical air bubble. The bubble was present up to two days post-surgery, indicating that the material had created a complete seal that did not allow the leakage of air. The rabbit histology showed that the patch was completely re-epithelialized. However, the 28-day duration of the study did not provide time for full stromal, endothelium and nerve regeneration.

The Göttingen mini-pigs used were genetically coherent or homogenous. Hence, grafts from one animal to another were considered syngeneic, i.e. they were sufficiently identical and immunologically compatible to allow for transplantation. The 12-month *in vivo* pig study confirmed that LiQD Cornea allowed regeneration of the corneal epithelium, stroma and nerves. Even if the material does not achieve the desired perfectly smooth surface directly after application, OCT results showed that the corneal thickness and curvature was restored to those matching the syngeneic grafts and unoperated controls (Fig. S2B). The primary difference in the clinical performance of the LiQD cornea and the syngeneic grafts was increased haze in the surgical site between three to six months post-operation, during the period of rapid keratocyte in-growth into the cell-free matrix. Syngeneic grafts were already populated with donor cells, so no rapid in-growth of host cells was expected. However, at one-year post surgery, the haze was reduced to a low grade in three out of four LiQD Cornea recipients, while the syngeneic graft outline was still clearly visible in the corneas. Neovascularization had accompanied the haze, as we had previously reported for solid CLP-PEG implants during the rapid cell population of cell-free grafts (20). However, as observed in previous solid implant studies (32, 33), the vessels receded over the 12-month observation period as haze cleared in three of four animals. While this small amount of vascularization and haze is not ideal, it is

unlikely to lead to immune rejection. LiQD Cornea does not activate dendritic cells *in vitro*, and is acellular and repopulated by the host cells, unlike traditional corneal transplants which bring with them allogeneic cells (25) whose surface proteins can trigger immune reactions. Vascularization could increase the risk of rejection of subsequent allografts (34), but LiQD Cornea is designed to regenerate the eye wall without the need for subsequent transplantation, avoiding problems with induced irregular astigmatism, rejection, and lack of access to transplant donor material. Where corneal perforations involve the central visual axis, at minimum, LiQD cornea aims to restore eye wall integrity as a viable pathway for future rehabilitation. In our pig model, steroid medication was only administered for 5 days. In a clinical setting, it may be possible to modulate neovascularization during healing through application of topical steroids for a longer period.

We also found that LiQD corneas had lower expression of mature type I collagen in the cornea. This is in keeping with the fact that the LiQD Cornea matrix had no collagen and hence, all collagen found at 12-months post-surgery was due to active remodeling of the gel, in comparison to syngeneic grafts which had a complete extracellular matrix at the time of grafting. When considering the relative performance of the LiQD cornea and the syngeneic grafts, it is important to note that the syngeneic grafts are likely less inflammatory than a standard clinical allograft, due to the genetic homogeneity of Göttingen mini-pigs. Interestingly, as previously reported for CLP-PEG (20), the LiQD Cornea also induced the production of copious amounts of EVs that included exosomes, in comparison to the syngeneic grafts, and the lack of EVs in the untreated, healthy controls. We currently hypothesize that the presence of the EVs is linked to the production of new extracellular matrix in the surgical site, as the reduced collagen content in the LiQD Cornea suggests that the new tissue is still undergoing ECM protein secretion to restore the matrix at 12 months.

Overall, LiQD Cornea performed equivalently to syngeneic grafts, indicating a possible role as an alternative to conventional donor corneal transplantation for conditions treatable by lamellar transplantation. However, as noted, it took the surgeon an average of two attempts to achieve the desired curvature, indicating that an appropriate point-of-care delivery device (Fig. S3) is needed for clinical application. The self-assembling, fully-defined, synthetic collagen-like LiQD Cornea is considerably less costly than human recombinant collagen and reduces any risk of allergy or immune rejection associated with xenogeneic materials. *in situ* gelation potentially allows for clinical application in an outpatient clinic instead of an operating theatre, thereby maximizing practicality while minimizing healthcare costs.

Materials and Methods

Synthesis of 8 arm CLP-PEG

The synthesis and characterization of CLP-PEG through conjugation of 8-Arm-PEG-Maleimide to the 38 A.A. CLP via the formation of a thio-ether linkage has been previously described (23, 35). Successful conjugation of the CLP to the PEG-maleimide is confirmed through the disappearance of the vinylic proton peak at 7 δ ppm by ^{1}H NMR spectroscopy and the appearance of characteristic vibrations in the FTIR spectrum.

Briefly, Collagen-like peptide [CLP: $CG(PKG)_4(POG)_{44}$] (AmbioPharm, SC, USA) was conjugated to a 40K 8 arm PEG-maleimide with hexa-glycerol core (Sinopeg Biotech Co. Ltd., Beijing, China) to give rise to CLP-PEG (35). Briefly, 20 mL of water was degassed by sparging with N_2 for 20 min. The flask was charged with 770 mg of 8 arm PEG-maleimide, and the solution was stirred until complete dissolution was achieved. CLP (625 mg) was added to the stirring solution (molar ratio of 8 arm PEG-maleimide:CLP is 1:8). The solution was allowed to stir for an additional 20 minutes (at this point all materials should be dissolved). The pH of the solution was adjusted to 4.5 through dropwise addition of 2 M NaOH. As the pH of the solution is adjusted, the reaction mixture becomes too viscous to be appropriately stirred. At this point another 30 mL of N_2 purged water was added. The reaction flask was covered in aluminum foil and allowed to stir for 5 days. The pH of the reaction mixture was monitored periodically during this time and adjusted accordingly. At the end of the 5 days, an additional 50 mL of water was added to the reaction mixture and again the pH was adjusted to 4.5. The solution was filtered through a 0.45 μm syringe filter. The filtered solution was transferred to dialysis tubing (MWCO 14 000). The tubes were dialyzed against pH 4.5 water for 7 days, while exchanging the water every 12 hours. The contents of the dialysis bags were transferred to 50 mL Falcon tubes as 25 mL aliquots. The solutions were frozen overnight at -80°C and freeze dried, resulting in a cotton-like solid CLP-PEG conjugate.

Reconstitution of CLP-PEG and Fibrinogen at 10% and 1% w/w respectively

The plunger of a 10 mL sterile syringe with luer lock was removed and the end fitted with a syringe cap. CLP-PEG and fibrinogen (clottable protein, Tisseel, Baxter International, Deerfield, IL, USA) were added to the barrel of the syringe. HyPure™ molecular biology grade water (GE Lifesciences, Logan, UT) was added to give a final dilution of 10% w/w and 1% w/w for the CLP-PEG and fibrinogen, respectively. The syringe was then sealed with parafilm and the CLP-PEG and fibrinogen was allowed to reconstitute at room temperature (RT) for 2-3 weeks. To facilitate the reconstitution process, the mixture was stirred periodically with a spatula and warmed up to 37°C in

a incubator. Once completely resuspended, the solution was heated above its melting temperature (>37°C) and centrifuged at 3000 rpm for 10 minutes. This process was repeated until all bubbles had been removed from the syringe.

Reconstitution of Thrombin

Thrombin was reconstituted at 250 U/mL by the addition of 4 mL of 10 mM PBS to the vial of thrombin contained within the Tisseel kit. The solution was mixed at RT for 20 minutes prior to use. The solution was either immediately used or aliquoted into several Eppendorf tube and frozen at -20 °C for future use. Frozen samples were thawed to RT before use.

Mixing and Application of LiQD Cornea

The solution within the syringe containing 10% w/w CLP-PEG and 1% w/w fibrinogen behaves as a liquid (injectable) at temperatures above 37°C, but sets as a gel when cooled to 25 °C due to the templated assembly of the CLPs. However, this sol-gel transition is reversible. In order to make this sol-gel transition irreversible to obtain a hydrogel, a solution of the crosslinker 4-(4,6-Dimethoxy-1,3,5-triazin-2-yl)-4-methylmorpholinium chloride (DMTMM) in 10 mM PBS was added to the mixture to obtain a final 2% w/w concentration of DMTMM, while cooling down the solution of CLP-PEG and fibrinogen from 50°C to 25°C. For application into the cornea, the stock solution of CLP-PEG/fibrinogen was heated to 50°C and transferred to a 2 mL glass syringe and assembled within a T-piece mixing system that had been primed with 10 mM PBS. The T-piece system was heated to 50 ºC and mixed until homogeneous. A 10% w/w solution of DMTMM in 10 mM PBS was introduced through the injection port of the mixing system to give a final concentration of 2% w/w DMTMM. The solution was mixed within the T-piece system until homogeneous and then dispensed into the wound bed to which the 250 U/mL solution of thrombin had been applied.

Physical and Mechanical Characterization

Collagenase Degradation Assay

Collagenase from Clostridium histolyticum (Sigma-Aldrich) at 5 U/mL in 0.1 M Tris-HCl buffer containing 5 mM $CaCl_2$ was used to evaluate the stability of the hydrogels as previously described. Briefly, samples were weighed after blotting off surface water at different time points to determine the rate of loss of mass. The percentage of residual weight was calculated using the following equation: Residual mass % = W_t / W_0 %, where W_t is the weight of hydrogel at a certain time point and W_0 is the initial weight of the hydrogel.

Fourier Transform Infrared (FTIR) Spectroscopy

Hydrogels were dried under vacuum for 3 days and measured using a Nicolet is5 FTIR spectrometer equipped with a iD7 Attenuated Total Reflectance (ATR) sampling accessory with 4 cm^{-1} resolution; a total of 300 individual spectra were collected for each sample.

Differential Scanning Calorimetry (DSC)

Denaturation temperature of the hydrogels was measured using a Q2000 DSC (TA Instruments, New Castle, DE, USA). Heating scans were recorded in the range of 8 to 210°C at a scan rate of 10°C/min. Glass transition temperature (T_g) was measured as the onset of the endothermic peak.

Refractive Index

The refractive index of the hydrogels was measured at RT on an Abbemat 300 (Anton Parr) refractometer. *Young's Modulus and Tensile Strength* The Young's Modulus and Tensile Strength of a 500 μM sheet of crosslinked material was evaluated in an Instron electromechanical universal tester (Model 3342, Instron, Norwood, MA) equipped with Series IX/S software, using a crosshead speed of 10 mm min-1. The hydrogel was equilibrated in 2× PBS for 1 h before being cut into a 10 x 5 mm rectangular piece. In order to remove surface water, the hydrogel was gently blotted with paper immediately prior to Instron measurement.

Water content of hydrogels

The water content of hydrogels was evaluated by weighing the "wet weight" (W_0) of the samples and then comparing this to the weight of the material after being dried at RT until a constant weight was achieved (W). The total water content of the hydrogels (W_t) was calculated according to the equation: W_t % = (W - W_0) / W %

Pore Size of hydrogels

Pore size measurements were made from SEM images obtained using a low temperature scanning electron microscope (Cryo-SEM) in a Tescan (model:Vega II – XMU) with cold stage sample holder at -50 °C.

Viscosity of hydrogels

The viscosity of 500 μm hydrogels were measured on a Brookfield RS-CPS+ Rheometer (Brookfield Engineering Laboratories, Inc., Middleboro, MA). The measurements were carried out at 37 °C under parallel-plate geometry.

Light Transmission of hydrogels

The light transmission of hydrogels between 250 nm and 800 nm was evaluated by placing a 5 mm x 10 mm strip of hydrogel on the inside wall of a quartz cuvette filled with PBS and reading its absorption in a Spectramax M2e series plate/cuvette spectrophotometer (Molecular Devices, San Jose, CA, USA). A cuvette filled with only PBS was used as the baseline reference. Measured absorbances were then converted to corresponding % transmission values.

Ex Vivo Model of Corneal Perforation and Sealing Evaluation

Corneoscleral buttons were excised from porcine eyes obtained from a local abattoir (Tom Henderson's Meats and Abattoir Inc., Chesterville, ON, Canada). The corneoscleral buttons were mounted on an artificial anterior chamber (Barron Artificial Anterior Chamber, Katena, NJ) and standardized corneal defects were made. Briefly, a 4 mm punch was used to partially trephine test corneas centrally to a depth of approximately 200 μm. Lamellar dissection of the cap was performed with a pediatric crescent blade, leaving a residual stromal depth which was then trephined with a 3 mm punch to a depth of 200 μm. A subsequent central full thickness defect was created in the central stromal bed with a 1 mm skin biopsy punch to mimic a full-thickness corneal perforation commonly encountered in clinical practice.

Sealing Methods

Once the standardized corneal perforations had been made, one of three different materials were used to seal the defect. Each condition was repeated four times. Cyanoacrylate glue was injected to completely fill the defect. After allowing the glue to dry the infusion was increased and the bursting pressures were measured. For fibrin glue evaluation, fibrinogen (2% w/w) and thrombin (250 U/mL) solutions were mixed (4:1) and transferred to completely fill the defect. After allowing the glue to dry, the infusion was increased and the bursting pressures were measured. For the LiQD Cornea, the defect was coated with 250 U/mL thrombin. The LiQD Cornea was injected to completely fill the defect. After allowing the glue to dry the infusion was increased and the bursting pressures were measured.

Bursting Pressure Evaluation

Artificial anterior chambers were connected via an intra-arterial blood pressure monitor (TruWave, Edwards Lifesciences) to a saline infusion bag using a pressure cuff to regulate infusion pressure. After application of test material, the infusion pressure was increased until the seal gave way, resulting in fluid egress. Bursting pressure (mmHg) was recorded as the peak in a continuous trace of infusion pressure versus time.

In vitro Evaluation of the LiQD Cornea

The *in vitro* compatibility of the LiQD Cornea was tested using green fluorescence protein (GFP) transfected immortalized human corneal epithelial cells (HCECs) (24). Briefly, 3 wells of a 24 well plate were coated with the LiQD Cornea. The glue was allowed to set for 1 hour before it was washed 3 times with 1 mL of 2× PBS. GFP-HCECs were seeded into the control wells and onto the materials at a density of 5,000 cells/well. GFP-HCECs were supplemented with keratinocyte serum-free medium (KSFM; Gibco, ThermoFisher, Waltham, MA, USA) containing 0.05 mg/mL bovine pituitary extract, 5 ng/mL epidermal growth factor, and 1 mg/mL penicillin/streptomycin and their growth monitored for 7 days in a humidified incubator at 37 °C and 5% CO2.

Bone-Marrow Derived Dendritic Cell Culture and Flow Cytometry Analysis

With ethical permission from the Animal Care and Use Committee of Maisonneuve-Rosemont Hospital, bone marrow was isolated from the tibia and femur of male, C57BL/6J mice (6-12 weeks old) (36, 37). Cells were seeded on suspension culture plates with 1×10^6 million cells per well in RPMI 1640 containing 10% (v/v) fetal bovine serum (Wisent), 0.5 mg/mL penicillin-streptomycin-glutamine, 10 mM HEPES, 1 mM sodium pyruvate, 55 μm β-mercaptoethanol and 2.5 ng/uL granulocyte-macrophage colony-stimulating factor (GM-CSF) (all Gibco, ThermoFisher, Waltham, MA, USA). BMDCs were cultured for six days. RPMI-C containing 5.0 ng/mL GM-CSF was exchanged for half of the media on days two and three of culture. On day six, the cells were collected and enlarged cells were selected using a Histodenz™ density gradient (Sigma-Aldrich, St. Louis, MO). The selected cells were seeded at a density of 1×10^6 cells/well on a 24 well plate for materials testing.

For materials testing, BMDCs were incubated for 24 hours with a 6mm, 500 μm thick hydrogel disk. Individual hydrogel components CLP, PEG, CLP-PEG, DMTMM, fibrinogen, and thrombin were applied to the cells at a concentration equivalent to the hydrogel volume (Table S1). LPS was used as a positive control for BMDC activation. BMDCs were labelled with direct-conjugate antibodies for CD11c, CD40, CD80 and CD86 (Table S2) and Zombie Aqua™ Fixable Viability Kit

(BioLegend, San Diego, CA). All samples were acquired using a BD LSR II and analyzed using FlowJo software (Becton, Dickinson & Company, Franklin Lakes, NJ, USA). BMDCs were selected using Zombie Aqua and CD11c as markers of a live, dendritic cell phenotype. Mean fluorescence for CD40, CD80 and CD86 was measured for the selected BMDCs and transformed into a ratio over the untreated BMDC control for analysis.

Macrophage Polarization Assay

Macrophages were isolated as previously described (38) with ethical permission from the Animal Care and Use Committee of the Ottawa Heart Research Institute. Briefly, bone marrow-derived macrophages (BMDMs) were generated from the tibial bones of C57BL/6 female mice (8-10 weeks old). BMDMs were maintained for 1 week in DMEM with 10% FBS, 15% L929 media containing macrophage colony-stimulating factor and penicillin-streptomycin.

For the assay, BMDM precursors from female C57BL/6 mice (8-10 weeks old) were used. The wells of a 24-well culture plate were fitted with 18 mm circular glass coverslips. A portion of the coverslips was then coated with the LiQD Cornea. The hydrogel was allowed to set for 1 hour before it was washed 3 times with 1 mL of 2× PBS, followed by two additional 1 mL rinses with media before the seeding of cells. The BMDMs were seeded into the control wells and onto the material at a density of 200,000 cells/well. The plate was then placed in a humidified incubator at 37 °C and 5% CO_2 with the media in each well being exchanged every 48 hours up to 7 days. On days 4 and 7 a subset of the wells was processed for immunofluorescence analysis to determine their polarization towards either an M1 or M2 phenotype. Briefly, media was removed, wells were washed 2× with Hank's buffer, and then cells were fixed with a solution of 4% PFA in 2× PBS at 4°C in the dark. Fixative was removed and wells were washed 2× with NH_4Cl in PBS, waiting 7 minutes between washes. The samples were then washed 3× with 2× PBS. On the final wash 0.2% NaN_3 was added from a 2% NaN_3 stock (10 μL/ 1 mL). When ready for staining, samples were washed with PBS and then blocked and permeabilized using a 2% BSA in PBS solution containing 0.5% Triton X-100 for 1.5 hours at RT. Primary antibodies for CD206 and CD86 (Table S1) were then diluted appropriately and added to the well plate to incubate overnight covered in foil at 4°C. The next day wells were washed with 2× PBS. Secondary antibodies (Table S1) were diluted and added to the plate and incubated at RT covered in foil for 1 hour. After 1 hour of incubation with the secondary antibodies, the wells were washed 3× with 2× PBS. The coverslips were removed from the wells and mounted onto a glass slide using Prolong™ Gold antifade reagent with DAPI (Invitrogen, P36931). Cells were imaged with a Zeiss Axiovert 200M Fluorescence microscope equipped with an AxioCam MR

camera using 63× oil immersion objective. The filters employed were DAPI blue filter (Ex: 352-402 / Em: 417-477), GFP green filter (Ex: 457-487 / Em: 502-538), Texas Red red filter (Ex: 542-582 / Em: 604-644).

Rabbit Perforation Study

All experiments had ethical approval from the Western Sydney Local Health District Animal Ethics Committee. Three New Zealand white rabbits underwent controlled surgical perforation of the right eye under general anaesthesia (sedation: 25 mg/kg medetomidine, analgesia: 0.5 mg/kg buprenorphine, anaesthesia: 50 mg/kg ketamine, 2% inhaled isofluorane). A 3 mm surgical trephine was used to make a partial thickness incision prior to full perforation using a 15 stab knife. The full incision was then enlarged to create a 1 mm full thickness perforation. The perforation was filled with LiQD Cornea hydrogel and allowed to crosslink *in situ*. Air was injected into the anterior chamber to ensure that the perforation was completely sealed. For the three days post-surgery, rabbits received 0.1% dexamethasone (Maxidex, Alcon Laboratories, Australia) and 0.5% chloramphenicol eyedrops (Chlorsig, Aspen Pharma, Australia) three times a day. Animals were monitored daily for signs of discomfort or glue leakage for the first week post-surgery, and then twice weekly for subsequent weeks. Rabbits underwent follow-up clinical evaluation and slit lamp exams on days 1, 2, 3, 7, 14, 21 and 28 post-surgery. At day 28 post-surgery, rabbits were euthanized and corneas from all operated and unoperated eyes were excised, fixed in 10% buffered formalin and processed for paraffin embedding for histopathological examination (33).

***In Vivo* Study in Göttingen Mini-Pigs**

In compliance with the Swedish Animal Welfare Ordinance and the Animal Welfare Act, and with ethical permission from the local ethical committee (Linköpings Djurförsöksetiska Nämnd), Göttingen mini-pigs underwent an anterior lamellar keratoplasty of the left eye. The left corneas were cut with a 6.5mm surgical trephine to a depth of 500 μm, followed by blunt dissection of corneal stroma with a blade to create a wound bed. Four pigs received the LiQD Cornea formulation, which was crosslinked *in situ* and subsequently covered with human amniotic membrane that was secured with overlying sutures. Four pigs received syngeneic grafts, i.e., they were grafted with the tissue removed from another, albeit genetically coherent, pig in the group. Syngeneic grafts were secured with conventional interrupted sutures. The right contralateral corneas served as unoperated controls. Post-operation, the operated eyes received dexamethasone/tobramycin eye drops (Tobrasone, Alcon, Sweden). Upon surgical completion, the pigs received a maintenance dose of

one drop, three time per day for five days post-surgery. Pigs were monitored daily for ocular health. Clinical exams were conducted under anaesthesia pre-surgery and at six weeks, 3, 6, and 12 months post-surgery. Clinical exams included slit lamp examination using a Kowa Sl-15 Portable slit lamp (Kowa Company, LTD., Aichi, Japan), anterior segment optical coherence tomography (AS-OCT) to conduct corneal pachymetry (Optovue, Fremont, CA, USA), Schirmer's tear test (tear strips from TearFlo, Hub Pharmaceuticals, Rancho Cucamonga, CA, USA), aesthesiometry to determine corneal sensitivity as a measure of nerve function (using a Cochet-Bonnet esthesiometer; Handaya Co., Tokyo, Japan), measurement of intraocular pressure (using a TonoVet tonometer, Icare Finland Oy, Vantaa, Finland) and in vivo confocal microscopy (Heidelberg HRT3 with a Rostock Cornea Module, Heidelberg Engineering GmbH, Dossenheim, Germany).

Central Collagen Content Analysis

Central corneal biopsies (3 mm) were taken from each cornea and snap frozen. For analyses, the samples were thawed and resuspended in 10 mM HCl at a ratio of 1:35 (w/v). Samples were digested using 1 mg/mL pepsin (Roche, Basel, Switzerland) at 2-8°C for 96 hours. The soluble fraction was recovered by centrifugation at 16,000xg for 30 min at 2-4°C. An aliquot of the pepsin soluble fraction was mixed with NuPAGE 4X LDS sample buffer (Life Technologies, ThermoFisher, Waltham, MA, USA) denatured at 75°C for 8 minutes and analyzed on 3 - 8 % Tris-acetate gels under non-reducing conditions. Proteins were visualized by staining with Gelcode Blue (Pierce, ThermoFisher, Waltham, MA, USA). Pre-stained broad range marker (New England Biolabs, P7712) and porcine skin type I collagen (Koken Co. Ltd., Tokyo, Japan) were used as molecular weight standards. To quantitate the amounts of type I and type V collagens in control and operated corneas, densitometric scans of the stained gels were made to obtain relative numerical units using GE Healthcare ImageQuant 350 (GE Healthcare, Chicago, IL, USA).

Histopathology and Immunohistochemistry

After removal of a central biopsy, a quarter of each operated and unoperated cornea was processed, paraffin-embedded and stained with hematoxylin and eosin as described previously (32). Another quarter of each operated and unoperated cornea was treated with a sucrose gradient and fixed in 4% paraformaldehyde. The samples were frozen in optimal cutting temperature medium and sectioned at 8 or 10 μm prior to mounting on glass slides. Slides were washed in PBS prior to permeabilization in PBS with 0.3% Triton-X-100 for 15 minutes. Slides were then washed in PBS. Sections stained using AlexaFluor 488 or 647 secondary antibodies were incubated for 30 minutes in Tris-buffered

saline (TBS) containing 50 mM ammonium chloride to reduce background fluorescence. All sections were blocked for 1 hour at RT in PBS containing 5% normal goat serum or FBS with 0.1 g/mL saponin. Sections were stained with primary antibodies for cytokeratin 12, CD163, α-smooth muscle actin, and lymphatic vessel endothelial hyaluronan receptor 1 (LYVE1) (Table S3) overnight at 4°C in blocking solution. Slides were washed in PBS or TBS buffer containing 5% FBS and incubated with secondary antibodies (Table S3) conjugated to AlexaFluor 488 or 594 diluted at 1:1000 in blocking solution for one hour at RT. Sections stained using AlexaFluor 488 or 647 secondary antibodies were quenched for autofluorescence using the Vector® TrueVIEW™ Autofluorescence Quenching Kit (Vector Laboratories, Burlingame, CA, USA). Slides were stained with DAPI (5 μg/mL) for 10 minutes prior to mounting in Vectashield Antifade Mounting Medium or Vectashield Vibrance Mounting Medium (Vector Laboratories, Burlingame, CA, USA). Slides stained using lectin were washed in PBS, stained with lectin overnight at 4°C, washed and counterstained with DAPI, before mounting in Vectashield Antifade Mounting Medium. All slides were imaged using a Zeiss LSM 880 confocal microscope (Zeiss, Oberkochen, Germany). Two dimensional images were processed using FIJI (40). Extracellular vesicle and exosome staining using CD9 and Tsg101 was reconstructed as surfaces in Imaris v9.2.1 (Bitplane Inc., Concord, MA, USA) with an intensity threshold of 1.5 and 2 for CD9 and Tsg101 respectively, with a minimum voxel threshold of 10. A co-localization channel was built using the same intensity threshold as the surface reconstructions and converted into surfaces using a fluorescent intensity threshold of 0.5 and a minimum voxel threshold of 2.

Transmission Electron Microscopy

For Transmission Electron Microscopy (TEM), a quarter of each cornea was fixed in 2.5% glutaraldehyde solution in 0.1 M sodium cacodylate-buffer (pH 7.4). Samples were then cut in 1mm wide strips and post-fixed in 1% OsO_4 solution for 2 hrs. After dehydration in an ethanol gradient (50% - 70% - 90% - 95% - 100% ethanol), whole mounts were embedded in EMbed 812 (Electron Microscopy Sciences, Hatfield, Pennsylvania). Ultrathin sections were stained with lead citrate and examined using Tecnai G2 Spirit Bio Twin Microscope (FEI, Eindhoven, The Netherlands) at 120 kV.

Central Cornea Nerve Analysis

In vivo confocal microscopy examinations were performed at various timepoints (pre-surgery, 3 months, 6 months, 9 months, and 12 months post-surgery) throughout the 12-month mini-pig

study. For each examination, all images with nerves were identified. For identification purposes, nerves were defined as bright, slender, straight, or branched structures; as substantially uniform in intensity along their length and width, and as having a marked contrast difference from the background intensity level. Nerve tracing and analysis software NeuronJ was used in combination with FIJI software to manually measure the total length of nerves present in each image identified as containing nerves (39). The central cornea nerve densities are reported from the average of the single-frame image displaying the highest nerve density for each treatment group and timepoint.

Evaluation of Preliminary Point-of-Care (POC) Delivery System

Testing of the preliminary POC delivery system (Fig. S3) was performed using the previously described *ex vivo* corneal perforation model. Briefly, a stock solution consisting of 10% CLP-PEG and 1% fibrinogen was heated to 50°C and transferred to a 1 mL disposable BD syringe. An equal volume of 10% w/w DMTMM in 10 mM PBS was added to a second 1 mL disposable BD syringe. The syringes were then attached to a dual syringe adapter (Medmix Systems AG, Switzerland), which was fitted with a 1:1 static mixer (Medmix Systems AG, Switzerland) and a 19 G x 25 mm flattened tip cannula. The mixing system was heated to 50°C and the material was dispensed through the mixing system into the wound bed to which a 250 U/mL solution of thrombin had been applied.

Statistical Analyses

The *in vitro* statistical analysis for BMDCs was performed using an unpaired, two-way t-test with a confidence interval of 95% for each marker (GraphPad Prism 8.3.0, GraphPad Software, LLC., San Diego, CA, USA). The unit of analysis was the mouse (n=6, per group). The unit of analysis for the clinical statistics was the eye. The clinical statistics were conducted on uneven population sizes (LiQD Cornea n=4; syngeneic graft n=4; unoperated n=8). For variables with repeated measures over time, a mixed-effects analysis with Geisser-Greenhouse's correction was performed (α=0.05) with a Tukey multiple comparison test for treatment effects by time point (GraphPad Prism 8.3.0). Post-mortem collagen content analysis was performed using a one-way ANOVA for each collagen type with a Tukey post-hoc test (α=0.05) (IMB® SPSS® Statistics Version 25, IMB Corp., Armonk, NY, USA). All graphs were prepared using GraphPad Prism and data is displayed as mean with individual data points or mean ± standard error of the mean (SEM).

References

(1) M. S. Oliva, T. Schottman, M. Gulati, Turning the tide of corneal blindness. *Indian J. Ophthalmol.* **60**, 423-427 (2012).

(2) P. Gain, R. Jullienne, Z. He, M. Aldossary, S. Acquart, F. Cognasse, G. Thuret, Global Survey of Corneal Transplantation and Eye Banking. *JAMA Ophthalmol.* **134**, 167-173 (2016).

(3) V. Jhanji, A. L. Young, J. S. Mehta, N. Sharma, T. Agarwal, R. B. Vajpayee, Management of Corneal Perforation. Surv. Ophthalmol. 56, 522-538 (2011).

(4) P. Jarrett, A. Coury, In *Joining and Assembly of Medical Materials and Devices*, Y. Zhou, M. D. Breyen, Eds. (Woodhead Publishing, 2013), pp. 449-490.

(5) B. J. Vote, M. J. Elder, Cyanoacrylate glue for corneal perforations: a description of a surgical technique and a review of the literature. *Clinical & experimental ophthalmology* **28**, 437-442 (2000).

(6) H. Yokogawa, A. Kobayashi, N. Yamazaki, T. Masaki, K. Sugiyama, Surgical therapies for corneal perforations: 10 years of cases in a tertiary referral hospital. *Clin. Ophthalmol.* **8**, 2165-2170 (2014).

(7) M. Vanathi, N. Sharma, J. S. Titiyal, R. Tandon, R. B. Vajpayee, Tectonic grafts for corneal thinning and perforations. *Cornea* **21**, 792-797 (2002).

(8) A. Khodadoust, A. Quinter, Microsurgical approach to the conjunctival flap. *Arch. Ophthalmol.* **121**, 1189-1193 (2003).

(9) K. Hanada, J. Shimazaki, S. Shimmura, K. Tsubota, Multilayered amniotic membrane transplantation for severe ulceration of the cornea and sclera. *Am. J. Ophthalmol.* **131**, 324-331 (2001).

(10) C. E. Hugkulstone, Use of a bandage contact lens in perforating injuries of the cornea. *J. R. Soc. Med.* **85**, 322-323 (1992).

(11) E. Shirzaei Sani, A. Kheirkhah, D. Rana, Z. Sun, W. Foulsham, A. Sheikhi, A. Khademhosseini, R. Dana, N. Annabi, Sutureless repair of corneal injuries using naturally derived bioadhesive hydrogels. *Sci. Adv.* **5**, eaav1281 (2019).

(12) S. Guhan, S. L. Peng, H. Janbatian, S. Saadeh, S. Greenstein, F. Al Bahrani, A. Fadlallah, T. C. Yeh, S. A. Melki, Surgical adhesives in ophthalmology: history and current trends. *Br. J. Ophthalmol.* **102**, 1328-1335 (2018).

(13) A. Sharma, R. Kaur, S. Kumar, P. Gupta, S. Pandav, B. Patnaik, A. Gupta, Fibrin glue versus N-butyl-2-cyanoacrylate in corneal perforations. *Ophthalmol.* **110**, 291-298 (2003).

(14) S. Hoshi, F. Okamoto, M. Arai, T. Hirose, Y. Sugiura, Y. Kaji, T. Oshika, In Vivo and In Vitro Feasibility Studies of Intraocular Use of Polyethylene Glycol-Based Synthetic Sealant to Close Retinal Breaks in Porcine and Rabbit Eyes. *Invest. Ophthalmol. Vis. Sci.* **56**, 4705-4711 (2015).

(15) T. Nakayama, C. Aizawa, Change in gelatin content of vaccines associated with reduction in reports of allergic reactions. *J. Allergy Clin. Immunol.* **106**, 591-592 (2000).

(16) G. Wollensak, E. Sporl, F. Reber, L. Pillunat, R. Funk, Corneal endothelial cytotoxicity of riboflavin/UVA treatment in vitro. *Ophthalmic Res.* **35**, 324-328 (2003).

(17) L. Koivusalo, M. Kauppila, S. Samanta, V. S. Parihar, T. Ilmarinen, S. Miettinen, O. P. Oommen, H. Skottman, Tissue adhesive hyaluronic acid hydrogels for sutureless stem cell delivery and regeneration of corneal epithelium and stroma. *Biomaterials* **225**, 119516 (2019).

(18) P. Fagerholm, N. S. Lagali, K. Merrett, W. B. Jackson, R. Munger, Y. Liu, J. W. Polarek, M. Söderqvist, M. Griffith, A Biosynthetic Alternative to Human Donor Tissue for Inducing Corneal Regeneration: 24-Month Follow-Up of a Phase 1 Clinical Study. *Sci. Transl. Med.* **2**, 46ra61 (2010).

(19) P. Fagerholm, N. S. Lagali, J. A. Ong, K. Merrett, W. B. Jackson, J. W. Polarek, E. J. Suuronen, Y. Liu, I. Brunette, M. Griffith, Stable corneal regeneration four years after implantation of a cell-free recombinant human collagen scaffold. *Biomaterials* **35**, 2420-2427 (2014).

(20) J. R. Jangamreddy, M. K. C. Haagdorens, M. Mirazul Islam, P. Lewis, A. Samanta, P. Fagerholm, A. Liszka, M. K. Ljunggren, O. Buznyk, E. I. Alarcon, N. Zakaria, K. M. Meek, M. Griffith, Short peptide analogs as alternatives to collagen in pro-regenerative corneal implants. *Acta Biomater.* **69**, 120-130 (2018).

(21) R. J. Mullins, C. Richards, T. Walker, Allergic reactions to oral, surgical and topical bovine collagen. Anaphylactic risk for surgeons. A*ust. N. Z. J. Ophthalmol.* **24**, 257-260 (1996).

(22) J. A. Fishman, Infectious disease risks in xenotransplantation. *Am. J. Transplant.* **18**, 1857-1864 (2018).

(23) C. Samarawickrama, A. Samanta, A. Liszka, P. Fagerholm, O. Buznyk, M. Griffith, B. Allan, Collagen-Based Fillers as Alternatives to Cyanoacrylate Glue for the Sealing of Large Corneal Perforations. *Cornea* **37**, 609-616 (2018).

(24) K. Araki-Sasaki, Y. Ohashi, T. Sasabe, K. Hayashi, H. Watanabe, Y. Tano, H. Handa, An SV40-immortalized human corneal epithelial cell line and its characterization. *Invest. Ophthalmol. Vis. Sci.* **36**, 614-621 (1995).

(25) Y. Qazi, P. Hamrah, Corneal Allograft Rejection: Immunopathogenesis to Therapeutics. *J. Clin. Cell Immunol.* 2013, 006 (2013).

(26) H. Simianer, F. Köhn, Genetic management of the Göttingen Minipig population. *J. Pharmacol. Toxicol. Methods* **62**, 221-226 (2010).

(27) I. Ahmed, Z. Akram, H. M. N. Iqbal, A. L. Munn, The regulation of Endosomal Sorting Complex Required for Transport and accessory proteins in multivesicular body sorting and enveloped viral budding - An overview. *Int. J. Biol. Macromol.* **127**, 1-11 (2019).

(28) C. Théry, K. W. Witwer, E. Aikawa, M. J. Alcaraz, J. D. Anderson, R. Andriantsitohaina, A. Antoniou, T. Arab, F. Archer, G. K. Atkin-Smith, D. C. Ayre, J.-M. Bach, D. Bachurski, H. Baharvand, L. Balaj, S. Baldacchino, N. N. Bauer, A. A. Baxter, M. Bebawy, C. Beckham, A. Bedina Zavec, A. Benmoussa, A. C. Berardi, P. Bergese, E. Bielska, C. Blenkiron, S. Bobis-Wozowicz, E. Boilard, W. Boireau, A. Bongiovanni, F. E. Borràs, S. Bosch, C. M. Boulanger, X. Breakefield, A. M. Breglio, M. Á. Brennan, D. R. Brigstock, A. Brisson, M. L. D. Broekman, J. F. Bromberg, P. Bryl-Górecka, S. Buch, A. H. Buck, D. Burger, S. Busatto, D. Buschmann, B. Bussolati, E. I. Buzás, J. B. Byrd, G. Camussi, D. R. F. Carter, S. Caruso, L. W. Chamley, Y.-T. Chang, C. Chen, S. Chen, L. Cheng, A. R. Chin, A. Clayton, S. P. Clerici, A. Cocks, E. Cocucci, R. J. Coffey, A. Cordeiro-da-Silva, Y. Couch, F. A. W. Coumans, B. Coyle, R. Crescitelli, M. F. Criado, C. D'Souza-Schorey, S. Das, A. Datta Chaudhuri, P. de Candia, E. F. De Santana, O. De Wever, H. A. del Portillo, T. Demaret, S. Deville, A. Devitt, B. Dhondt, D. Di Vizio, L. C. Dieterich, V. Dolo, A. P. Dominguez Rubio, M. Dominici, M. R. Dourado, T. A. P. Driedonks, F. V. Duarte, H. M. Duncan, R. M. Eichenberger, K. Ekström, S. El Andaloussi, C. Elie-Caille, U. Erdbrügger, J. M. Falcón-Pérez, F. Fatima, J. E. Fish, M. Flores-Bellver, A. Försönits, A. Frelet-Barrand, F. Fricke, G. Fuhrmann, S. Gabrielsson, A. Gámez-Valero, C. Gardiner, K. Gärtner, R. Gaudin, Y. S. Gho, B. Giebel, C. Gilbert, M. Gimona, I. Giusti, D. C. I. Goberdhan, A. Görgens, S. M. Gorski, D. W. Greening, J. C. Gross, A. Gualerzi, G. N. Gupta, D. Gustafson, A. Handberg, R. A. Haraszti, P. Harrison, H. Hegyesi, A. Hendrix, A. F. Hill, F. H. Hochberg, K. F. Hoffmann, B. Holder, H. Holthofer, B. Hosseinkhani, G. Hu, Y. Huang, V. Huber, S. Hunt, A. G.-E. Ibrahim, T. Ikezu, J. M. Inal, M. Isin, A. Ivanova, H. K. Jackson, S. Jacobsen, S. M. Jay, M. Jayachandran, G. Jenster, L. Jiang, S. M. Johnson, J. C. Jones, A. Jong, T. Jovanovic-Talisman, S. Jung, R. Kalluri, S.-i. Kano, S. Kaur, Y. Kawamura, E. T. Keller, D. Khamari, E. Khomyakova, A. Khvorova, P. Kierulf, K. P. Kim, T. Kislinger, M. Klingeborn, D. J. Klinke, M. Kornek, M. M. Kosanović, Á. F. Kovács, E.-M. Krämer-Albers, S. Krasemann, M. Krause, I. V. Kurochkin, G. D. Kusuma,

S. Kuypers, S. Laitinen, S. M. Langevin, L. R. Languino, J. Lannigan, C. Lässer, L. C. Laurent, G. Lavieu, E. Lázaro-Ibáñez, S. Le Lay, M.-S. Lee, Y. X. F. Lee, D. S. Lemos, M. Lenassi, A. Leszczynska, I. T. S. Li, K. Liao, S. F. Libregts, E. Ligeti, R. Lim, S. K. Lim, A. Linē, K. Linnemannstöns, A. Llorente, C. A. Lombard, M. J. Lorenowicz, Á. M. Lörincz, J. Lötvall, J. Lovett, M. C. Lowry, X. Loyer, Q. Lu, B. Lukomska, T. R. Lunavat, S. L. N. Maas, H. Malhi, A. Marcilla, J. Mariani, J. Mariscal, E. S. Martens-Uzunova, L. Martin-Jaular, M. C. Martinez, V. R. Martins, M. Mathieu, S. Mathivanan, M. Maugeri, L. K. McGinnis, M. J. McVey, D. G. Meckes, K. L. Meehan, I. Mertens, V. R. Minciacchi, A. Möller, M. Møller Jørgensen, A. Morales-Kastresana, J. Morhayim, F. Mullier, M. Muraca, L. Musante, V. Mussack, D. C. Muth, K. H. Myburgh, T. Najrana, M. Nawaz, I. Nazarenko, P. Nejsum, C. Neri, T. Neri, R. Nieuwland, L. Nimrichter, J. P. Nolan, E. N. M. Nolte-'t Hoen, N. Noren Hooten, L. O'Driscoll, T. O'Grady, A. O'Loghlen, T. Ochiya, M. Olivier, A. Ortiz, L. A. Ortiz, X. Osteikoetxea, O. Østergaard, M. Ostrowski, J. Park, D. M. Pegtel, H. Peinado, F. Perut, M. W. Pfaffl, D. G. Phinney, B. C. H. Pieters, R. C. Pink, D. S. Pisetsky, E. Pogge von Strandmann, I. Polakovicova, I. K. H. Poon, B. H. Powell, I. Prada, L. Pulliam, P. Quesenberry, A. Radeghieri, R. L. Raffai, S. Raimondo, J. Rak, M. I. Ramirez, G. Raposo, M. S. Rayyan, N. Regev-Rudzki, F. L. Ricklefs, P. D. Robbins, D. D. Roberts, S. C. Rodrigues, E. Rohde, S. Rome, K. M. A. Rouschop, A. Rughetti, A. E. Russell, P. Saá, S. Sahoo, E. Salas-Huenuleo, C. Sánchez, J. A. Saugstad, M. J. Saul, R. M. Schiffelers, R. Schneider, T. H. Schøyen, A. Scott, E. Shahaj, S. Sharma, O. Shatnyeva, F. Shekari, G. V. Shelke, A. K. Shetty, K. Shiba, P. R. M. Siljander, A. M. Silva, A. Skowronek, O. L. Snyder, R. P. Soares, B. W. Sódar, C. Soekmadji, J. Sotillo, P. D. Stahl, W. Stoorvogel, S. L. Stott, E. F. Strasser, S. Swift, H. Tahara, M. Tewari, K. Timms, S. Tiwari, R. Tixeira, M. Tkach, W. S. Toh, R. Tomasini, A. C. Torrecilhas, J. P. Tosar, V. Toxavidis, L. Urbanelli, P. Vader, B. W. M. van Balkom, S. G. van der Grein, J. Van Deun, M. J. C. van Herwijnen, K. Van Keuren-Jensen, G. van Niel, M. E. van Royen, A. J. van Wijnen, M. H. Vasconcelos, I. J. Vechetti, T. D. Veit, L. J. Vella, é. Velot, F. J. Verweij, B. Vestad, J. L. Viñas, T. Visnovitz, K. V. Vukman, J. Wahlgren, D. C. Watson, M. H. M. Wauben, A. Weaver, J. P. Webber, V. Weber, A. M. Wehman, D. J. Weiss, J. A. Welsh, S. Wendt, A. M. Wheelock, Z. Wiener, L. Witte, J. Wolfram, A. Xagorari, P. Xander, J. Xu, X. Yan, M. Yáñez-Mó, H. Yin, Y. Yuana, V. Zappulli, J. Zarubova, V. Žėkas, J.-y. Zhang, Z. Zhao, L. Zheng, A. R. Zheutlin, A. M. Zickler, P. Zimmermann, A. M. Zivkovic, D. Zocco, E. K. Zuba-Surma, Minimal information for studies of extracellular vesicles 2018

(MISEV2018): a position statement of the International Society for Extracellular Vesicles and update of the MISEV2014 guidelines. *J. Extracell. Vesicles* **7**, 1535750 (2018).

(29) R. J. Barry, A. K. Denniston, *A Dictionary of Ophthalmology.* (Oxford University Press, 2017).

(30) Y. Sano, B. R. Ksander, J. W. Streilein, Minor H, rather than MHC, alloantigens offer the greater barrier to successful orthotopic corneal transplantation in mice. *Transpl. Immunol.* **4**, 53-56 (1996).

(31) M. M. Alvarez, J. C. Liu, G. Trujillo-de Santiago, B.-H. Cha, A. Vishwakarma, A. M. Ghaemmaghami, A. Khademhosseini, Delivery strategies to control inflammatory response: Modulating M1-M2 polarization in tissue engineering applications. *J. Control Release* **240**, 349-363 (2016).

(32) M. K. Ljunggren, R. A. Elizondo, E. Edin, D. Olsen, K. Merrett, C.-J. Lee, G. Salerud, J. Polarek, P. Fagerholm, M. Griffith, Effect of Surgical Technique on Corneal Implant Performance. *Transl. Vis. Sci. Technol.* **3**, 6-6 (2014).

(33) Y. Liu, L. Gan, D. J. Carlsson, P. Fagerholm, N. Lagali, M. A. Watsky, R. Munger, W. G. Hodge, D. Priest, M. Griffith, A Simple, Cross-linked Collagen Tissue Substitute for Corneal Implantation. *Invest. Ophthalmol. Vis. Sci.* **47**, 1869-1875 (2006).

(34) K. A. Williams, M. C. Keane, N. E. Coffey, V. J. Jones, R. A. D. Mills, D. J. Coster, *The Australian Corneal Graft Registry*, (Flinders University, 2018).

(35) M. M. Islam, R. Ravichandran, D. Olsen, M. K. Ljunggren, P. Fagerholm, C. J. Lee, M. Griffith, J. Phopase, Self-assembled collagen-like-peptide implants as alternatives to human donor corneal transplantation. *RSC Adv.* **6**, 55745-55749 (2016).

(36) Y. I. Son, S. Egawa, T. Tatsumi, R. E. Redlinger, Jr., P. Kalinski, T. Kanto, A novel bulk-culture method for generating mature dendritic cells from mouse bone marrow cells. *J. Immunol. Methods* **262**, 145-157 (2002).

(37) K. Inaba, M. Inaba, N. Romani, H. Aya, M. Deguchi, S. Ikehara, S. Muramatsu, R. M. Steinman, Generation of large numbers of dendritic cells from mouse bone marrow cultures supplemented with granulocyte/macrophage colony-stimulating factor. *J. Exp. Med.* **176**, 1693-1702 (1992).

(38) J. Weischenfeldt, B. Porse, Bone Marrow-Derived Macrophages (BMM): Isolation and Applications. *C.S.H. Protoc.* **2008**, pdb.prot5080 (2008).

(39) J. Schindelin, I. Arganda-Carreras, E. Frise, V. Kaynig, M. Longair, T. Pietzsch, S. Preibisch, C. Rueden, S. Saalfeld, B. Schmid, J.-Y. Tinevez, D. J. White, V. Hartenstein,

K. Eliceiri, P. Tomancak, A. Cardona, Fiji: an open-source platform for biological-image analysis. *Nat. Methods* **9**, 676–682 (2012).

Acknowledgments: We thank Dr. Sylvie Lesage and Dr. Cindy Audiger for help with the dendritic cell assay design; and Ms. Janet Laganiere and Ms. Bahareh Hosseinpour for assistance with histopathological processing.

Funding: We acknowledge research funding from EuronanomedII-Swedish Research Council (Dnr IKE-2014-00597), EuronanomedIII-FRQS (file no. 278653), Quebec Vision Health Research Network-FRQS (File no. 2017-3). BDA receives partial salary support for research from the NIHR Biomedical Research Centre (BRC-1215-20002) at Moorfields Eye Hospital NHS Foundation Trust and UCL Institute of Ophthalmology. CS acknowledges support from a Westmead Charitable Trust Early Career Research Fellowship (CC368629-8245), and FCS acknowledges support for her doctoral studies from the Faculté des études supérieures et postdoctorales de l'Université de Montréal, Fonds de recherche en ophtalmologie de l'Université de Montréal (FROUM), Fonds de recherche du Québec - Nature et technologies (FRQNT), and the Natural Sciences and Engineering Research Council of Canada (NSERC).

Author contributions: BDA and MG developed the LiQD Cornea concept. CDM and MG designed the material, CDM performed all optical, physical, mechanical and chemical characterization, BMDM assays and assisted with animal surgeries and analyses of the results. FCS performed the dendritic assays, immunohistochemistry and analyses of the clinical results from the pig study. BDA and CS designed the LiQD Corneal animal studies for feasibility evaluation. CS and DH performed the rabbit perforation study. OB and PF performed the pig surgeries and follow-ups. MH and MKL contributed to the pig study design, assisted with pig clinical exams. DO conducted the collagen content analysis. MH, IP and PL contributed to the transmission electron microscopy and interpretation of the results. MG2 contributed to the immunohistochemistry experiments. EE contributed in IHC protocol development and statistical analysis. MG developed the overall study plan, supervised all research and analyses. All authors contributed to the writing, revisions and final approval of the manuscript.

Competing interests: MG is a named inventor on PCT PCT/IB2017/056342 Collagen and collagen like peptide-based hydrogels, corneal implants, filler glue and uses thereof, which was assigned to the Hyderabad Eye Research Foundation, and then subsequently assigned to North Grove Investments, Inc. wherein PCT national phase applications have been filed in the USA, EU, India and

China, and an impending application to be filed in Canada. CDM and MG are named inventors on a US provisional patent application no. 62916765, subsequent to a disclosure to Univalor, technology transfer agent to Maisonneuve-Rosemont Hospital and Université de Montréal.

Data and materials availability: All data associated with this study are available in the main text or supplementary materials.

Figure Legends

Figure 1. Biological evaluation of LiQD Cornea. (A) Immortalized human corneal epithelial cells cultured on LiQD Cornea hydrogels and control tissue culture plastic, showing that the hydrogels support epithelial growth. (B) Expression of T-cell co-stimulatory molecules in bone marrow-derived dendritic cells (BMDCs). Expression of CD40, CD80, and CD86 was measured by flow cytometry and data is presented as a ratio of mean fluorescent intensity of the experimental samples to untreated BMDCs. Lipopolysaccharide (LPS) acted as a positive control for BMDC activation; * $p \leq 0.05$ by Student's t-test. (C) Expression of pro-inflammatory M1(CD 86) and anti-inflammatory M2 (CD 206) phenotypic markers at 4 and 7 days after exposure of naïve bone marrow-derived macrophage precursors to LiQD Cornea hydrogels. (D) Example of a human corneal perforation. (E) Post-surgical photos of rabbits immediately after injecting LiQD Cornea into a perforated cornea. The two-stepped surgically-induced perforation can be seen. At Day 2 post surgery, the air bubble placed under the cornea during surgery is prominent, indicating that the perforation was completely sealed. The perforated cornea was completed healed by 28 days post-operation Photo Credit: Damien Hunter, University of Sydney. (F) Mini-pig corneas where the LiQD Cornea was tested as an alternative to a donor allograft, showing the gross appearance of the LiQD Cornea, syngeneic graft and an unoperated eye at 12 months post-surgery. Photo Credit: Monika K. Ljunggren, Linköping University.

Figure 2. Clinical exam progression of LiQD Cornea in Göttingen mini-pigs. (A) Pachymetry showing corneal thickness measured by OCT, showing no significant differences in thickness compared to controls. There was a normal increase in corneal thickness in unoperated controls as the pigs matured. (B) Intraocular pressures were similar in all three groups, showing a slight overall increase over the normal aging process of the pigs. (C) Central corneal haze measured using a modified McDonald-Shadduck scoring system on a scale from 0-4. An increase of haze corresponds to the period of in-growth of stromal cells into the cell-free implants. By 12 months post-operation, the cells appeared to have attained quiescence. (D) Corneal neovascularization was seen in the LiQD Cornea, mainly from the animal that sustained an unintended perforation. (E) Corneal blink response measured by Cochet-Bonnet aesthesiometry showed no significant differences amongst the three groups. (F) Corneal nerve density in the LiQD Cornea group was significantly lower than the unoperated corneas during months 3 through 9 post-operation when the severed nerves were regenerating. (G) Schirmer's tear test showed similar responses in all three groups tested. (H) Expression of high molecular weight collagens (HMW, γ, β), type V collagen, and type I collagen (α1

and $\alpha 2$) in the central portion of the cornea. Figures A-B, and E-H were assessed using a mixed-effect model with a Tukey post-hoc test for multiple comparisons. Figures C-D were analyzed using a Mann-Whitney U test for ordinal data. * $p \leq 0.05$ for LiQD Cornea to unoperated, † $p \leq 0.05$ for LiQD Cornea to syngeneic graft, ‡ $p \leq 0.05$ syngeneic graft to unoperated. All data is plotted from as mean ± SEM or mean with individual values.

Figure3. Histopathology, transmission electron microscopy (TEM), and immunohistochemistry of the LiQD Cornea at 12 months. (A-C) Paraffin-embedded sections of porcine cornea stained with hematoxylin and eosin show multi-layered, non-keratinizing epithelia in all three samples. (D-F) TEM images of corneal epithelium in all three samples. (G-I) Epithelial cells showed abundance of desmosomes between cells (arrowhead). (J-L). A fully regenerated corneal tear film mucin stained with FITC-conjugated lectin (green) from Ulex Europeaus is seen in the LiQD Cornea. This is similar to the tear film in the controls. (M-O) Cytokeratin 12 (red), a marker for fully differentiated corneal epithelial cells is present in the regenerated LiQD Cornea as in controls. (P-R) CD163 staining (red) shows that a few mononuclear cells are present in stroma of all three samples. Cell nuclei were stained blue with DAPI.

Figure 4 Extracellular vesicle (EV) and exosome secretion of the regenerated LiQD Cornea compared to a healthy unoperated cornea and a syngeneic graft. (A) Transmission electron micrograph of a LiQD Cornea sample showing the presence of basal epithelial cells invaginations into the stroma. A basement membrane was present. Vesicles can be seen inside the epithelial cell (an example is indicated with a red arrow). EVs are seen (white arrows) in the underlying stromal compartment. (B, C) TEM of syngeneic graft and untreated cornea, respectively. (D-F) Surface reconstructions of corneal sections stained with the cytosolic, extracellular vesicle marker Tsg101 (red) and DAPI (blue) (G-I) Surface reconstruction of colocalized CD9 and Tsg101 staining indicating the presence of exosomes in the basal epithelium and upper stroma of the LiQD cornea sample. There was less staining in the syngeneic graft and minimal in the untreated control. Scale bars, red: 500 nm, white: 20 μm.

Figure 5. *In vivo* confocal microscopy images of the LiQD Cornea (left column) compared to a healthy unoperated cornea (right column) and a syngeneic graft (centre column) at 12 months post-surgery. Regenerated corneal epithelial cells cover the surface of the LiQD cornea (A) as with the syngeneic graft (B) and untreated cornea (C). Regenerated nerves (arrows) found at the sub-basal epithelium within the LiQD cornea (D), ran parallel to one another and were morphologically similar to those found in the unoperated cornea (F). Nerves in the syngeneic graft were less distinct

(E). Keratocytes were present in all corneas (G-I). The unoperated endothelium remained intact and healthy in all corneas (J-L). Scale bars, 100 μm.

Supplementary Figure Legends **Figure S1.** Cryo-scanning electron microscopy (SEM) and Fourier-transform infrared spectroscopy (FTIR) of LiQD Cornea hydrogels. (A) Representative cryo-SEM image of the LiQD cornea and corresponding pore size histogram, which illustrates the mean pore size of the resulting hydrogel. Mean was determined from the measurement of $>$ 250 different pores. Scale bar, 50 μm. (B) Overlay of the representative ATR-FTIR spectra of CLP-PEG (red), fibrinogen (blue), and crosslinked LiQD Cornea (black). The characteristic amide peaks of both the CLP-PEG conjugate and fibrinogen are present in the crosslinked LiQD cornea.

Figure S2. Clinical progression of the LiQD Cornea in all four Göttingen mini-pigs. (A) Surgical microscope images showing the presence of haze at 3 months post-surgery as stromal cells are migrating into the implant. The haze is diminished at 12 months except in one animal where an unintended perforation and suture placement resulted in haze. Representative images of a syngeneic corneal graft and an untreated contralateral cornea are shown as controls. Haze is seen at the graft-host interface of the syngeneic cornea. Photo Credit: Monika K. Ljunggren, Linköping University. (B) Optical coherence tomography images of representative samples of LiQD Cornea, syngeneic grafts and unoperated corneas over 12 months post-surgery. The filling of the surgical wound bed was not always optimal as shown by the over-filled LiQD Cornea that had gelled in situ (a). Remodeling over the initial 3 months resulted in a regenerated cornea with a smooth external curvature that conforms to the overall shape of the host cornea (p). The initially cell-free hydrogel (a-d) became populated with cells (m-p, s-v, w-z, cc-ff).

Figure S3. Towards point-of-care (POC) delivery of LiQD Cornea. Comparison of the current T-piece mixing system (A) with the preliminary POC delivery system (B). (C) Representative image of an ex-vivo perforation model sealed using LiQD Cornea that was mixed and dispensed to the wound bed using the preliminary POC delivery system. (D) POC delivered LiQD Cornea after failure in bursting pressure testing. Red arrows indicate the interface of the applied material and the perforated cornea. Photo Credit: Christopher D. McTiernan, Université de Montréal.

Figure S4. Immunohistochemistry of the cornea at 12 months. (A-C) The operated corneas show minimal staining for α-SMA, and no large vessels present in the operated region although they are present in the scleral positive control (D). (E-G) LYVE1 was not observed in the central cornea,

although lymphatic vessels were seen in the corneal limbus and sclera (H). Cell nuclei were stained blue with DAPI.

Figure S5. Schematic for the preparation of CLP-PEG conjugate.

Figures

Figure 1.

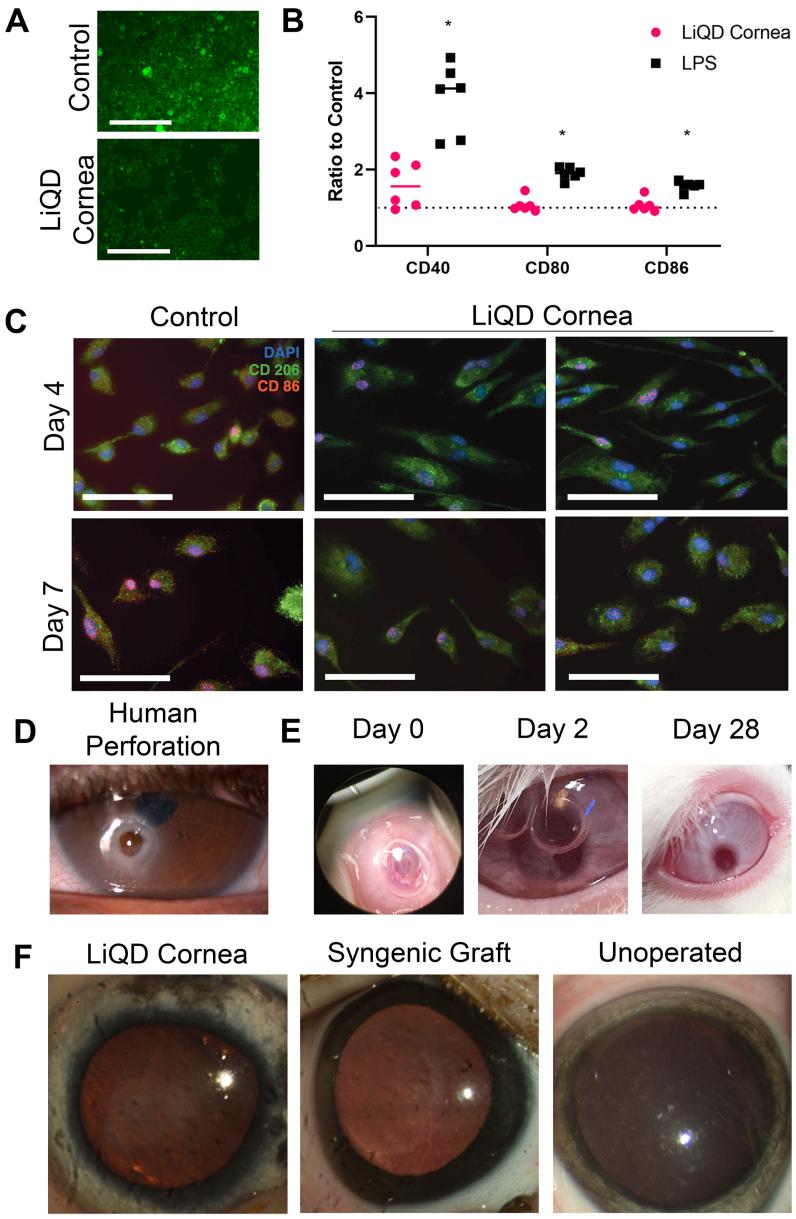

Figure 2.

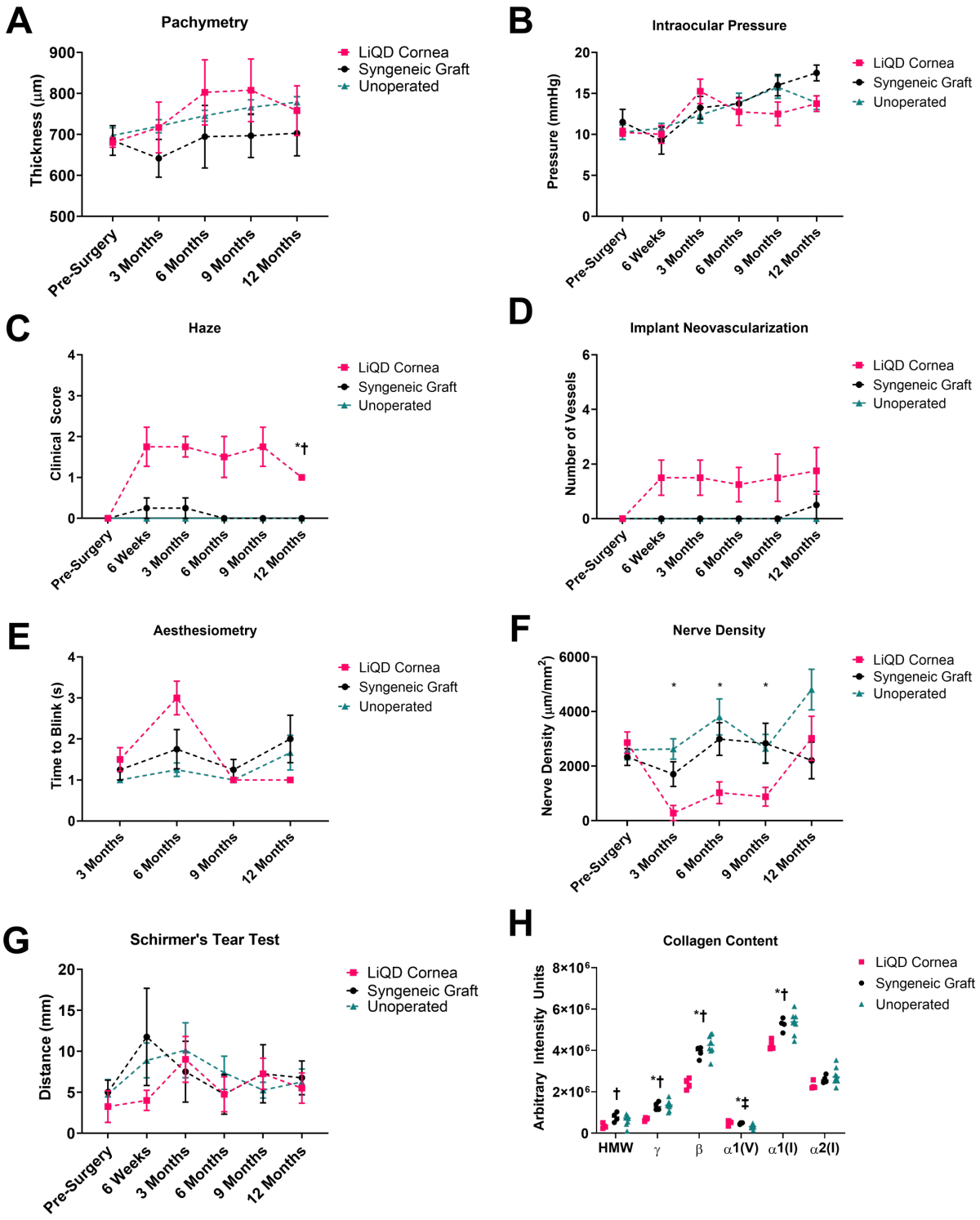
A
Pachymetry
Thickness (µm)
900
800
700
600
500
Pre-Surgery
3 Months
6 Months
9 Months
12 Months
LiQD Cornea
Syngeneic Graft
Unoperated
B
Intraocular Pressure
Pressure (mmHg)
20
15
10
5
0
Pre-Surgery
6 Weeks
3 Months
6 Months
9 Months
12 Months
LiQD Cornea
Syngeneic Graft
Unoperated
C
Haze
Clinical Score
4
3
2
1
0
*†
Pre-Surgery
6 Weeks
3 Months
6 Months
9 Months
12 Months
LiQD Cornea
Syngeneic Graft
Unoperated
D
Implant Neovascularization
Number of Vessels
6
4
2
0
Pre-Surgery
6 Weeks
3 Months
6 Months
9 Months
12 Months
LiQD Cornea
Syngeneic Graft
Unoperated
E
Aesthesiometry
Time to Blink (s)
4
3
2
1
0
3 Months
6 Months
9 Months
12 Months
LiQD Cornea
Syngeneic Graft
Unoperated
F
Nerve Density
Nerve Density (µm/mm²)
6000
4000
2000
0
*
*
*
Pre-Surgery
3 Months
6 Months
9 Months
12 Months
LiQD Cornea
Syngeneic Graft
Unoperated
G
Schirmer's Tear Test
Distance (mm)
20
15
10
5
0
Pre-Surgery
6 Weeks
3 Months
6 Months
9 Months
12 Months
LiQD Cornea
Syngeneic Graft
Unoperated
H
Collagen Content
Arbitrary Intensity Units
8×10⁶
6×10⁶
4×10⁶
2×10⁶
0
†
*†
*†
*‡
*†
HMW
γ
β
α1(V)
α1(I)
α2(I)
LiQD Cornea
Syngeneic Graft
Unoperated

Figure 3.

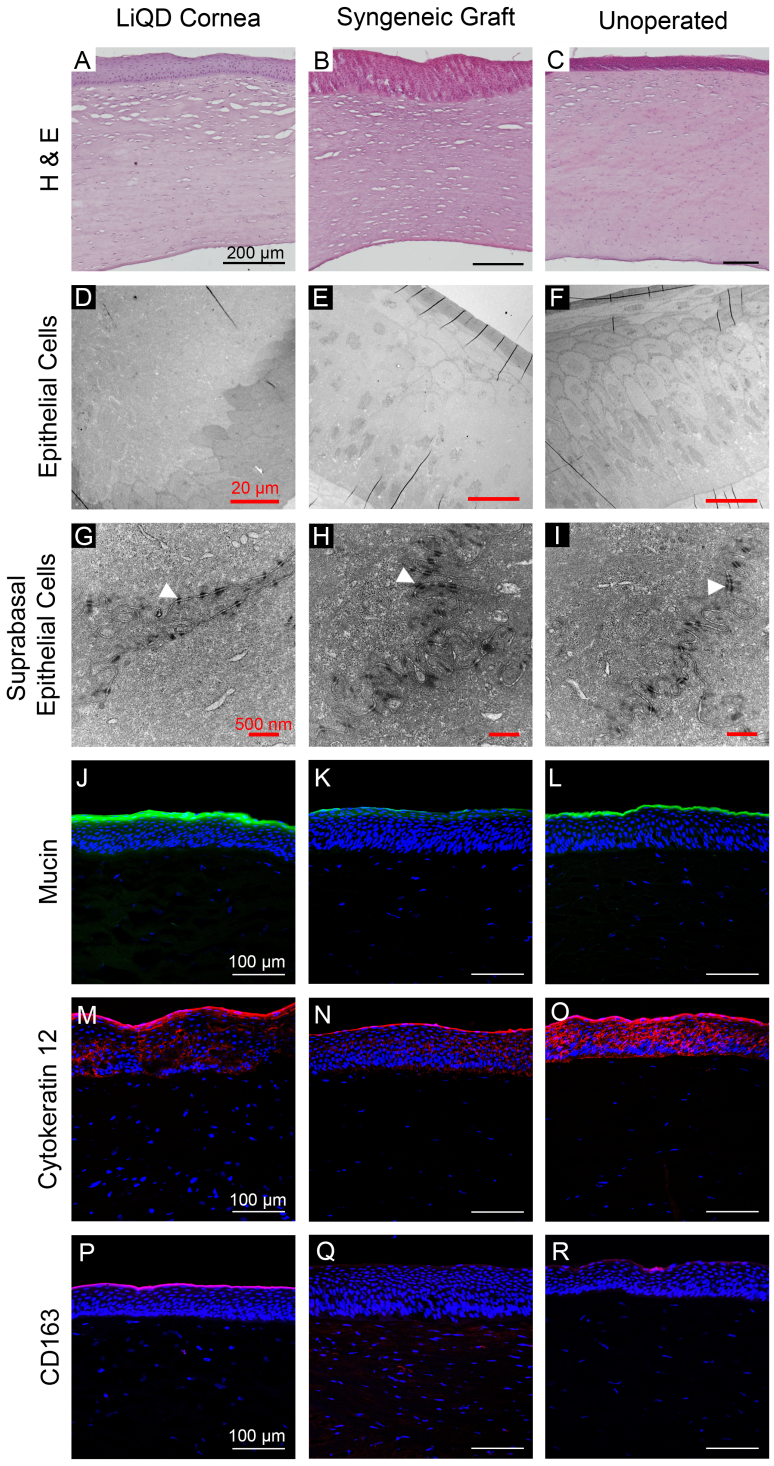
LiQD Cornea
Syngeneic Graft
Unoperated
H & E
Epithelial Cells
Suprabasal Epithelial Cells
Mucin
Cytokeratin 12
CD163
A
B
C
D
E
F
G
H
I
J
K
L
M
N
O
P
Q
R
200 µm
20 µm
500 nm
100 µm
100 µm
100 µm

Figure 4.

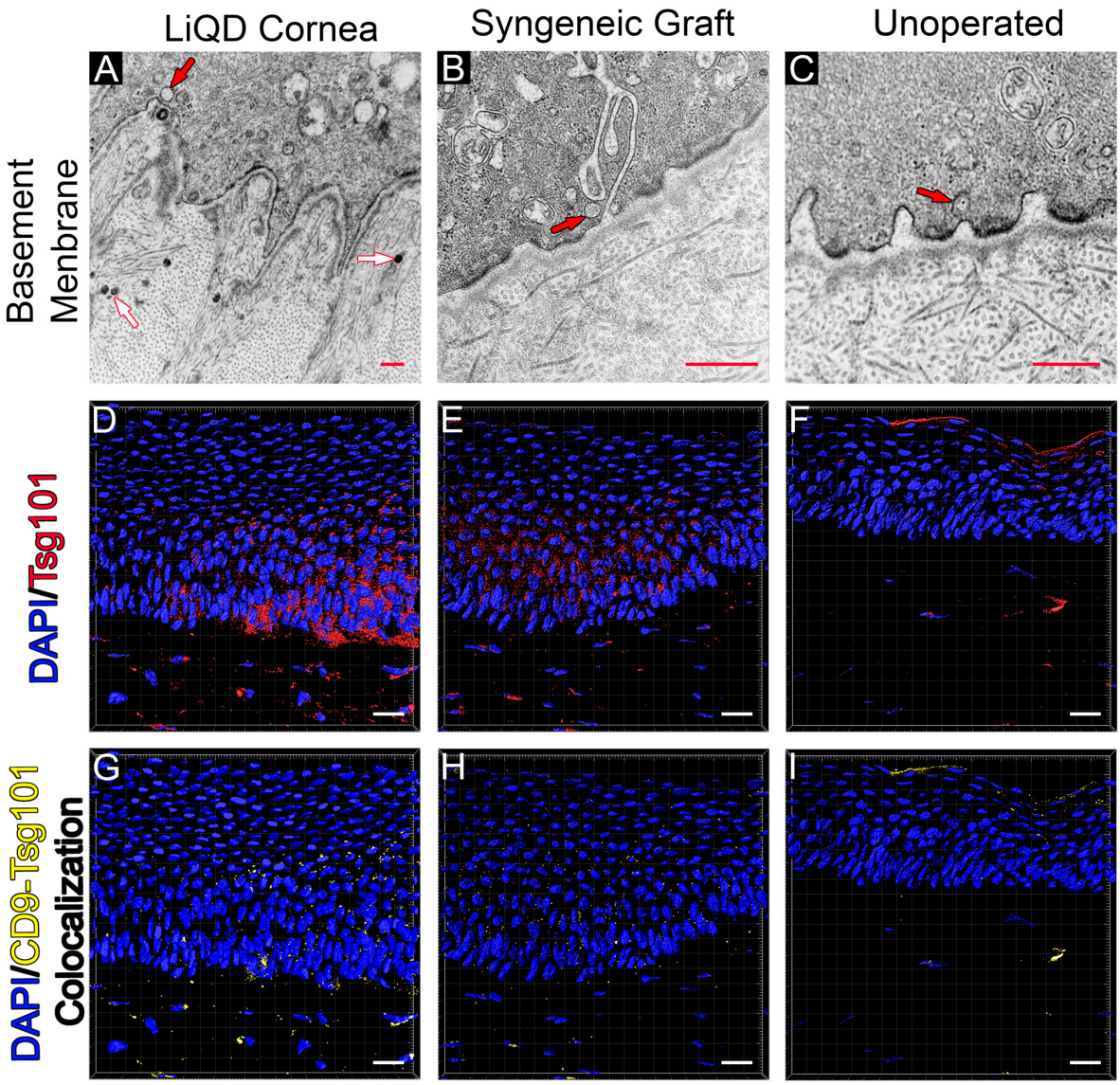
LiQD Cornea
Syngeneic Graft
Unoperated
A
B
C
Basement Menbrane
D
E
F
DAPI/Tsg101
G
H
I
DAPI/CD9-Tsg101 Colocalization

Figure 5.

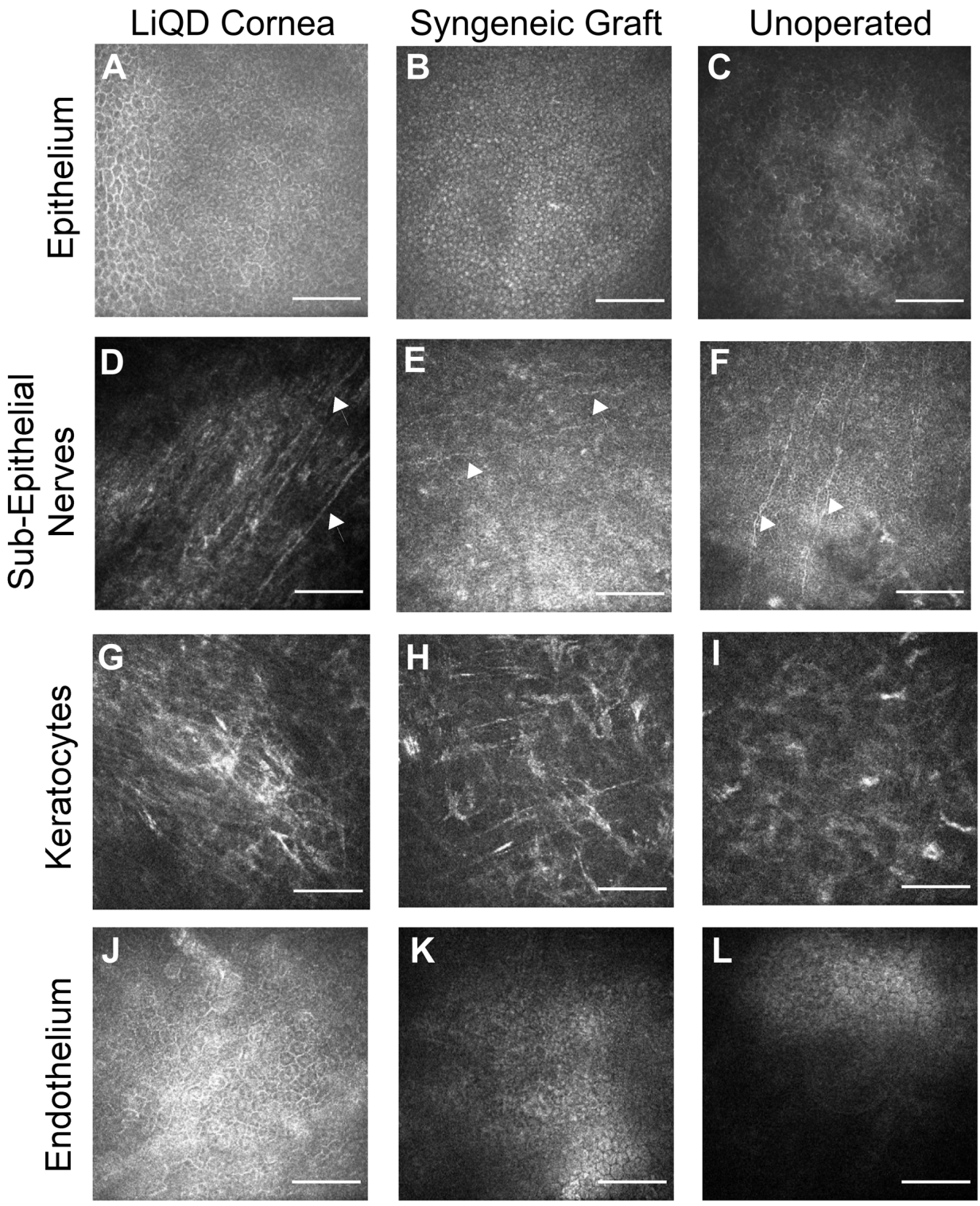
LiQD Cornea
Syngeneic Graft
Unoperated
Epithelium
Sub-Epithelial Nerves
Keratocytes
Endothelium
A
B
C
D
E
F
G
H
I
J
K
L

Supplementary Figures

Figure S1.

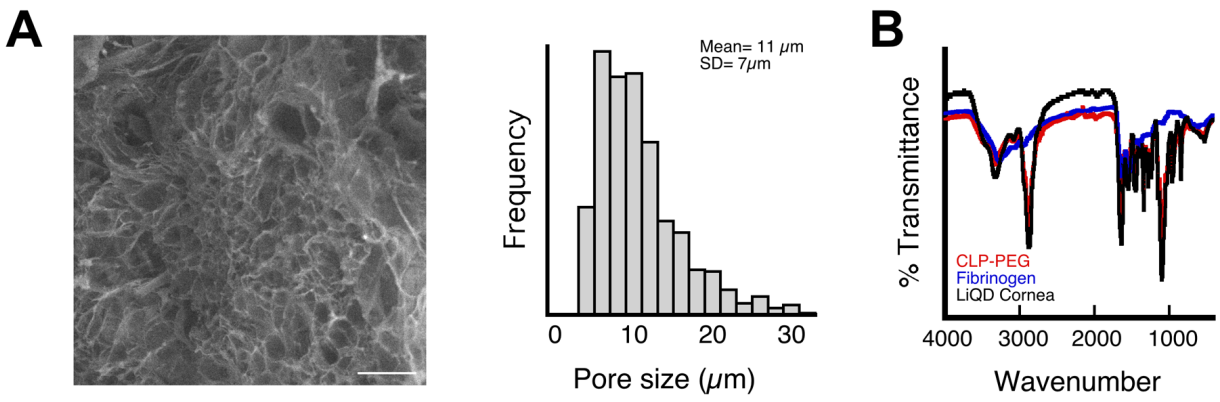

Figure S2.

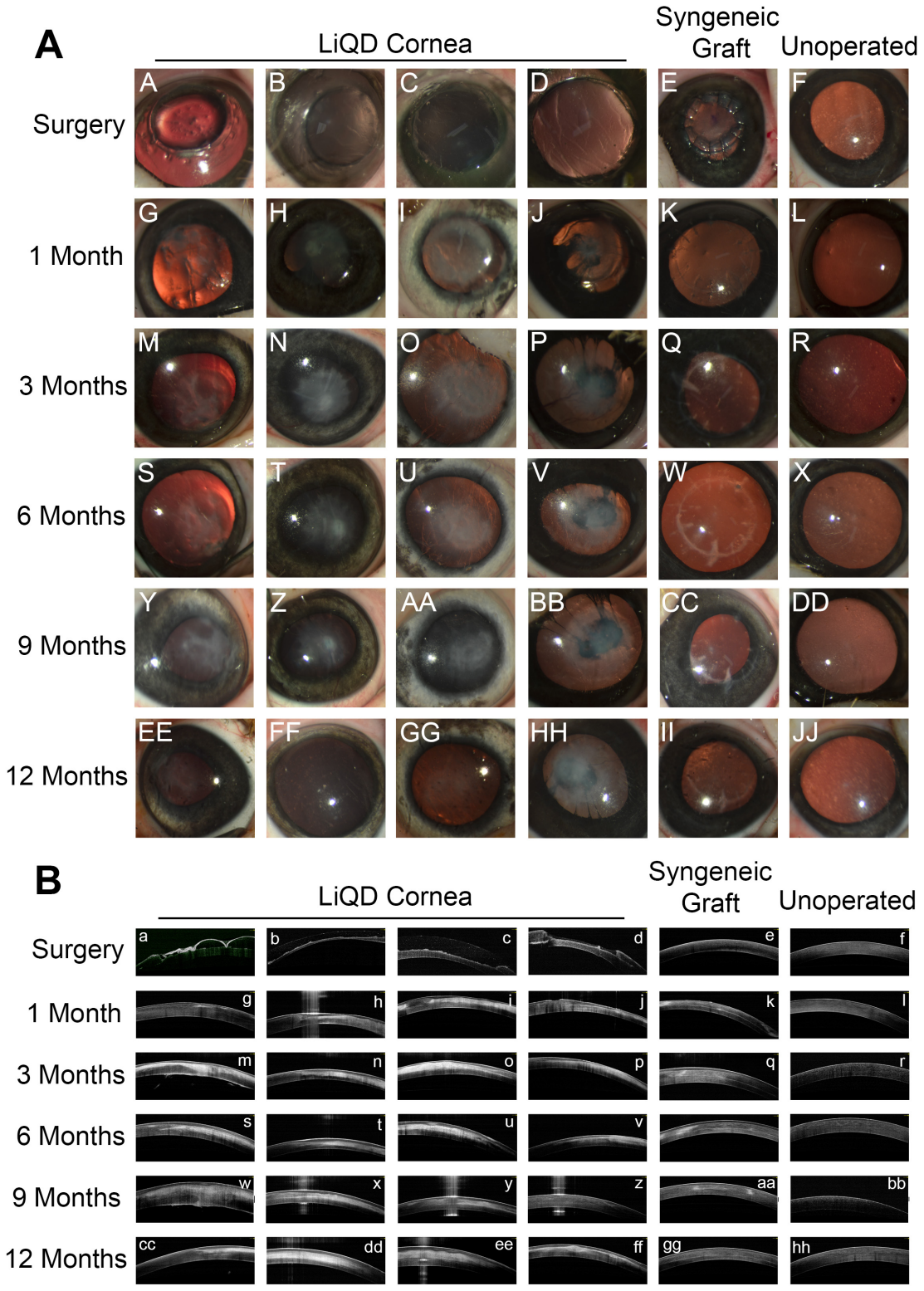
A
LiQD Cornea
Syngeneic Graft
Unoperated
Surgery
1 Month
3 Months
6 Months
9 Months
12 Months
A B C D E F
G H I J K L
M N O P Q R
S T U V W X
Y Z AA BB CC DD
EE FF GG HH II JJ
B
LiQD Cornea
Syngeneic Graft
Unoperated
Surgery
1 Month
3 Months
6 Months
9 Months
12 Months
a b c d e f
g h i j k l
m n o p q r
s t u v
w x y z aa bb
cc dd ee ff gg hh

Figure S3.

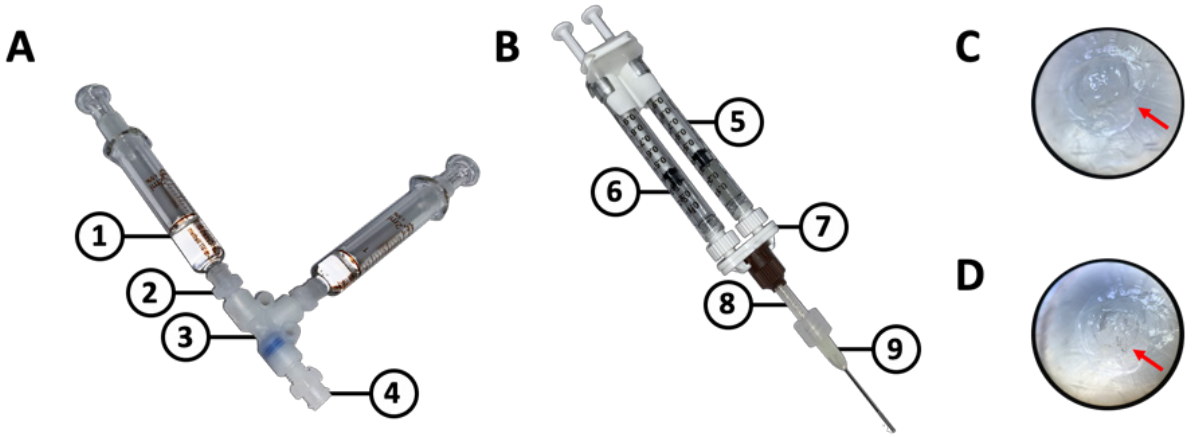

① 2 mL glass syringe
② syringe port adapter
③ T-piece (3-way) adapter
④ injection port with rubber septum
⑤ BD 1 mL syringe with LiQD Cornea
⑥ BD 1 mL syringe with 10% w/w DMTMM
⑦ dual syringe adapter (L-System, 15mm)
⑧ static mixer (DN2.0x16, 1:1)
⑨ 19 G x 25 mm flattened tip

Figure S4.

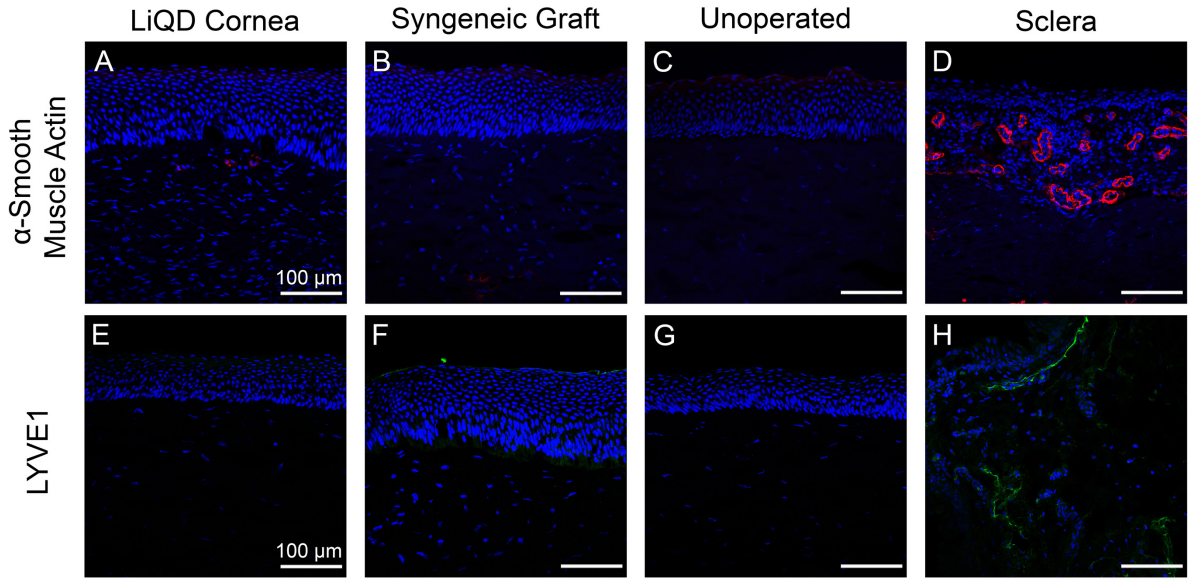
LiQD Cornea
Syngeneic Graft
Unoperated
Sclera
α-Smooth Muscle Actin
LYVE1
A
B
C
D
E
F
G
H
100 µm
100 µm

Figure S5.

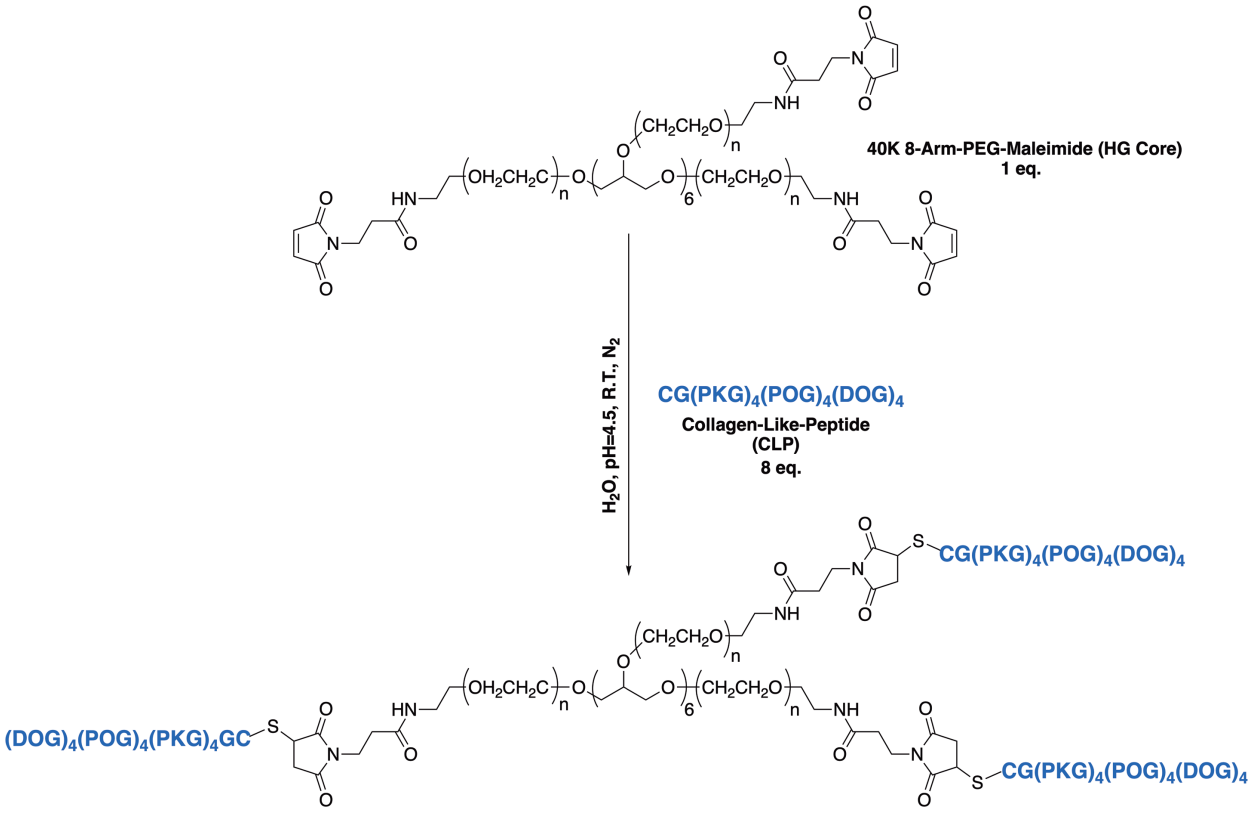
40K 8-Arm-PEG-Maleimide (HG Core)
1 eq.
H2O, pH=4.5, R.T., N2
CG(PKG)4(POG)4(DOG)4
Collagen-Like-Peptide
(CLP)
8 eq.
CG(PKG)4(POG)4(DOG)4
(DOG)4(POG)4(PKG)4GC
CG(PKG)4(POG)4(DOG)4

Tables

Table 1.

Tensile Strength (MPa)	**Modulus** (MPa)	**Viscosity** (Pa/s)	**Transmission** (%)
0.02	0.16	31.7 ± 27.6	19-93% (UV) 93-99% (Vis)
Refractive Index	**Water Content** (%)	**Collagenase** (mg/min)	**T_d** (°C)
1.354 ± 0.037	91.2 ± 2.3	7.3E-7 ± 6.1E-7	64 ± 8.5

Material	**Average Bursting Pressure (mmHg)**[a]	**Representative Image of sealed *ex-vivo* perforation model**[b]
Cyanoacrylate Glue	>300 mmHg	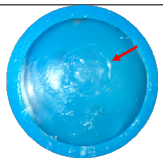
Fibrin Glue	259 ± 14.5	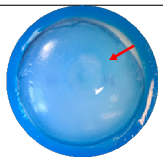
LiQD Cornea	170 ± 16.9	

Supplementary Tables

Table S1. Antibodies for Immunocytochemistry

Target	**Antibody (or Lectin)**	**Dilution Factor**
CD206	Anti-Mannose Receptor antibody, AbCam, ab64693	1/1000
CD86	Anti-CD86 antibody [GL-1], AbCam, ab119857	1/500
Rat IgG	Donkey anti-rat IgG (H+L) Highly Cross-Adsorbed Secondary Antibody, Alexa Fluor 488 (Invitrogen, A-21208)	1/2000
Rabbit IgG	Goat anti-Rabbit IgG (H+L) Cross-Adsorbed Secondary Antibody, Alexa Fluor 568 (Invitrogen, A-11011)	1/2000

Table S2. Antibodies for Immunohistochemistry

Target	**Antibody**	**Dilution Factor**
Mucin	Lectin from Ulex europaeus (gorse, furze) FITC conjugate, Sigma-Aldrich, L9006	1/500
Cytokeratin 12	Recombinant Anti-Keratin 12/K12 antibody [EPR17882], AbCam, ab185627	1/500
α-SMA	Anti-alpha smooth muscle Actin antibody [1A4], AbCam, ab7817	1/500
LYVE1	Anti-LYVE1 antibody, AbCam, ab33682	1/100
CD163	CD163 antibody | 2A10/11, Bio-Rad, MCA2311GA	1/500
β3-tubulin	beta Tubulin Antibody, Novus Biologicals, NB-600-936	1/1000
CD31	Anti-CD31 antibody [C31.3 + JC/70A]. AbCam, ab199012	1/500
CD9	CD9 Mouse anti-Bovine, Canine, Equine, Feline, Human, Mink, Mustelid, Non-human primate, Porcine, Rabbit, Clone: MM2/57, Invitrogen^{TM}, MA180307	1/100
Tsg101	Recombinant Anti-TSG101 antibody [EPR7130(B)], AbCam, ab125011	1/100
Mouse IgG	IgG (H+L) Highly Cross-Adsorbed Goat anti-Mouse, Alexa Fluor® 488, Invitrogen, A11029	1/1000
Rabbit IgG	IgG (H+L) Highly Cross-Adsorbed Goat anti-Rabbit, Alexa Fluor® 594, Invitrogen, A11037	1/1000
Mouse IgG	IgG (H+L) Highly Cross-Adsorbed Goat anti-Mouse, Alexa Fluor® Plus 647, Invitrogen^{TM}, PIA32728	1/1000

Table S3. Antibodies for Flow Cytometry

Target	**Antibody**	**Dilution Factor**
CD11c	Brilliant Violet 650^{TM} anti-mouse CD11c,(Clone: N418),(IsoType: Armenian Hamster IgG),(Reactivity: Mouse),(Format: BV650),(APP: FC),(Species: Hamster), Biolegend, 117339	1/1600
IA-IE (MHC Class II)	PerCP/Cy5.5 anti-mouse I-A/I-E,(Clone: M5/114.15.2),(IsoType: Rat IgG2b, κ),(Reactivity: Mouse),(Format: PerCP/Cy5.5),(APP: FC),(Species: Rat), Biolegend, 107626	1/3200
CD40	CD40, APC, clone: 1C10, eBioscience^{TM}, 501129392	1/400
CD80	PE anti-mouse CD80,(Clone: 16-10A1),(IsoType: Armenian Hamster IgG),(Reactivity: Mouse, Cross-Reactivity: Dog (Canine)),(Format: PE),(APP: FC),(Species: Hamster), Biolegend, 104708	1/100
CD86	FITC anti-mouse CD86,(Clone: GL-1),(IsoType: Rat IgG2a, κ),(Reactivity: Mouse),(Format: FITC),(APP: FC),(Species: Rat), Biolegend, 105006	1/50

Table S4. Clinical Results – Mixed-effects model

Pachymetry			
Fixed effects (type III)	**P value**	**F (DFn, DFd)**	**Geisser-Greenhouse's ϵ**
Time	0.0045	F (1.830, 23.79) = 7.150	0.4575
Treatment	0.3941	F (2, 13) = 1.001	
Time x Treatment	0.2117	F (8, 52) = 1.417	
Random effects	**SD**	**Variance**	
Pig	73.13	5348	
Residual	47.1	2218	
Was the matching effective?		Chi-square, df	12.06, 1
		P value	0.0005
IOP			
Fixed effects (type III)	**P value**	**F (DFn, DFd)**	**Geisser-Greenhouse's ϵ**
Time	<0.0001	F (3.682, 47.87) = 11.68	0.7365
Treatment	0.6255	F (2, 13) = 0.4866	
Time x Treatment	0.0943	F (10, 65) = 1.723	
Random effects	**SD**	**Variance**	
Pig	1.342	1.801	
Residual	2.342	5.486	
Was the matching effective?		Chi-square, df	7.991, 1
		P value	0.0047
Haze			
Fixed effects (type III)	**P value**	**F (DFn, DFd)**	**Geisser-Greenhouse's ϵ**
Time	0.0002	F (2.661, 34.59) = 9.092	0.5322
Treatment	<0.0001	F (2, 13) = 47.40	
Time x Treatment	<0.0001	F (10, 65) = 6.769	
Random effects	**SD**	**Variance**	

Pig	0.1826	0.03333	
Residual	0.3232	0.1045	
Was the matching effective?		Chi-square, df	7.693, 1
		P value	0.0055
Implant Neovascularization			
Fixed effects (type III)	**P value**	**F (DFn, DFd)**	**Geisser-Greenhouse's ϵ**
Time	0.0186	F (2.444, 31.77) = 4.173	0.4887
Treatment	0.0055	F (2, 13) = 7.977	
Time x Treatment	0.0041	F (10, 65) = 2.949	
Random effects	**SD**	**Variance**	
Pig	0.4974	0.2474	
Residual	0.4557	0.2077	
Was the matching effective?		Chi-square, df	33.92, 1
		P value	<0.0001
Aesthesiometry			
Fixed effects (type III)	**P value**	**F (DFn, DFd)**	**Geisser-Greenhouse's ϵ**
Time	0.0207	F (1.019, 7.136) = 8.702	0.3398
Treatment	0.2408	F (1.311, 9.178) = 1.631	0.6556
Time x Treatment	0.2251	F (2.080, 1.734) = 3.999	0.3467
Random effects	**SD**	**Variance**	
Pig	0.1652	0.0273	
Pig x Time	0	0	
Pig x Treatment	0.2884	0.08317	
Residual	0.5188	0.2691	
Was the matching effective?		Chi-square, df	5.236, 2
		P value	0.0729
Nerve Density			

Fixed effects (type III)	**P value**	**F (DFn, DFd)**	**Geisser-Greenhouse's ϵ**
Time	0.0243	F (2.773, 34.67) = 3.653	0.6933
Treatment	0.0033	F (2, 13) = 9.160	
Time x Treatment	0.0745	F (8, 50) = 1.939	
Random effects	**SD**	**Variance**	
Pig	309.9	96028	
Residual	1275	1625511	
Was the matching effective?		Chi-square, df	0.3532, 1
		P value	0.5523
Schirmer's Tear Test			
Fixed effects (type III)	**P value**	**F (DFn, DFd)**	**Geisser-Greenhouse's ϵ**
Time	0.1752	F (3.187, 41.44) = 1.719	0.4575
Treatment	0.796	F (2, 13) = 0.2322	
Time x Treatment	0.7514	F (10, 65) = 0.6660	
Random effects	**SD**	**Variance**	
Pig	73.13	10.64	
Residual	147.1	23.51	
Was the matching effective?		Chi-square, df	12.06, 1
		P value	0.0005

Table S5. Collagen Content One-Way ANOVAs

Collagen Type	**Comparison**	**Sum of Squares**	**df**	**Mean Square**	**F**	**Sig.**
HMW	Between Groups	3.89E+11	2	1.94E+11	3.707	0.053
	Within Groups	6.82E+11	13	5.25E+10		
	Total	1.07E+12	15			
γ	Between Groups	1.26E+12	2	6.30E+11	14.922	0.000
	Within Groups	5.49E+11	13	4.22E+10		
	Total	1.81E+12	15			
β	Between Groups	9.61E+12	2	4.80E+12	28.254	0.000
	Within Groups	2.21E+12	13	1.70E+11		
	Total	1.18E+13	15			
α1(V)	Between Groups	1.11E+11	2	5.56E+10	6.479	0.011
	Within Groups	1.12E+11	13	8.59E+09		
	Total	2.23E+11	15			
α 1(I)	Between Groups	3.17E+12	2	1.59E+12	8.498	0.004
	Within Groups	2.43E+12	13	1.87E+11		
	Total	5.60E+12	15			
α2(I)	Between Groups	5.90E+11	2	2.95E+11	2.729	0.102
α2(I)	Within Groups	1.40E+12	13	1.08E+11		
	Total	1.99E+12	15			

Chapter 7

Synthesis and application of collagens for assembling a corneal implant

Elle Edin[1,2], Fiona Simpson[1,2], May Griffith[1,2] Email may.griffith@umontreal.ca

[1]Maisonneuve-Rosemont Hospital Research Centre, Montréal, QC, Canada [2]Department of Ophthalmology and Institute of Biomedical Engineering, Université de Montréal, Montréal, QC, Canada

Abstract

Recombinant or artificial designer collagens have developed to a point where they are viable candidates for replacing extracted animal collagens in regenerative medicine applications. Biomimetic corneas made have shown promise as replacements for human donor corneas, and have previously been fabricated from several different collagens or collagen-like peptides (CLPs). Prokaryotic expression systems allow for cheap, rapid, gram scale production of collagens/CLPs. Here, we describe a procedure for production of collagen-like peptides for the manufacturing of a biomimetic cornea.

Key words

Biomimetic · Artificial Cornea · Artificial collagen · Collagen · Corneal regeneration · Transgenic

1. Introduction

1.1. Collagen and Collagen-Like Peptides

Collagen is the most abundant protein present in the extracellular matrix that surrounds the cells of various tissues and organs in the mammalian body, including the cornea [1]. The defining feature of collagen is its unique supercoiled triple-helix structure [2, 3]. Fibrillar collagens, in particular, are robust structural macromolecules that contain cell-interactive domains. Hence, they have excellent properties for creating regenerative, cell-free scaffolds for corneal repair as seen in early clinical evaluation (Fig. 1) [4].

Most commercially available collagen is extracted from animal sources and purified using different methods, resulting in heterogeneity of size and helicity [5]. Recombinantly produced human collagens and short collagen mimetic peptides (CMPs) or collagen-like peptides (CLPs) developed as alternatives to animal collagens. Both have the benefit of low heterogeneity. Also, unlike xenogeneic collagens [6], there is little/no risk of allergy to xenogeneic protein or zoonotic disease transfer. Collagen was initially considered a protein that is unique to multicellular animals, as hydroxyproline residues within collagen have been considered the main determinants for structural stability [7]. However, CLPs have since been identified in prokaryotes, such as bacteria [8, 9]. These proteins have been isolated from biofilm, and they have been shown to also have triple helical structures and similar thermal stability to mammalian collagens [10]. As such, researchers have been able to design new CLPs that are based on bacterial collagen sequences and analyzed the structure-mechanical property relationships between these fibrils [8, 11, 12]. Collagens are chains of G-X-Y amino acid motifs, where the G amino acid (Gaa) is glycine [12]. The amino acidat the X (Xaa) position is frequently proline, and in animal collagens, the Y amino acid (Yaa) is oftenhydroxyproline. Important features that are known to affect collagen assembly, stability, as well as the relatedmelting temperature include the Grand Average of Hydropathicity (GRAVY) score, hydroxyproline spacing, andthe frequency of the six amino acid sequence Xaa1Yaa1Gaa1Xaa2Yaa2Gaa2 where the Yaa1 position hosts alysine and the Xaa2 is occupied by a negatively charged residue (glutamic, or aspartic acid) [12, 13, 14, 15]. In longer collagen peptides (>50 amino acids), assembly regions are often necessary for collagen fibril formation [16, 17]. In small CLPs that have high inter-strand interactions, assembly regions are not needed. Therefore, when selecting or designing a CLP, the experimenter needs to consider the availability of functional groups that can be used to stabilize the collagen helix, as well as stabilizing inter-fibrillar interactions.

1.2. CLP Production

Solid state synthesis is the method of choice for shorter CLPs (<40–50 amino acids). However, longer peptideshave been produced using a combination of solid phase peptide synthesis, polymerization, and self-assembly [18]. The final products of such a combination strategy are triple helical nanofibers of 10–20 nm. The Hartgerink group used an N-terminal cysteine and C-terminal thioester to achieve selective head to tail polymerization of peptides under aqueous conditions, without the need for protecting groups [18]. However, this method is not cost-effective for producing longer polypeptides. Recombinant DNA technology is more efficient and cost-effective for production of full-length recombinant human collagens. Full-length human and recombinant human collagens have been produced in a range of transgenic species ranging from yeast (Pichia pastoris for types 1 and III human collagen [19]) to human fibroblasts [20], silkworms [21], and plants (tobacco for type I human collagen) [22]. CLPs (in this case, gelatins) have also been recombinantly produced, e.g., in silkworms [23].

1.3. CLP Protocols

The protocols that we provide cover the production of recombinantly produced CLP to fabrication of corneal shaped and sized implants (Fig. 2). This protocol covers in particular CLPs that are based on bacterial sequences or synthetic sequences that lack hydroxyproline residues, as these are significantly less demanding to produce. If a sequence is reliant on hydroxyprolines for stable fibril formation, a system designed particularly for allowing this type of post-translational modification must be used. For shorter sequences, however, solid state synthesis is recommended and hydroxyprolines can be incorporated more easily.

We have not provided any specific CLP sequence but instead have provided a general protocol that can be used in its entirety or in part for fabrication of implants, using a CLP that the reader has access to. The specific cloning protocol given here is optimized for CLPs that are between 20 and 50 kDa, with either an assembly initiation region or which can fold in the absence of such a region. For convenience we have named the generic CLP we are preparing "exColA." For preparation of hydrogel implants, various crosslinkers can be used. Water-soluble carbodiimides such as 1-ethyl-3-(3-dimethylaminopropyl)carbodiimide hydrochloride (EDC) and its co-reactant, N-hydroxysuccinimide (NHS) can be used to stabilize hydrogels. A protocol for making hydrogels for implantation into mini-pig corneal models based on the CLP sequence from O'Leary et al. [24] and EDC-NHS crosslinking can be found in Islam et al. [25]. Here, the CLP was conjugated to

an 8-arm PEG prior to crosslinking. Our exColA peptide, however, is crosslinked without prior conjugation to a polymeric backbone. In Samarawickrama et al. [26], 4-(4,6-dimethoxy-1,3,5-triazin-2-yl)-4-methyl-morpholinium chloride (DMTMM) was used as a crosslinker. Unlike EDC-based crosslinking, DMTMM does not require accurate pH control or pH shift during the reaction to be effective [27].

2. Materials

Please note that examples of equipment given are those we have used. The can be substituted with equipment or reagents from other manufacturers or suppliers.

2.1. Synthetic DNA

(1) pUC57-exColA: Commercially available DNA cloning vector with recombinant CLP sequence, exColA. The exColA sequence should be codon optimized. This vector contains a Tobacco Etch Virus (TEV) endoprotease cleavage site after His-tag (see Notes 1 and 2). The name exColA is a placeholder for the CLP selected by the reader.

2.2. Preparation of Cloning System and Expression System

(1) E. coli cloning strain: 5-α cold shock competent E. coli.
(2) E. coli expression strain: ClearColi BL21(DE3) Electrocompetent Cells (see Note 3).
(3) Expression plasmid: pColdIII.
(4) Ampicillin stock solution: 3 g of ampicillin in 30 mL distilled water. The ampicillin solution is decanted into a 60 mL syringe and filtered through a 0.22 μm syringe filter. The sterile filtered solution is divided into 3 mL aliquots and stored at -20 °C.
(5) LB Miller broth: 100 g of powdered LB broth is weighed and placed in a 6 L glass flask. The flask is filled to 4 L with distilled water. The flask is covered with aluminum foil and sealed with autoclaving tape. The bottle is autoclaved for 20 min at 121 °C and then allowed to cool. When the broth has cooled to below 45 °C, 4 mL of ampicillin stock is added to make a final concentration of 100 μg/mL.
(6) LB Miller agar plates: 5 g of LB broth is added to a 1 L bottle. 2 g of agar is added and the volume is made up to 200 mL by adding distilled water. The powder is dissolved by heating in a microwave oven at high intensity until boiling. The solution is boiled by microwaving at 30% intensity for an additional 5 min. When flask has cooled to below 55 °C, 4 mL

of ampicillin stock is added to make a final concentration of 100 μg/mL. The solution is poured into 35 mm petri dishes (see Note 4).

(7) Culture tubes: 100 mm size, translucent microbiology polypropylene tubes.

(8) Shaking incubator: A closed, temperature-controlled, shaking incubator capable of maintaining 250 RPM and 37 °C.

(9) Incubator: A closed, temperature-controlled, incubator capable of maintaining 37 °C.

(10) Agar gel electrophoresis system: Horizontal electrophoresis system with combs to make 30 μL wells.

(11) 1% Agar gels prepared according to external protocol [28].

(12) Tris, Acetic acid, EDTA (TAE) buffer: Ready-made TAE buffer concentrate is diluted 1:50 in water.

(13) Loading buffer.

(14) Invitrogen™ SYBR™ Safe™ DNA Gel Stain.

(15) Blue light table: Light source capable of exciting at 470 nm.

(16) Gel imaging box: Imaging system with light source capable of exciting at 470 nm.

(17) Freezing solution: 10 mL glycerol solution and 10 mL water.

(18) Miniprep kits.

(19) Vacuum manifold.

(20) Centrifuge.

2.3. Expression of CLP

(1) Culture flasks.

(2) Shaking incubator.

(3) Magnetic stirrer.

(4) Thermometer.

(5) LB Miller broth (see Subheading 2.2, item 5).

(6) 1 M Isopropyl β-D-1-thiogalactopyranoside (IPTG): 2.38 g IPTG in 10 mL of water. The solution is filtered using a 0.22 μM syringe filter and stored at -20°C.

(7) Lysis buffer: 690 mM NaCl, 13.5 mM KCl, 50 mM Na_2HPO_4, 9 mM KH_2PO_4, 20 mM imidazole, 5 M urea, 5 g/L Triton X100, 10% v/v glycerol.

(8) 1 mM phenylmethanesulfonyl fluoride (PMSF) in ethanol.

(9) Probe sonicator.

(10) Ultracentrifuge. 1

(11) SDS-PAGE system.

(12) SDS-PAGE Precast Protein gels. 1

(13) SDS-PAGE running buffer: 10× Tris/Glycine/SDS, diluted 1:10 in water.

(14) Laemmli buffer.

(15) Coomassie solution.

(16) Gel imaging box: Imaging system with white light illumination.

2.4. FPLC Purification of CLP

(1) FPLC system.

(2) FPLC columns.

(3) Loading/washing buffer: PBS powder, pH 7.4, 5 M urea, 20 mM imidazole to make 1 L.

(4) Elution buffer: PBS powder, pH 7.4, 5 M urea, 500 mM imidazole to make 1 L.

(5) 20% ethanol: Prepared from sterile water and 100% ethanol. Filter with 0.20 μm bottle filters.

(6) TEV reaction buffer: 500 mM NaCl, 20 mM Tris, pH 7.5 in water.

(7) Bradford solution:

2.5. Preparation of Lyophilized CLP

(1) Dialysis tubing (see Note 5).

(2) Dialysis buffer container (see Note 6).

(3) Urea in water: 4 M, 3 M, 2 M, and 1 M solutions of urea in ultrapure water is prepared and sterile filtered using a 0.2 μm bottle filter.

(4) Liquid nitrogen.

(5) Lyophilizer.

2.6. Preparation of Corneal-Shaped Implants The apparatus used for molding is identical to that used for making collagen-based implants and can be found in Islam et al. [29].

(1) Pre-weighed 4-(4,6-dimethoxy-1,3,5-triazin-2-yl)-4-methyl-morpholinium chloride (DMTMM) powder aliquots of 50–100 mg. Store at -20 °C.

(2) T-junction connector and fittings.

(3) Glass syringes: 2 mL, Luer lock.

(4) Rubber septum: 2 mm thickness.

(5) Biopsy punch: 4 mm diameter.

(6) 500 μL, 100 μL and 50 μL Hamilton syringes.

(7) Needle (22 s/51/2)L for 500 μL syringe.

(8) Needle (22 s/51/2)S for 100 μL and 50 μL syringes.

(9) Wide glass dish.

(10) Metal jigs: stainless steel jigs machined to tightly hold PTFE corneal molds.

(11) Polypropylene corneal implant molds: 500 μm thick, 10 mm diameter, x curvature (custom-made).

(12) Allen key.

(13) Hydrated chamber (a pipette tip box can be used).

3. Methods

3.1. Preparation of Cloning System

(1) Transform 5-α cold shock competent E. coli with pUC57-exColA according to the bacterial strain supplier protocol.

(2) Pick at least 10 colonies by touching the colony with a 10 μm sterile pipette tip and place the pipette tip in 6 mL of Miller media in a bacterial culture tube.

(3) Culture the 5-α E. coli clones for 24 h at 37°C at 250 RPM; cultures can be taken to the next step after the optical density (OD) reaches 0.6 or higher.

(4) Freeze stocks of 5-α pUC57-exColA. 500 μL of bacterial culture is mixed with 500 μL of freezing solution in a 2 mL cryotube and placed in -80°C.

(5) Clone exColA from pUC57 to pColdIII according to any conventional cloning protocol [30, 31].

(6) Transform 5-α E. coli with pColdIII-exColA according to the protocol supplier with the bacterial strain.

(7) Pick at least 10 colonies by touching the colony with a 10 μm sterile pipette tip and place the pipette tip in 6 mL of Miller media within a bacterial culture tube.

(8) Culture the 5-α E. coli pColdIII-exColA clones for 24 h at 37°C at 250 RPM; cultures can be taken to the next step after OD reaches 0.6 or higher.

(9) Freeze stocks of 5-α pUC57-exColA. 500 μL of bacterial culture is mixed with 500 μL of freezing solution in a 2 mL cryotube and placed in -80°C.

(10) Perform Miniprep plasmid isolation according to manufacturer protocol on the 10 clones. 1

(11) Digest the 10 clones with restriction enzymes, or run analytical PCR. Use a different set of enzymes than was used for the cloning in step 5.

(12) Run agarose gels according to external protocol (see Notes 7 and 8) [28].

(13) Image and validate the presence of expected bands using a gel imaging system.

(14) Discard any clones that do not cut/amplify in expected manner.

3.2. Preparation of CLP Expression System

(1) Transform ClearColi with pColdIII-exColA according to supplier protocol.

(2) Pick at least 10 colonies by touching each colony with a 10 μm sterile pipette tip and then placing the pipette tip in 6 mL of Miller media in a bacterial culture tube.

(3) Culture the ClearColi clones for 24–48 h at 37 °C at 250 RPM; cultures can be taken to the next step after OD reaches 0.6 or higher.

(4) Freeze stocks of ClearColi pColdIII-exColA. To freeze, 500 μL of bacterial culture is mixed with 500 μL of freezing solution in a 2 mL cryotube and placed in a -80 °C freezer.

(5) Perform a diagnostic restriction digestion according to external protocol [32].

(6) Run agarose gels [28].

(7) Image and validate the presence of expected bands.

(8) Discard any clone that does not show the appropriate restriction digested bands or amplifies in expected manner.

(9) Optional: perform sequencing of plasmid.

3.3. Expression of CLP

(1) ClearColi pColdIII-exColA is scraped on 10 μm pipette tip and placed in 40 mL of culture media.

(2) Culture is maintained at 37 °C until OD $>$ 0.5.

(3) 40 mL of bacterial culture is added to 3 L of media in baffled culture flask.

(4) Culture is maintained at 37 °C at 250 RPM until an OD of 1 is reached (see Note 9).

(5) IPTG is added to culture to a final concentration of 1 mM.

(6) Culture is brought to 5–8 °C by placing in ice bath on a stir-plate at 250 RPM. Monitor temperature with an analog thermometer.

(7) Culture is placed at 5–16 °C at 250 RPM for 24 h.

(8) Culture is divided into 1 L centrifugation flasks and pelleted at 4 °C, 4000 rcf.

(9) Supernatant is discarded.

(10) Pellet is dissolved in lysis buffer: 5$\times$ the pellet volume of buffer is used.

(11) Bacteria is lysed with sonication: 60% amplitude; 1 s on, 200 ms off; 4$\times$ 2 min with 10 min of cooling on ice between each cycle.

3.2. Preparation of CLP Expression System

(1) Transform ClearColi with pColdIII-exColA according to supplier protocol.
(2) Pick at least 10 colonies by touching each colony with a 10 μm sterile pipette tip and then placing the pipette tip in 6 mL of Miller media in a bacterial culture tube.
(3) Culture the ClearColi clones for 24–48 h at 37 °C at 250 RPM; cultures can be taken to the next step after OD reaches 0.6 or higher.
(4) Freeze stocks of ClearColi pColdIII-exColA. To freeze, 500 μL of bacterial culture is mixed with 500 μL of freezing solution in a 2 mL cryotube and placed in a -80 °C freezer.
(5) Perform a diagnostic restriction digestion according to external protocol [32].
(6) Run agarose gels [28].
(7) Image and validate the presence of expected bands.
(8) Discard any clone that does not show the appropriate restriction digested bands or amplifies in expected manner.
(9) Optional: perform sequencing of plasmid.

3.3. Expression of CLP

(1) ClearColi pColdIII-exColA is scraped on 10 μm pipette tip and placed in 40 mL of culture media.
(2) Culture is maintained at 37 °C until OD $>$ 0.5.
(3) 40 mL of bacterial culture is added to 3 L of media in baffled culture flask.
(4) Culture is maintained at 37 °C at 250 RPM until an OD of 1 is reached (see Note 9).
(5) IPTG is added to culture to a final concentration of 1 mM.
(6) Culture is brought to 5–8 °C by placing in ice bath on a stir-plate at 250 RPM. Monitor temperature with an analog thermometer.
(7) Culture is placed at 5–16 °C at 250 RPM for 24 h.
(8) Culture is divided into 1 L centrifugation flasks and pelleted at 4 °C, 4000 rcf.
(9) Supernatant is discarded.
(10) Pellet is dissolved in lysis buffer: 5$\times$ the pellet volume of buffer is used.
(11) Bacteria is lysed with sonication: 60% amplitude; 1 s on, 200 ms off; 4$\times$ 2 min with 10 min of cooling on ice between each cycle. Solution is centrifuged at 15 kRCF at 4 °C for 30 min.
(12) Supernatant is decanted and combined in a sterile glass flask.
(13) Pellets are resuspended in 5 mL of lysis buffer with fresh PMSF.
(14) Suspension is sonicated using the same parameters as above.

(15) Perform SDS-PAGE of the supernatant from step 13 and solution from step 14 according to external protocol [33].

(16) If either of solutions from step 13 or 14 is devoid of target protein, that fraction is discarded.

(17) Pool fractions that contain significant amounts of exColA.

3.4. FPLC Purification of CLP

(1) The HisPrep^{TM} FF 16/10 column containing Ni-loaded sepharose is attached to FPLC system (see Note 10).

(2) System cleaning is performed according to FPLC system manufacturer handbook.

(3) Column is equilibrated with 5 column volumes (CVs) of running buffer (see Note 11).

(4) Sample from step X 3.3.18 is loaded by direct injection at 3 mL/min flow (see Note 12). AQ1

(5) Wash the sample flow path with 1 CV of washing buffer.

(6) Column with bound sample is washed with 10 CVs of washing buffer (see Note 13).

(7) A linear gradient from washing buffer to elusion buffer is performed over 10 CVs. Fraction collection is performed over the whole span of the gradient, and one additional CV. Fraction volume is set to 20 mL (see Note 14).

(8) FPLC system and column is washed according to manufacturer instructions.

(9) Chromatogram is used to identify which fractions contain eluted protein. The peak is expected in the range of 100–400 mM of imidazole. Peak base width is expected to be no wider than 30 mL (see Note 15).

(10) Dialysis tubing should be cut to the correct length for the sample volume. The length can be calculated using the formula:

$$\frac{4 + \frac{\frac{376.992 \times SampleVolume}{TubingFlatWidth}}{TubingFlatWidth} \times 100 + 0.5}{100}$$

It is recommended to add 5–10 cm of tubing to this measurement to have space to attach the dialysis tubing clamps.

(11) The dialysis tubing should be pre-equilibrated in the buffer to remove the residual preservatives from the tubing before use.

(12) Clamp the bottom end of the dialysis tube by folding over the end of the tubing and attaching the weighted clamp over the folded edge.

(13) Carefully pipette the solution into the tubing.

(14) Open the tubing fully at the top end to allow air into the tubing above the sample. Fold the top end of the tubing over and clamp at the top ensuring that the air bubble remains between the clamp and the sample. The air is critical for the buoyancy of the sample during dialysis.

(15) Fill the buffer container 80% with buffer and an appropriately sized stir bar. Add the sample and fill to 100% of the volume to prevent spillover.

(16) Dialysis is performed by stepwise dialysis against urea solution. The sample is dialyzed against a total of 50 dialysis volumes of urea solution for a total of 12H per buffer step. 4 M, 3 M, 2 M, and 1 M is used and finally the solution is dialyzed against 100 dialysis volumes of TEV reaction buffer (see Notes 16 and 17).

(17) The protein content is quantified using a Bradford assay according to the manufacturer instructions.

(18) The sample is digested with TEV protease. 0.25 mg of TEV protease is used per mg of protein.

(19) FPLC column is equilibrated with 5 CV of running buffer.

(20) The sample is loaded on the column. Due to the lack of His-tag after digestion, only His-rich bacterial proteins should bind to the column while the protein of interest should run straight through. The flowthrough is run to outlet and collected in a sterile glass bottle. Do not run to waste (see Note 18).

(21) Wash buffer is run for 1 CV and collected in the same vessel as sample load flow through.

(22) Bound protein is eluted using 3 CV of elution buffer. Flow-through goes to waste (see Note 19) .

3.5. Preparation of Lyophilized CLP

The protein flow-through should be dialyzed again from FPLC buffer until it is in ultrapure water.

(1) Dialyzed exColA is transferred into 50 mL liquid nitrogen-safe tubes.

(2) Sample tubes are frozen in liquid nitrogen for 10 min (see Note 20).

(3) Sample tubes are opened slightly to allow air flow and placed in lyophilizer flasks.

(4) The lyophilizer system is closed, and cycle is started.

3.6. Preparation of Corneal-Shaped Implants

(1) Remove the plunger from a sterile 10 mL syringe and wipe the interior of the barrel with a particle-free wipe to remove the syringe's coating as it can interfere with hydrogel formation. Cap the syringe using a rubber cap held in place with parafilm.

(2) Weigh the empty syringe and record the weight. Carefully transfer the lyophilized exColA into the syringe and weigh the assembly to determine the exColA mass.

(3) Add ddH O for a final concentration of 20% w/w. Cap the top of the syringe with a rubber stopper and parafilm. Centrifuge for 1 min at 200 rcf to ensure protein and water are in contact with one another. Dissolving can be expedited by cycles of heating to 37 °C for 30 min followed by cooling on ice. Store at 4 °C (see Note 21).

(4) Centrifuge dissolved exColA at 1000 RCF at 4 °C for 1 h; repeat until solution is free of visible bubbles.

(5) Transfer 0.7 g of exColA solution from plastic syringe to a glass syringe using a 2 mm inner diameter PTFE tube to connect the two syringes. Ensure that no bubbles are produced during the transfer.

(6) Prepare water bath in large glass beaker using ultrapure water (dd-water).

(7) Fill syringe mixing system with dd-water and violently expel any trapped air bubbles into a water bath. Eject all water from the attached syringe and keep the mixing system submerged. Attach the glass syringe containing collagen to the empty Luer adapter on the mixing system, take care not to introduce bubbles. Place assembled mixing system on ice (see Note 22).

(8) Dissolve DMTMM to 20% w/w in H O. Sterile filter through a 0.2 μm syringe filter.

(9) Inject dissolved DMTMM through the septum of the mixing system; use a volume equivalent to 0.7 times the molar amount of primary amines in exColA (see Note 23).

(10) Mix the solution by alternating pressing the two plungers of the mixing system; pass the solution through the central t-piece 40 times to ensure sufficient homogeneity.

(11) Eject 150 μL of exColA/DMTMM solution to each cornea mold. Assemble molds and jigs, expelling any surplus CLP/DMTMM solution around the edges of the molds. Place in a hydrated chamber overnight at room temperature.

(12) Open the jigs and place the mold assemblies in PBS overnight at 4 °C. 1

(13) Carefully pry the jigs open and incubate the open molds overnight in PBS at 4 °C.

(14) Gently lift the corneal implants out of the molds once fully hydrated. Wash in PBS at 4 °C for 7 days, changing the buffer daily.

4. Notes

(1) When an appropriate CLP has been designed or selected, codon optimization for the desired expression system must be performed. This service can be performed by commercial entities such as GenScript. We suggest incorporation of an N-terminal 6x His tag and TEV endoprotease cutting site. The design should take into account the nucleases that will be used for future enzymatic cloning, ensuring that these are avoided within the coding sequence.

(2) Cleavage sites other than the TEV site can be used. TEV endoprotease was chosen due to high specificity and due to the rarity of the motif.

(3) Endonuclease deficient bacterial strains are required for long-term stability of cloning strains. This protocol uses a cold shock competent bacterial strain. If different competency bacteria is used, the reader should follow the protocols supplied together with that cloning strain for transformation. We use ClearColi , an E. coli strain that was modified to have diminished or non-existent activation of LPS response in mammalian cells. A distinction should be made between endotoxin pathway activation and lack of immunogenicity. LPS is not the only bacterial constituent that can trigger inflammation or rejection [34].

(4) Microwaving will sterilize the solution sufficiently for no spontaneous growth to occur for several weeks on properly stored agar plates, even in the absence of antibiotics.

(5) Dialysis tubing made from nitrocellulose can generally be used. Mw cutoff needs to be based on target protein Mw. Dialysis tubing should be purchased with a pore size that is at least 5 kDa smaller than a single subunit of your protein of interest. The dialysis tubing width should be chosen so that a standard batch results in tubing that is the correct length for your dialysis chamber. If necessary, use two shorter lengths of dialysis tubing for the sample to fit the beaker, so it floats free and unencumbered within the chamber.

(6) The dialysis buffer container should be sufficiently large to hold a minimum of 50× the sample volume. A large graduated cylinder may be ideal as it allows for longer lengths of dialysis tubing for large samples than a large beaker.

(7) Optional: at this point sequencing can be used in place of restriction digestion to ensure that no mutations have been introduced into the sequence.

(8) We recommend use of SYBR Safe in place of toxic and mutagenic ethidium bromide.

(9) Oxygenation is of critical importance during the initial growth of the bacterial colony. The culture conditions outlined here assumes a large aerated space in the shaking incubator, or a ventilated/actively oxygenated incubator.

(10) Binding capacity is heavily dependent upon the geometry and surface chemistry of the electrophoresis matrix. If a different matrix is used, the reader must reference manufacturer instructions and adjust bed volume to facilitate a sufficient protein binding capacity.

(11) Depending on the predisposition of the protein used, a higher ionic strength might be needed for wash/bind buffer and elution buffer. If the protein is noted to form insoluble particles when exposed to the wash/bind buffer, 5× PBS can be used instead of 1×.

(12) Ensure that the column manufacturer-specified max delta pressure is not exceeded in this step. If column becomes visibly compressed or the delta pressure exceeds manufacturer recommendations, a lower pump speed should be used.

(13) If this is a routine run, the flow-through in this step can be run to waste. If this is an early optimization run, the sample should be collected by running it to an outlet valve with a clean collection vessel.

(14) Average peak base width using HisPrep™ FF 16/10 columns is 1 CV, which is why 20 mL fractions are used.

(15) If yields are poor the imidazole absorption at 280 nm can make resolving the exact range of target elusion difficult; in these cases, a "dry run" with all the same parameters but without protein in the loading buffer can supply a baseline that can be deducted from the absorbance chromatogram.

(16) The first dialysis stage should be no more than 3 h before the buffer is changed.

(17) The stepwise dialysis is necessary to avoid protein falling out of solution.

(18) This flow-through contains your target protein. Only bacterial His rich proteins will bind the column.

(19) This step is a cleaning step, removing His rich bacterial proteins, TEV protease, and digested His-tags from the column.

(20) Samples should be frozen and lyophilized according to the instructions provided by the lyophilizer manufacturer. These instructions are based on protocols for most research lyophilizers.

(21) If the protein cannot be kept soluble in water at room temperature, other buffers can be used. Note that many collagens do not lyophilize well in phosphate-based buffers; PB and PBS should be avoided in this step.

(22) Depending on the size and inter-strand interaction strength, the viscosity of different CLPs at any given concentration will vary. A mechanical syringe mixer can facilitate mixing of solutions that are not possible to safely mix by hand.

(23) DMTMM has a MW of 276.72 Da. The volume of exColA is 0.7 mL. The concentration of exColA is 0.2 g/mL. The concentration of DMTMM is 0.2 g/mL. To calculate the volume to inject use the formula:

$$V_{DMTMM} = \frac{(0.7 \times (0.2/MW_{exColA}) \times (1^{\circ}A_{exColA}) \times MW_{DMTMM})}{0.2}$$

References

(1) Montes GS, Junqueira LC (1982) Biology of collagen. Rev Can Biol Exp 41(2):143–156

(2) Brodsky B, Persikov AV (2005) Molecular structure of the collagen triple helix. In: Advances in protein chemistry, vol 70. Academic Press, Cambridge, pp 301–339

(3) Kadler KE, Holmes DF, Trotter JA, Chapman JA (1996) Collagen fibril formation. Biochem J 316(1):1. http s://doi.org/10.1042/bj3160001

(4) Islam MM, Buznyk O, Reddy JC, Pasyechnikova N, Alarcon EI, Hayes S, Lewis P, Fagerholm P, He C, Iakymenko S, Liu W, Meek KM, Sangwan VS, Griffith M (2018) Biomaterials-enabled cornea regeneration in patients at high risk for rejection of donor tissue transplantation. NPJ Regen Med 3:2. https://doi.org/10.103 8/s41536-017-0038-8

(5) Zeugolis DI, Paul RG, Attenburrow G (2008) Factors influencing the properties of reconstituted collagenfibers prior to self-assembly: animal species and collagen extraction method. J Biomed Mater Res A 86A(4):892–904. https://doi.org/10.1002/jbm.a.31694

(6) Lynn AK, Yannas IV, Bonfield W (2004) Antigenicity and immunogenicity of collagen. J Biomed Mater Res B Appl Biomater 71B(2):343–354. https://doi.org/10.1002/jbm.b.30096

(7) Jenkins CL, Bretscher LE, Guzei IA, Raines RT (2003) Effect of 3-hydroxyproline residues on collagen stability. J Am Chem Soc 125(21):6422–6427. https://doi.org/10.1021/ja034015j

(8) Yu Z, An B, Ramshaw JAM, Brodsky B (2014) Bacterial collagen-like proteins that form triple-helical structures. J Struct Biol 186(3):451–461. https://doi.org/10.1016/j.jsb.2014.01.003

(9) Peng YY, Yoshizumi A, Danon SJ, Glattauer V, Prokopenko O, Mirochnitchenko O, Yu Z, Inouye M, Werkmeister JA, Brodsky B, Ramshaw JA (2010) A streptococcus pyogenes derived collagen-like protein as a non-cytotoxic and non-immunogenic cross-linkable biomaterial. Biomaterials 31(10):2755–2761. https://do i.org/10.1016/j.biomaterials.2009.12.040

10. An B, Kaplan DL, Brodsky B (2014) Engineered recombinant bacterial collagen as an alternative collagenbased biomaterial for tissue engineering. Front Chem 2(40). https://doi.org/10.3389/fchem.2014.00040

(10) Cosgriff-Hernandez E, Hahn MS, Russell B, Wilems T, Munoz-Pinto D, Browning MB, Rivera J, Hook M (2010) Bioactive hydrogels based on designer collagens. Acta Biomater 6(10):3969–3977. https://doi.org/10. 1016/j.actbio.2010.05.002

(11) Xu C, Yu Z, Inouye M, Brodsky B, Mirochnitchenko O (2010) Expanding the family of collagen proteins: recombinant bacterial collagens of varying composition form triple-helices of similar stability. Biomacromolecules 11(2):348–356. https://doi.org/10.1021/bm900894b

(12) Shoulders MD, Raines RT (2009) Collagen structure and stability. Annu Rev Biochem 78:929–958. https://d oi.org/10.1146/annurev.biochem.77.032207.120833 14. Fallas JA, Gauba V, Hartgerink JD (2009) Solution structure of an abc collagen heterotrimer reveals a single-register helix stabilized by electrostatic interactions. J Biol Chem 284(39):26851–26859. https://doi.or g/10.1074/jbc.M109.014753

(13) Nassa M, Anand P, Jain A, Chhabra A, Jaiswal A, Malhotra U, Rani V (2012) Analysis of human collagen sequences. Bioinformation 8(1):26–33. https://doi.org/10.6026/97320630008026 AQ2

(14) Boudko SP, Engel J, Bächinger HP (2012) The crucial role of trimerization domains in collagen folding. Int J Biochem Cell Biol 44(1):21–32. https://doi.org/10.1016/j.biocel.2011.09.009

(15) Sundaramoorthy M, Meiyappan M, Todd P, Hudson BG (2002) Crystal structure of nc1 domains. Structural basis for type iv collagen assembly in basement membranes. J Biol Chem 277(34):31142–31153. https://doi. org/10.1074/jbc.M201740200

(16) Paramonov SE, Gauba V, Hartgerink JD (2005) Synthesis of collagen-like peptide polymers by native chemical ligation. Macromolecules 38(18):7555–7561. https://doi.org/10.1021/ma0514065

(17) Olsen D, Yang C, Bodo M, Chang R, Leigh S, Baez J, Carmichael D, Perala M, Hamalainen ER, Jarvinen M, Polarek J (2003) Recombinant collagen and gelatin for drug delivery. Adv Drug Deliv Rev 55(12):1547–1567

(18) Bagley D (2019) Declaration of source material - vitricol. https://www.advancedbiomatrix.com/wp-content/uploads/2011/09/Declaration-of-Source-Material-9-3-15.pdf. Accessed 10 June 2019

(19) Tomita M, Munetsuna H, Sato T, Adachi T, Hino R, Hayashi M, Shimizu K, Nakamura N, Tamura T, Yoshizato K (2003) Transgenic silkworms produce recombinant human type iii procollagen in cocoons. Nat Biotechnol 21(1):52–56. https://doi.org/10.1038/nbt771

(20) Shoseyov O, Posen Y, Grynspan F (2014) Human collagen produced in plants: more than just another molecule. Bioengineered 5(1):49–52. https://doi.org/10.4161/bioe.26002

(21) Adachi T, Wang X, Murata T, Obara M, Akutsu H, Machida M, Umezawa A, Tomita M (2010) Production of a non-triple helical collagen alpha chain in transgenic silkworms and its evaluation as a gelatin substitute for cell culture. Biotechnol Bioeng 106(6):860–870. https://doi.org/10.1002/bit.22752

(22) O'Leary LER, Fallas JA, Bakota EL, Kang MK, Hartgerink JD (2011) Multi-hierarchical self-assembly of a collagen mimetic peptide from triple helix to

nanofibre and hydrogel. Nat Chem 3:821. https://doi.org/10.10 38/nchem.1123. https://www.nature.com/articles/nchem.1123#supplementary-information 25. Islam MM, Ravichandran R, Olsen D, Ljunggren MK, Fagerholm P, Lee CJ, Griffith M, Phopase J (2016) Self-assembled collagen-like-peptide implants as alternatives to human donor corneal transplantation. RSC Adv 6(61):55745–55749. https://doi.org/10.1039/C6RA08895C 26. Samarawickrama C, Samanta A, Liszka A, Fagerholm P, Buznyk O, Griffith M, Allan B (2018) Collagenbased fillers as alternatives to cyanoacrylate glue for the sealing of large corneal perforations. Cornea 37(5):609–616. https://doi.org/10.1097/ico.0000000000001459

(23) D'Este M, Eglin D, Alini M (2014) A systematic analysis of dmtmm vs edc/nhs for ligation of amines to hyaluronan in water. Carbohydr Polym 108:239–246. https://doi.org/10.1016/j.carbpol.2014.02.070

(24) Voytas D (2000) Agarose gel electrophoresis. Curr Protoc Mol Biol 51(1):2.5A.1–2.5A.9. https://doi.org/10. 1002/0471142727.mb0205as51

(25) Islam MM, Griffith M, Merrett K (2013) Fabrication of a human recombinant collagen-based corneal substitute using carbodiimide chemistry. Methods Mol Biol 1014:157–164. https://doi.org/10.1007/978-1-62 703-432-6_10

(26) Plasmid cloning by restriction enzyme digest. addgene. https://www.addgene.org/protocols/subcloning/. Accessed 10 June 2019

(27) Struhl K (1991) Subcloning of DNA fragments. Curr Protoc Mol Biol 13(1):3.16.11-13.16.12. https://doi.org/10.1002/0471142727.mb0316s13

(28) Diagnostic restriction digest (2018) addgene. https://www.addgene.org/protocols/diagnostic-digest/. Accessed 10 June 2019

(29) Gallagher SR (2006) One-dimensional sds gel electrophoresis of proteins. Curr Protoc Mol Biol 75(1):10.12.11–10.12A.37. https://doi.org/10.1002/0471142727.mb1002as75

(30) Mamat U, Wilke K, Bramhill D, Schromm AB, Lindner B, Kohl TA, Corchero JL, Villaverde A, Schaffer L, Head SR, Souvignier C, Meredith TC, Woodard RW (2015) Detoxifying escherichia coli for endotoxin-free production of recombinant proteins. Microb Cell Factories 14(1):57. https://doi.org/10.1186/s12934-015-024 1-5

Figure Legends

Figure 1. Before and after photos of patients who had been grafted with recombinant human collagen-based implants to treat ulcers and scarring due to infection or burns. These patients showed stable integration of the implants and regenerated neo-corneas after an average of 2 years post-surgery. Modified from Fig. 2, Islam et al. [4]

Figure 2. Collagen-like peptide-based implant manufactured according to Subheading 3.6 of this chapter.

Figures

Figure 1.

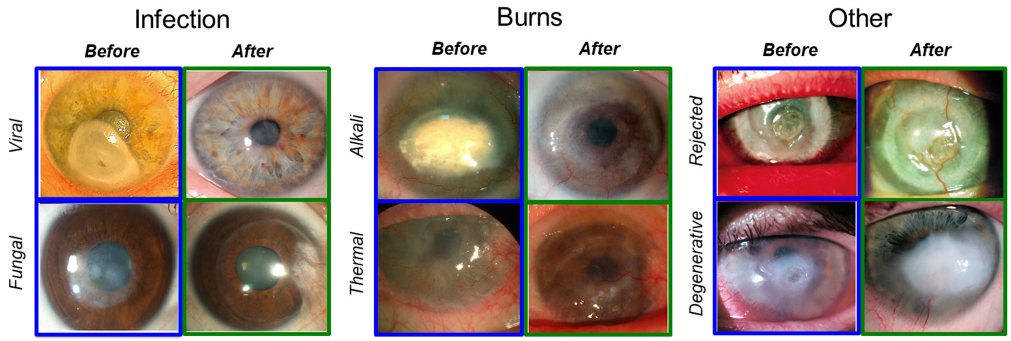

Figure 2.

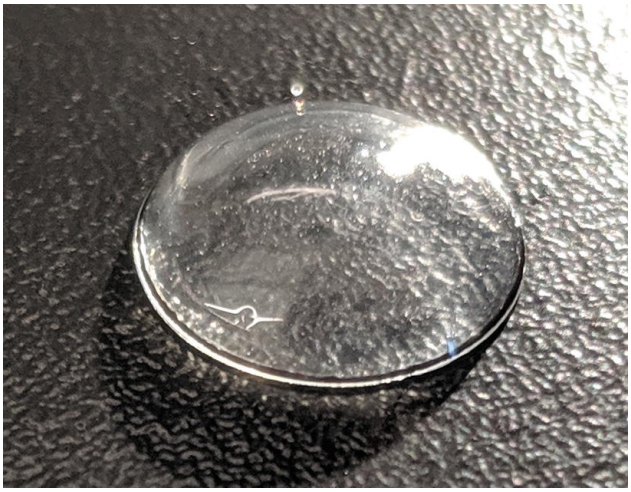

Chapter 8

Discussion

8.1. Solid Corneal Implants

The first objective presented in this thesis examines methods to improve the manufacture of solid corneal implants. Here, we validated the hypothesis that an interpenetrating network of polyphosphorylcholine could improve the anti-inflammatory properties of CLP-PEG (Hypothesis 1A, that peptide-capped silver nanoparticles can be used to improve the anti-microbial properties of solid corneal implants (Hypothesis 1B), and that e-beam can be used to terminally sterilize RHCIII-MPC implants (Hypothesis 1C). Appendix B compares aligned vs random recombinant human collagen type I (RHCI) solid corneal implants.

8.1.1. Impact of phosphorylcholine on cornea regeneration

The addition of polyphosphorylcholine to a collagen or peptide base-material fundamentally alters the mechanical properties of the gel. Despite the increase in total solid content, polyphosphorylcholine increases elongation at break and decreases the Young's modulus, leading to a more elastic hydrogel material [272, 273, 326]. Polyphosphorylcholine was originally conceptualized as a phospholipid mimetic, due to its phosphate group and hyrgoscopic properties [327]. It was originally used to create anti-microbial coatings on medical devices like stents (For review see [328]. In our composite hydrogels, polyphosphorylcholine acts as a GAG-mimetic retaining water content, so it adds an additional structural mimic for the corneal ECM.

The anti-inflammatory properties of polyphosphorylcholine are the outcome of complex structure/function relationship mediated by rapid re-epithelialization by CEpCs on the surface of the

hydrogel, encapsulating the hydrogel inside the cornea. This creates an environment where the fibroblasts and myofibroblasts at the edge of the surgical incision interact directly with the CLP-PEG-MPC material. The CLP-PEG-MPC material is resistant to collagenase, but it is still subject to degradation by macrophages and other enzymatic degradation. As long as the fibroblasts sense the presence of a non-native material, and they aren't anchored in the full corneal ECM with adjacent cells they can still secrete factors that promote the slow degradation of the hydrogel material and its replacement with newly secreted ECM that can support fibroblast attachment. We observe the outcome of this slow remodelling via decreased haze, central corneal neovascularization, and a lack of corneal thickening.

8.1.2. Suitability of collagen-based constructs for anti-bacterial additives

Chapter 4 discusses a porcine collagen hydrogel crosslinked with an epoxide crosslinker, BDDGE, and surface functionalized with peptide-capped silver nanoparticles to improve the implant's anti-microbial properties (Hypothesis 1B). BDDGE was used as a crosslinker because carbodiimide chemistry is incompatible with the incorporation of silver nanoparticles [329]. Capping the AgNPs with CLKRS peptides is a successful strategy to mitigate the cytotoxic effects of AgNP. The CLKRS-AgNP coated corneal implants successfully supported HCEpCs and promoted an M2 tolerogenic macrophage phenotype *in vitro*. This functionalized corneal implant was successful in inhibiting *P. aeruginosa*, *S. aureus*, and *S. epidermidis in vitro* and preventing biofilm formation at the air-liquid interface.

Collagen-based hydrogels are excellent base substrates for anti-bacterial additives. They have a wide range of amino-acids present to serve as attachment points for other chemistries. The primary limitation for collagen or other protein-based hydrogels is degradation. The lifespan of a conjugate or entrapped active ingredient depends on the rate of breakdown of either the conjugate bond or the collagen matrix within the material. Depending on the rate of breakdown, a surface coating may only be effective for a span of hours to days before the mechanical action of the eyelid and the enzymatic action of tears removes the coating from the surface. Ideally, functional additives that are evenly distributed throughout the hydrogel are not released from the central region until cells reach the area and begin the degradation and remodeling process. We currently do not have longitudinal data on the persistence of NPs in this type of system. It is likely that the persistence of functional additives is highly specific to the entrapment or linkage, hydrogel pore size, and rate of

remodeling. Care should also be taken in selection of a crosslinker with the incorporation of metallic nanoparticles.

8.1.3. Effect of e-beam on collagen-derived biomaterials

Low dose e-beam was successfully used to sterilize RHCIII-MPC solid corneal implants (Hypothesis 1C); however, this process was not without caveats. The industrial standard dose for gamma or e-beam irradiation is 25 kGy [330]. Previous literature suggested that this range was too high for biomaterials, so the RHCIII-MPC implants were tested at 17, 19 and 21 kGy [137]. Irradiation did not result in significant changes in tensile strength, elongation at break and Young's modulus, but a trend towards a change was present and may have been identified with a larger sample size. Given this data, the lowest dose at 17 kGy was used to test biocompatibility in rabbits. The irradiated and control RHCIII-MPC implants successfully regenerated the corneal tissue in the rabbit model. The control implants resulted in a decrease in corneal thickness, but the irradiated implants were comparable to the unoperated controls. The ability to use terminal sterilization in the manufacturing process for RHCIII-MPC provides it an advantage over HDC, which can be contaminated by bacteria and fungi. Overall, e-beam was demonstrated to be a successful technique for the sterilization of RHCIII-MPC corneal implants.

Interestingly, we did not observe the phenomenon reported for ACG, where the Young's modulus was maintained, but there was a significant alteration in melting temperature after γ-irradiation [138]. The downwards shift in T_m suggests that the γ-irradiation is causing free-radical damage to the peptide backbone, lowering the threshold for complete fibril unwinding. Our result indicate that the e-beam is not causing a comparable shift in T_m in the RHCIII-MPC material, this could either be due to fewer free radicals generated by e-beam or a protective effect from the polyphosphorylcholine.

8.2. Liquid Corneal Fillers

8.2.1. Adhesive Properties

Hypothesis 2A was confirmed, showing that 1% fibrinogen, in combination with thrombin application to the wound bed, would attach the LiQD Cornea to the surrounding wound bed. The fibrinogen is cleaved into fibrin by the thrombin applied to the wound bed, to attach to fibrin present on the wound surface using coiled coil interaction. It may also provide additional structural support for

the biomaterial after cross-linking. The presence of fibrinogen in LiQD Cornea may affect the environment of the corneal wound healing response. Fibrinogen is cleaved by thrombin into the active form fibrin that forms fibrils due to the action of its coiled coil domains. Fibrin(ogen) is associated with a pro-inflammatory, pro-angiogenic wound healing response [331]. It contains binding sites for Tissue-type plasminogen activator, plasminogen, plasmin inhibitor, α2-PI, Lipoprotein(a) [LP(a)], Histidine-rich glycoprotein (HRGP), heparin, vascular endothelial (VE)-cadherin, intercellular adhesion molecule-1 (ICAM-1) and the integrins $\alpha_{\mathrm{IIb}}\beta_3$, $\alpha_{\mathrm{V}}\beta_3$, $\alpha_{\mathrm{M}}\beta_2$ or $\alpha_{\mathrm{x}}\beta_2$ (CD11c/CD18) [331, 332]. This means that it has direct interactions with platelets (αIIbβ3), VECs (VE-cadherin, ICAM-1) and dendritic cells (αxβ2) that promote angiogenesis. The peptides cleaved by thrombin, fibrinopeptides A and B, act as chemoattractants for neutrophils, monocytes and macrophages [331, 333–335]. Overall, the presence of fibrinogen throughout the hydrogel material may accelerate wound healing, but it may also create a pro-inflammatory environment and lead to increased myofibroblast formation and neovascularization. LiQD Cornea is an excellent proof of concept for the viability of *in situ* collagen mimetic peptide-based hydrogels, but the incorporation of commercial fibrin glue limits its future as a medical device.

8.2.2. Tissue Regeneration by CLP-PEG-fibrinogen

CLP-PEG-fibrinogen successfully regenerated the corneal epithelium and stroma (Hypothesis 2B). Interestingly, the remodelling process appears to have occurred more slowly than in the CLP-PEG and CLP-PEG-MPC solid implants, with visible haze up to 9 months post-operatively. This is reflected in the collagen quantification analysis, which shows decreased fibril formation in the LiQD Cornea, compared to the the syngeneic graft and unoperated cornea, a pattern that is not observed in the solid implants. This may be due to the pro-inflammatory properties of the fibrinogen described above or to a difference in the structural properties of the material. As the LiQD Cornea has a higher CLP-PEG content than the CLP-PEG-MPC implants, it is difficult to compare them directly.

8.3. Design of Collagen Mimetics

There is a fourth option for a primary protein matrix for hydrogel design, beyond xenogeneic collagen, recombinant human collagens and solid state peptides. Chapter 7 presents a method for the production of a fully recombinant collagen mimetic protein in low endotoxin *E. coli* (Hypothesis 3A). This allows for the design of collagens that do not require enzymatic addition of hydroxyprolines.

It also allows their creator to tune their thermal properties and their isoelectric point to achieve solubility at neutral pH and the ability to repeatedly thermally assemble and disassemble into fibrils. Their sequences can also be designed to carry cell attachment sequences (RGD, IKVAV, YIGSR) to faciliate cellular attachment to the fibrils. Recombinant collagen mimetics' greater molecular weight, combined with their adaptive thermal properties, provides the strengths of both collagens and collagen mimetic peptides to create a unique hydrogel matrix. Their *in silico* design also makes them patentable intellectual property, which can assist in protecting the formulations during development and expanding the options for their future use.

8.4. Perspectives

8.4.1. Collagen vs. Peptide Implants

This thesis presents four collagen-based solid corneal implants: RHCIII-MPC, CLKRS-NP-porcine collagen I (PCI), aligned recombinant human collagen type I (RHCI), and random RHCI (For RHCI study, please see Appendix B. Of these three implants, the rRHCI has the highest tensile strength and the second lowest elongation at break (Table 8.1). As it is manufactured using a crosslinking, dehydration and rehydration method, it can have an extremely high solid collagen content when rehydrated for use. The CLKRS-NP-PCI hydrogel had the second highest modulus, followed by RHCIII-MPC corneal implants. This is likely due to the fact that the RHCIII-MPC implants contain a network of polyphosphorylcholine that has been previously demonstrated to decrease tensile strength and increase elongation at break in RHCIII and PCI implants [272]. However, the phosporylcholine networked increased the elasticity of the implants from 28% for RHCI up to 49% for type I porcine collagen, making them more flexible for handling [272]. All three collagen-based implants were not as tough as the human cornea.

Corneal implants need to be flexible so the surgeon can manipulate them in the operating theater and elastic so they can retain single sutures without cracking or cheese-wiring. The manufacture of collagen-based biomaterials needs to be optimized to balance the high tensile strength of collagen fibers with the brittleness that can occur as a result of over-crosslinking. The methods for mixing collagen hydrogels are inherently limited by the thermal properties of the collagen fibers. Collagens rely on coiled-coil domains to assemble into their triple helical quaternary structure, but these domains are cleaved after assembly. This means that if collagen is heated, unwinding the fibrillar structure, it cannot re-assemble in its original conformation. This converts it to gelatin during

manufacturing. The manufacturing techniques used to make the collagen-based materials are all temperature controlled to prevent disassembly of the collagen from occurring. When dissolved in water, collagens form a highly viscous, non-Newtonian liquid that is difficult to manipulate. As a result, collagen hydrogels are either manufactured in acidic conditions and dehydrated (rRHCI), use a lower concentration of collagen (CLKRS-NP-PCI), or require robotic assisted mixing (RHCIII-MPC) [336–338]. These methods all require strict process controls to ensure that the collagen does not lose its structural integrity during processing.

The production of collagen-based biomaterials can also be limited by the supply line issues. RHCIII and RHCI are only manufactured by a single company, both of whom manufacture collagen primarily for internal use in their medical device programs (Eluminex Inc. [formerly Fibrogen Inc.] and CollPlant Inc. respectively). This means that these materials must be co-developed with the supplier and any process deviations or business solvency issues can entirely close off the supply of these materials for the corneal implant manufacturing process. Similarly, medical grade animal collagens are supplied by a limited number of companies. While there are more companies supplying this market, re-validating a collagen product may require design modifications if there are differences in the extraction process that affect the size and assembly of the fibrils. Supply line issues are an important front-end consideration for the manufacture of collagen-based materials and the long-term accessibility of the base material for the product. Overall, collagen-based materials provide good mechanical properties, but have a lot of undesirable manufacturing considerations.

Peptide-based biomaterials solve both of the primary concerns of collagen-based biomaterials. Peptides can be synthesized by any company providing active pharmaceutical ingredient-grade peptides for the biotechnology industry. It is significantly easier to validate a new peptide supplier, as all manufacturers use comparable solid state synthesis methods and it is possible to directly compare the certificates of analysis for the existing and new peptides. CLPs are synthesized as monomers and designed to use thermal assembly to form self-assembled structures. There are no concerns that heat-mediated fibrillar disassembly will result in changes to the material, as these gels can easily reform their quaternary structure as they cool. The CLP-PEG only material has a lower tensile strength than the RHCIII or rRHCI biomaterials, but greater elongation at break [271, 326, 339]. The addition of MPC to the biomaterial reproduces the trend of decreased tensile strength and greater elasticity that was observed with both RHCIII vs RHCIII-MPC and porcine collagen vs. porcine collagen-MPC materials [272, 326].

The CLP-PEG biomaterials provide a unique opportunity to simplify the manufacturing process by exploiting the thermal gelation properties of the peptide. It is possible to heat the CLP-PEG stock solution to 55°C to reduce the viscosity during manufacturing, removing the need to use a T-piece for manufacturing. This makes it easier to precision fill the molds when manufacturing corneal implants.

Tab. 8.1. Summary of Mechanical Properties for Solid and Liquid Corneal Biomaterials

	RHCIII-MPC	**CLP-PEG-MPC**	**CLP-PEG**	**rRHCI**	**LiQD Cornea**	**Cornea**
Tensile Strength	0.3 ± 0.1	0.022 ± 0.004	0.56 ± 0.21	2.67 ± 0.8	0.02	3.81 ± 0.04
Elongation at Break	20.1 ± 7.6	59.5 ± 7.7	50 ± 8	28 ± 6	N/A	N/A
Young's Modulus	1.7 ± 0.8	0.04 ± 0.01	0.15 ± 0.02	52.8 ± 13.1	0.2	3 to 13
Refractive Index	1.351 ± 0.001	1.340 ± 0.005	1.338 ± 0.004		1.354 ± 0.037	1.423 – 1.436
Water Content	91.5 ± 0.92	90.9 ± 0.78	92.7 ± 0.85	89.2 ± 0.003	91.2 ± 2.3	78

8.4.2. Primary Matrix Design of Liquid-to-Solid Hydrogel Formulations

The thermal properties of the CLP-PEG hydrogels make them uniquely suited to the production of liquid to solid corneal fillers. The ability to monomerize the CLP-PEG, then re-form the thermal network allows for the liquid application of the material to fill the corneal wound, prior to irreversibly crosslinking the hydrogel with DMTMM. Collagen-based biomaterials are unsuitable for the formation of thermal gels, as they need to be applied at temperatures under 37°C. In order to get a complete fill, the collagen would need to be applied at extremely low concentrations in order to have a sufficiently low viscosity to fill the wound bed.

Gelatin-methacrylate (Gel-MA), which is photocrosslinkable, has been developed as a liquid to solid injectable corneal filler [315, 325]. In GelMA-based biomaterials, a photoinitiator is used to generate free-radicals to initiate the polymerization reaction between methacryl groups [340]. This allows

for indiscriminate crosslinking to the surrounding tissue. The smaller molecular size of the gelatin allows for the hydrogel to penetrate and polymerize through the damaged native ECM to adhere it to the wound bed. Unfortunately, free radicals can damage ribosomes, DNA and RNA if they infiltrate surrounding cells [341]. Given that gelatin may already be recognized as a DAMP by the immune system (see section 1.3.1.1), the addition of free radical damage increases the likelihood that the repair will initiate a strong inflammatory response in the host tissue, preventing scar-free repair. Gelatin is susceptible to enzymatic degradation, so it is more likely to be degraded by MMP and macrophage activity in the short term [342]. Unmodified gelatin could be directly substituted for CLP-PEG in the LiQD Cornea, but our group does not use xenogeneic protein sources for our clinical development pipeline. This means that we would be turning expensive, recombinant human collagens into gelatin to enable thermal disassembly and re-assembly, which is both expensive and illogical.

8.4.3. General Design for *in situ* tissue regeneration

There is a trade-off between ease of use and ease of point of care delivery. Solid implants require a dedicated corneal surgeon, and the outcomes are dependent on the surgeon's skill, as well as their experience with the device. The shelf life of a solid device after terminal sterilization is one the scale of 1-2 years and easy to test. Solid corneal implants do not need particular considerations when it comes to shipping, and while refrigerated storage is preferable, there is a high likelihood that extended storage at room temperature can be validated. The outcomes using a liquid filler are less affected by surgical skill, as the device doesn't require the extensive use of surgical procedures. Ideally, the LiQD Cornea could be administered by an emergency medical technician, combat medic, or equivalent to stabilize an injury for transfer to an ophthalmic surgeon for assessment. Liquid hydrogel formulations present greater hurdles in packaging, storage and stability. Hydrogels designed to crosslink *in situ* need to be shipped and stored in a way that minimizes premature crosslinking of the bulk material and breakdown of the crosslinker, which likely involves aseptic fill, freezing, and/or packaging under inert gas.

8.4.4. Should sterilization technique be integral to biomaterials design?

Sterilization technique should be accounted for in the design of biomaterials, especially as irradiation-based methods are known to increase covalent crosslinking in dECM and collagen-based biomaterials. This may decrease elasticity and increase brittleness of the biomaterial. If terminal

sterilization is considered integral to the manufacturing process, it's important to plan this into the device design. Ideally, a research team would develop an optimal biomaterial and determine a sterilization dose that does not affect its mechanical properties. If this is not possible, it may be necessary to generate biomaterials with varying degrees of chemical crosslinking and test them at varying doses of irradiation, in order to optimize the relationship between these two processes and ensure that the final product meets the required mechanical characteristics.

If it's determined that terminal sterilization is unwanted or impossible to quality control, biomaterials can be processed using aseptic techniques. This outcome is undesirable because it places a significantly higher burden on the manufacturing process to certify that all incoming materials are sterile and that all processes conform to strict environmental monitoring criteria.

Overall, it's important to design biomaterials with a sterilization technique in mind, because it would be extremely work-intensive and expensive to re-design a material that fails during a required terminal sterilization procedure, or to re-design a manufacturing process to be aseptic.

8.4.5. Recommendation of sterilization methods for future efforts

We have shown that low dosage e-beam sterilization is compatible with solid corneal implants; being an industry standard as well as a well validated terminal sterilization method, this approach is unlikely to be supplanted in the near future. When working with liquid formulations that need to be assembled or crosslinked *in situ*, further work is needed to determine the optimal route. There is some evidence of increased peptide or protein stability in aqueous solutions at the point of sterilization; however, crosslinking is limited by physical distance, which means that the benefits of a lower degree of radical formation on the polymer might be offset by the higher mobility of the molecule in a solution. The first big risk of irradiating a liquid formulation compared to a solid implant is crosslinking of the polymer or protein which can inhibit assembly, thermo-responsive properties, and introduce graininess in the material. The second risk with irradiation of a liquid in a pre-crosslinked state is breakdown of the crosslinking agent, which may cause poor adhesion to the wound bed, changes in modulus, and a reduced tolerance to elevated temperatures.

8.5. Future Work

8.5.1. Primary Hydrogel Components

Recombinant collagens, xenogeneic collagens and CLP-PEG based collagen implants all have inherent limitations. The collagens are limited by their pre-assembly and susceptibility to thermal disassembly and CLP-PEG is limited by minimal self-assembly due to low peptide monomer content and steric hindrance from the PEG.

Chapter 7 discusses the methods for producing a custom collagen mimetic protein. In the future, collagen inspired proteins can be designed with tuneable properties, including the ability to self-assemble, cell adhesion motifs, and the removal of hydroxyprolines to streamline production of the protein. Unlike collagen, these custom recombinant proteins can be patented because they are designed *in silico*. This means that both the protein material and the composite hydrogel can undergo patent protection, to ensure the ability to commercialize a medical device.

8.5.2. Anti-Inflammatory Properties

The next obvious design step for the rRHCI solid corneal implant and the LiQD Cornea is the incorporation of polyphosphorylcholine. The rRHCI material can easily be designed to incorporate the existing free radical chemistry used in the RHCIII-MPC and CLP-PEG-MPC solid implants. The LiQD Cornea presents a significantly larger design issue, as free radical chemistry to too toxic for direct application *in situ*. The polyphosphorylcholine network will require a re-design to be compatible with the LiQD Cornea format for hydrogels.

8.5.3. Adhesives

The LiQD Cornea requires a re-design to eliminate the fibrinogen and thrombin from the biomaterial. Although this system created an effective seal for the hydrogel in the wound bed, fibrin glue's status as a biologic and inflammatory properties cannot be overlooked as obstacles in the development of a liquid corneal wound sealant.

Biology provides us with many examples of natural adhesives that can be employed in improving the LiQD Cornea formulation including catecholamines used by barnacles, activated esters, and

biotin and (strept)avidin systems. This adhesive could be developed as a separate glue to attach the hydrogel or incorporated into the primary formula to simplify application.

8.5.4. Anti-microbial Properties

CLKRS-NPs were successfully shown to adhere to collagen-based hydrogels in a single synthesis reaction. This method could be used to attach them to the surface of RHCI or CLP-PEG based solid corneal implants, to improve their immediate anti-microbial properties. Anti-microbial drugs or NPs can also be mixed into liquid corneal sealants, although it is currently unclear if they would provide a sufficient dose in the hydrogel material, or if they would require adjunctive topical application.

Chapter 9

References

1. Formisano, N. *et al.* Nanoscale Topographies for Corneal Endothelial Regeneration. *Applied Sciences 2021, Vol. 11, Page 827* **11,** 827 (2021).
2. Al-Aqaba, M. A., Fares, U., Suleman, H., Lowe, J. & Dua, H. S. Architecture and distribution of human corneal nerves. *British Journal of Ophthalmology* **94,** 784–789 (2010).
3. Müller, L. J., Marfurt, C. F., Kruse, F. & Tervo, T. M. Corneal nerves: Structure, contents and function. *Experimental Eye Research* **76,** 521–542 (2003).
4. Dua, H. S. & Said, D. G. Clinical evidence of the pre-Descemets layer (Dua's layer) in corneal pathology. *Eye* **30,** 1144–1145 (2016).
5. Amitai-Lange, A. *et al.* Lineage tracing of stem and progenitor cells of the murine corneal epithelium. *Stem Cells* **33,** 230–239 (2015).
6. Di Girolamo, N. *et al.* Tracing the fate of limbal epithelial progenitor cells in the murine cornea. *Stem Cells* **33,** 157–169 (2015).
7. Dorà, N. J., Hill, R. E., Collinson, J. M. & West, J. D. Lineage tracing in the adult mouse corneal epithelium supports the limbal epithelial stem cell hypothesis with intermittent periods of stem cell quiescence. *Stem Cell Research* **15,** 665–677 (2015).
8. Kasetti, R. B. *et al.* Study of corneal epithelial progenitor origin and the Yap1 requirement using keratin 12 lineage tracing transgenic mice. *Scientific Reports* **6** (2016).
9. Lobo, E. P. *et al.* Self-organized centripetal movement of corneal epithelium in the absence of external cues. *Nature Communications* **7** (2016).

10. Pflugfelder, S. C. & Stern, M. E. Biological functions of tear film. *Experimental Eye Research* **197,** 108115 (2020).
11. Wiesner, J. & Vilcinskas, A. Antimicrobial peptides: the ancient arm of the human immune system. *Virulence* **1,** 440–464 (2010).
12. Dartt, D. A. Tear Lipocalin: structure and Function. *The Ocular Surface* **9,** 126–138 (2011).
13. Fluckinger, M., Haas, H., Merschak, P., Glasgow, B. J. & Redl, B. Human tear lipocalin exhibits antimicrobial activity by scavenging microbial siderophores. *Antimicrobial Agents and Chemotherapy* **48,** 3367–3372 (2004).
14. Sack, R. A., Nunes, I., Beaton, A. & Morris, C. Host-defense mechanism of the ocular surfaces. *Bioscience Reports* **21,** 463–480 (2001).
15. Merindano, M. D., Costa, J., Canals, M., Potau J. M. & Ruano, D. A comparative study of Bowman's layer in some mammals: Relationships with other constituent corneal structures. *European Journal of Anatomy* **6,** 133–139 (2002).
16. Germundsson, J., Karanis, G., Fagerholm, P. & Lagali, N. Age-Related Thinning of Bowman's Layer in the Human Cornea In Vivo. *Investigative Ophthalmology & Visual Science* **54,** 6143–6149 (2013).
17. Gordon, M., Foley, J., Birk, D., Fitch, J. & Linsenmayer, T. Type V collagen and Bowman's membrane. Quantitation of mRNA in corneal epithelium and stroma. *Journal of Biological Chemistry* **269,** 24959–24966 (1994).
18. Nakayasu, K., Tanaka, M., Konomi, H. & Hayashi, T. Distribution of Types I, II, III, IV and V Collagen in Normal and Keratoconus Corneas. *Ophthalmic Research* **18,** 1–10 (1986).
19. Kayes, J. & Holmberg, Å. The Fine Structure of Bowman's Layer and the Basement Membrane of the Corneal Epithelium. *American Journal of Ophthalmology* **50,** 1013–1021 (1960).
20. Birk, D. E. & Trelstad, R. L. Extracellular compartments in matrix morphogenesis: Collagen fibril, bundle, and lamellar formation by corneal fibroblasts. *Journal of Cell Biology* **99,** 2024–2033 (1984).

21. Birk, D. E., Zycband, E. I., Winkelmann, D. A. & Trelstad, R. L. Collagen fibrillogenesis in situ: Fibril segments are intermediates in matrix assembly. *Proceedings of the National Academy of Sciences of the United States of America* **86,** 4549–4553 (1989).
22. Ploetz, C., Zycband, E. I. & Birk, D. E. Collagen fibril assembly and deposition in the developing dermis: Segmental deposition in extracellular compartments. *Journal of Structural Biology* **106,** 73–81 (1991).
23. Chen, S., Mienaltowski, M. J. & Birk, D. E. Regulation of corneal stroma extracellular matrix assembly. *Experimental Eye Research* **133,** 69–80 (2015).
24. Carlson, E. C. *et al.* Keratocan, a cornea-specific keratan sulfate proteoglycan, is regulated by lumican. *Journal of Biological Chemistry* **280,** 25541–25547 (2005).
25. Zhang, G. *et al.* Genetic evidence for the coordinated regulation of collagen fibrillogenesis in the cornea by decorin and biglycan. *Journal of Biological Chemistry* **284,** 8888–8897 (2009).
26. Gültekin, O. *Computational Inelasticity of Fibrous Biological Tissues with a Focus on Viscoelasticity, Damage and Rupture* PhD thesis (Graz University of Technology, Graz, 2018).
27. Wang, L. *et al.* Lateral growth limitation of corneal fibrils and their lamellar stacking depend on covalent collagen cross-linking by transglutaminase-2 and lysyl oxidases, respectively. *Journal of Biological Chemistry* **289,** 921–929 (2014).
28. De Jong, O. G., van Balkom, B. W., Gremmels, H. & Verhaar, M. C. Exosomes from hypoxic endothelial cells have increased collagen crosslinking activity through up-regulation of lysyl oxidase-like 2. *Journal of Cellular and Molecular Medicine* **20,** 342–350 (2016).
29. Dudakova, L. *et al.* Changes in lysyl oxidase (LOX) distribution and its decreased activity in keratoconus corneas. *Experimental Eye Research* **104,** 74–81 (2012).
30. Shetty, R. *et al.* Outcomes of Corneal Cross-Linking Correlate with Cone-Specific Lysyl Oxidase Expression in Patients with Keratoconus. *Cornea* **37,** 369–374 (2018).
31. Han, K. Y., Dugas-Ford, J., Seiki, M., Chang, J. H. & Azar, D. T. Evidence for the involvement of MMP14 in MMP2 processing and recruitment in exosomes of corneal fibroblasts. *Investigative Ophthalmology & Visual Science* **56,** 5323–5329 (2015).

32. Chang, J.-H. *et al.* Matrix metalloproteinase 14 modulates signal transduction and angiogenesis in the cornea. *Survey of Ophthalmology* **61,** 478–497 (2016).
33. Han, K. Y., Chang, J. H. & Azar, D. T. MMP14-containing exosomes cleave VEGFR1 and promote VEGFA-induced migration and proliferation of vascular endothelial cells. *Investigative Ophthalmology & Visual Science* **60,** 2321–2329 (2019).
34. Wolf, M. *et al.* Overexpression of mmps in corneas requiring penetrating and deep anterior lamellar keratoplasty. *Investigative Ophthalmology & Visual Science* **60,** 1734–1747 (2019).
35. Zhang, J., Wang, S., He, Y., Yao, B. & Zhang, Y. Regulation of matrix metalloproteinases 2 and 9 in corneal neovascularization. eng. *Chemical Biology and Drug Design* **1,** 1–8 (2020).
36. Johnson, D. H., Bourne, W. M. & Campbell, R. J. The Ultrastructure of Descemet's Membrane: I. Changes With Age in Normal Corneas. *Archives of Ophthalmology* **100,** 1942–1947 (1982).
37. Bourne, W. M., Johnson, D. H. & Campbell, R. J. The Ultrastructure of Descemet's Membrane: III. Fuchs' Dystrophy. *Archives of Ophthalmology* **100,** 1952–1955 (1982).
38. Srinivas, S. Dynamic regulation of barrier integrity of the corneal endothelium. *Optometry and Vision Science* **87,** E239–E254 (2010).
39. Kumagai, A., Glasgow, B. & Pardridge, W. GLUT1 glucose transporter expression in the diabetic and nondiabetic human eye. *Investigative Ophthalmology & Visual Science* **35,** 2887–2894 (1994).
40. Riley, M. Glucose and oxygen utilization by the rabbit cornea. *Experimental Eye Research* **8,** 193–200 (1969).
41. Williams, K. K. & Watsky, M. A. Gap junctional communication in the human corneal endothelium and epithelium. *Current Eye Research* **25,** 29–36 (2002).
42. Kwok, L. S. & Klyce, S. D. Theoretical basis for an anomalous temperature coefficient in swelling pressure of rabbit corneal stroma. *Biophysical Journal* **57,** 657–662 (1990).
43. Gain, P. *et al.* Global Survey of Corneal Transplantation and Eye Banking. eng. *JAMA Ophthalmology* **134,** 167 (2016).
44. World Health Organization. *Blindness and vision impairment* 2019.

45. Flaxman, S. R. *et al.* Global causes of blindness and distance vision impairment 1990–2020: a systematic review and meta-analysis. *The Lancet Global Health* **5,** e1221–e1234 (2017).
46. World Health Organization. *Priority eye diseases: Corneal opacities*
47. Asimellis, G. & Kaufman, E. J. Keratoconus. *StatPearls* (2021).
48. Moshirfar, M., Somani, A. N., Vaidyanathan, U. & Patel, B. C. Fuchs Endothelial Dystrophy. *Acta Ophthalmologica* **60,** 38–40 (2021).
49. Ting, D. S. J., Ho, C. S., Deshmukh, R., Said, D. G. & Dua, H. S. Infectious keratitis: an update on epidemiology, causative microorganisms, risk factors, and antimicrobial resistance. *Eye 2021 35:4* **35,** 1084–1101 (2021).
50. Joint United Kingdom (UK) Blood Transfusion and Tissue Transplantation Services Professional Advisory Committee. in *Guidelines for the Blood Transfusion Services* 8th ed. (TSO (The Stationery Office), Norwich, 2016).
51. Tan, D. T., Dart, J. K., Holland, E. J. & Kinoshita, S. Corneal transplantation. *Lancet* **379,** 1749–1761 (2012).
52. George, A. J. T. & Larkin, D. F. P. Corneal Transplantation: The Forgotten Graft. *American Journal of Transplantation* **4,** 678–685 (2004).
53. Dunker, S. L. *et al.* Practice patterns of corneal transplantation in Europe: first report by the European Cornea and Cell Transplantation Registry. *Journal of Cataract and Refractive Surgery* (2021).
54. Dunker, S. L. *et al.* Outcomes of corneal transplantation in Europe: report by the European Cornea and Cell Transplantation Registry. *Journal of Cataract and Refractive Surgery* **47,** 780–785 (2021).
55. Williams, K. A. *et al.* How effective is penetrating corneal transplantation? Factors influencing long-term outcome in multivariate analysis. *Transplantation.* **81,** 896–901 (2006).
56. Claesson, M., Armitage, W. J., Fagerholm, P. & Stenevi, U. Visual outcome in corneal grafts: A preliminary analysis of the Swedish Corneal Transplant Register. *British Journal of Ophthalmology* **86,** 174–180 (2002).
57. Borderie, V. M. *et al.* Predicted Long-term Outcome of Corneal Transplantation. *Ophthalmology* **116,** 2354–2360 (2009).

58. Joshi, S., Jagdale, S., More, P. & Deshpande, M. Outcome of optical penetrating keratoplasties at a tertiary care eye institute in Western India. *Indian Journal of Ophthalmology* **60,** 15–21 (2012).

59. Hu, V. H. *et al.* in *Organ Tissue Engineering* 557–587 (Springer, Cham, 2020).

60. Aboshiha, J., Jones, M. N. A., Hopkinson, C. L. & Larkin, D. F. P. Differential Survival of Penetrating and Lamellar Transplants in Management of Failed Corneal Grafts. *JAMA Ophthalmology* **136,** 859–865 (2018).

61. Yamagami, S. *et al.* Distinct populations of dendritic cells in the normal human donor corneal epithelium. *Investigative Ophthalmology & Visual Science* **46,** 4489–4494 (2005).

62. Chen, W. *et al.* Cauterization of Central Cornea Induces Recruitment of Major Histocompatibility Complex Class II+ Langerhans Cells From Limbal Basal Epithelium. *Cornea* **29,** 73–79 (2010).

63. Hamrah, P., Liu, Y., Zhang, Q. & Dana, M. R. Alterations in corneal stromal dendritic cell phenotype and distribution in inflammation. *Archives of Ophthalmology* **121,** 1132–1140 (2003).

64. Li, Z., Burns, A. R. & Smith, C. W. Two waves of neutrophil emigration in response to corneal epithelial abrasion: Distinct adhesion molecule requirements. *Investigative Ophthalmology & Visual Science* **47,** 1947–1955 (2006).

65. Marrazzo, G. *et al.* The role of neutrophils in corneal wound healing in HO-2 null mice. *PLoS ONE* **6,** 7–9 (2011).

66. Li, Z., Burns, A. R., Han, L., Rumbaut, R. E. & Smith, C. W. IL-17 and VEGF are necessary for efficient corneal nerve regeneration. *American Journal of Pathology* **178,** 1106–1116 (2011).

67. Pan, Z., Fukuoka, S., Karagianni, N., Guaiquil, V. H. & Rosenblatt, M. I. Vascular endothelial growth factor promotes anatomical and functional recovery of injured peripheral nerves in the avascular cornea. *FASEB Journal* **27,** 2756–2767 (2013).

68. O'Brien, T. P. *et al.* Inflammatory response in the early stages of wound healing after excimer laser keratectomy. *Archives of Ophthalmology* **116,** 1470–1474 (1998).

69. Li, S. *et al.* Macrophage Depletion Impairs Corneal Wound Healing after Autologous Transplantation in Mice. *PLoS ONE* **8,** 1–8 (2013).

70. Liu, Q., Smith, C. W., Zhang, W., Burns, A. R. & Li, Z. NK cells modulate the inflammatory response to corneal epithelial abrasion and thereby support wound healing. *American Journal of Pathology* **181,** 452–462 (2012).

71. Gao, Y. *et al.* NK cells are necessary for recovery of corneal CD11c + dendritic cells after epithelial abrasion injury. *Journal of Leukocyte Biology* **94,** 343–351 (2013).

72. Zieske, J. D. Extracellular matrix and wound healing. *Current Opinion in Ophthalmology* **12,** 237–41 (2001).

73. Kamiyama, K., Iguchi, I., Wang, X. & Imanishi, J. Effects of PDGF on the migration of rabbit corneal fibroblasts and epithelial cells. *Cornea* **17,** 315–25 (1998).

74. Fini, M. E. & Stramer, B. M. How the cornea heals: Cornea-specific repair mechanisms affecting surgical outcomes. *Cornea* **24,** 2–11 (2005).

75. Singh, V. *et al.* TGFβ and PDGF-B signaling blockade inhibits myofibroblast development from both bone marrow-derived and keratocyte-derived precursor cells invivo. *Experimental Eye Research* **121,** 35–40 (2014).

76. Marino Gustavo K. Santhiago, M. R., Santhanam, A., Torricelli, A. A. M. & Wilson, S. E. Regeneration of defective epithelial basement membrane and restoration of corneal transparency. *Journal of Refractive Surgery* **33,** 337–346 (2017).

77. Carlos De Oliveira, R., Wilson, S. E., de Oliveira, R. C. & Wilson, S. E. Fibrocytes, Wound Healing, and Corneal Fibrosis. *Investigative Ophthalmology & Visual Science* **61,** 28 (2020).

78. Ling, C., Yamashita, M., Zhang, J., Bless, D. M. & Welham, N. V. Reactive response of fibrocytes to vocal fold mucosal injury in rat. *Wound Repair and Regeneration* **18,** 514–523 (2010).

79. Garana, R. M. *et al.* Radial keratotomy. II. Role of the myofibroblast in corneal wound contraction. *Investigative Ophthalmology & Visual Science* **33,** 3271–82 (1992).

80. Jester, J. V., Petroll, W. M., Barry, P. A. & Cavanagh, H. D. Expression of alpha-smooth muscle (alpha-SM) actin during corneal stromal wound healing. *Investigative Ophthalmology & Visual Science* **36,** 809–819 (1995).

81. Tomasek, J. J., Gabbiani, G., Hinz, B., Chaponnier, C. & Brown, R. A. Myofibroblasts and mechano: Regulation of connective tissue remodelling. *Nature Reviews Molecular Cell Biology* **3,** 349–363 (2002).

82. Jester, J. V. *et al.* The cellular basis of corneal transparency: Evidence for 'corneal crystallins'. *Journal of Cell Science* **112,** 613–622 (1999).

83. Chaurasia, S. S., Kaur, H., de Medeiros, F. W., Smith, S. D. & Wilson, S. E. Dynamics of the expression of intermediate filaments vimentin and desmin during myofibroblast differentiation after corneal injury. *Experimental Eye Research* **89,** 133–139 (2009).

84. Cintron, C., Covington, H. I. & Kublin, C. L. Morphologic analyses of proteoglycans in rabbit corneal scars. *Investigative Ophthalmology & Visual Science* **31,** 1789–1798 (1990).

85. Hassell, J. R., Cintron, C. & Newsome, D. A. Proteoglycan changes during restoration of transparency in corneal scars. *Archives of Biochemistry and Biophysics* **222,** 362–369 (1983).

86. Wilson, S. E., Chaurasia, S. S. & Medeiros, F. W. Apoptosis in the initiation, modulation and termination of the corneal wound healing response. *Experimental Eye Research* **85,** 305–311 (2007).

87. Kaur, H., Chaurasia, S. S., Agrawal, V., Suto, C. & Wilson, S. E. Corneal myofibroblast viability: Opposing effects of IL-1 and TGF β1. *Experimental Eye Research* **89,** 152–158 (2009).

88. Wilson, S. E., Marino, G. K., Torricelli, A. A. & Medeiros, C. S. Injury and defective regeneration of the epithelial basement membrane in corneal fibrosis: A paradigm for fibrosis in other organs? *Matrix Biology* **64,** 17–26 (2017).

89. Garcia-Hirschfeld, J., Lopez-Briones, L. G. & Belmonte, C. Neurotrophic influences on corneal epithelial cells. *Experimental Eye Research* **59,** 597–605 (1994).

90. Reid, T. W., Murphy, C. J., Iwahashi, C. K., Foster, B. A. & Mannis, M. J. Stimulation of epithelial cell growth by the neuropeptide substance P. *Journal of Cellular Biochemistry* **52,** 476–485 (1993).

91. Nakamura, M., Chikama, T. I. & Nishida, T. Up-regulation of integrin α5 expression by combination of substance P and insulin-like growth factor-1 in rabbit corneal epithelial cells. *Biochemical and Biophysical Research Communications* **246,** 777–782 (1998).

92. Mikulec, A. A. & Tanelian, D. L. CGRP increases the rate of corneal re-epithelialization in an in vitro whole mount preparation. *Journal of Ocular Pharmacology and Therapeutics* **12,** 417–423 (1996).

93. Lambiase, A., Bonini, S., Aloe, L., Rama, P. & Bonini, S. Anti-inflammatory and healing properties of nerve growth factor in immune corneal ulcers with stromal melting. *Archives of Ophthalmology* **118,** 1446–1449 (2000).

94. Nicholas, M. P. & Mysore, N. Corneal neovascularization. *Experimental Eye Research* **202,** 108363 (2021).

95. Penn, J. S. *et al.* Vascular endothelial growth factor in eye disease. *Progress in Retinal and Eye Research* **27,** 331–371 (2008).

96. Cursiefen, C. *et al.* VEGF-A stimulates lymphangiogenesis and hemangiogenesis in inflammatory neovascularization via macrophage recruitment. *Journal of Clinical Investigation* **113,** 1040–1050 (2004).

97. Chung, E.-S. *et al.* Contribution of Macrophages to Angiogenesis Induced by Vascular Endothelial Growth Factor Receptor-3-Specific Ligands. *The American Journal of Pathology* **175,** 1984–1992 (2009).

98. Tammela, T. *et al.* Blocking VEGFR-3 suppresses angiogenic sprouting and vascular network formation. *Nature* **454,** 656–660 (2008).

99. Cui, N., Hu, M. & Khalil, R. A. Biochemical and Biological Attributes of Matrix Metalloproteinases. *Progress in Molecular Biology and Translational Science* **147,** 1–73 (2017).

100. Shi, W., Liu, J., Li, M., Gao, H. & Wang, T. Expression of MMP, HPSE, and FAP in Stroma Promoted Corneal Neovascularization Induced by Different Etiological Factors. *Current Eye Research* **35,** 967–977 (2010).

101. Kvanta, A., Sarman, S., Fagerholm, P., Seregard, S. & Steen, B. Expression of Matrix Metalloproteinase-2 (MMP-2) and Vascular Endothelial Growth Factor (VEGF) in Inflammation-associated Corneal Neovascularization. *Experimental Eye Research* **70,** 419–428 (2000).

102. Dean, R. A. *et al.* Identification of Candidate Angiogenic Inhibitors Processed by Matrix Metalloproteinase 2 (MMP-2) in Cell-Based Proteomic Screens: Disruption of Vascular Endothelial Growth Factor (VEGF)/Heparin Affin Regulatory Peptide (Pleiotrophin) and VEGF/Connective Tissue Growth Factor Angiogenic Inhibitory Complexes by MMP-2 Proteolysis. *Molecular and Cellular Biology* **27,** 8454–8465 (2007).

103. Ma, J. J. K., Graney, J. M. & Dohlman, C. H. Repeat Penetrating Keratoplasty versus the Boston Keratoprosthesis in Graft Failure. *International Ophthalmology Clinics* **45,** 49–59 (2005).

104. Akpek, E. K., Alkharashi, M., Hwang, F. S., Ng, S. M. & Lindsley, K. Artificial corneas versus donor corneas for repeat corneal transplants. *Cochrane Database of Systematic Reviews* (2014).

105. Avadhanam, V. S. & Liu, C. S. A brief review of Boston type-1 and osteo-odonto keratoprostheses. Eng. *British Journal of Ophthalmology* **99,** 878–887 (2015).

106. Salvador-Culla, B. & Kolovou, P. E. Keratoprosthesis: A Review of Recent Advances in the Field. eng. *Journal of Functional Biomaterials* **7,** 13 (2016).

107. European Medicines Agency. *Holoclar* 2021.

108. Walkden, A. Amniotic Membrane Transplantation in Ophthalmology: An Updated Perspective. *Clinical Ophthalmology (Auckland, N.Z.)* **14,** 2057 (2020).

109. Nakamura, T. *et al.* The successful culture and autologous transplantation of rabbit oral mucosal epithelial cells on amniotic membrane. *Investigative Ophthalmology & Visual Science* **44,** 106–116 (2003).

110. Nishida, T. & Tanaka, T. Extracellular matrix and growth factors in corneal wound healing. *Current Opinion in Ophthalmology* **7,** 2–11 (1996).

111. Nakamura, T. *et al.* Transplantation of cultivated autologous oral mucosal epithelial cells in patients with severe ocular surface disorders. *British Journal of Ophthalmology* **88,** 1280–1284 (2004).

112. Inatomi, T. *et al.* Ocular surface reconstruction with combination of cultivated autologous oral mucosal epithelial transplantation and penetrating keratoplasty. *American Journal of Ophthalmology* **142** (2006).

113. Nakamura, T., Takeda, K., Inatomi, T., Sotozono, C. & Kinoshita, S. Long-term results of autologous cultivated oral mucosal epithelial transplantation in the scar phase of severe ocular surface disorders. *British Journal of Ophthalmology* **95,** 942–946 (2011).

114. Sotozono, C. *et al.* Visual improvement after cultivated oral mucosal epithelial transplantation. *Ophthalmology* **120,** 193–200 (2013).

115. Sotozono, C. *et al.* Cultivated oral mucosal epithelial transplantation for persistent epithelial defect in severe ocular surface diseases with acute inflammatory activity. *Acta Ophthalmologica* **92,** 447–453 (2014).

116. Dobrowolski, D. *et al.* Cultivated Oral Mucosa Epithelium in Ocular Surface Reconstruction in Aniridia Patients. *BioMed Research International* **2015** (2015).

117. Sangwan, V., Basu, S., MacNeil, S. & Balasubramanian, D. Simple limbal epithelial transplantation (SLET): a novel surgical technique for the treatment of unilateral limbal stem cell deficiency. *British Journal of Ophthalmology* **96,** 931–934 (2012).

118. Basu, S. *et al.* Simple Limbal Epithelial Transplantation: Long-Term Clinical Outcomes in 125 Cases of Unilateral Chronic Ocular Surface Burns. *Ophthalmology* **123,** 1000–1010 (2016).

119. Thokala, P. *et al.* Economic, clinical and social impact of simple limbal epithelial transplantation for limbal stem cell deficiency. *British Journal of Ophthalmology* **0,** 1–6 (2021).

120. Rama, P. *et al.* Limbal Stem-Cell Therapy and Long-Term Corneal Regeneration. *http://dx.doi.org/10.1056/NEJMoa0905955* **363,** 147–155 (2010).

121. Basu, S. *et al.* Human limbal biopsy–derived stromal stem cells prevent corneal scarring. *Science Translational Medicine* **6,** 266ra172 (2014).

122. Okumura, N., Kinoshita, S. & Koizumi, N. Cell-based approach for treatment of corneal endothelial dysfunction. Eng. *Cornea* **33,** 37–41 (2014).

123. Okumura, N., Kinoshita, S. & Koizumi, N. The Role of Rho Kinase Inhibitors in Corneal Endothelial Dysfunction. *Current Pharmaceutical Design* **23,** 660–666 (2017).

124. Tan, T.-E. *et al.* A Cost-Minimization Analysis of Tissue-Engineered Constructs for Corneal Endothelial Transplantation. *PLoS ONE* **9,** e100563 (2014).

125. Sano, Y., Ksander, B. R. & Streilein, J. W. Minor H, rather than MHC, alloantigens offer the greater barrier to successful orthotopic corneal transplantation in mice. eng. *Transplant Immunology* **4,** 53–56 (1996).

126. Gilbert, T. W., Sellaro, T. L. & Badylak, S. F. Decellularization of tissues and organs. *Biomaterials* **27,** 3675–3683 (2006).

127. Marino, J., Paster, J. & Benichou, G. Allorecognition by T lymphocytes and allograft rejection. *Frontiers in Immunology* **7,** 1–9 (2016).

128. Wu, Z. *et al.* The use of phospholipase A2 to prepare acellular porcine corneal stroma as a tissue engineering scaffold. *Biomaterials* **30,** 3513–3522 (2009).

129. Lin, X. C. *et al.* Lamellar keratoplasty with a graft of lyophilized acellular porcine corneal stroma in the rabbit. *Veterinary Ophthalmology* **11,** 61–66 (2008).

130. Xiao, J. *et al.* Construction of the recellularized corneal stroma using porous acellular corneal scaffold. *Biomaterials* **32,** 6962–6971 (2011).

131. Zhang, M.-C. *et al.* Lamellar Keratoplasty Treatment of Fungal Corneal Ulcers With Acellular Porcine Corneal Stroma. *American Journal of Transplantation* **15,** 1068–1075 (2015).

132. Liu, X.-N. *et al.* Acellular ostrich corneal stroma used as scaffold for construction of tissue-engineered cornea. *International Journal of Ophthalmology* **9,** 325 (2016).

133. Xu, B., Song, Z. & Fan, T. Construction of Anterior Hemi-Corneal Equivalents Using Nontransfected Human Corneal Cells and Transplantation in Dog Models. *Artificial Organs* **41,** 1004–1016 (2017).

134. Zheng, J. *et al.* Short-term results of acellular porcine corneal stroma keratoplasty for herpes simplex keratitis. *Xenotransplantation* **26,** e12509 (2019).

135. Chen, L., Wei, L., Shao, A. & Xu, L. Immune risk assessment of residual αGal in xenogeneic decellularized cornea using GTKO mice. *Regenerative Biomaterials* **7,** 427–434 (2020).

136. CorneaGen. *VisionGraft ® THE CLEAR CHOICE ®*

137. Daoud, Y. J. *et al.* The intraoperative impression and postoperative outcomes of gamma-irradiated corneas in corneal and glaucoma patch surgery. *Cornea* **30,** 1387–1391 (2011).

138. Chae, J., Choi, J., Stark, W. & Elisseeff, J. Extracellular matrix characterization of the acellular gamma-irradiated cornea. Poster Presented at the Association for Research in Vision and Ophthalmology Annual Meeting May 5-9, Seattle Washington. *Investigative Ophthalmology & Visual Science* **54,** 5257 (2013).

139. Dearth, C. L. *et al.* The effect of terminal sterilization on the material properties and in vivo remodeling of a porcine dermal biologic scaffold. *Acta Biomaterialia* **33,** 78–87 (2016).

140. Herbert, A., Edwards, J. H., Jones, G. L., Ingham, E. & Fisher, J. The effects of irradiation dose and storage time following treatment on the viscoelastic properties of decellularised porcine super flexor tendon. *Journal of Biomechanics* **57,** 157–160 (2017).

141. Monaco, G., Cholas, R., Salvatore, L., Madaghiele, M. & Sannino, A. Sterilization of collagen scaffolds designed for peripheral nerve regeneration: Effect on microstructure, degradation and cellular colonization. *Materials Science and Engineering: C* **71,** 335–344 (2017).

142. Cao, X. Self-regulation and cross-regulation of pattern-recognition receptor signalling in health and disease. *Nature Reviews Immunology 2015 16:1* **16,** 35–50 (2015).

143. Chen, G. Y. & Nuñez, G. Sterile inflammation: sensing and reacting to damage. *Nature Reviews Immunology 2010 10:12* **10,** 826–837 (2010).

144. Genicio, N., Paramo, J. G. & Shortt, A. J. Quantum Dot Labeling and Tracking of Cultured Limbal Epithelial Cell Transplants In Vitro. *Investigative Ophthalmology & Visual Science* **56,** 3051–3059 (2015).

145. Hashimoto, Y. *et al.* Corneal regeneration by deep anterior lamellar keratoplasty (DALK) using decellularized corneal matrix. *PLoS ONE* **10,** 1–10 (2015).

146. Zhang, Z. *et al.* Bioengineered multilayered human corneas from discarded human corneal tissue. *Biomedical Materials* **10,** 035012 (2015).

147. Lin, H. J. *et al.* Development of Decellularized Cornea by Organic Acid Treatment for Corneal Regeneration. *Tissue Engineering - Part A* **25,** 652–662 (2019).

148. Da Mata Martins, T. M. *et al.* Epithelial basement membrane of human decellularized cornea as a suitable substrate for differentiation of embryonic stem cells into corneal epithelial-like cells. *Materials Science and Engineering: C* **116,** 111215 (2020).

149. Wang, Y. *et al.* Development of Transparent Acellular Dermal Matrix as Tissue-Engineered Stroma Substitute for Central Lamellar Keratoplasty. *Investigative Ophthalmology & Visual Science* **61,** 5–5 (2020).

150. Proulx, S. S. *et al.* Transplantation of a tissue-engineered corneal endothelium reconstructed on a devitalized carrier in the feline model. *Investigative Ophthalmology & Visual Science* **50,** 2686–2694 (2009).

151. Choi, J. S. *et al.* Bioengineering endothelialized neo-corneas using donor-derived corneal endothelial cells and decellularized corneal stroma. *Biomaterials* **31,** 6738–6745 (2010).

152. Du, L. & Wu, X. Development and Characterization of a Full-Thickness Acellular Porcine Cornea Matrix for Tissue Engineering. *Artificial Organs* **35,** 691–705 (2011).

153. Huang, M. *et al.* Using acellular porcine limbal stroma for rabbit limbal stem cell microenvironment reconstruction. *Biomaterials* **32,** 7812–7821 (2011).

154. Shafiq, M. A., Milani, B. Y. & Djalilian, A. R. In Vivo Evaluation of a Decellularized Limbal Graft for Limbal Reconstruction. *International Journal of Tissue Engineering* **2014,** 1–6 (2014).

155. Alio del Barrio, J. L. *et al.* Acellular human corneal matrix sheets seeded with human adipose-derived mesenchymal stem cells integrate functionally in an experimental animal model. *Experimental Eye Research* **132,** 91–100 (2015).

156. Wilson, S. L., Sidney, L. E., Dunphy, S. E., Dua, H. S. & Hopkinson, A. Corneal Decellularization: A Method of Recycling Unsuitable Donor Tissue for Clinical Translation? *Current Eye Research* **41,** 769–782 (2016).

157. He, M. *et al.* Artificial Polymeric Scaffolds as Extracellular Matrix Substitutes for Autologous Conjunctival Goblet Cell Expansion. Eng. *Investigative Ophthalmology & Visual Science* **57,** 6134–6146 (2016).

158. Yam, G. H. F. *et al.* Decellularization of human stromal refractive lenticules for corneal tissue engineering. *Scientific Reports* **6** (2016).

159. Yin, H. *et al.* Construction of a Corneal Stromal Equivalent with SMILE-Derived Lenticules and Fibrin Glue. *Scientific Reports 2016 6:1* **6,** 1–10 (2016).

160. Guler, S., Aslan, B., Hosseinian, P. & Aydin, H. M. Supercritical Carbon Dioxide-Assisted Decellularization of Aorta and Cornea. *Tissue Engineering - Part C: Methods* **23,** 540–547 (2017).

161. Alió del Barrio, J. L. *et al.* Corneal Stroma Enhancement With Decellularized Stromal Laminas With or Without Stem Cell Recellularization for Advanced Keratoconus. *American Journal of Ophthalmology* **186,** 47–58 (2018).

162. Huh, M. I. *et al.* Generation of femtosecond laser-cut decellularized corneal lenticule using hypotonic trypsin-EDTA solution for corneal tissue engineering. *Journal of Ophthalmology* **2018** (2018).

163. Shi, C., Ulke-Lemée, A., Deng, J., Batulan, Z. & O'Brien, E. R. Characterization of heat shock protein 27 in extracellular vesicles: A potential anti-inflammatory therapy. *FASEB Journal* **33,** 1617–1630 (2019).

164. Ahearne, M. Corneal extracellular matrix decellularization. *Methods in Cell Biology* **157,** 81–95 (2020).

165. Uyanıklar, M., Günal, G., Tevlek, A., Hosseinian, P. & Aydin, H. M. Hybrid Cornea: Cell Laden Hydrogel Incorporated Decellularized Matrix. *ACS Biomaterials Science & Engineering* **6,** 122–133 (2019).

166. Amano, S., Shimomura, N., Yokoo, S., Araki-Sasaki, K. & Yamagami, S. Decellularizing corneal stroma using N2 gas. *Molecular Vision* **14,** 878 (2008).

167. Lee, S. E. *et al.* Characterization of Porcine Corneal Endothelium for Xenotransplantation. *http://dx.doi.org/10.3109/08820538.2013.787104* **29,** 127–135 (2014).

168. Bhogal, M., Lwin, C. N., Seah, X.-Y., Peh, G. & Mehta, J. S. Allogeneic Descemet's Membrane Transplantation Enhances Corneal Endothelial Monolayer Formation and Restores Functional Integrity Following Descemet's Stripping. *Investigative Ophthalmology & Visual Science* **58,** 4249–4260 (2017).

169. Aslan, B., Guler, S., Tevlek, A. & Aydin, H. M. Evaluation of collagen foam, poly(l-lactic acid) nanofiber mesh, and decellularized matrices for corneal regeneration. *Journal of Biomedical Materials Research - Part B Applied Biomaterials* **106,** 2157–2168 (2018).

170. Liu, Y. C. *et al.* Biological corneal inlay for presbyopia derived from small incision lenticule extraction (SMILE). *Scientific Reports* **8** (2018).

171. An, J. H. *et al.* Tissue engineered ultra-thin descemet stripping corneal endothelial layers using porcine cornea and stem cells. *Experimental Eye Research* **199,** 108192 (2020).

172. Yin, H. *et al.* Tissue-Derived Biological Particles Restore Cornea Properties in an Enzyme-Mediated Corneal Ectatic Model. *Bioengineering* **6,** 90 (2019).

173. Yin, H. *et al.* Tissue-derived microparticles reduce inflammation and fibrosis in cornea wounds. *Acta Biomaterialia* **85,** 192–202 (2019).

174. Chandru, A. *et al.* Human Cadaveric Donor Cornea Derived Extra Cellular Matrix Microparticles for Minimally Invasive Healing/Regeneration of Corneal Wounds. *Biomolecules* **11,** 532 (2021).

175. Wang, F. *et al.* Decellularized porcine cornea-derived hydrogels for the regeneration of epithelium and stroma in focal corneal defects. *The Ocular Surface* **18,** 748–760 (2020).

176. Ahearne, M. & Lynch, A. P. Early Observation of Extracellular Matrix-Derived Hydrogels for Corneal Stroma Regeneration. *Tissue Engineering - Part C: Methods* **21,** 1059–1069 (2015).

177. Hong, H. *et al.* Decellularized corneal lenticule embedded compressed collagen: Toward a suturable collagenous construct for limbal reconstruction. *Biofabrication* **10** (2018).

178. Kim, H. *et al.* Characterization of cornea-specific bioink: high transparency, improved in vivo safety. *Journal of Tissue Engineering* **10** (2019).

179. Ahearne, M. & Fernández-Pérez, J. Fabrication of Corneal Extracellular Matrix-Derived Hydrogels. *Methods in Molecular Biology* **2145,** 159–168 (2020).

180. Zhou, Q. *et al.* Hydrogels derived from acellular porcine corneal stroma enhance corneal wound healing. *Acta Biomaterialia* (2021).

181. Priyadarsini, S., Sarker-Nag, A., Rowsey, T. G., Ma, J.-X. & Karamichos, D. Establishment of a 3D In Vitro Model to Accelerate the Development of Human Therapies against Corneal Diabetes. *PLoS ONE* **11,** e0168845 (2016).

182. Karamichos, D. *et al.* Novel in Vitro Model for Keratoconus Disease. *Journal of Functional Biomaterials* **3,** 760–775 (2012).

183. Thériault, M., Gendron, S. P., Brunette, I., Rochette, P. J. & Proulx, S. Function-Related Protein Expression in Fuchs Endothelial Corneal Dystrophy Cells and Tissue Models. *American Journal of Pathology* **188,** 1703–1712 (2018).

184. Zhang, C. *et al.* Construction of tissue-engineered full-thickness cornea substitute using limbal epithelial cell-like and corneal endothelial cell-like cells derived from human embryonic stem cells. *Biomaterials* **124,** 180–194 (2017).

185. Syed-Picard, F. N. *et al.* Scaffold-free tissue engineering of functional corneal stromal tissue. *Journal of Tissue Engineering and Regenerative Medicine* **12,** 59–69 (2018).

186. Peh, G. *et al.* Functional Evaluation of Two Corneal Endothelial Cell-Based Therapies: Tissue-Engineered Construct and Cell Injection. *Scientific Reports* **9** (2019).

187. Rico-Sánchez, L. *et al.* Successful development and clinical translation of a novel anterior lamellar artificial cornea. *Journal of Tissue Engineering and Regenerative Medicine* **13,** 2142–2154 (2019).

188. Le-Bel, G. *et al.* Grafting of an autologous tissue-engineered human corneal epithelium to a patient with limbal stem cell deficiency (LSCD). *American Journal of Ophthalmology Case Reports* **15,** 100532 (2019).

189. Zhang, J., Huang, C., Feng, Y., Li, Y. & Wang, W. Comparison of beneficial factors for corneal wound-healing of rat mesenchymal stem cells and corneal limbal stem cells on the xenogeneic acellular corneal matrix in vitro. *Molecular Vision* **18,** 161–173 (2012).

190. Luo, H. *et al.* Construction of tissue-engineered cornea composed of amniotic epithelial cells and acellular porcine cornea for treating corneal alkali burn. *Biomaterials* **34,** 6748–6759 (2013).

191. Zhao, H., Qu, M., Wang, Y., Wang, Z. & Shi, W. Xenogeneic Acellular Conjunctiva Matrix as a Scaffold of Tissue-Engineered Corneal Epithelium. *PLoS ONE* **9,** e111846 (2014).

192. Wu, Z. *et al.* Reconstruction of Auto-Tissue-Engineered Lamellar Cornea by Dynamic Culture for Transplantation: A Rabbit Model. *PLoS ONE* **9,** e93012 (2014).

193. Proulx, S. *et al.* Tissue engineering of feline corneal endothelium using a devitalized human cornea as carrier. *Tissue Engineering - Part A* **15,** 1709–1718 (2009).

194. Yoeruek, E. *et al.* Decellularization of porcine corneas and repopulation with human corneal cells for tissue-engineered xenografts. *Acta Ophthalmologica* **90,** e125–e131 (2012).

195. Zieske, J. D. *et al.* Basement Membrane Assembly and Differentiation of Cultured Corneal Cells: Importance of Culture Environment and Endothelial Cell Interaction. *Experimental Cell Research* **214,** 621–633 (1994).

196. Guo, X. *et al.* Morphologic Characterization of Organized Extracellular Matrix Deposition by Ascorbic Acid–Stimulated Human Corneal Fibroblasts. *Investigative Ophthalmology & Visual Science* **48,** 4050–4060 (2007).

197. Carrier, P. *et al.* Characterization of wound reepithelialization using a new human tissue-engineered corneal wound healing model. *Investigative Ophthalmology & Visual Science* **49,** 1376–1385 (2008).

198. Ren, R. *et al.* Human primary corneal fibroblasts synthesize and deposit proteoglycans in long-term 3-D cultures. *Developmental Dynamics* **237,** 2705–2715 (2008).

199. González-Andrades, M. *et al.* Sequential development of intercellular junctions in bioengineered human corneas. *Journal of Tissue Engineering and Regenerative Medicine* **3,** 442–449 (2009).

200. Carrier, P. *et al.* Impact of Cell Source on Human Cornea Reconstructed by Tissue Engineering. *Investigative Ophthalmology & Visual Science* **50,** 2645–2652 (2009).

201. Guillemette, M. D. *et al.* Surface topography induces 3D self-orientation of cells and extracellular matrix resulting in improved tissue function. *Integrative Biology* **1,** 196–204 (2009).

202. Proulx, S. *et al.* Reconstruction of a human cornea by the self-assembly approach of tissue engineering using the three native cell types. *Molecular Vision* **16,** 2192–2201 (2010).

203. Karamichos, D., Guo, X. Q., Hutcheon, A. E. K. & Zieske, J. D. Human Corneal Fibrosis: An In Vitro Model. *Investigative Ophthalmology & Visual Science* **51,** 1382–1388 (2010).

204. Karamichos, D., Hutcheon, A. E. K. & Zieske, J. D. Transforming growth factor-β3 regulates assembly of a non-fibrotic matrix in a 3D corneal model. *Journal of Tissue Engineering and Regenerative Medicine* **5,** e228–e238 (2011).

205. Wu, J., Du, Y., Watkins, S. C., Funderburgh, J. L. & Wagner, W. R. The engineering of organized human corneal tissue through the spatial guidance of corneal stromal stem cells. *Biomaterials* **33,** 1343–1352 (2012).

206. Lake, J. *et al.* Expression of the α5 integrin gene in corneal epithelial cells cultured on tissue-engineered human extracellular matrices. *Biomaterials* **34,** 6367–6376 (2013).

207. Zaniolo, K., Carrier, P., Guérin, S. L., Auger, F. A. & Germain, L. A Tissue-Engineered Corneal Wound Healing Model for the Characterization of Reepithelialization. *Methods in Molecular Biology* **1037,** 59–78 (2013).

208. Karamichos, D. *et al.* TGF-β3 Stimulates Stromal Matrix Assembly by Human Corneal Keratocyte-Like Cells. *Investigative Ophthalmology & Visual Science* **54,** 6612–6619 (2013).

209. Karamichos, D. *et al.* A Role for Topographic Cues in the Organization of Collagenous Matrix by Corneal Fibroblasts and Stem Cells. *PLoS ONE* **9,** e86260 (2014).

210. Wu, J. *et al.* Corneal stromal bioequivalents secreted on patterned silk substrates. *Biomaterials* **35,** 3744–3755 (2014).

211. Abidin, F. Z., Gouveia, R. M. & Connon, C. J. Application of retinoic acid improves form and function of tissue engineered corneal construct. *Organogenesis* **11,** 122–136 (2015).

212. Bourget, J. M. & Proulx, S. Characterization of a corneal endothelium engineered on a self-assembled stromal substitute. *Experimental Eye Research* **145,** 125–129 (2016).

213. Couture, C. *et al.* The tissue-engineered human cornea as a model to study expression of matrix metalloproteinases during corneal wound healing. *Biomaterials* **78,** 86–101 (2016).

214. Ghezzi, C. E. C., Marelli, B., Omenetto, F. G. F., Funderburgh, J. J. L. & Kaplan, D. D. L. 3D functional corneal stromal tissue equivalent based on corneal stromal stem cells and multi-layered silk film architecture. *PLoS ONE* **12,** 1–18 (2017).

215. Deardorff, P. M. *et al.* Modeling Diabetic Corneal Neuropathy in a 3D In Vitro Cornea System. *Scientific Reports 2018 8:1* **8,** 1–12 (2018).

216. McKay, T. B., Karamichos, D., Hutcheon, A. E. K., Guo, X. & Zieske, J. D. Corneal Epithelial–Stromal Fibroblast Constructs to Study Cell–Cell Communication in Vitro. *Bioengineering* **6,** 110 (2019).

217. Doane, M., Dohlman, C. & Bearse, G. Fabrication of a keratoprosthesis. *Cornea* **15,** 179–184 (1996).

218. Patel, S., Thakar, R. G., Wong, J., McLeod, S. D. & Li, S. Control of cell adhesion on poly(methyl methacrylate). *Biomaterials* **27,** 2890–2897 (2006).

219. Wang, L. *et al.* Hydroxyapatite for Keratoprosthesis Biointegration. *Investigative Ophthalmology & Visual Science* **52,** 7392–7399 (2011).

220. Riau, A. K. *et al.* Surface Modification of PMMA to Improve Adhesion to Corneal Substitutes in a Synthetic Core–Skirt Keratoprosthesis. *ACS Applied Materials & Interfaces* **7,** 21690–21702 (2015).

221. Riau, A. K. *et al.* Functionalization of the Polymeric Surface with Bioceramic Nanoparticles via a Novel, Nonthermal Dip Coating Method. *ACS Applied Materials & Interfaces* **8,** 35565–35577 (2016).

222. Baino, F. *et al.* Novel antibacterial ocular prostheses: Proof of concept and physicochemical characterization. *Materials Science and Engineering: C* **60,** 467–474 (2016).

223. Behlau, I. *et al.* Biocompatibility and biofilm inhibition of N,N-hexyl,methyl-polyethylenimine bonded to Boston Keratoprosthesis materials. *Biomaterials* **32,** 8783–8796 (2011).

224. Musiime, M. *et al.* Collagen Assembly at the Cell Surface: Dogmas Revisited. *Cells* **10** (2021).

225. Yamauchi, M., London, R., Guenat, C., Hashimoto, F. & Mechanic, G. Structure and formation of a stable histidine-based trifunctional cross-link in skin collagen. *Journal of Biological Chemistry* **262,** 11428–11434 (1987).

226. Shoulders, M. D. & Raines, R. T. Collagen Structure and Stability. *http://dx.doi.org/10.1146/annurev.biochem.77.032207.120833* **78,** 929–958 (2009).

227. Hayashi, T. & Nagai, Y. Effect of pH on the Stability of Collagen Molecule in Solution. *J. Biochem* **73,** 999–1006 (1973).

228. Miyata, T. & Taira, T. *Aqueous atelocollagen solution and method of preparing same* 1984.

229. Djagny, K. B., Wang, Z. & Xu, S. Gelatin: A valuable protein for food and pharmaceutical industries: Review. *Critical Reviews in Food Science and Nutrition* **41,** 481–492 (2001).

230. Vuorela, A., Myllyharju, J., Nissi, R., Pihlajaniemi, T. & Kivirikko, K. I. Assembly of human prolyl 4-hydroxylase and type III collagen in the yeast Pichia pastoris: formation of a stable enzyme tetramer requires coexpression with collagen and assembly of

a stable collagen requires coexpression with prolyl 4-hydroxylase. *The EMBO Journal* **16,** 6702–12 (1997).

231. Stein, H. *et al.* Production of Bioactive, Post-Translationally Modified, Heterotrimeric, Human Recombinant Type-I Collagen in Transgenic Tobacco†. *Biomacromolecules* **10,** 2640–2645 (2009).

232. Orwin, E. J. & Hubel, A. In vitro culture characteristics of corneal epithelial, endothelial, and keratocyte cells in a native collagen matrix. *Tissue Engineering* **6,** 307–319 (2000).

233. Orwin, E. J., Borene, M. L. & Hubel, A. Biomechanical and optical characteristics of a corneal stromal equivalent. *Journal of Biomechanical Engineering* **125,** 439–444 (2003).

234. Mimura, T. *et al.* Cultured human corneal endothelial cell transplantation with a collagen sheet in a rabbit model. *Investigative Ophthalmology & Visual Science* **45,** 2992–2997 (2004).

235. Borene, M. L., Barocas, V. H. & Hubel, A. Mechanical and cellular changes during compaction of a collagen-sponge- based corneal stromal equivalent. *Annals of Biomedical Engineering* **32,** 274–283 (2004).

236. Crabb, R. A., Chau, E. P., Evans, M. C., Barocas, V. H. & Hubel, A. Biomechanical and Microstructural Characteristics of a Collagen Film-Based Corneal Stroma Equivalent. *Tissue Engineering* **12,** 1565–1575 (2006).

237. Duan, X. & Sheardown, H. Dendrimer crosslinked collagen as a corneal tissue engineering scaffold: Mechanical properties and corneal epithelial cell interactions. *Biomaterials* **27,** 4608–4617 (2006).

238. Duan, X., McLaughlin, C., Griffith, M. & Sheardown, H. Biofunctionalization of collagen for improved biological response: Scaffolds for corneal tissue engineering. *Biomaterials* **28,** 78–88 (2007).

239. Vrana, N. E. *et al.* Development of a reconstructed cornea from collagen-chondroitin sulfate foams and human cell cultures. *Investigative Ophthalmology & Visual Science* **49,** 5325–5331 (2008).

240. Mi, S., Chen, B., Wright, B. & Connon, C. J. Plastic compression of a collagen gel forms a much improved scaffold for ocular surface tissue engineering over conventional collagen gels. *Journal of Biomedical Materials Research - Part A* **95 A,** 447–453 (2010).

241. Builles, N. *et al.* Use of magnetically oriented orthogonal collagen scaffolds for hemicorneal reconstruction and regeneration. *Biomaterials* **31,** 8313–8322 (2010).

242. Ahearne, M. *et al.* Online monitoring of the mechanical behavior of collagen hydrogels: Influence of corneal fibroblasts on elastic modulus. *Tissue Engineering - Part C: Methods* **16,** 319–327 (2010).

243. Ahearne, M. *et al.* Influence of cell and collagen concentration on the cell-matrix mechanical relationship in a corneal stroma wound healing model. *Experimental Eye Research* **91,** 584–591 (2010).

244. Ke, Q. *et al.* Carrier-free epithelial cell sheets prepared by enzymatic degradation of collagen gel. *Journal of Tissue Engineering and Regenerative Medicine* **5,** 138–145 (2011).

245. Kilic, C., Girotti, A., Rodriguez-Cabello, J. C. & Hasirci, V. A collagen-based corneal stroma substitute with micro-designed architecture. *Biomaterials Science* **2,** 318–329 (2014).

246. Xiao, X. *et al.* In vivo study of the biocompatibility of a novel compressed collagen hydrogel scaffold for artificial corneas. *Journal of Biomedical Materials Research - Part A* **102,** 1782–1787 (2014).

247. Chae, J. J. *et al.* Regeneration of corneal epithelium utilizing a collagen vitrigel membrane in rabbit models for corneal stromal wound and limbal stem cell deficiency. *Acta Ophthalmologica* **93,** e57–e66 (2015).

248. Koulikovska, M. *et al.* Enhanced regeneration of corneal tissue via a bioengineered collagen construct implanted by a nondisruptive surgical technique. *Tissue Engineering - Part A* **21,** 1116–1130 (2015).

249. Kureshi, A. K., Dziasko, M., Funderburgh, J. L. & Daniels, J. T. Human corneal stromal stem cells support limbal epithelial cells cultured on RAFT tissue equivalents. *Scientific Reports* **5,** 1–9 (2015).

250. Palchesko, R. N., Funderburgh, J. L. & Feinberg, A. W. Engineered Basement Membranes for Regenerating the Corneal Endothelium. *Advanced Healthcare Materials* **5,** 2942–2950 (2016).

251. Rafat, M. *et al.* Composite core-and-skirt collagen hydrogels with differential degradation for corneal therapeutic applications. *Biomaterials* **83,** 142–155 (2016).

252. Vázquez, N. *et al.* Human bone derived collagen for the development of an artificial corneal endothelial graft. in Vivo results in a rabbit model. *PLoS ONE* **11,** 1–18 (2016).

253. Kishore, V., Iyer, R., Frandsen, A. & Nguyen, T. U. In vitro characterization of electrochemically compacted collagen matrices for corneal applications. *Biomedical Materials (Bristol)* **11,** 55008 (2016).

254. Kong, B. *et al.* Tissue-engineered cornea constructed with compressed collagen and laser-perforated electrospun mat. *Scientific Reports* **7** (2017).

255. Isaacson, A., Swioklo, S. & Connon, C. J. 3D bioprinting of a corneal stroma equivalent. *Experimental Eye Research* **173,** 188–193 (2018).

256. Cen, Y. J. & Feng, Y. Constructing a novel three-dimensional biomimetic corneal endothelium graft by culturing corneal endothelium cells on compressed collagen gels. *Chinese Medical Journal* **131,** 1710–1714 (2018).

257. Shojaati, G. *et al.* Compressed Collagen Enhances Stem Cell Therapy for Corneal Scarring. *Stem Cells Translational Medicine* **7,** 487–494 (2018).

258. Mukhey, D., Phillips, J. B., Daniels, J. T. & Kureshi, A. K. Controlling human corneal stromal stem cell contraction to mediate rapid cell and matrix organization of real architecture for 3-dimensional tissue equivalents. *Acta Biomaterialia* **67,** 229–237 (2018).

259. Miotto, M. *et al.* 4D Corneal Tissue Engineering: Achieving Time-Dependent Tissue Self-Curvature through Localized Control of Cell Actuators. *Advanced Functional Materials* **29** (2019).

260. Gouveia, R. M. *et al.* Assessment of corneal substrate biomechanics and its effect on epithelial stem cell maintenance and differentiation. *Nature Communications 2019 10:1* **10,** 1–17 (2019).

261. Liu, Y. *et al.* A collagen film with micro-rough surface can promote the corneal epithelization process for corneal repair. *International Journal of Biological Macromolecules* **121,** 233–238 (2019).

262. Arabpour, Z. *et al.* Design and characterization of biodegradable multi layered electrospun nanofibers for corneal tissue engineering applications. *Journal of Biomedical Materials Research Part A* **107,** 2340–2349 (2019).

263. Xeroudaki, M. *et al.* A porous collagen-based hydrogel and implantation method for corneal stromal regeneration and sustained local drug delivery. *Scientific Reports* **10,** 1–18 (2020).

264. Chen, F., Le, P., Fernandes-Cunha, G. M., Heilshorn, S. C. & Myung, D. Bio-orthogonally crosslinked hyaluronate-collagen hydrogel for suture-free corneal defect repair. *Biomaterials* **255,** 120176 (2020).

265. Fernandes-Cunha, G. M. *et al.* In situ-forming collagen hydrogel crosslinked via multi-functional PEG as a matrix therapy for corneal defects. *Scientific Reports 2020 10:1* **10,** 1–13 (2020).

266. Wang, X. *et al.* Multifunctional synthetic Bowman's membrane-stromal biomimetic for corneal reconstruction. *Biomaterials* **241,** 119880 (2020).

267. Islam, M. M. *et al.* Optimization of Collagen Chemical Crosslinking to Restore Biocompatibility of Tissue-Engineered Scaffolds. *Pharmaceutics* **13,** 832 (2021).

268. Na, K.-S. *et al.* Effect of mesenchymal stromal cells encapsulated within polyethylene glycol-collagen hydrogels formed in situ on alkali-burned corneas in an ex vivo organ culture model. *Cytotherapy* **23,** 500–509 (2021).

269. Merrett, K. *et al.* Tissue-engineered recombinant human collagen-based corneal substitutes for implantation: Performance of type I versus type III collagen. *Investigative Ophthalmology & Visual Science* **49,** 3887–3894 (2008).

270. Fagerholm, P. *et al.* A Biosynthetic Alternative to Human Donor Tissue for Inducing Corneal Regeneration: 24-Month Follow-Up of a Phase 1 Clinical Study. *Science Translational Medicine* **2,** 46ra61 (2010).

271. Fagerholm, P. *et al.* Stable corneal regeneration four years after implantation of a cell-free recombinant human collagen scaffold. *Biomaterials* **35,** 2420–2427 (2014).

272. Liu, W. *et al.* Collagen-phosphorylcholine interpenetrating network hydrogels as corneal substitutes. **30,** 1551–1559 (2009).

273. Hackett, J. M. *et al.* Biosynthetic Corneal Implants for Replacement of Pathologic Corneal Tissue: Performance in a Controlled Rabbit Alkali Burn Model. eng. *Investigative Ophthalmology & Visual Science* **52,** 651–657 (2011).

274. Islam, M. M. *et al.* Biomaterials-enabled cornea regeneration in patients at high risk for rejection of donor tissue transplantation. eng. *NJP Regenerative Medicine* **3,** 2 (2018).

275. Engel, J., Chen, H.-T., Prockop, D. J. & Klump, H. The triple helix coil conversion of collagen-like polytripeptides in aqueous and nonaqueous solvents. Comparison of the thermodynamic parameters and the binding of water to (L-Pro-L-Pro-Gly)n and (L-Pro-L-Hyp-Gly)n. *Biopolymers* **16,** 601–622 (1977).

276. O'Leary, L. E., Fallas, J. A., Bakota, E. L., Kang, M. K. & Hartgerink, J. D. Multi-hierarchical self-assembly of a collagen mimetic peptide from triple helix to nanofibre and hydrogel. eng. *Nature Chemistry* **3,** 821–828 (2011).

277. Jangamreddy, J. R. *et al.* Short peptide analogs as alternatives to collagen in pro-regenerative corneal implants. eng. *Acta Biomaterialia* **69,** 120–130 (2018).

278. Islam, M. M. *et al.* Self-assembled collagen-like-peptide implants as alternatives to human donor corneal transplantation. *RSC Advances* **6,** 55745–55749 (2016).

279. Jones, R. R., Castelletto, V., Connon, C. J. & Hamley, I. W. Collagen Stimulating Effect of Peptide Amphiphile C16–KTTKS on Human Fibroblasts. *Molecular Pharmaceutics* **10,** 1063–1069 (2013).

280. Castelletto, V. *et al.* Alanine-rich amphiphilic peptide containing the RGD cell adhesion motif: a coating material for human fibroblast attachment and culture. *Biomaterials Science* **2,** 362–369 (2014).

281. Gouveia, R. M., Castelletto, V., Alcock, S. G., Hamley, I. W. & Connon, C. J. Bioactive films produced from self-assembling peptide amphiphiles as versatile substrates for tuning cell adhesion and tissue architecture in serum-free conditions. *Journal of Materials Chemistry B* **1,** 6157–6169 (2013).

282. Walter, M. N., Dehsorkhi, A., Hamley, I. W. & Connon, C. J. Supra-molecular assembly of a lumican-derived peptide amphiphile enhances its collagen-stimulating activity. *Biomaterials Science* **4,** 346–354 (2016).

283. Dehsorkhi, A. *et al.* Self-assembly of a dual functional bioactive peptide amphiphile incorporating both matrix metalloprotease substrate and cell adhesion motifs. *Soft Matter* **11,** 3115–3124 (2015).

284. Gouveia, R. M., Hamley, I. W. & Connon, C. J. Bio-fabrication and physiological self-release of tissue equivalents using smart peptide amphiphile templates. *Journal of Materials Science: Materials in Medicine* **26,** 1–8 (2015).

285. Gouveia, R. M. *et al.* Controlling the 3D architecture of Self-Lifting Auto-generated Tissue Equivalents (SLATEs) for optimized corneal graft composition and stability. *Biomaterials* **121,** 205–219 (2017).

286. Duarte Campos, D. F. *et al.* Corneal bioprinting utilizing collagen-based bioinks and primary human keratocytes. *Journal of Biomedical Materials Research Part A* **107,** 1945–1953 (2019).

287. Park, J. *et al.* Biocompatibility evaluation of bioprinted decellularized collagen sheet implanted in vivo cornea using swept-source optical coherence tomography. *Journal of Biophotonics* **12,** e201900098 (2019).

288. Kutlehria, S. *et al.* High-throughput 3D bioprinting of corneal stromal equivalents. *Journal of Biomedical Materials Research Part B: Applied Biomaterials* **108,** 2981–2994 (2020).

289. Bektas, C. K. & Hasirci, V. Cell loaded 3D bioprinted GelMA hydrogels for corneal stroma engineering. *Biomaterials Science* **8,** 438–449 (2019).

290. Mahdavi, S. S. *et al.* Stereolithography 3D Bioprinting Method for Fabrication of Human Corneal Stroma Equivalent. *Annals of Biomedical Engineering 2020 48:7* **48,** 1955–1970 (2020).

291. Gibney, R., Patterson, J. & Ferraris, E. High-Resolution Bioprinting of Recombinant Human Collagen Type III. *Polymers 2021, Vol. 13, Page 2973* **13,** 2973 (2021).

292. Tseng, T.-C. *et al.* An Injectable, Self-Healing Hydrogel to Repair the Central Nervous System. *Advanced Materials* **27,** 3518–3524 (2015).

293. Wu, H. D. *et al.* Development of a chitosan-polyglutamate based injectable polyelectrolyte complex scaffold. *Carbohydrate Polymers* **85,** 318–324 (2011).

294. Ma, Z., Nelson, D. M., Hong, Y. & Wagner, W. R. Thermally Responsive Injectable Hydrogel Incorporating Methacrylate-Polylactide for Hydrolytic Lability. *Biomacromolecules* **11,** 1873–1881 (2010).

295. Sà-Lima, H., Caridade, S. G., Mano, J. F. & Reis, R. L. Stimuli-responsive chitosan-starch injectable hydrogels combined with encapsulated adipose-derived stromal cells for articular cartilage regeneration. *Soft Matter* **6,** 5184–5195 (2010).

296. Rodell, C. B., Kaminski, A. L. & Burdick, J. A. Rational Design of Network Properties in Guest–Host Assembled and Shear-Thinning Hyaluronic Acid Hydrogels. *Biomacromolecules* **14,** 4125–4134 (2013).

297. Mealy, J. E., Rodell, C. B. & Burdick, J. A. Sustained small molecule delivery from injectable hyaluronic acid hydrogels through host–guest mediated retention. *Journal of Materials Chemistry B* **3,** 8010–8019 (2015).

298. Saekhor, K., Udomsinprasert, W., Honsawek, S. & Tachaboonyakiat, W. Preparation of an injectable modified chitosan-based hydrogel approaching for bone tissue engineering. *International Journal of Biological Macromolecules* **123,** 167–173 (2019).

299. Cui, H. *et al.* PLA-PEG-PLA and Its Electroactive Tetraaniline Copolymer as Multiinteractive Injectable Hydrogels for Tissue Engineering. *Biomacromolecules* **14,** 1904–1912 (2013).

300. Nam, H. G., Nam, M. G., Yoo, P. J. & Kim, J.-H. Hydrogen bonding-based strongly adhesive coacervate hydrogels synthesized using poly(N-vinylpyrrolidone) and tannic acid. *Soft Matter* **15,** 785–791 (2019).

301. Ossipov, D. A. & Hilborn, J. Poly(vinyl alcohol)-Based Hydrogels Formed by "Click Chemistry". *Macromolecules* **39,** 1709–1718 (2006).

302. DeForest, C. A., Polizzotti, B. D. & Anseth, K. S. Sequential click reactions for synthesizing and patterning three-dimensional cell microenvironments. *Nature Materials 2009 8:8* **8,** 659–664 (2009).

303. Hardy, J., Lin, P. & Schmidt, C. Biodegradable hydrogels composed of oxime crosslinked poly(ethylene glycol), hyaluronic acid and collagen: a tunable platform for soft tissue engineering. *Journal of Biomaterials Science. Polymer Edition* **26,** 143–161 (2015).

304. Grover, G. N., Lam, J., Nguyen, T. H., Segura, T. & Maynard, H. D. Biocompatible Hydrogels by Oxime Click Chemistry. *Biomacromolecules* **13,** 3013–3017 (2012).

305. Tseng, T. C., Hsieh, F. Y., Theato, P., Wei, Y. & Hsu, S. h. Glucose-sensitive self-healing hydrogel as sacrificial materials to fabricate vascularized constructs. *Biomaterials* **133,** 20–28 (2017).

306. Zhou, Y. *et al.* Photopolymerized maleilated chitosan/thiol-terminated poly (vinyl alcohol) hydrogels as potential tissue engineering scaffolds. *Carbohydrate Polymers* **184,** 383–389 (2018).

307. Dahlmann, J. *et al.* Fully defined in situ cross-linkable alginate and hyaluronic acid hydrogels for myocardial tissue engineering. *Biomaterials* **34,** 940–951 (2013).

308. Martínez-Sanz, E. *et al.* Bone reservoir: Injectable hyaluronic acid hydrogel for minimal invasive bone augmentation. *Journal of Controlled Release* **152,** 232–240 (2011).

309. Smith, L. J. *et al.* Diels–Alder Click-Cross-Linked Hydrogels with Increased Reactivity Enable 3D Cell Encapsulation. *Biomacromolecules* **19,** 926–935 (2018).

310. Abandansari, H. S. *et al.* In situ formation of interpenetrating polymer network using sequential thermal and click crosslinking for enhanced retention of transplanted cells. *Biomaterials* **170,** 12–25 (2018).

311. Li, R. *et al.* Synthesis of in-situ formable hydrogels with collagen and hyaluronan through facile Michael addition. *Materials Science and Engineering: C* **77,** 1035–1043 (2017).

312. Levit, R. D. *et al.* Cellular Encapsulation Enhances Cardiac Repair. *Journal of the American Heart Association: Cardiovascular and Cerebrovascular Disease* **2** (2013).

313. Weber, L. M., Lopez, C. G. & Anseth, K. S. The effects of PEG hydrogel crosslinking density on protein diffusion and encapsulated islet survival and function. *Journal of Biomedical Materials Research. Part A* **90,** 720–729 (2009).

314. Noshadi, I. *et al.* In vitro and in vivo analysis of visible light crosslinkable gelatin methacryloyl (GelMA) hydrogels. *Biomaterials Science* **5,** 2093–2105 (2017).

315. Sani, E. S. *et al.* Sutureless repair of corneal injuries using naturally derived bioadhesive hydrogels. *Science Advances* **5,** 1281 (2019).

316. Sharifi, S. *et al.* Photo-cross-linked Gelatin Glycidyl Methacrylate/N-Vinylpyrrolidone Copolymeric Hydrogel with Tunable Mechanical Properties for Ocular Tissue Engineering Applications. *ACS Applied Bio Materials,* acsabm.1c00905 (2021).

317. Liu, J. *et al.* In situ forming hydrogel of natural polysaccharides through Schiff base reaction for soft tissue adhesive and hemostasis. *International Journal of Biological Macromolecules* **147,** 653–666 (2020).

318. Hozumi, T., Kageyama, T., Ohta, S., Fukuda, J. & Ito, T. Injectable Hydrogel with Slow Degradability Composed of Gelatin and Hyaluronic Acid Cross-Linked by Schiff's Base Formation. *Biomacromolecules* **19,** 288–297 (2018).

319. Jin, R. *et al.* Enzymatically-crosslinked injectable hydrogels based on biomimetic dextran–hyaluronic acid conjugates for cartilage tissue engineering. *Biomaterials* **31,** 3103–3113 (2010).

320. Wang, L. S., Chung, J. E., Pui-Yik Chan, P. & Kurisawa, M. Injectable biodegradable hydrogels with tunable mechanical properties for the stimulation of neurogenesic differentiation of human mesenchymal stem cells in 3D culture. *Biomaterials* **31,** 1148–1157 (2010).

321. Poudel, B. K. *et al.* In situ Tissue Regeneration in the Cornea from Bench to Bedside. *Cells Tissues Organs,* 1–21 (2021).

322. Anumolu, S. N. S. *et al.* Doxycycline loaded poly(ethylene glycol) hydrogels for healing vesicant-induced ocular wounds. *Biomaterials* **31,** 964–974 (2010).

323. Daza, J. H. U. *et al.* PVA/anionic collagen membranes as drug carriers of ciprofloxacin hydrochloride with sustained antibacterial activity and potential use in the treatment of ulcerative keratitis. *Journal of Biomaterials Applications* **35,** 301–312 (2020).

324. Chang, M.-C. *et al.* Liposomal dexamethasone–moxifloxacin nanoparticle combinations with collagen/gelatin/alginate hydrogel for corneal infection treatment and wound healing. *Biomedical Materials* **15,** 055022 (2020).

325. Khalil, I. A. *et al.* Ciprofloxacin-loaded bioadhesive hydrogels for ocular applications. *Biomaterials Science* **8,** 5196–5209 (2020).

326. Simpson, F. C. *et al.* Collagen analogs with phosphorylcholine are inflammation-suppressing scaffolds for corneal regeneration from alkali burns in mini-pigs. *Communications Biology* **4,** 1–15 (2021).

327. Kyun Kim, H., Kim, K. & Byun, Y. Preparation of a chemically anchored phospholipid monolayer on an acrylated polymer substrate. *Biomaterials* **26,** 3435–3444 (2005).

328. Lewis, A. L. & Stratford, P. W. A Review on Phosphorylcholine-Coated Stents. *Journal of long-term effects of medical implants* **27,** 233–252 (2017).

329. Alarcon, E. I. *et al.* The biocompatibility and antibacterial properties of collagen-stabilized, photochemically prepared silver nanoparticles. *Biomaterials* **33,** 4947–4956 (2012).

330. International Standards Organization. *ISO 11137-2:2012 Sterilization of health care products – Radiation – Part 2: Establishing the sterilization dose* 2012.

331. Jennewein, C. *et al.* Novel Aspects of Fibrin(ogen) Fragments during Inflammation. *Molecular Medicine* **17,** 568–573 (2011).

332. Mosesson, M. W. Fibrinogen and fibrin structure and functions. *Journal of Thrombosis and Haemostasis* **3,** 1894–1904 (2005).

333. Richardson, D. L., Pepper, D. S. & Kay, A. B. Chemotaxis for Human Monocytes by Fibrinogen-derived Peptides. *British Journal of Haematology* **32,** 507–514 (1976).

334. Senior, R. M., Skogen, W. F., Griffin, G. L. & Wilner, G. D. Effects of fibrinogen derivatives upon the inflammatory response. Studies with human fibrinopeptide B. *Journal of Clinical Investigation* **77,** 1014–1019 (1986).

335. Singh, T. M., Kadowaki, M. H., Glagov, S. & Zarins, C. K. Role of fibrinopeptide B in early atherosclerotic lesion formation. *American Journal of Surgery* **160,** 156–159 (1990).

336. Khatoon, Z. *et al.* Nanoengineering the surface of corneal implants: towards functional anti-microbial and biofilm materials. *RSC Advances* **10,** 23675–23681 (2020).

337. Haagdorens, M. *et al.* Plant Recombinant Human Collagen Type I Hydrogels for Corneal Regeneration. *Regenerative Engineering and Translational Medicine,* 1–15 (2021).

338. Islam, M. M. *et al.* Functional fabrication of recombinant human collagen-phosphorylcholine hydrogels for regenerative medicine applications. *Acta Biomaterialia* **12,** 70–80 (2015).

339. Liu, W. *et al.* Recombinant human collagen for tissue engineered corneal substitutes. *Biomaterials* **29,** 1147–1158 (2008).

340. Ahmady, A. & Abu Samah, N. A review: Gelatine as a bioadhesive material for medical and pharmaceutical applications. *International Journal of Pharmaceutics* **608,** 121037 (2021).

341. Von Sonntag, C. The chemistry of free-radical-mediated DNA damage. *Basic Life Sciences* **58,** 287–317 (1991).

342. Zhu, M. *et al.* Gelatin methacryloyl and its hydrogels with an exceptional degree of controllability and batch-to-batch consistency. *Scientific Reports* **9,** 1–13 (2019).

Appendix A

In situ Tissue Regeneration in the Cornea from Bench-to-Bedside.

Bijay K. Poudel[a, b] Marie-Claude Robert[a, b, c] Fiona C. Simpson[a, b, c, d] Kamal Malhotra[a, b, c] Ludovic Jacques[a, b] Paul LaBarre[e] May Griffith[a, b, c, d]

[a]Département d'Ophtalmologie, Université de Montréal, Montréal, QC, Canada; [b]Centre de Recherche, Hôpital Maisonneuve-Rosemont, Montréal, QC, Canada; [c]Département d'Opthalmologie, Centre hospitalier de l'Université de Montréal, Montréal, QC, Canada; [d]Institut du Génie Biomédicale, Université de Montréal, Montréal, QC, Canada; [e]SightLife, Seattle, WA, USA

Keywords

Cornea · Transplantation · Biomaterials · Regeneration ·Clinical trial · Exosomes · Regulatory considerations

Abstract

Corneal blindness accounts for 5.1% of visual deficiency and is the fourth leading cause of blindness globally. An additional 1.5–2 million people develop corneal blindness each year, including many children born with or who later develop corneal infections. Over 90% of corneal blind people globally live in low- and middle-income regions (LMIRs), where corneal ulcers are approximately 10-fold higher compared to high-income countries. While corneal transplantation is an effective option for patients in high-income countries, there is a considerable global shortage of corneal graft tissue and limited corneal transplant programs in many LMIRs. In situ tissue regeneration aims to restore diseases or damaged tissues by inducing organ regeneration. This can be achieved in the cornea using biomaterials based on extracellular matrix (ECM) components like collagen, hyaluronic acid, and silk. Solid corneal implants based on recombinant human collagen type III were successfully implanted into patients resulting in regeneration of the corneal epithelium, stroma, and sub-basal nerve plexus. As ECM crosslinking and manufacturing methods improve, the focus of biomaterial development has shifted to injectable, in situ gelling formulations. Collagen, collagen- mimetic, and gelatin-based in situ gelling formulas have shown the ability to repair corneal wounds, surgical incisions, and perforations in in-vivo models. Biomaterial approaches may not be sufficient to treat inflammatory conditions, so other cell-free therapies such as treatment with tolerogenic exosomes and extracellular vesicles may improve treatment outcomes. Overall, many of the technologies described here show promise as future medical devices or combination products with cell or drug-based therapies. In situ tissue regeneration, particularly with liquid formulas, offers the ability to triage and treat corneal injuries and disease with a single regenerative solution, providing alternatives to organ transplantation and improving patient outcomes.

Introduction

Conventional Tissue Engineering versus In Situ Tissue Engineering

Tissue engineering aims at regenerating new tissues to replace and restore damaged body parts. Biomaterials play an important role, providing the scaffolds or templates for the therapeutic cells to repair or recreate a target tissue. The biomaterial scaffolds provide optimal anchorage, microenvironment, and topology for seeded or migrating cells (from adjacent tissues) for proliferation, alignment, and integration with host tissue before and after transplantation [Mano et al., 2007].

Conventionally, bioresorbable polymers like polycaprolactone and poly(lactic acid) were prefabricated into solid state scaffolds/matrices of desired shape and size, incubated with therapeutic cells from autologous or allogeneic sources expanded in vitro, and then surgically transplanted to target sites in patients [Cima et al., 1991]. The tissue construct is pre-conditioned prior to implantation to allow smooth graft-host integration. This has been referred to as ex vivo tissue engineering by Gaharwar et al. [2020].

More recently, cell-free scaffolds have been implanted into target organ sites to stimulate the patient's own endogenous cells to migrate into the scaffold, expand and regrow the tissues or organs. This has been referred to as in situ tissue engineering [Gaharwar et al., 2020]. Examples of scaffolds developed include the use of cell-free solid implants in human clinical trials [Fagerholm et al., 2010] to development of flowable, gel-forming precursors that could be delivered using injection devices and crosslinked in-situ [Elisseeff et al., 1999; McTiernan et al., 2020]. These stimuli or triggers for in-situ gelation range from exogenous or endogenous chemical cues, such as pH [Chiu et al., 2009], metabolites, ionic factors [Jaikumar et al., 2015], and crosslinkers [McTiernan et al., 2020], to physical stimuli such as temperature [Yeon et al., 2013], UV light [Shirzaei Sani et al., 2019] and electrical potential.

An extensive review of in situ tissue engineering can be found in Gaharwar et al. 2020 [Gaharwar et al., 2020]. Essentially, bioresponsive materials are developed to serve as templates that recapitulate the conditions in organogenesis to enable regeneration of targeted tissues and organs. In the present review, we focus on in situ tissue engineering in the human cornea as a treatment for corneal blindness and how it compares with more traditional therapeutic methods. While Gaharwar et al. cite difficulty to monitor the regenerative process as a disadvantage of in situ tissue engineering in general, this is not a problem in the cornea. The transparency of the human cornea allows the

tracking of the regeneration process in real time, particularly by in vivo confocal microscopy (IVCM) or anterior segment optical coherence tomography (ASOCT).

The human cornea

The cornea is the transparent window at the front of the eye. As such, the cornea has two important roles in ensuring the proper function of the visual system. First, the cornea forms the eye wall, providing tensile strength and protecting the intraocular contents. Second, through its optical clarity and by providing two thirds of the eye's refractive power, the cornea is essential for the formation of a clear image on the retina.

The cornea is composed of five main layers (Fig. 1) [Rowsey and Karamichos, 2017]. From the ocular surface, these layers are the epithelium, the Bowman layer, the stroma, the Descemet membrane and the endothelium. A more recent sixth pre-Descemetic layer referred to the Dua layer has also been described [Dua et al., 2013] .

The epithelium consists of 5-6 layers of non-keratinized stratified squamous epithelial cells. The epithelium renews itself every 7 to 10 days from stem cells located in the limbal palisades of Vogt, at the periphery of the cornea [DelMonte and Kim, 2011; Eghrari et al., 2015]. The epithelium creates a physical barrier with the exterior to protect the eye. Immunoglobulins, lysozyme, lactoferrin and other proteins in the tears add further safeguard against ocular surface pathogens [McDermott, 2013]. Cell-surface associated mucins of the epithelium enhance ocular surface protection and lubrication, allowing for a smooth tear film to optimize the cornea's refractive function.[Sack et al., 2001; DelMonte and Kim, 2011].

The stroma, which in human corneas includes a Bowman layer, is about 80 to 85% of the thickness of the cornea. Stromal cells called keratocytes populate the stroma and produce its extracellular matrix (ECM), composed of collagen (types I and V) and proteoglycan, organized into lamellae. The stroma derives its transparency from a precise alignment of collagen fibers. In addition, the stroma must maintain a turgescence of approximately 78% water to maintain optimal alignment and transparency [DelMonte and Kim, 2011]. The Bowman layer is a 12 μm thick acellular layer anterior to the stroma, generated through interactions between the epithelial cells and stromal keratocytes. The precise functional role of Bowman Layer has not been scientifically demonstrated and absence of adverse complications in individuals lacking the Bowman layer suggests that its role is minor [Wilson and Hong, 2000]. The Descemet membrane is composed of collagen (Type IV and VIII) and ranges from 8–10 μm thickness in adults. It is the endothelium's basement membrane. The

endothelium is composed of a single cell layer lining the most posterior aspect of the cornea. Being in direct contact with the aqueous humor of the anterior chamber of the eye, the endothelium controls the degree of stromal hydration through Na/K ATPase pumps and maintains the transparency of the stroma [Eghrari et al., 2015]. The hexagonal corneal endothelial cells are the only cell layer of the cornea that do not proliferate [Joyce, 2012].

To maintain its transparency and immune privilege, the cornea must remain avascular. Thus, the perilimbal vasculature, as well as the aqueous humor and tear film, provide all the nutrients required for the cornea's metabolic activity. The cornea is also richly innervated. Branches of the ophthalmic branch of the trigeminal nerve enter the cornea within the mid stroma, travel anteriorly and pierce through the Bowman membrane to create a complex network of nerves just below the epithelium [DelMonte and Kim, 2011].

Corneal blindness and need for bioengineered solutions

According to the World Health Organization, corneal diseases rank as the 4th most prevalent cause of blindness, representing 5.1% of blindness overall [World Health Organization, 2020a]. Globally, 4.2 million people suffer from bilateral corneal blindness and 23 million people suffer from corneal moderate to severe visual impairment [World Health Organization, 2019]. The most common causes of corneal blindness are infectious keratitis and ocular trauma [Porth et al., 2019]. While most epidemiological data captures vision as a function of both eyes, many corneal diseases present unilaterally. These diseases, while not causing blindness, causes monocular vision loss, severe or chronic pain, patient suffering and loss of quality of life are additional consequences of corneal disease.

Corneal diseases and injuries affect all ages and all populations. However, they disproportionately affect the young and populations of developing economies, contributing to the high societal burden of corneal diseases. For example, corneal diseases such as xerophthalmia (vitamin A deficiency) and ophthalmia neonatorum (neonatal keratoconjunctivitis) represent approximately 20% of childhood blindness [Oliva et al., 2012]. Trachoma, an infectious cause of corneal scarring and neovascularization that has left 2 million persons blind or visually impaired, disproportionately targets children and their mothers [Courtright and West, 2004; International Agency for the Prevention of Blindness, 2020; World Health Organization, 2020b].

Overall, over 90% of of corneal blindness occurs in low and middle income regions [Whitcher et al., 2001]. The burden of corneal disease is heightened in these countries as access to corneal

transplantation is limited. Fifty-three percent of corneal blind patients live in countries where corneal transplant surgery is simply not accessible [Gain et al., 2016]. Availability of human donor corneal tissue is a critical barrier to transplantation. Indeed, it is estimated that globally only one corneal donor tissue is available for every 70 patients in need of surgery [Gain et al., 2016]. However, even if donated corneas were readily available, patients with inflammation or severe pathologies may not respond well to conventional donor transplantation using allograft corneas. These corneas are already highly sensitized and therefore are often at high risk of graft failure or rejection [Pleyer, 2009]. With each subsequent rejection, the chances of rejection escalates as the patients draw closer to permanent blindness [Pleyer, 2009]. Alternatives or supplements to human donor corneas are therefore urgently needed.

State-of-the-art available treatments in clinical application

Human corneal transplantation

Many advances in corneal surgical technique have been made since the first corneal transplantation performed by Zirm in 1905, including surgical microscopes, microsurgical instrumentation and suturing material. These advances have improved the outcomes of traditional penetrating keratoplasty (PKP) [Zirm, 1906]. Traditional PKP aims to remove the entire thickness of the diseased central cornea and replace it by clear human donor corneal tissue. More recent advances have focused on the development of partial thickness lamellar techniques. For example, deep anterior lamellar keratoplasty (DALK) replaces the diseased stroma but leaves the posterior corneal layers in place. Endothelial keratoplasty (EK), using Descemet stripping automated endothelial keratoplasty (DSAEK) or Descemet membrane endothelial keratoplasty (DMEK) allows the targeted removal of diseased endothelium and Descemet membrane. While endothelial keratoplasty is the most often performed corneal transplantation procedure in North America, PKP remains the most commonly performed corneal transplantation globally [Gain et al., 2016; Mathews et al., 2018].

Modern reports of the outcome of PKP demonstrate survival rates of 59-82% at 5 years and of 50-65% at 10 years [Muraine et al., 2003; Williams et al., 2007; Williams et al., 2008; Barraquer et al., 2019].The primary risk factors for graft failure are preoperative corneal diagnosis and previous graft failure. Inflammatory diseases of the cornea, such as infectious keratitis, trauma and chemical burn, have significantly worse prognosis. As well, corneal transplantation success rates precipitously drop in the setting of prior corneal graft failure. In one retrospective study of 895 penetrating

keratoplasties, the 10 years success rate was 81% for a first graft, 33% for a second graft and 16% for 3 or more grafts.

The cost of a human cornea from the eye bank ranges from US $1800 to 2000 (figures from co-authors' organizations – hospital and eyebank). The costs of various bioengineered alternatives to donated tissues vary. Keratoprostheses that utilize human donor corneas as part of the device would therefore also need to bear the cost of screening donated corneas. Stem cell transplantation that involves expansion of cells in specialized cleanrooms operating under Good Manufacturing Practice (GMP) are expensive procedures due to the cost of GMP cell production [National Institute for Health and Care Excellence, 2017]. Cell-free alternatives made from synthetic materials that can potentially be produced in large batches under controlled conditions have to potential to be produced within $100 to $1000.

Keratoprostheses

Keratoprosthesis development is the earliest bioengineering approach to replace damage and diseased cornea in humans. Over the years, multiple keratoprosthesis procedures and devices have been tested, but only few are used in clinics. The Boston keratoprosthesis (Boston KPro), the osteo-odonto-keratoprosthesis (OOKP), MICOF (Moscow eye microsurgery complex in Russia), AlphaCor and Keraklear are several keratoprostheses that are used clinically.

The Boston KPro is the most widely used model with 11000 units implanted worldwide as of 2015 (https://www.masseyeandear.org/assets/MEE/pdfs/professionals/kpro/kpro- newsletter-2015.pdf). It comprises a polymethylmethacrylate (PMMA) optic and a human corneal donor graft as the carrier interface for securing onto the host cornea. The human donor cornea is sandwiched between a polymethylmethacrylate (PMMA) front plate and a titanium back plate. The Boston KPro suffers from complications such as glaucoma development (Fig. 2) and sight-threatening infections. More importantly, this device requires donor corneal tissue, and therefore cannot overcome the shortage of donor corneas.

To improve outcomes and reduce the risk of sight-threatening complications such as glaucoma, extrusion, retinal detachment and retroprosthetic membrane formation [Liu et al., 2005], research is focused on improving the conception of KPro using biocompatible materials for better integration [36]. The major limitation of current KPros is insufficient amount of cellular invasion into the implant which is important for long term stability and integration. Lack of adhesion of cells at the interface between the corneal carrier graft and the optical stem of the B-KPro can result in growth of

microbes causing corneal necrosis, or endophthalmitis, loosening of implant/device, leakage of aqueous humor, stromal downgrowth or device extrusion. It is therefore important to have a biomaterial which is biocompatible, biostable, supports integration and immunological acceptance and provides some anti-microbial protection. These biomaterials should support cell adhesion, allow movement of nutrients and glucose into the implant while supporting an infection free environment [Griffith et al., 2012; Riau et al., 2015]. Two very recent reviews from our team discuss the technologies being developed to overcome the short-comings in current KPros and we refer the reader to them [Griffith et al., 2020; Hu et al., 2020].

Stem cell transplantation To date, corneal limbal epithelial stem cells (LESCs) are being used for re-surfacing of the cornea where stem cells of the patient's eyes have been depleted by damage or injury. Two main methods are used in the clinic. The first is the expansion of LESCs in culture and then grafting onto the cornea after removal of the damaged epithelium on a carrier. Various carriers used include human amniotic membrane [Tsubota et al., 1999], fibrin [Pellegrini et al., 1997] and compressed collagen [Levis et al., 2015]. Other substrates such as silk are also being tested. The second method is the Simple Limbal Epithelial Transplantation (SLET), where small biopsies of LESCs are minced and spread over the corneal surface and glued in place after removal of the pathologic epithelium (Sangwan et al., 2012).

Corneal mesenchymal stromal (or stem) cells (MSCs) have also been expanded in culture and reinjected into the cornea. To date, clinical studies show restoration of clarity to corneas with opacifications [Basu et al., 2014].

Corneal endothelial cells (CNCs) do not proliferate in situ but they have been induced to expand in culture. CNC sheets [Okumura et al., 2014; Tan et al., 2014] and cells [Okumura et al., 2017] have been developed for use as replacements to damaged or dysfunctional endothelium.

A comprehensive review has been published by Stern et al. [Stern et al., 2018]. We also discussed this topic more recently in Hu et al. [Hu et al., 2020]. While these techniques using ex vivo tissue engineering has seen clinical success, drawbacks include donor-tissue morbidity, requirement for large quantities of immune-acceptable therapeutic cells and the lack of reliable and reproducible cell sources and the loss of cellular phenotype [Gaharwar et al., 2020].

In situ tissue engineering with solid implants

A range of implants with and without cells have been developed as alternatives to human corneal donor transplantation. These have been reviewed previously [Brunette et al., 2017; Griffith et al., 2020; Hu et al., 2020] so here, we discuss the design characteristics of one corneal implant that has been successfully evaluated in a clinical trial.

In 2010, Fagerholm et al. [Fagerholm et al., 2010] reported the 2-year results of the first- in-human in situ tissue regeneration of the human cornea, a tissue that does not normally regenerate on its own. Cell-free biosynthetic corneal implants made from crosslinked recombinant human collagen type III (RHCIII) integrated stably with the patients' own tissues and stimulate endogenous re-growth of corneal cells and nerves, and overall improved vision. Patients at four years post-operative were still stable and required no immunosuppression compared to allografted patients, where an 11% rejection episode occurred (the reported rejection rate at 1-2 years post-operation is 10-15%) [Fagerholm et al., 2014]. Implanted patients had a 4-year average corrected visual acuity of 20/54 and gained more than 5 Snellen lines of vision on an eye chart [Fagerholm et al., 2014].

Implant design considerations

The hydrogel RHCIII implants used in Fagerholm et al. [Fagerholm et al., 2010, 2014] were designed to mimic the native ECM of the cornea. The ECM has an important role in early organogenesis by providing the environment needed for cellular migration, proliferation and differentiation. As regeneration tends to recapitulate organogenesis, collagen was selected because it is the main scaffolding of the corneal ECM. Recombinant human collagen (RHC) was selected to avoid lot-to-lot heterogeneity and obtain a homogenous source of scaffolding material, important in the production of implants for clinical use. RHC use also avoids animal source xenogeneic proteins that could cause allergies or other adverse immune reactions or transmit zoonotic disease [Manuelidis et al., 1977; Wong and Griffiths, 2014]. RHCIII was used even though the native cornea contains RHC type I, because a comparison done in a 12-month study in the corneas of mini-pigs showed that they were equivalent [Merrett et al., 2008] and the homotrimeric RHCIII [Linsenmayer, 1991] was easier to produce in cGMP grade. RHCIII fibrils were finer and had a tendency towards higher optical clarity [Assouline et al., 1992]. Hydrogels were selected as the scaffold type to mimic the highly hydrated cornea ECM, and to keep the collagen fibrils well below 300 nm (half the wavelength of visible light) to prevent scattering [Hayes et al., 2015]. Finally, the hydrogels were crosslinked to increase the mechanical strength of the implants to allow for surgical handling and to increase the resistance of the fibers against proteolysis to enhance their stability [Vater et al., 1979]. It should be noted that the choice of crosslinkers and amounts used should be very carefully determined, to maintain

transparency and elasticity of the hydrogels. For example, the crosslinked RHCIII implants used by Fagerholm and co-workers showed white light transmittance of 95%, well within the accepted level for healthy human corneas at around 8% [Fagerholm et al., 2014].

Patients with corneas that are inflamed or have severe pathologies, are often at high risk for rejecting donor human corneas. These inflamed corneas are already immune sensitized and grafting of allograft tissues into these corneas often results in graft failure. Therefore, for subsequent use in patients diagnosed with severe pathologies associated with high- graft rejection risk, 2-methacryloyloxyethyl phosphorylcholine (MPC) was incorporated into the RHCIII implants as interpenetrating networks [Islam et al., 2018]. MPC has been shown to have inflammation suppressing properties [Yumoto et al., 2015], which may be due to its anti-fouling properties that includes preventing the adhesion of inflammatory cells such as macrophages [Ham et al., 2020]. The resulting RHCIII-MPC implants were able to promote stable regeneration in high-risk corneas with ulcers and scarring over the observation period of an average of 2 years [Islam et al., 2018].

Implant characterization Prior to entry into clinical evaluation, both RHCIII and RHCIII-MPC were extensively tested in vitro and then in vivo. Table 1 shows the steps taken from the laboratory to clinical trials. Regulatory details are given below in the Regulatory Considerations section.

Animal model testing must be conducted to establish a degree of safety and efficacy prior to first in human trials. For example, in McLaughlin et al (2010) [McLaughlin et al., 2010], implants were tested for their ability to promote regeneration of functional innervation, i.e. regeneration of all the different sensory nerves supplying the cornea and not just one type. The implants were also tested in multiple animal species prior to human clinical trials to minimize errors of extrapolation. For example, type I porcine collagen-MPC (used for research) and RHCIII-MPC was tested in mice [Lee et al., 2014], rabbits [Liu et al., 2009; Hackett et al., 2011], guinea pigs [McLaughlin et al., 2010] and two sub-species of mini-pigs (Göttingen and Yucatan) [Liu et al., 2009; Islam et al., 2018] prior to clinical evaluation.

In situ tissue regeneration in clinical trials

Fig. 3 shows ASOCT and IVCM images of regenerated neo-corneas after implantation of RHCIII scaffolds into the wound bed after excision of pathologic tissue. The biosynthetic RHCIII implant was cell-free when implanted, but at 24 months post-operation, shows comparable morphology to the control, normal human cornea, complete with a regenerated sub- epithelial nerve plexus. The posterior stroma and endothelium that were unoperated remained unaffected.

More importantly, there was no recruitment of inflammatory dendritic cells into the implant area, whereas, even with immunosuppression, donor cornea recipients had dendritic cells present and one out of nine grafts had a rejection episode. At four years post-operation, the nerves within donor cornea grafted corneas were abnormally long and tortuous whereas a more normally appearing sub-basal nerve plexus of parallel nerve fibres was present in the in situ tissue regenerated neo-corneas. However, it is pertinent to note that in corneas with severe pathologies where the patients' stem cells are depleted, in situ tissue regeneration will only partially treat the condition and requires supplementation with exogenous therapeutic cells [Islam et al., 2018].

Tissue regeneration from in situ gelling formulations

In-situ forming hydrogels in tissue regeneration

Recently, injectable, in-situ forming hydrogels have gained growing interest in the tissue engineering field as they offer several advantages over the preformed solid scaffold counterparts. Fluidic precursors can adapt or mold to complex tissue cavities/irregular wounds or shapes in real time resulting in the better integration. Minimally invasive percutaneous injection via needles or endoscopic catheters in lieu of specialized surgical interventions for transplantation, thus reducing the risk of infection, scar tissue formation and patient discomfort. They can also easily incorporate therapeutic molecules, exosomes, nanoparticles and growth factors; and are ultimately more cost-effective. Apart from biocompatibility and non-immunogenicity, an ideal in-situ forming hydrogel and the crosslinking mechanism should meet additional design specifications: (a) Sol-gel transition under mild, physiological condition (not requiring toxic reagents, initiators or catalysts and extreme stimulus such as elevated temperature, pH, and ionic concentrations) with no toxic by-products and degradation products; (b) Modulated biodegradation profile that accommodate the rapid proliferation of cells and tissue integration while maintaining necessary mechanical stability; (c) Sufficient gelation/crosslinking time to avoid the infiltration to the surrounding tissues and adjacent blood streams or blockage of the needle/catheters due to early polymerization; (d) Suitable rheological properties of hydrogel precursors to allow flowability through small diameter needle so as not to exert undue shear forces on encapsulated cells (e.g., using shear-thinning precursors [Samimi Gharaie et al., 2018].

To achieve these criteria, in situ forming hydrogels have been designed using naturally derived materials chitosan [Jin et al., 2009], alginate [Bidarra et al., 2014], collagen [Yuan et al., 2016],

gelatin [Li et al., 2018], hyaluronic acids (HA) [Dorsey et al., 2015], decellularized ECMs), synthetic polymers (polyethylene glycols (PEGs), polyacrylamides [Alexander et al., 2013], polyesters) and composite/hybrid materials. Naturally derived materials tend to be inherently biocompatible, biodegradable and biointegrable owing to innate integrin binding motifs, but might suffer from inter-batch variability, potential antigenicity and low mechanical stability. They may require significant chemical modification to enable in-situ crosslinking to increase the stability of hydrogels. Conversely, synthetic polymers can be precisely tailored to provide required mechanical and chemical properties with sufficient inter-batch consistency and minimal immunogenicity but can lack bio-functionality to support cell adhesion and cellular coordination. These polymers are crosslinked locally at the target site in patients using physical (weak secondary bonds) or chemical (covalent bonds) methods. Different in situ crosslinking mechanisms, their strengths and weakness and some examples are summarized in Table 2 [Ossipov and Hilborn, 2006; DeForest et al., 2009; Weber et al., 2009; Jin et al., 2010; Ma et al., 2010; Sá-Lima et al., 2010; Wang et al., 2010; Martínez-Sanz et al., 2011; Wu et al., 2011; Grover et al., 2012; Cui et al., 2013; Dahlmann et al., 2013; Levit et al., 2013; Rodell et al., 2013; Hardy et al., 2015; Tseng et al., 2015; Li et al., 2017; Noshadi et al., 2017; Tseng et al., 2017; Abandansari et al., 2018; Hozumi et al., 2018; Smith et al., 2018; Zhou et al., 2018; Nam et al., 2019; Saekhor et al., 2019; Liu et al., 2020].

Uses of in situ forming hydrogels for corneal regeneration

In-situ forming hydrogels are suitable for soft tissue (superficial skin wound, corneal defects) regeneration as they have similar viscoelastic compositions [Khunmanee et al., 2017]. These hydrogels have been studied for tissue regeneration in skin defects [Zhu et al., 2017], cardiac tissue defects [Frey et al., 2014; Peña et al., 2018], nerve defects [Lin and Marra, 2012] and retinal degeneration [Tang et al., 2019].

In the ophthalmic field, in-situ gelling systems have been investigated for topical administration to prolong the drug residence time which otherwise is impeded by rapid tear turnover rate, reflex blinking, penetration barriers and nasolacrimal drainage resulting in the bioavailability of $<5\%$ of the applied dose [Choi and Kim, 2018; Bhattacharjee et al., 2019; Wu et al., 2019]. In-situ forming hydrogels for corneal regeneration must allow for cellular contacts between cells and support neuronal in-growth. As hydrogels are nano-porous, they can allow diffusion of growth factors and nutrients. However, they need to degrade at optimally balanced rates to permit gradual replacement via migration, mitosis and differentiation of micron-sized cells (epithelial cells, stromal fibroblast,

limbal stem cells etc.) while maintaining structural stability. They should also provide: (a) sufficient mechanical strength to withstand intraocular pressure (IOP) fluctuations of up to 268 mmHg (ca. 250 KPa); (b) optical transparency and refractive index comparable to cornea; (c) sufficient adhesivity to the native tissue [Griffith et al., 2020].

To date, there are no clinically evaluated nor approved in situ gelling formulations that induce corneal regeneration. There are a few hydrogel-based commercial adhesives or sealants approved for closure of tissue incisions that have found "off-label" use in the management of corneal wounds. However, these are mostly used in acute, short-term management of corneal wounds and not designed to promote regeneration. Below are several examples of systems that are under development to promote in situ tissue regeneration.

Collagen-based hydrogels

A range of injectable in situ gelling hydrogels that are based on collagen, their derivatives and analogs have been developed for use in corneal wound repair. Several of these are discussed here.

Lee et al. (2018) modified full-length, type I collagen with azide and dibenzocyclooctyne groups, co-cultured keratinocytes (on surface) and keratocytes (in bulk) in precursor solution and used copper free, strain-promoted azide–alkyne cycloaddition (SPAAC) click chemistry for in-situ gelling in stromal wound of rabbit cornea organ culture model. The hydrogels adhered well to the host stromal layer and support the growth of stratified epithelium [Lee et al., 2018]. Subsequently the same group developed a hydrogel comprising two simultaneous interpenetrating networks (IPN) of crosslinked collagen (via thiol-ene Michael click reaction) for cell adhesion and hyaluronic acid (HA; via a strain-promoted azide-alkyne cycloaddition reaction). The resulting hydrogel successfully filled stroma defects created in rabbits corneas, restoring corneal curvature, promoted re-epithelialization and allowed stromal regeneration with minimal activation of myofibroblastic scar-forming cells [Chen et al., 2020].

Gelatin is essentially denatured collagen that exists as smaller fragments. Li et al. (2018) used acrylated and thiolated gelatin as UV photopolymerizable precursor of in-situ forming hydrogels with tunable mechanical properties for the repair of corneal wounds. Accelerated epithelialization and reduced scarring were observed after hydrogel application in focal corneal injury rabbit model [Li et al., 2018]. Another group also used modified gelatin (GelCORE) but used visible light for in-situ photo-polymerization. Shirzaei Sani et al. (2019) used cell-free gelatin-methacrylate as precursor, Eosin Y as photoinitiator and N- vinylcaprolactam as co-monomer and photo-crosslinked

by exposing to visible light (450 to 550 nm) in a rabbit corneal defect model. In vitro cell studies with corneal fibroblast showed that the hydrogels were cell-friendly while in vivo experiments showed that hydrogels effectively sealed corneal defects and promoted epithelial and stromal regeneration [Shirzaei Sani et al., 2019].

Researchers have also developed fully-defined collagen-like or collagen mimetic peptides as alternatives to both gelatin and collagen for regenerative medicine applications [Strauss and Chmielewski, 2017]. McTiernan et al. (2020) developed the LiQD Cornea, a synthetic injectable hydrogel comprising a collagen analog and fibrinogen. The collagen analog comprised a short 36 amino acid collagen-like peptide [O'Leary et al., 2011] conjugated with an 8 arm PEG maleimide through a short cysteine-glycine peptide linker [Islam et al., 2016] and mixed with fibrinogen. The hydrogel showed excellent in vitro cytocompatibility with human corneal epithelial cells. As an alternative to donor tissue in an anterior lamellar keratoplasty surgery in mini-pig corneas, the LiQD Cornea gelled in situ and promoted successful corneal epithelium and stroma regeneration and neuronal restoration over a 12- month follow-up period (Fig. 4) [McTiernan et al., 2020]. This collagen analog with fibrinogen was also able to seal full-thickness perforations in rabbit corneas (Fig. 4). A similar "in-situ forming" PEG-collagen hydrogel has been described by Fernandes-Cunha and co-workers [Fernandes-Cunha et al., 2020].

The idea behind these in situ gelling hydrogels is to potentially eliminate costly operating room costs needed for grafting of solid implants as the aim was to repair perforations in the ophthalmologist's clinic in a similar way to dentists filling cavities. The costs of operating rooms is averaged as US $37.45 per minute [Childers et al., 2018].

Other in situ gelling hydrogels

Zarembinski et al. (2014) used cytocompatible glutathione disulfide to crosslink thiolated HA and thiolated gelatin, which gelled in under 5 minutes. This disulfide-linked hydrogel supported the 3-D culture of adipose-derived stem cells in-vitro and showed biocompatibility in preliminary intracutaneous and subconjunctival experiments in-vivo in rabbits [Zarembinski et al., 2014].

Other in situ gelling hydrogels have been developed using other biomimetic materials. However, they have mainly been used in conjunction with stem cell delivery such human adipose derived stems [Koivusalo et al., 2018] or corneal endothelial [Liang et al., 2011] or stromal [Chien et al. 2012] cells to affect the regeneration.

Extracellular vesicles, exosomes and in situ tissue regeneration

Extracellular vesicles (EVs) are lipid bilayer-delimited particles released from cells as a form of intercellular communication. Exosomes are an EV subtype ranging in size from 30 - 150 nm [Boriachek et al., 2018]. EV are derived from plasma membrane invaginations that form the early endosome. The destiny of the multivesicular bodies is primarily regulated by Rab7, which is associated with both trafficking to lysozymes for degradation and exosomal release [Song et al., 2016]. Lipid compositions affects Rab7 targeting, with cholesterol rich exosomes destined for extracellular release [Möbius et al., 2003; Rocha et al., 2009] Exosomal cargo is loaded using endosomal sorting complex required for transport (ESCRT) machinery (containing ESCRT-0, ESCRT-I, ESCRT-II, and ESCRT-III) and ESCRT-independent machinery (involving lipids, syndecan, and syntenin) [van Niel et al., 2018; Mathieu et al., 2019]. Exosomes are associated with the transfer of miRNAs between cells, in addition to the transport of protein cargo [Valadi et al., 2007]. Exosomes are also associated with the presentation of antigens in inflammatory states [Arima et al., 2019]. In transplantation, exosomes containing self-antigens have been associated with organ transplant rejection [Sharma et al., 2018a; Sharma et al., 2018b].

Exosomes in corneal wound healing and regeneration

Mesenchymal stromal cells (MSCs) are pluripotent stromal cells that are associated with immunomodulation through the secretion of paracrine factors [Zhao et al., 2010]. They have been used extensively in ischemic diseases to reduce inflammation and promote healing at the ischemic site [Akyurekli et al., 2015; Vizoso et al., 2017]. Exosomes were identified as one of the primary mediators of the paracrine effects of MSCs, allowing for the treatment efficacy of MSCs without the safety concerns surrounding cell therapies [Maguire, 2013; Yu et al., 2014; Rani et al., 2015].MSC-derived exosomes have been associated with dermal wound healing and collagen secretion [Zhang et al., 2015; Hu et al., 2016].

In 2018, Shen et al. published the first paper examining the effects of adipose MSC-derived exosomes in the cornea [Shen et al., 2018]. Cornea stromal keratocytes treated with AMSC-derived exosomes showed increased cell proliferation, and collagen and fibronectin expression. These cells also showed downregulation of matrix metalloproteinases (MMPs) 1, 2, 3 and 9. MMPs are enzymes that degrade ECM proteins. Building on these findings, Samaeekia et al. isolated corneal MSCs (cMSCs) and collected exosomes from cMSC conditioned-media [Samaeekia et al., 2018]. In a mouse corneal epithelium debridement model, cMSC-exosomes application resulted in 77.5 $\pm$ 3% corneal wound

closure due to epithelial re-growth after 72 hours, whereas the untreated control group only showed $41.6 \pm 7\%$ wound healing.

The effects of MSC-derived exosomal miRNAs were examined by Shojaati et al. [Shojaati et al., 2019]. In a mouse corneal wound model, the wound was treated with fibrin glue containing MSCs from corneal stromal stem cells (CSSC) with and without CSSC-EVs. Both the CSSC and CSSC-EV groups had full prevention of corneal scarring. When the experiment was repeated with EVs derived from CSSCs or HEK293T cells, only the CSSC-derived exosomes prevented corneal scar formation. The CSSC EVs also decreased neutrophil infiltration after wounding, which is consistent with previous results for treatment with CSSCs. CSSC-derived EVs carrying synthetic ath-miR159a, a molecular tool used to track exosome fate, fused with human corneal fibroblasts and HCECs, delivering the cargo miRNA. The packaging of miRNA into CSSC-EVs is dependent on Alix (or programmed cell death 6-interacting protein), and a knockout of Alix (Alix-KD) resulted in an 85% decrease in EV cargo miRNA. When corneal wounds were treated with CSSC-EVs or Alix-KD-CSSC-EVs, the knockout resulted in a decrease in suppression of genes associated with fibrosis.

These studies show that sub-cellular exosomes have the potential promote cell-free in situ tissue regeneration in the cornea, without the possible adverse immune reactions caused by the introduction of foreign cells. However, before exosomes can be routinely used in clinical application, their isolation and processing have to be made more uniform for regulatory approval. At present, they would be classified as medicinal products, like therapeutic cells, and hence subject to more stringent regulatory guidelines for cGMP production than cell-free biomaterials.

Regulatory Considerations

In situ tissue regeneration is dependent on the use of bio-responsive materials to reproduce the conditions in organogenesis for development of various tissue and organs. The regulatory classification of implants used to promote in situ tissue regeneration dependent on what components the constructs or implants contain, and how these act to achieve the desired effect. Essentially, the implants will be classified as medical devices, medicinal products or combination products. The regulatory considerations for each of these are discussed below.

Medical Device Regulation

The regulation of medical products, including those used in the field of ophthalmology, reduces risks to patients through a rigorous process of in vitro and in vivo testing that is used to demonstrate

safety and efficacy. The pathways for regulatory approval vary by country and by the type of product whether it is a device, a drug, a biologic, or a combination of any of these three. Building on the strong foundational support of the Global Harmonization Task Force, the International Medical Device Regulators Forum was conceived in 2011 to discuss future directions in medical device regulatory harmonization. International standards such as ISO 13485 [141] for medical devices provide a basis for countries to adopt entire or partial components of their regulatory system that have been developed iteratively by an international group of expert stakeholders.

The first stage of medical device approval is classification. Most countries have developed risk-based classification systems whereby more novel or risky products are subjected to higher levels of rigor prior to market authorization. The Global Harmonization Task Force (GHTF) classifies medical devices into the 3 classes. Canada, however, has a Class IV designation for medical devices that are considered high-risk and requires invasive surgery for implantation. Class I: generally regarded as low risk; Class IIa&b: generally regarded as medium risk; and Class III: generally regarded as high risk. These have been adapted in the Medical Devices Directive 93/42/EEC which defines safety and performance requirements for medical equipment sold in the European Union. Whereas, in the USA, the FDA specifies three classes of medical devices: Class I (least risk), Class II, and Class III (greatest risk). The FDA determines the device classification by the device's intended use and the risk that it presents to the patient. If proposed medical devices can be compared to legally-marketed predicate devices with the same intended use, very often the pathway is via Class II with a 510(k) application that may not require extensive clinical demonstration of safety and effectiveness. Alternatively, for the highest risk devices and for those so novel that there is no predicate, Class III is often designated requiring the most stringent regulatory controls including a pivotal clinical study, GMP inspections, pre-market-notification as well as post- market studies. While similar classes exist between countries, the class can vary by jurisdiction. For example, keratoprostheses are considered Class II medical devices by the US FDA, but Class III medical devices by Health Canada.

Requirements for biocompatibility testing medical devices are derived from ISO 10993- 1:2018 Biological evaluation of medical devices — Part 1: Evaluation and testing within a risk management process, which outlines the necessary testing based on the type of tissue contact and duration of contact following Annex A in ISO 10993-1:2018 [142]. In the case of biosynthetic corneas, testing must meet the requirements for permanent implantation with tissue contact. Based on this categorization, researchers can use Annexe A to determine the biocompatibility testing necessary for their device. All medical devices require cytotoxicity and sensitization studies. Implantable

medical devices that remain longer then 24 hours also require irritation or subcutaneous reactivity, acute systemic toxicity, sub-chronic toxicity, genotoxicity and implantation. Each of these tests has approved protocols outlined in subsequent parts of ISO 10993. It is critical that these tests be conducted by an external, GLP certified lab to meet the requirements for submission to regulatory agencies. These pre-clinical tests form the basis for the application for clinical trials and it is critical that consult your regulatory agency to identify current best practices such as the correct species of large and small animal models for these trials. For cornea research, rabbits are often used as small animal models, while mini-pigs are used as large animal models. The collected results of the biocompatibility testing form the basis of the application for clinical trials.

Prior to conducting clinical studies involving a novel medical device, federal approval is often required, as well as an ethics committee review and clearance. In the United States, that would require an application for an Investigational Device Exemption (IDE) for permission to conduct clinical trials. Clinical trials for medical devices are generally divided into pilot safety trials with limited enrollment and pivotal efficacy studies with wide enrollment. These studies conclude the scientific evaluation of the medical device the results of which comprise the main section of a dossier submitted to regulatory agencies.

QMS certification ensures that medical devices are produced so that they conform to the technical specifications set out by the manager. The regulations for the development and manufacture of medical devices are based on ISO 13485:2016 Medical devices — Quality management systems — Requirements for regulatory purposes. Each signatory to the GHS system has a legal framework based on this standard. Manufacturing for medical devices must be monitored by a notified body or regulatory agency to ensure compliance to the standards and laws that apply to each medical device. Records for the history of the both the design and the iterations device, as well as the current technical specifications need to be maintained in a Design History File (DHF) and supplied to the regulatory agencies for review. Once the manufacturer has met the conditions to issue a declaration of conformity for the product, they can pursue a license application for the sale of the device.

Drug products

Drug products are required to meet the standards and laws regulating cGMP in their jurisdiction. Unlike medical devices, drugs do not have a central international standard that underpins all legislation. Drugs that have undergone pre-clinical toxicology and multi-species animal studies can

be submitted for investigational drug exemptions that facilitate human clinical trials. This usually requires three phases of clinical trials. Phase I trials are safety trials conducted in healthy individuals. Phase 2 trials are limited enrollment efficacy studies, which are usually examined by the regulatory agency before proceeding to Phase 3 trials which are large multisite trials designed to extensively test the efficacy of the drug. Once clinical testing has concluded, the results and the labelling and manufacture of the drug is reviewed to ensure the safety and efficacy of the product. Phase 4 post-regulatory approval studies may be conducted to evaluate product efficacy when in public health use.

Combination Products

Combination products arise when a product qualifies for more than one classification: drug, device, or biologic for example, an implant designed to deliver drugs or therapeutic cells. They are typically regulated by the agency that governs the primary mode of action and their manufacturing requirements are usually based on the more stringent of the two requirements. For, example a biomaterial implant containing drug-delivery nanoparticles would likely be required to manufacture to the cGMP standard for pharmaceutical products, and not ISO 13485.

Key Considerations for Researchers

The pathways for regulatory approval have very clear objectives: safety and efficacy. However, there are aspects of manufacturing and pre-clinical testing that can be hard to visualize clearly for researchers. Early design choices in the reagents and protocols that are used to manufacture your future product can have a significant impact on your manufacturing feasibility in the future. There are aspects of both GLP and GMP practices that should be implemented early on in development to have adequate documentation later. Table 2 lists some early considerations for QMS development that can be implemented during development, to facilitate QMS implementation in the future.

Conclusion

We have shown that in situ tissue regeneration has several advantages over ex vivo tissue engineered products or cell-based therapies. However, in certain conditions such as in hosts with depleted stem or progenitor cells, the technique is not effective. The use of cell-derived extracellular vesicles is a potential source of therapeutic agent for promoting in situ tissue regeneration. Finally, the regulatory pathway is a consideration for design of therapies to promote in situ tissue regeneration as a new therapeutic modality.

Statements

Conflict of Interest Statement

MG is a named inventor on PCT PCT/IB2017/056342 Collagen and collagen like peptide-based hydrogels, corneal implants, filler glue and uses thereof, which was assigned to the Hyderabad Eye Research Foundation, and then subsequently assigned to North Grove Investments, Inc. wherein PCT national phase applications have been filed in the USA, EU, India and China, and an impending application to be filed in Canada. MG is also a named inventor on US provisional patent application #62916765, following a disclosure to Univalor, technology transfer agent to Maisonneuve-Rosemont Hospital and Université de Montréal.

MG holds the Canada Research Chair for Biomaterials and Stem Cells in Ophthalmology and the Caroline Durand Foundation Research Chair for Cellular Therapy in the Eye. FCS is currently supported by a Natural Sciences and Engineering Research Council of Canada (NSERC) studentship for her doctoral studies.

Funding Sources

Research referenced from the Griffith group was funded by CIHR and NSERC Canada, the Canadian Stem Cell Network, Swedish Research Council, VINNOVA Sweden, Euronanomed 2 and 3 and Fonds de la recherche en santé du Québec (FRQS).

Author Contributions

All authors contributed to the writing, revisions and final approval of this review paper.

References

Abandansari HS, Ghanian MH, Varzideh F, Mahmoudi E, Rajabi S, Taheri P, et al. In situ formation of interpenetrating polymer network using sequential thermal and click crosslinking for enhanced retention of transplanted cells. Biomaterials. 2018 Jul;170:12-25.

Akyurekli C, Le Y, Richardson RB, Fergusson D, Tay J, Allan DS. A systematic review of preclinical studies on the therapeutic potential of mesenchymal stromal cell-derived microvesicles. Stem Cell Rev Rep. 2015 Feb;11(1):150-60.

Alexander A, Ajazuddin, Khan J, Saraf S, Saraf S. Poly(ethylene glycol)-poly(lactic-co-glycolic acid) based thermosensitive injectable hydrogels for biomedical applications. J Control Release. 2013 Dec 28;172(3):715-29.

Arima Y, Liu W, Takahashi Y, Nishikawa M, Takakura Y. Effects of Localization of Antigen Proteins in Antigen-Loaded Exosomes on Efficiency of Antigen Presentation. Mol Pharm. 2019 Jun;16(6):2309-14.

Assouline M, Chew SJ, Thompson HW, Beuerman R. Effect of growth factors on collagen lattice contraction by human keratocytes. Invest Ophthalmol Vis Sci. 1992 Apr;33(5):1742-55.

Barraquer RI, Pareja-Aricò L, Gómez-Benlloch A, Michael R. Risk factors for graft failure after penetrating keratoplasty. Medicine. 2019 Apr;98(17):e15274.

Basu S, Hertsenberg AJ, Funderburgh ML, Burrow MK, Mann MM, Du Y, et al. Human limbal biopsy-derived stromal stem cells prevent corneal scarring. Sci Transl Med. 2014 Dec;6(266):266ra172.

Bhattacharjee A, Das PJ, Adhikari P, Marbaniang D, Pal P, Ray S, et al. Novel drug delivery systems for ocular therapy: With special reference to liposomal ocular delivery. Eur J Ophthalmol. 2019 Jan;29(1):113-26.

Bidarra SJ, Barrias CC, Granja PL. Injectable alginate hydrogels for cell delivery in tissue engineering. Acta Biomaterialia. 2014 Apr;10(4):1646-62.

Boriachek K, Islam MN, Möller A, Salomon C, Nguyen N-T, Hossain MSA, et al. Biological Functions and Current Advances in Isolation and Detection Strategies for Exosome Nanovesicles. Small. 2018 Feb;14(6):1702153.

Brown TE, Carberry BJ, Worrell BT, Dudaryeva OY, McBride MK, Bowman CN, et al. Photopolymerized dynamic hydrogels with tunable viscoelastic properties through thioester exchange. Biomaterials. 2018 Sep; 178: 496–503.

Brunette I, Roberts CJ, Vidal F, Harissi-Dagher M, Lachaine J, Sheardown H, et al. Alternatives to eye bank native tissue for corneal stromal replacement. Prog Retin Eye Res. 2017 Jul;59:97-130.

Chen F, Le P, Lai K, Fernandes-Cunha GM, Myung D. Simultaneous Interpenetrating Polymer Network of Collagen and Hyaluronic Acid as an In Situ-Forming Corneal Defect Filler. Chem Mater. 2020 Jun;32(12):5208-16.

Chien Y, Liao YW, Liu DM, Lin HL, Chen SJ, Chen HL, et al. Corneal repair by human corneal keratocyte-reprogrammed iPSCs and amphiphatic carboxymethyl-hexanoyl chitosan hydrogel. Biomaterials. 2012 Nov;33(32):8003-16.

Childers CP, Maggard-Gibbons M. Understanding Costs of Care in the Operating Room. JAMA Surg. 2018 Apr 18;153(4):e176233.

Chiu Y-L, Chen S-C, Su C-J, Hsiao C-W, Chen Y-M, Chen H-L, et al. pH-triggered injectable hydrogels prepared from aqueous N-palmitoyl chitosan: In vitro characteristics and in vivo biocompatibility. Biomaterials. 2009 Oct;30(28):4877-88.

Choi SW, Kim J. Therapeutic Contact Lenses with Polymeric Vehicles for Ocular Drug Delivery: A Review. Materials (Basel). 2018 Jul;11(7).

Cima LG, Vacanti JP, Vacanti C, Ingber D, Mooney D, Langer R. Tissue engineering by cell transplantation using degradable polymer substrates. J Biomech Eng. 1991 May;113(2):143-51.

Courtright P, West SK. Contribution of sex-linked biology and gender roles to disparities with trachoma. Emerg Infect Dis. 2004 Nov;10(11):2012.

Cui H, Shao J, Wang Y, Zhang P, Chen X, Wei Y. PLA-PEG-PLA and Its Electroactive Tetraaniline Copolymer as Multi-interactive Injectable Hydrogels for Tissue Engineering. Biomacromolecules. 2013 Jun;14(6):1904-12.

Dahlmann J, Krause A, Möller L, Kensah G, Möwes M, Diekmann A, et al. Fully defined in situ cross- linkable alginate and hyaluronic acid hydrogels for myocardial tissue engineering. Biomaterials. 2013 Jan;34(4):940-51.

DeForest CA, Polizzotti BD, Anseth KS. Sequential click reactions for synthesizing and patterning three-dimensional cell microenvironments. Nat Mater. 2009 Aug;8(8):659-64. DelMonte DW, Kim T. Anatomy and physiology of the cornea. J Cataract Refract Surg. 2011 Mar;37(3):588-98.

Dorsey SM, McGarvey JR, Wang H, Nikou A, Arama L, Koomalsingh KJ, et al. MRI evaluation of injectable hyaluronic acid-based hydrogel therapy to limit ventricular remodeling after myocardial infarction. Biomaterials. 2015 Nov;69:65-75.

Dua HS, Faraj LA, Said DG, Gray T, Lowe J. Human Corneal Anatomy Redefined: A Novel Pre-Descemet's Layer (Dua's Layer). Ophthalmology. 2013 Sep;120(9):1778-85.

Eghrari AO, Riazuddin SA, Gottsch JD. Overview of the Cornea: Structure, Function, and Development. Prog Mol Biol Transl Sci. 2015;134:7-23.

Elisseeff J, Anseth K, Sims D, McIntosh W, Randolph M, Langer R. Transdermal photopolymerization for minimally invasive implantation. Proc Natl Acad Sci U S A. 1999 Mar;96(6):3104-7.

Fagerholm P, Lagali NS, Merrett K, Jackson WB, Munger R, Liu Y, et al. A Biosynthetic Alternative to Human Donor Tissue for Inducing Corneal Regeneration: 24-Month Follow-Up of a Phase 1 Clinical Study. Sci Transl Med. 2010 Aug;2(46):46ra61-46ra61.

Fagerholm P, Lagali NS, Ong JA, Merrett K, Jackson WB, Polarek JW, et al. Stable corneal regeneration four years after implantation of a cell-free recombinant human collagen scaffold. Biomaterials. 2014 Mar;35(8):2420-7.

Fernandes-Cunha GM, Chen KM, Chen F, Le P, Han JH, Mahajan LA, et al. In situ-forming collagen hydrogel crosslinked via multi-functional PEG as a matrix therapy for corneal defects. Scientific Reports. 2020 Oct;10(1):16671.

Frey N, Linke A, Süselbeck T, Müller-Ehmsen J, Vermeersch P, Schoors D, et al. Intracoronary delivery of injectable bioabsorbable scaffold (IK-5001) to treat left ventricular remodeling after ST-elevation myocardial infarction: a first-in-man study. Circ Cardiovasc Interv. 2014 Dec;7(6):806-12.

Gaharwar AK, Singh I, Khademhosseini A. Engineered biomaterials for in situ tissue regeneration. Nat Rev Mat. 2020 Sep;5(9):686-705.

Gain P, Jullienne R, He Z, Aldossary M, Acquart S, Cognasse F, et al. Global Survey of Corneal Transplantation and Eye Banking. JAMA Ophthalmol. 2016 Feb;134(2):167-73.

Griffith M, Polisetti N, Kuffova L, Gallar J, Forrester J, Vemuganti GK, et al. Regenerative Approaches as Alternatives to Donor Allografting for Restoration of Corneal Function. Ocul Surf. 2012 Jul;10(3):170-83.

Griffith M, Poudel BK, Malhotra K, Akla N, González-Andrades M, Courtman D, et al. Biosynthetic alternatives for corneal transplant surgery. Exp Rev Ophthalmol. 2020 May;15(3):129-43.

Grover GN, Lam J, Nguyen TH, Segura T, Maynard HD. Biocompatible Hydrogels by Oxime Click Chemistry. Biomacromolecules. 2012 Oct;13(10):3013-17.

Hackett JM, Lagali N, Merrett K, Edelhauser H, Sun Y, Gan L, et al. Biosynthetic Corneal Implants for Replacement of Pathologic Corneal Tissue: Performance in a Controlled Rabbit Alkali Burn Model. Invest Ophthalmol Vis Sci. 2011 Feb;52(2):651-57.

Ham J, Kim Y, An T, Kang S, Ha C, Wufue M, et al. Covalently Grafted 2-Methacryloyloxyethyl Phosphorylcholine Networks Inhibit Fibrous Capsule Formation around Silicone Breast Implants in a Porcine Model. ACS Applied Materials & Interfaces. 2020 Jul;12(27):30198-212.

Hardy JG, Lin P, Schmidt CE. Biodegradable hydrogels composed of oxime crosslinked poly(ethylene glycol), hyaluronic acid and collagen: a tunable platform for soft tissue engineering. J Biomater Sci Polym Ed. 2015 Jan;26(3):143-61.

Hayes S, Lewis P, Islam MM, Doutch J, Sorensen T, White T, et al. The structural and optical properties of type III human collagen biosynthetic corneal substitutes. Acta Biomater. 2015 Oct;25:121-30.

Hozumi T, Kageyama T, Ohta S, Fukuda J, Ito T. Injectable Hydrogel with Slow Degradability Composed of Gelatin and Hyaluronic Acid Cross-Linked by Schiff's Base Formation. Biomacromolecules. 2018 Feb;19(2):288-97.

Hu L, Wang J, Zhou X, Xiong Z, Zhao J, Yu R, et al. Exosomes derived from human adipose mensenchymal stem cells accelerates cutaneous wound healing via optimizing the characteristics of fibroblasts. Sci Rep. 2016 Sep;6(1):32993.

Hu VH, Kanda P, Malhotra K, Alarcon EI, Gonzalez-Andrades M, Burton M, et al. Bioengineered Corneas Entering the Clinical Realm. In: Eberli D, Lee SJ, Traweger A, editors. Organ Tissue Engineering. Cham: Springer International Publishing; 2020. p. 1-31. International Agency for the Prevention of Blindness. Global Burden Vision Impairment-Global Cause Estimates. 2020.

Islam MM, Buznyk O, Reddy JC, Pasyechnikova N, Alarcon EI, Hayes S, et al. Biomaterials-enabled cornea regeneration in patients at high risk for rejection of donor tissue transplantation. npj Regenerative Medicine. 2018 Jan;3(1):2.

Islam MM, Ravichandran R, Olsen D, Ljunggren MK, Fagerholm P, Lee CJ, et al. Self-assembled collagen-like-peptide implants as alternatives to human donor corneal transplantation. RSC Advances. 2016 Jun;6(61):55745-49.

Jaikumar D, Sajesh KM, Soumya S, Nimal TR, Chennazhi KP, Nair SV, et al. Injectable alginate-O- carboxymethyl chitosan/nano fibrin composite hydrogels for adipose tissue engineering. Int J Biol Macromol. 2015 Mar;74:318-26.

Jin R, Moreira Teixeira LS, Dijkstra PJ, Karperien M, van Blitterswijk CA, Zhong ZY, et al. Injectable chitosan-based hydrogels for cartilage tissue engineering. Biomaterials. 2009 May;30(13):2544-51.

Jin R, Moreira Teixeira LS, Dijkstra PJ, van Blitterswijk CA, Karperien M, Feijen J. Enzymatically-crosslinked injectable hydrogels based on biomimetic dextran–hyaluronic acid conjugates for cartilage tissue engineering. Biomaterials. 2010 Apr;31(11):3103-13.

Joyce NC. Proliferative capacity of corneal endothelial cells. Exp Eye Res. 2012 Feb;95(1):16-23.

Khunmanee S, Jeong Y, Park H. Crosslinking method of hyaluronic-based hydrogel for biomedical applications. J Tissue Eng. 2017 Sep;8:2041731417726464.

Koivusalo L, Karvinen J, Sorsa E, Jönkkäri I, Väliaho J, Kallio P, et al. Hydrazone crosslinked hyaluronan-based hydrogels for therapeutic delivery of adipose stem cells to treat corneal defects. Mat Sci End C Mater Biol Appl. 2018 Apr;85:68-78.

Lee CJ, Buznyk O, Kuffova L, Rajendran V, Forrester JV, Phopase J, et al. Cathelicidin LL-37 and HSV-1 Corneal Infection: Peptide Versus Gene Therapy. Transl Vis Sci Technol. 2014 May;3(3):4.

Lee HJ, Fernandes-Cunha GM, Na KS, Hull SM, Myung D. Bio-Orthogonally Crosslinked, In Situ Forming Corneal Stromal Tissue Substitute. Adv Healthc Mater. 2018 Oct;7(19):e1800560.

Levis HJ, Kureshi AK, Massie I, Morgan L, Vernon AJ, Daniels JT. Tissue Engineering the Cornea: The Evolution of RAFT. J Funct Biomater. 2015 Jan 22;6(1):50-65.

Levit RD, Landázuri N, Phelps EA, Brown ME, García AJ, Davis ME, et al. Cellular encapsulation enhances cardiac repair. J Am Heart Assoc. 2013 Oct;2(5):e000367.

Li L, Lu C, Wang L, Chen M, White J, Hao X, et al. Gelatin-Based Photocurable Hydrogels for Corneal Wound Repair. ACS Appl Mater Interfaces. 2018 Apr;10(16):13283-92.

Li R, Cai Z, Li Z, Zhang Q, Zhang S, Deng L, et al. Synthesis of in-situ formable hydrogels with collagen and hyaluronan through facile Michael addition. Mat Sci End C Mater Biol Appl. 2017 Aug;77:1035-43.

Liang Y, Liu W, Han B, Yang C, Ma Q, Song F, et al. An in situ formed biodegradable hydrogel for reconstruction of the corneal endothelium. Colloids Surf B Biointerfaces. 2011 Jan 1;82(1):1-7.

Lin YC, Marra KG. Injectable systems and implantable conduits for peripheral nerve repair. Biomed Mater. 2012 Apr;7(2):024102.

Linsenmayer TF. Collagen. In: Hay ED, editor. Cell Biology of Extracellular Matrix. Springer US; 1991. p. 7-40.

Liu C, Paul B, Tandon R, Lee E, Fong K, Mavrikakis I, et al. The osteo-odonto-keratoprosthesis (OOKP). Semin Ophthalmol. 2005 Jul;20(2):113-28.

Liu J, Li J, Yu F, Zhao YX, Mo XM, Pan JF. In situ forming hydrogel of natural polysaccharides through Schiff base reaction for soft tissue adhesive and hemostasis. Int J Biol Macromol. 2020 Mar;147:653-66.

Liu W, Deng C, McLaughlin CR, Fagerholm P, Lagali NS, Heyne B, et al. Collagen-phosphorylcholine interpenetrating network hydrogels as corneal substitutes. Biomaterials. 2009 Mar;30(8):1551-9.

Ma Z, Nelson DM, Hong Y, Wagner WR. Thermally Responsive Injectable Hydrogel Incorporating Methacrylate-Polylactide for Hydrolytic Lability. Biomacromolecules. 2010 Jul;11(7):1873-81. Maguire G. Stem cell therapy without the cells. Commun Integr Biol. 2013 Nov;6(6):e26631.

Mano JF, Silva GA, Azevedo HS, Malafaya PB, Sousa RA, Silva SS, et al. Natural origin biodegradable systems in tissue engineering and regenerative medicine: present status and some moving trends. J R Soc Interface. 2007 Dec;4(17):999-1030.

Manuelidis EE, Angelo JN, Gorgacz EJ, Kim JH, Manuelidis L. Experimental Creutzfeldt-Jakob Disease Transmitted Via the Eye with Infected Cornea. New Engl J Med. 1977 Jun;296(23):1334-36.

Martínez-Sanz E, Ossipov DA, Hilborn J, Larsson S, Jonsson KB, Varghese OP. Bone reservoir: Injectable hyaluronic acid hydrogel for minimal invasive bone augmentation. J Control Release. 2011 Jun 10;152(2):232-40.

Mathews PM, Lindsley K, Aldave AJ, Akpek EK. Etiology of Global Corneal Blindness and Current Practices of Corneal Transplantation: A Focused Review. Cornea. 2018 Sep;37(9):1198-203.

Mathieu M, Martin-Jaular L, Lavieu G, Théry C. Specificities of secretion and uptake of exosomes and other extracellular vesicles for cell-to-cell communication. Nat Cell Biol. 2019 Jan;21(1):9-17.

McDermott AM. Antimicrobial compounds in tears. Exp Eye Res. 2013 Dec;117:53-61.

McLaughlin CR, Acosta MC, Luna C, Liu W, Belmonte C, Griffith M, et al. Regeneration of functional nerves within full thickness collagen-phosphorylcholine corneal substitute implants in guinea pigs. Biomaterials. 2010 Apr;31(10):2770-8.

McTiernan CD, Simpson FC, Haagdorens M, Samarawickrama C, Hunter D, Buznyk O, et al. LiQD Cornea: Pro-regeneration collagen mimetics as patches and alternatives to corneal transplantation. Sci Adv. 2020 Jun;6(25):eaba2187.

Merrett K, Fagerholm P, McLaughlin CR, Dravida S, Lagali N, Shinozaki N, et al. Tissue-engineered recombinant human collagen-based corneal substitutes for implantation: performance of type I versus type III collagen. Invest Ophthalmol Vis Sci. 2008 Sep;49(9):3887-94.

Möbius W, Van Donselaar E, Ohno-Iwashita Y, Shimada Y, Heijnen HFG, Slot JW, et al. Recycling Compartments and the Internal Vesicles of Multivesicular Bodies Harbor Most of the Cholesterol Found in the Endocytic Pathway. Traffic. 2003 Apr;4(4):222-31.

Muraine M, Sanchez C, Watt L, Retout A, Brasseur G. Long-term results of penetrating keratoplasty. A 10-year-plus retrospective study. Graefes Arch Clin Exp Ophthalmol. 2003 Jul;241(7):571-76.

Nam HG, Nam MG, Yoo PJ, Kim J-H. Hydrogen bonding-based strongly adhesive coacervate hydrogels synthesized using poly(N-vinylpyrrolidone) and tannic acid. Soft Matter. 2019 Jan;15(4):785-91.

National Institute for Health and Care Excellence, 2017: https://www.nice.org.uk/guidance/ta467/documents/appr consultation-document-2].

Noshadi I, Hong S, Sullivan KE, Shirzaei Sani E, Portillo-Lara R, Tamayol A, et al. In vitro and in vivo analysis of visible light crosslinkable gelatin methacryloyl (GelMA) hydrogels. Biomater Sci. 2017 Sep;5(10):2093-105.

O'Leary LER, Fallas JA, Bakota EL, Kang MK, Hartgerink JD. Multi-hierarchical self-assembly of a collagen mimetic peptide from triple helix to nanofibre and hydrogel. Nat Chem. 2011 Oct;3(10):821-28.

Okumura N, Kinoshita S, Koizumi N. Cell-based approach for treatment of corneal endothelial dysfunction. Cornea. 2014 Nov;33 Suppl 11:S37-41.

Okumura N, Kinoshita S, Koizumi N. The Role of Rho Kinase Inhibitors in Corneal Endothelial Dysfunction. Curr Pharm Des. 2017;23(4):660-66.

Oliva MS, Schottman T, Gulati M. Turning the tide of corneal blindness. Indian J Ophthalmol. 2012 Sep-Oct;60(5):423-7. Ossipov DA, Hilborn J. Poly(vinyl alcohol)-Based Hydrogels Formed by "Click Chemistry". Macromolecules. 2006 Mar;39(5):1709-18.

Pellegrini G, Traverso CE, Franzi AT, Zingirian M, Cancedda R, De Luca M. Long-term restoration of damaged corneal surfaces with autologous cultivated corneal epithelium. Lancet. 1997 Apr;349(9057):990-3.

Peña B, Laughter M, Jett S, Rowland TJ, Taylor MRG, Mestroni L, et al. Injectable Hydrogels for Cardiac Tissue Engineering. Macromol Biosci. 2018 Jun;18(6):e1800079.

Pleyer U. Prevention of corneal graft rejection. Acta Ophthalmol. 2009 Sep;87(s244):0-0.

Porth JM, Deiotte E, Dunn M, Bashshur R. A Review of the Literature on the Global Epidemiology of Corneal Blindness. Cornea. 2019 Dec;38(12):1602-09.

Rani S, Ryan AE, Griffin MD, Ritter T. Mesenchymal Stem Cell-derived Extracellular Vesicles: Toward Cell-free Therapeutic Applications. Mol Ther. 2015 May;23(5):812-23.

Riau AK, Mondal D, Yam GH, Setiawan M, Liedberg B, Venkatraman SS, et al. Surface Modification of PMMA to Improve Adhesion to Corneal Substitutes in a Synthetic Core-Skirt Keratoprosthesis. ACS Appl Mater Interfaces. 2015 Oct;7(39):21690-702.

Rocha N, Kuijl C, van der Kant R, Janssen L, Houben D, Janssen H, et al. Cholesterol sensor ORP1L contacts the ER protein VAP to control Rab7-RILP-p150 Glued and late endosome positioning. J Cell Biol. 2009 Jun;185(7):1209-25.

Rodell CB, Kaminski AL, Burdick JA. Rational Design of Network Properties in Guest–Host Assembled and Shear-Thinning Hyaluronic Acid Hydrogels. Biomacromolecules. 2013 Nov;14(11):4125-34.

Rowsey TG, Karamichos D. The role of lipids in corneal diseases and dystrophies: a systematic review. Clin Transl Med. 2017 Dec;6(1):30.

Sá-Lima H, Caridade SG, Mano JF, Reis RL. Stimuli-responsive chitosan-starch injectable hydrogels combined with encapsulated adipose-derived stromal cells for articular cartilage regeneration. Soft Matter. 2010 Aug;6(20):5184-95.

Sack RA, Nunes I, Beaton A, Morris C. Host-Defense Mechanism of the Ocular Surfaces. Biosci Rep. 2001 Aug;21(4):463-80.

Saekhor K, Udomsinprasert W, Honsawek S, Tachaboonyakiat W. Preparation of an injectable modified chitosan-based hydrogel approaching for bone tissue engineering. Int J Biol Macromol. 2019 Feb;123:167-73.

Samaeekia R, Rabiee B, Putra I, Shen X, Park YJ, Hematti P, et al. Effect of Human Corneal Mesenchymal Stromal Cell-derived Exosomes on Corneal Epithelial Wound Healing. Invest Ophthalmol Vis Sci. 2018 Oct;59(12):5194-200.

Samimi Gharaie S, Dabiri SMH, Akbari M. Smart Shear-Thinning Hydrogels as Injectable Drug Delivery Systems. Polymers (Basel). 2018 Nov;10(12).

Sangwan VS, Basu S, MacNeil S, Balasubramanian D. Simple limbal epithelial transplantation (SLET): a novel surgical technique for the treatment of unilateral limbal stem cell deficiency. Br J Ophthalmol. 2012 Jul;96(7):931-4. doi: 10.1136/bjophthalmol-2011-301164.

Sharma M, Liu W, Perincheri S, Gunasekaran M, Mohanakumar T. Exosomes expressing the self-antigens myosin and vimentin play an important role in syngeneic cardiac transplant rejection induced by antibodies to cardiac myosin. Am J Transplant. 2018a Jul;18(7):1626-35.

Sharma M, Ravichandran R, Bansal S, Bremner RM, Smith MA, Mohanakumar T. Tissue-associated self-antigens containing exosomes: Role in allograft rejection. Hum Immunol. 2018b Sep;79(9):653-58.

Shen T, Zheng QQ, Shen J, Li QS, Song XH, Luo HB, et al. Effects of Adipose-derived Mesenchymal Stem Cell Exosomes on Corneal Stromal Fibroblast Viability and Extracellular Matrix Synthesis. Chin Med J (Engl). 2018 Mar;131(6):704-12.

Shirzaei Sani E, Kheirkhah A, Rana D, Sun Z, Foulsham W, Sheikhi A, et al. Sutureless repair of corneal injuries using naturally derived bioadhesive hydrogels. Sci Adv. 2019 Mar;5(3):eaav1281.

Shojaati G, Khandaker I, Funderburgh ML, Mann MM, Basu R, Stolz DB, et al. Mesenchymal Stem Cells Reduce Corneal Fibrosis and Inflammation via Extracellular Vesicle-Mediated Delivery of miRNA. Stem Cells Transl Med. 2019 Nov;8(11):1192-201.

Smith LJ, Taimoory SM, Tam RY, Baker AEG, Binth Mohammad N, Trant JF, et al. Diels–Alder Click- Cross-Linked Hydrogels with Increased Reactivity Enable 3D Cell Encapsulation. Biomacromolecules. 2018 Mar;19(3):926-35.

Song P, Trajkovic K, Tsunemi T, Krainc D. Parkin Modulates Endosomal Organization and Function of the Endo-Lysosomal Pathway. J Neurosci. 2016 Feb;36(8):2425-37.

Stern JH, Tian Y, Funderburgh J, Pellegrini G, Zhang K, Goldberg JL, et al. Regenerating Eye Tissues to Preserve and Restore Vision. Cell Stem Cell. 2018 Jun;22(6):834-49.

Strauss K, Chmielewski J. Advances in the design and higher-order assembly of collagen mimetic peptides for regenerative medicine. Current Opinion in Biotechnology. 2017 Aug; 46: 34-41.

Tan TE, Peh GS, George BL, Cajucom-Uy HY, Dong D, Finkelstein EA, et al. A cost-minimization analysis of tissue-engineered constructs for corneal endothelial transplantation. PLoS One. 2014 Jun;9(6):e100563.

Tang Z, Jiang F, Zhang Y, Zhang Y, YuanYang, Huang X, et al. Mussel-inspired injectable hydrogel and its counterpart for actuating proliferation and neuronal differentiation of retinal progenitor cells. Biomaterials. 2019 Feb;194:57-72.

Tseng T-C, Hsieh F-Y, Theato P, Wei Y, Hsu S-h. Glucose-sensitive self-healing hydrogel as sacrificial materials to fabricate vascularized constructs. Biomaterials. 2017 Jul;133:20-28.

Tseng T-C, Tao L, Hsieh F-Y, Wei Y, Chiu I-M, Hsu S-h. An Injectable, Self-Healing Hydrogel to Repair the Central Nervous System. Advanced Materials. 2015 May;27(23):3518-24.

Tsubota K, Satake Y, Kaido M, Shinozaki N, Shimmura S, Bissen-Miyajima H, et al. Treatment of Severe Ocular-Surface Disorders with Corneal Epithelial Stem-Cell Transplantation. New Engl J Med. 1999 Jun;340(22):1697-703.

Valadi H, Ekström K, Bossios A, Sjöstrand M, Lee JJ, Lötvall JO. Exosome-mediated transfer of mRNAs and microRNAs is a novel mechanism of genetic exchange between cells. Nat Cell Biol. 2007 Jun;9(6):654-9.

van Niel G, D'Angelo G, Raposo G. Shedding light on the cell biology of extracellular vesicles. Nat Rev Mol Cell Biol. 2018 Apr;19(4):213-28.

Vater CA, Harris ED, Jr., Siegel RC. Native cross-links in collagen fibrils induce resistance to human synovial collagenase. Biochem J. 1979 Sep;181(3):639-45.

Vizoso FJ, Eiro N, Cid S, Schneider J, Perez-Fernandez R. Mesenchymal Stem Cell Secretome: Toward Cell-Free Therapeutic Strategies in Regenerative Medicine. Int J Mol Sci. 2017 Aug;18(9).

Wang LS, Chung JE, Chan PP, Kurisawa M. Injectable biodegradable hydrogels with tunable mechanical properties for the stimulation of neurogenesic differentiation of human mesenchymal stem cells in 3D culture. Biomaterials. 2010 Feb;31(6):1148-57.

Weber LM, Lopez CG, Anseth KS. Effects of PEG hydrogel crosslinking density on protein diffusion and encapsulated islet survival and function. J Biomater Res A. 2009 Sep;90(3):720-29.

Whitcher JP, Srinivasan M, Upadhyay MP. Corneal blindness: a global perspective. Bull World Health Organ. 2001 Apr;79(3):214-21.

Williams K, Lowe M, Keane M, Jones VJ, Loh RS, Coster D. The Australian Corneal Graft Registry 2012 Report. 2007. Williams KA, Lowe M, Bartlett C, Kelly TL, Coster DJ. Risk factors for human corneal graft failure within the Australian corneal graft registry. Transplantation. 2008 Dec;86(12):1720-4.

Wilson SE, Hong JW. Bowman's layer structure and function: critical or dispensable to corneal function? A hypothesis. Cornea. 2000 Jul;19(4):417-20.

Wong ML, Griffiths LG. Immunogenicity in xenogeneic scaffold generation: antigen removal vs. decellularization. Acta Biomater. 2014 May;10(5):1806-16. World Health Organization. World report on vision. 2019. World Health Organization. Blindness and vision impairment prevention. 2020a.

World Health Organization. Trachoma. 2020b. Wu H-D, Yang J-C, Tsai T, Ji D-Y, Chang W-J, Chen C-C, et al. Development of a chitosan–polyglutamate based injectable polyelectrolyte complex scaffold. Carbohydr Polym. 2011 May;85(2):318-24.

Wu Y, Liu Y, Li X, Kebebe D, Zhang B, Ren J, et al. Research progress of in-situ gelling ophthalmic drug delivery system. Asian J Pharm Sci. 2019 Jan;14(1):1-15.

Yeon B, Park MH, Moon HJ, Kim SJ, Cheon YW, Jeong B. 3D culture of adipose-tissue-derived stem cells mainly leads to chondrogenesis in poly(ethylene glycol)-poly(L-alanine) diblock copolymer thermogel. Biomacromolecules. 2013 Sep;14(9):3256-66.

You Y, Yang J, Zheng Q, Wu N, Lv Z, Jiang Z. Ultra-stretchable hydrogels with hierarchical hydrogen bonds. Sci Rep. 2020 Jul; 10(1): 11727.

Yu B, Zhang X, Li X. Exosomes derived from mesenchymal stem cells. Int J Mol Sci. 2014 Mar;15(3):4142-57. Yuan L, Li B, Yang J, Ni Y, Teng Y, Guo L, et al. Effects of Composition and Mechanical Property of Injectable Collagen I/II Composite Hydrogels on Chondrocyte Behaviors. Tissue Eng Part A. 2016 Jun;22(11-12):899-906.

Yumoto H, Hirota K, Hirao K, Miyazaki T, Yamamoto N, Miyamoto K, et al. Anti-inflammatory and protective effects of 2-methacryloyloxyethyl phosphorylcholine polymer on oral epithelial cells. J Biomed Mater Res A. 2015 Feb;103(2):555-63.

Zarembinski TI, Doty NJ, Erickson IE, Srinivas R, Wirostko BM, Tew WP. Thiolated hyaluronan-based hydrogels crosslinked using oxidized glutathione: An injectable matrix designed for ophthalmic applications. Acta Biomater. 2014 Jan;10(1):94-103.

Zhang J, Guan J, Niu X, Hu G, Guo S, Li Q, et al. Exosomes released from human induced pluripotent stem cells-derived MSCs facilitate cutaneous wound healing by promoting collagen synthesis and angiogenesis. J Transl Med. 2015 Feb;13:49.

Zhao S, Wehner R, Bornhäuser M, Wassmuth R, Bachmann M, Schmitz M. Immunomodulatory properties of mesenchymal stromal cells and their therapeutic consequences for immune- mediated disorders. Stem Cells Dev. 2010 May;19(5):607-14.

Zhou Y, Zhao S, Zhang C, Liang K, Li J, Yang H, et al. Photopolymerized maleilated chitosan/thiol-terminated poly (vinyl alcohol) hydrogels as potential tissue engineering scaffolds. Carbohydr Polym. 2018 Mar;184:383-89.

Zhu F, Wang C, Yang S, Wang Q, Liang F, Liu C, et al. Injectable tissue adhesive composite hydrogel with fibroblasts for treating skin defects. J Mater Chem B. 2017 Apr;5(13):2416-24.

Zirm EK. Eine erfolgreiche totale Keratoplastik (A successful total keratoplasty). 1906. Refract Corneal Surg. 1989 Jul;5(4):258-61.

Figure Legends

Fig. 1. Structure of the human cornea. Reproduced under the terms of the Creative Commons CC BY license from Springer Nature, from Rowsey and Karamichos, 2017.

Fig. 2. Eye of a 66 year-old with herpes simplex keratitis and dense corneal neovascularization after Boston KPro implantation. Despite marked improvement in vision initially, visual acuity declined to 20/400 due to glaucoma.

Fig. 3. Corneal features in a healthy, unoperated subject, compared to those of patients grafted with a biosynthetic RHCIII implant or a human donor cornea, at 24 months post-operation. (Top row) ASOCT images where areas of wound-healing activity exhibit high reflectivity (white areas). (A to O) IVCM images. Intact epithelium of the unoperated cornea (A), regenerated corneal epithelial cells on the implant surface (B), and regenerated epithelium of the penetrating graft (C). Regenerated nerves (E) at the sub-basal epithelium in an implanted cornea were parallel and morphologically similar to the normal cornea (D), whereas regenerated sub-basal nerves were also observed in a cornea transplanted with human donor tissue (F). Anterior stromal cell (keratocyte) nuclei (G to I) and posterior keratocytes (J to L) were present, with varying density, in all corneas. The endothelium (M to O) in all corneas had a characteristic mosaic pattern. Scale bars, 2 mm (ASOCT), 100 mm (IVCM). Reproduced from Fagerholm et al. 2010, with copyright permission from AAAS.

Fig. 4. In vitro and in vivo biological evaluation of the LiQD Cornea. (A) Immortalized human corneal epithelial cells cultured on LiQD Cornea hydrogels and control tissue culture plastic, showing that the hydrogels support epithelial growth. (B) Expression of T-cell co-stimulatory molecules in bone marrow-derived dendritic cells (BMDCs). Expression of CD40, CD80, and CD86 was measured by flow cytometry and data is presented as a ratio of mean fluorescent intensity of the experimental samples to untreated BMDCs. Lipopolysaccharide (LPS) acted as a positive control for BMDC activation; * $p \leq 0.05$ by Student's t-test. (C) Expression of pro- inflammatory M1(CD 86) and anti-inflammatory M2 (CD 206) phenotypic markers at 4 and 7 days after exposure of naïve bone marrow-derived macrophage precursors to LiQD Cornea hydrogels. (D) Example of a human corneal perforation. (E) Post-surgical photos of rabbits immediately after injecting LiQD Cornea into a perforated cornea. The two-stepped surgically- induced perforation can be seen. At Day 2 post surgery, the air bubble placed under the cornea during surgery is prominent, indicating that the

perforation was completely sealed. The perforated cornea was completed healed by 28 days post-operation. (F) Mini-pig corneas where the LiQD Cornea was tested as an alternative to a donor allograft, showing the gross appearance of the LiQD Cornea, syngeneic graft and an unoperated eye at 12 months post-surgery. Reproduced from McTiernan et al. 2020, by a Creative Commons license from AAAS.

Figures

Figure 1.

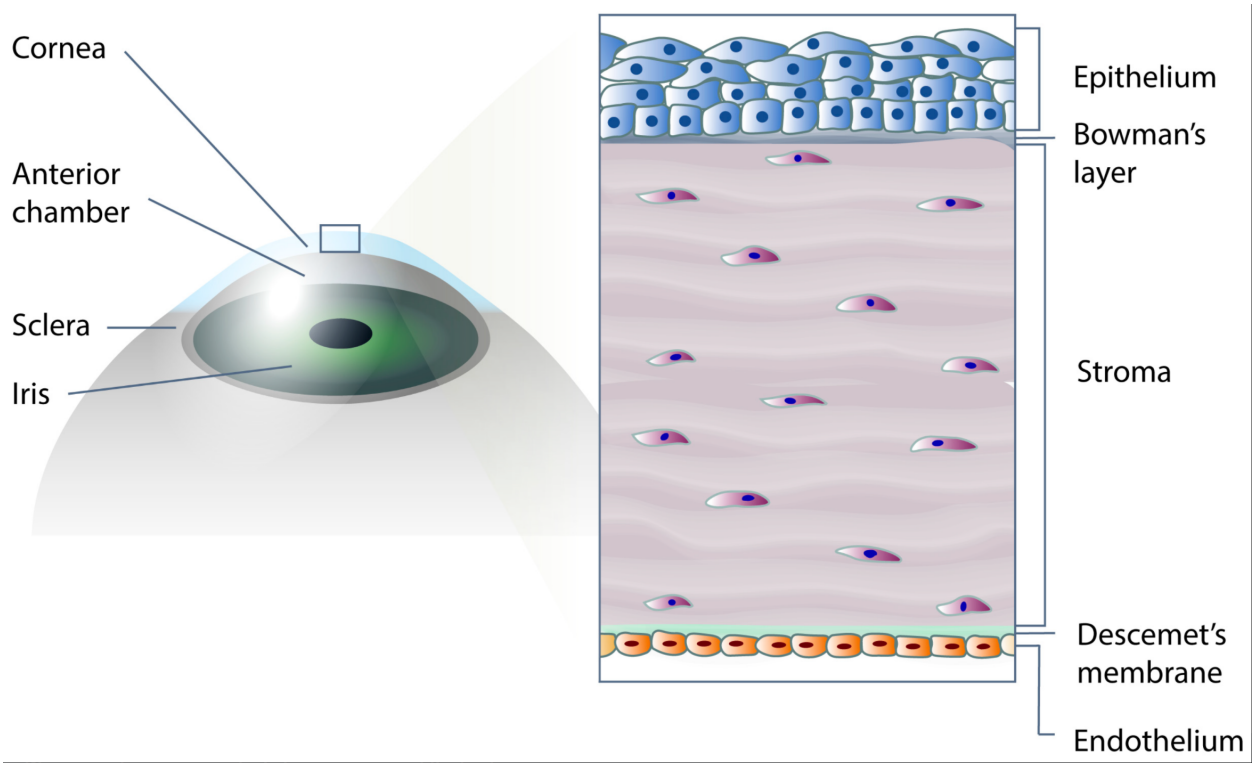

Figure 2.

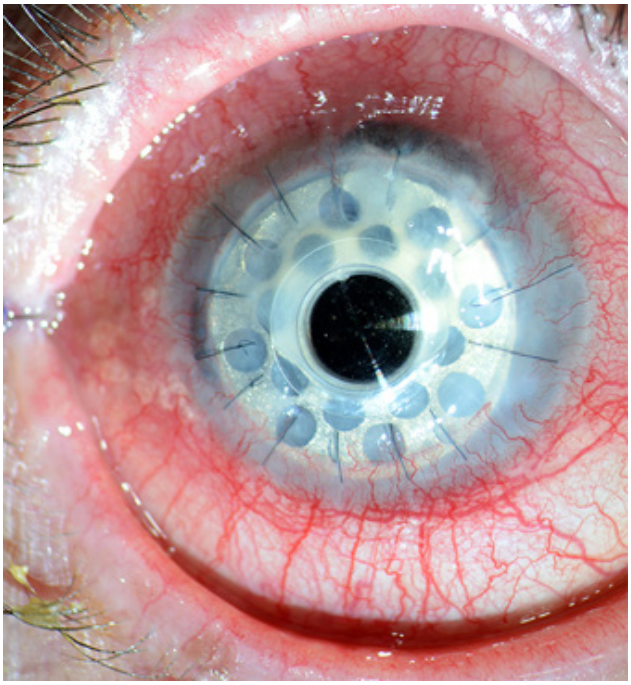

Figure 3.

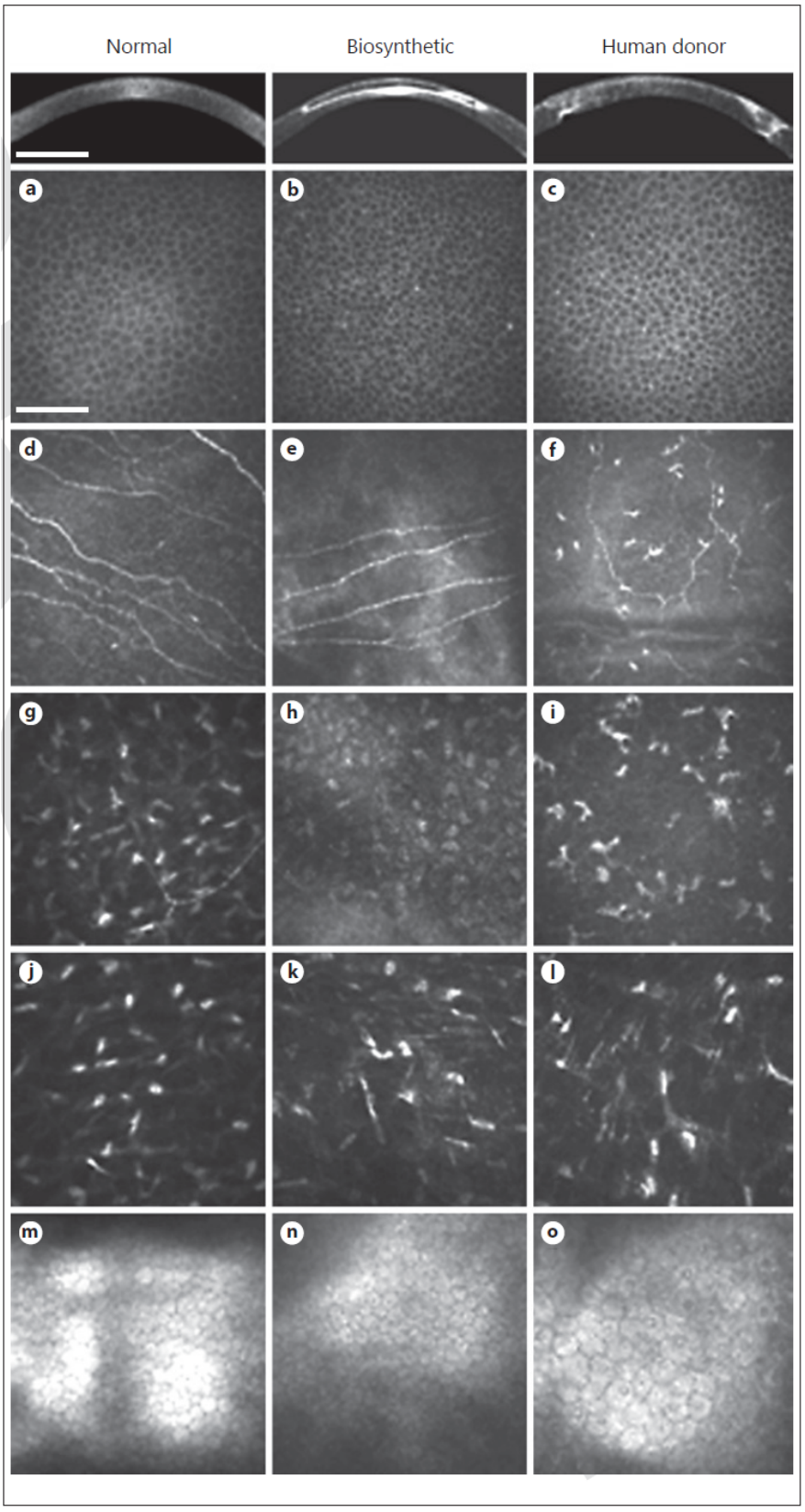

Figure 4.

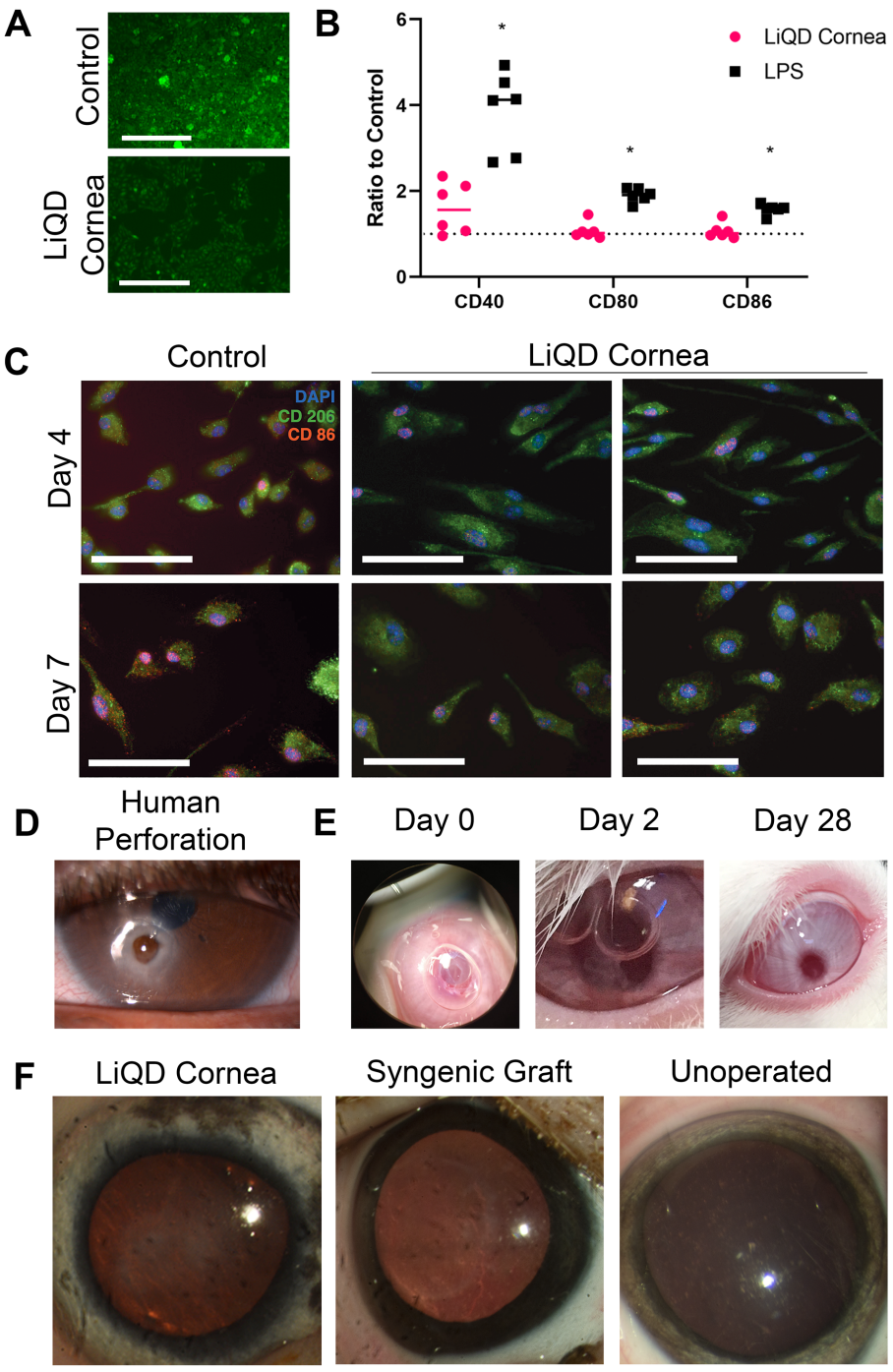
A
Control
LiQD Cornea
B
Ratio to Control
LiQD Cornea
LPS
CD40
CD80
CD86
C
Control
LiQD Cornea
Day 4
Day 7
DAPI
CD 206
CD 86
D
Human Perforation
E
Day 0
Day 2
Day 28
F
LiQD Cornea
Syngenic Graft
Unoperated

Appendix B

Plant Recombinant Human Collagen Type I Hydrogels for Corneal Regeneration

Michel Haagdorens[1,2] · Elle Edin[3,4,5] · Per Fagerholm[6] · Marc Groleau[4,5] · Zvi Shtein[7,8] · Artūras Ulčinas[9] · Amit Yaari[7,8] · Ayan Samanta[10] · Vytautas Cepla[9,12] · Aneta Liszka[6] · Marie-José Tassignon[1,2] · Fiona Simpson[3,4,5] · Oded Shoseyov[7,8,13] · Ramūnas Valiokas[9] · Isabel Pintelon[11] · Monika Kozak Ljunggren[6] · May Griffith[3,4,5]

Monika Kozak Ljunggren: Monika.Ljunggren@liu.se

May Griffith: May.Griffith@umontreal.ca

Isabel Pintelon: isabel.pintelon@uantwerpen.be

[1]Department of Ophthalmology, Visual Optics and Visual Rehabilitation, University of Antwerp, Antwerp, Belgium

[2]Department of Ophthalmology, Antwerp University Hospital,Antwerp, Belgium

[3]Department of Ophthalmology and Institute of Biomedical Engineering, University of Montreal, Montreal, Quebec, Canada

[4]Maisonneuve-Rosemont Hospital Research Centre, Montreal,Quebec, Canada

[5]CHUM Research Centre, Montreal, Quebec, Canada

[6]Department of Clinical and Experimental Medicine, Linköping University, Linköping, Sweden

[7]The Robert H. Smith Faculty of Agriculture, Food and Environment,Rehovot, Israel

[8]The Center for Nanoscience and Nanotechnology, The Hebrew University of Jerusalem, Jerusalem, Israel

[9]Department of Nanoengineering, Center for Physical Sciences andTechnology, Vilnius, Lithuania

[10]Department of Chemistry–Ångström Laboratory, Uppsala, Sweden

[11]Laboratory of Cell Biology and Histology, Antwerp University,Antwerp, Belgium

[12]Ferentis UAB, Vilnius, Lithuania

[13]CollPlant Ltd., Ness-Ziona, Israel Regenerative Engineering and Translational Medicine

Abstract

Purpose

To determine feasibility of plant-derived recombinant human collagen type I (RHCI) for use in corneal regenerative implants

Methods

RHCI was crosslinked with 1-ethyl-3-(3-dimethyl aminopropyl) carbodiimide (EDC) and N-hydroxysuccinimide (NHS) to form hydrogels. Application of shear force to liquid crystalline RHCI aligned the collagen fibrils. Both aligned and random hydrogels were evaluated for mechanical and optical properties, as well as in vitro biocompatibility. Further evaluation was performed in vivo by subcutaneous implantation in rats and corneal implantation in Göttingen minipigs.

Results

Spontaneous crosslinking of randomly aligned RHCI (rRHCI) formed robust, transparent hydrogels that were sufficient for implantation. Aligning the RHCI (aRHCI) resulted in thicker collagen fibrils forming an opaque hydrogel with insufficient transverse mechanical strength for surgical manipulation. rRHCI showed minimal inflammation when implanted subcutaneously in rats. The corneal implants in minipigs showed that rRHCI hydrogels promoted regeneration of corneal epithelium, stroma, and nerves; some myofibroblasts were seen in the regenerated neo-corneas.

Conclusion

Plant-derived RHCI was used to fabricate a hydrogel that is transparent, mechanically stable, and biocompatible when grafted as corneal implants in minipigs. Plant-derived collagen is determined to be a safe alternative to allografts, animal collagens, or yeast-derived recombinant human collagen for tissue engineering applications. The main advantage is that unlike donor corneas or yeast-produced collagen, the RHCI supply is potentially unlimited due to the high yields of this production method.

Lay Summary

A severe shortage of human-donor corneas for transplantation has led scientists to develop synthetic alternatives. Here, recombinant human collagen type I made of tobacco plants through genetic engineering was tested for use in making corneal implants. We made strong, transparent hydrogels that were tested by implanting subcutaneously in rats and in the corneas of minipigs. We showed

that the plant collagen was biocompatible and was able to stably regenerate the corneas of minipigs comparable to yeast-produced recombinant collagen that we previously tested in clinical trials. The advantage of the plant collagen is that the supply is potentially limitless.

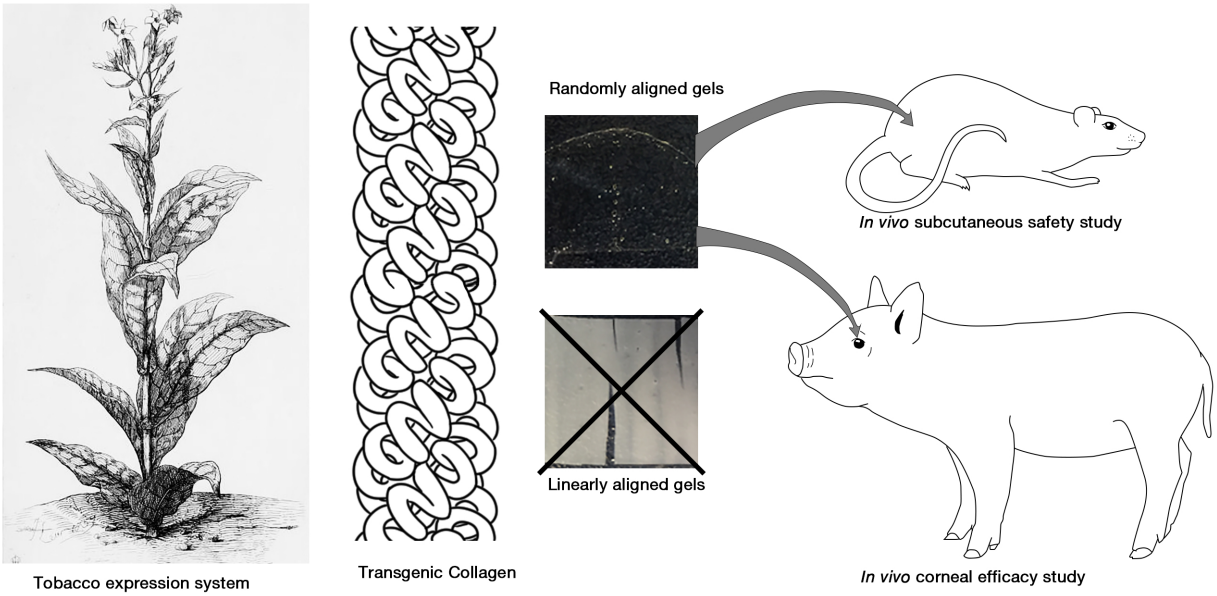

Introduction

The human cornea is the transparent front of the eye that focuses incoming light onto the retina for vision. Its cellular layers comprise an outermost epithelium, a middle stroma composed of collagenous extracellular matrix (ECM) with interconnected keratocytes, and an innermost endothelium. It is heavily innervated, but avascular. Damage or disease leading to permanent transparency loss or surface distortion can result in corneal blindness. Historically, the only widely used treatment for restoring vision is human donor cornea (HDC) transplantation. However, a serious donor shortage has left an estimated 12.7 million patients worldwide waiting for corneal transplants [1]. Moreover, the outcome of conventional corneal transplantation is limited by immune rejection, ocular infection, and premature graft failure. Artificial corneas in the form of prostheses have been introduced in clinics, most notably the Boston KPro, AlphaCor, and osteo-odonto-keratoprosthesis (OOKP) [2,3,4]. All three prostheses are associated with potentially serious side effects and are regarded as a last resort treatment for patients with severe pathology or previous conventional graft failures [5]. Given the shortcomings of conventional corneal transplantation and insufficient performance of prostheses, various research groups have focused on the development of a range of corneal replacements [6, 7].

In 2010, Fagerholm et al. published the 2-year results of a clinical trial describing the first-in-human in situ tissue regeneration of the cornea. Tissue regeneration was achieved by implanting cell-free, bio-responsive recombinant human collagen type III (RHCIII) hydrogels [8]. RHCIII was selected as a homogenous, non-xenogeneic protein that minimizes the risk of allergic reactions to animal source collagens, or zoonotic disease transmission [9]. The results of the RHCIII hydrogels are promising, but the human cornea is primarily composed of type I collagen. Here, we examine the biocompatibility and efficacy of recombinant human collagen type I (RHCI) collagen hydrogels as implants in minipig corneas, compared to syngeneic grafts.

The RHCI implants designed for this study are the first to use plant-derived type I collagen. A prior comparison of RHCI and RHCIII has been made, but both collagens were produced in Pichia pastoris. Protein production in yeast is a fermentation-based process that requires the additional expression of two enzymes: prolyl 4-hydroxylase (P4H) and pepsin. PH4 is the enzyme that catalyzes the formation of 4-hydroxyproline amino acids from proline [10]. The 4-hydroxyproline amino acids are needed for stable triple helix formation. The recombinant pepsin is needed to cleave the telopeptides from the full-length protein before use [9]. This process is inherently limited by the fermentation batch size.

Plant-derived RHCI is generated from genetically modified tobacco plants, which allows the production of theoretically unlimited quantities of protein and supports agricultural development. The two genes encoding RHCI were co-expressed in tobacco plants with P4H and lysyl hydroxylase 3 (LH3) enzymes that were responsible for key post-translational modifications of the RHC [11]. Tobacco plants co-expressing all five vacuole-targeted proteins generated intact RHCI pro-collagen with stable triple helical structures. Tobacco plant–derived RHCI was shown to have equivalent biofunctionality to human tissue–derived collagen in other applications [11,12,13]. We recently reported that RHCI hydrogels were fully biocompatible with corneal cells and served as excellent substrates for corneal limbal epithelial stem cells, showing comparable efficacy to human amniotic membrane, the current gold standard for their culture [14].

Previous studies of collagen implants did not include attempts to align the collagen fibrils, although there have been numerous reports of attempts to align collagen fibrils for use as corneal implants, citing the need for transparency and mechanical strength [15, 16]. Here, we examined the properties of RHCI with aligned and random fibrils in vitro and their biocompatibility in vivo in a rat model. The RHCI hydrogel showing the most optimal properties for use as corneal implants was tested in a minipig model, where its efficacy was compared to that of allografting, simulating donor cornea transplantation.

Materials and Methods

The study followed the tenets of the Declaration of Helsinki and was approved by the Antwerp University Hospital Ethical Committee (EC: 14/30/319) for use of human amniotic membrane. Animal experiments in rats and Gottingen minipigs were performed in accordance with the Association for Research in Vision and Ophthalmology Statement for the Use of Animals in Ophthalmic and Vision Research, and the Swedish Animal Welfare Ordinance and the Animal Welfare Act, after ethical approval was acquired from the local Linkoping ethical committee (Linköpings Djurförsöksetiska Nämnd).

Materials All inorganic salts, enzymes, basic chemicals, and reagents were purchased from Sigma-Aldrich (St. Louis, MO, USA), unless stated otherwise. Plant-derived RHCI was provided by Collplant (Ness Ziona, Israel).

Recombinant Human Collagen Hydrogels

RHCI Hydrogels

To fabricate RHCI hydrogels with random fibrillogenesis (rRHCI), we use the protocol described in Haagdorens et al. [14]. Briefly, a 30% v/v solution of tobacco-derived RHCI in 10mM HCl was prepared by diluting with 100% ethanol. Fibrillogenesis was initiated by addition of 160 mM sodium phosphate buffer that was adjusted to pH 7.5 with 100 mM NaOH. The buffer was added at a ratio of 1:10 v/v to the original collagen-HCl volume. The solution was stirred for 2 h at 25°C; after which, water-diluted EDC and NHS were added to attain a 50 mM 1-ethyl-3-(3-dimethyl aminopropyl) carbodiimide (EDC) and 100 mM N-hydroxysuccinimide (NHS) concentration. The collagen solution was then stirred for 24 h at 4°C on a magnetic stirrer at 200 rpm. The solution was then transferred into a 50 mL tube for 6 cycles of washing to remove all excess EDC/NHS. Each cycle consisted of centrifuging the mixture at full-speed (5000 rpm, 10 min), discarding the supernatant and resuspending the collagen in 40 mL distilled water (DW). During the final wash cycle, the RHCI suspension was dispensed into a rectangular Teflon mold (4.5 × 4.5 cm) for in vitro characterization or into curved corneal-shaped and corneal-sized molds (10 mm diameter, 500-μm thick) as implants. The collagen was then air-dried under a sterile hood and immersed in 100% ethanol to promote detachment from the mold. The gels were stored in 100% ethanol until further use. Gels were rehydrated by five 2-h soaks in phosphate-buffered saline (PBS).

RHCI Hydrogels with Aligned Collagen Fibrils

For production of aligned RHCI membranes (aRHCI), shear force was applied to the collagen solution prior to fibrillogenesis and chemical crosslinking. Shear force was effected using a motorized automatic film applicator, Elcometer 4340 (Elcometer Ltd, Manchester, UK) and an Elcometer 3570 "Doctor Blade" that served as the orthogonal force. After ethanol dilution, the acidic RHCI was cast onto a glass plate that was mounted in the Elcometer. The glass plate had previously been surface-coated with a hydrophobic siloxane solution. After collagen casting, shear force was applied at a constant speed of 0.02 m/s and a thickness of 50 μm. After the RHCI had spread, the glass plate was immediately lifted from the Elcometer and immersed in a bath of fibrillogenesis buffer. This was performed very carefully in order not to disrupt the collagen membrane. Membranes were then crosslinked for 24 h in fibrillogenesis buffer and 50 mM EDC and 100 mM NHS. Crosslinked membranes were then rinsed four times in DW and peeled from the glass plate. Hydrogels were kept in 100% ethanol until further use.

Human Amniotic Membrane

Human amniotic membrane (HAM), prepared following our previous protocol, was used as a benchmark [14]. Written informed consent was collected from the donors, women undergoing scheduled cesarean section. Briefly, HAM was washed in an antibiotic cocktail and then flattened onto sterilized nitrocellulose filter paper, epithelial side up. The paper-supported HAM was then cut into 5cm × 5cm pieces and cryopreserved at -80°C in 50% Dulbecco's Modified Eagle Medium (DMEM), 50% glycerol. The membrane was quarantined for 4 weeks during which time sterility and serology testing were performed to confirm safety. Prior to use, HAM was thawed, epithelial cells removed, and the cell-free membrane was washed. For use, HAM is oriented spongy layer up, after which excessive water is mechanically expelled using cell scrapers. For stabilization, HAM was mounted "spongy layer" down in a CellCrown or interlockable ring [17].

Physical and Mechanical Characterization

To measure water content, samples were DW equilibrated for 24 h. Water content of samples was determined by weighing membranes that were blotted dry to remove excess surface liquid to obtain the wet weight (W0). These samples were then dried in a drying oven (60°C) for 24 h to obtain the dry weight (W). Equilibrated water content of hydrogels (Wt%) was obtained according to the following equation: Wt% = (W0 - W)/W0 × 100%.

The refractive index (RI) of samples was measured of fully hydrated membranes using an Abbe refractometer (Model C10, VEE GEE Scientific Inc., Kirkland, WA, USA) at 21°C with DW as the calibration agent.

To test membrane light transmission, 6-mm acellular discs of the sample were punched out and placed in a glass bottom 96-well plate. Using the previously published protocol [18], light absorbance was measured at room temperature for specific wavelengths of the visual spectrum (405, 450, 490, 530, and 630 nm) with the VICTOR3 microplate reader (PerkinElmer). Percentage of light transmittance was calculated with the following equation: transmission (%) = 10(2 - absorbance). Wells mounted with 100 μL of trypan blue or DW served as negative and positive controls, respectively. Transmittance values were normalized to demineralized water.

Oscillatory rheology was performed on a Discovery Hybrid Rheometer (DHR2; TA Instruments, Sollentuna, Sweden) using 8 mm diameter, parallel-plate, stainless steel geometry. Frequency sweeps were performed at a constant shear strain amplitude of 0.267% at 25°C.

Tensile testing of the membrane samples was performed on a vertical stress-strain testing device (Instron 3345, Canton, MA, USA) fitted with a 100 N load cell. Testing was performed at a 2 mm/min rate. Membrane samples where cut into 4 × 0.5-cm-long strips and fixed at both ends to a 1-mm-thick polypropylene frame. The ultimate tensile strength (UTS) was calculated based on the area of the sample (sample thickness measured with optical coherence tomography; RTVue 100–2, Optovue, California, USA).

Hydrogel Stability and Susceptibility to Enzymes and Microbial Attack

The stability of the hydrogels was tested against in vitro degradation by collagenase enzyme [19]. In brief, samples (n = 3) equilibrated in Tris-HCl buffer (0.1 M, pH 7.4) were incubated in 5 mL 5 U/mL type I collagenase dissolved in Tris-HCl at 37°C. The undigested mass was weighed at time 0 (W'0) and every 60 min (W't) until the sample was completely digested. At every interval, surface water was blotted away, and samples were weighed three times independently using an ultra-microbalance (SE2, Sartorius, Göttingen, Germany). The percentage of mass remaining after digestion was calculated according to the following equation: Residual mass (%) = (W't/W'0) × 100%. As a control, HAM was incubated in Tris–HCl buffer only and weighed at the same time points.

For determination of attack by common bacteria causing blindness, such as Gram-negative Pseudomonas aeruginosa, fully hydrated samples equilibrated in PBS were cut into 1 cm2 pieces. Hydrogels were mounted in a 24 well-plate and fixed using a CellCrown. As previously described by Dravida et al. [20], a dilution of 10-1 of two P. aeruginosa strains (ATCC 15442 and ATCC 9027) was made in Tryptic Soy Broth (TSB). Using a 22 gauge needle, 100 μL solution was injected into the scaffold (n = 3 for each ATCC strain). The inoculated scaffolds were incubated in an oven (37°C) for 24 h. The samples were homogenized in PBS using a tissue grinder. The homogenized extracts were diluted in the range of 10-10-8 and plated on agar (TSA). The number of colony-forming units (CFU)/mL was determined 24 h later. To have sufficiently thick amnion to inject the solution, mechanical scraping of the spongy layer was not performed for this experiment. Injection of 100 μL bacterial solution in 10 mL TSB and 10 mL PBS served as negative and positive controls respectively.

Ultrastructural Characterization

Atomic Force Microscopy

Membrane samples of 10 × 10 mm^2 were cut out and placed onto a rigid support carrier. The carrier, a glass slide that had functional aldehyde surface groups (developed in-house), was then immersed in PBS to allow full rehydration of the sample prior to atomic force microscopy (AFM) imaging. HAM samples received additional gentle mechanical scraping with cell scrapers to remove excess spongy layer, thus exposing the underlying membrane and reducing height variation. While imaging, samples were kept hydrated. AFM imaging was carried out in PBS by a NanoWizard 3 (JPK Instruments, Germany) system using NSC35 probes (MicroMasch, Germany) and the force curve acquisition-based Quantitative Imaging™ (QI) mode. Topography images were generated with the setpoint height channel in the QI-mode, setpoint force 5–10 of nN. Fibril diameters were estimated from height cross-sections extracted from the AFM images. Full-width at half-maximum was measured where the image resolution was sufficient. In other cases (e.g., rRHCI characterized by very fine fibrils), a trained operator's estimates were used.

Electron Microscopy

Samples of biomaterials were fixed and prepared for scanning electron microscopy (SEM) and transmission electron microscopy (TEM) as we previously described in Haagdorens et al. [14]. Gold sputter-coated samples were imaged on a SEM 515 Microscope (Philips, Eindhoven, The Netherlands) for surface features [14]. Ultra-thin sections were cut from osmicated samples embedded in EMbed 812 (Electron Microscopy Sciences, Hatfield, PA). Ultrathin sections were stained with lead citrate and examined using a Tecnai G2 Spirit Bio Twin Microscope (FEI, Eindhoven, The Netherlands) at 120 kV.

In vivo Biocompatibility Testing in Rats

Random RHCI hydrogels, 11 mm in diameter and 1-mm thick, were implanted subcutaneously in rats (following ISO standard 10993-6:2007). Denuded HAM was also implanted as a comparison for RHCI. To achieve samples of sufficient thickness, 7 layers of HAM were stacked upon each other and sealed with fibrin glue (Tisseel, Baxter, Deerfield, IL, USA). Clotted fibrin sealant molded into 1-cm3 blocks were implanted as a control. In total, 5 collagen hydrogels, 4 HAM samples, and 3 fibrin clots were implanted subcutaneously. Two sham surgeries were performed to ensure that the skin healing process does not affect the outcome of biocompatibility testing. Postoperatively, extended assessment of health conditions of animals was performed based on an observational grading scheme (not shown).

At 3 months post-implantation, the animals were euthanized, and the implants and surrounding tissues were collected. Each rRHCI samples was subdivided into quarters for analysis. Quarters one and two were fixed in formalin, then embedded in paraffin or O.C.T. compound, respectively for histology and immunohistochemistry. One quarter was fixed in glutaraldehyde for EM. The final quarter was not analyzed. Recovered HAM, fibrin, and sham samples were similarly processed for histology and immunohistochemistry.

Non-consecutive paraffin sections, cut at 7-μm thick, were stained with hematoxylin and eosin (H&E) for histological evaluation. Based on H&E staining, two slides, each containing three tissue sections of the same sample, were used to assess biocompatibility as per Table S1 (adapted from ISO10993-6:2007 Table E3). According to this grading table, the test sample was considered a non-irritant (0 up to 2.9), slight irritant (3.0 up to 8.9), moderate irritant (9.0 up to 15.0), or severe irritant ($>$ 15). Grading was performed double-blinded. In brief, each H&E section was graded at five different sites, two at each respective end, and one in the middle of the sample. If remnants of the implant could be identified, the area of grading was at the junction of the sample and surrounding tissue.

Cryosections, 7-μm thick, were stained with antibodies to identify plasma cells (anti-syndecan-1), granulocytes (anti-myeloperoxidase), macrophages (anti-CD68), T-lymphocytes (anti-CD3), blood vessels (anti-vWF), and activated myofibroblasts (anti-αSMA) as previously described (Table S2) [38]. Immunofluorescent (IF) images were recorded using an inverted LSM-800 Zeiss confocal microscope (LSM800, Carl Zeiss Microscopy, Germany), and the percentage of positive staining area per view was calculated for each sample using the ImageJ software (National Institutes of Health, Bethesda, MD, USA). In each stained sample, the analysis was performed for three IF images at standard locations (left end, middle, and right end of the sample). A Kruskal-Wallis nonparametric test was used with a Dunn's multiple comparisons post hoc test. Statistical analysis was performed in GraphPad Prism 8.4.3. P $\leq$0.05 was considered significant.

In vivo Efficacy Testing as Corneal Implants in Minipigs

To test in vivo safety and efficacy of corneal regeneration, the implants were evaluated in Göttingen minipigs, which are genetically uniform. Four animals were used in each treatment group. The left eyes of the pigs underwent surgical treatment, while the right eyes served as unoperated controls. All animals were subjected to anterior keratoplasty. The central section of corneal epithelium and stroma was removed to a depth of 500μm using a 6.5-mm surgical trephine and a scalpel. Solid

rRHCI gels were grafted into the wound bed, covered with HAM, and secured in place using interrupted sutures. In the control group, cornea excised from the other pigs in this study was used as implants, being secured with interrupted sutures. These were syngeneic grafts rather than conventional allografts, as they are from genetically identical donors and recipients. The syngeneic grafts were secured using interrupted sutures. All operated eyes received corticosteroids and antibiotics in the form of topical dexamethasone/tobramycin eye drops (Tobrasone, Alcon, Sweden). The dexamethasone/tobramycin was applied 3 times daily for the first 5 postoperative days. The pigs were monitored daily for any eye-related complications for the entire study duration. Clinical exams were performed pre-operation, and then at 6 weeks, and 3, 6, 9, and 12 months post-operation according to protocols as we described in McTiernan et al. [21]. Briefly, all operated and control corneas were examined by slit lamp biomicroscopy (for haze, redness), anterior segment optical coherence tomography (for corneal changes including thickness), Schirmer's tear test (for tear production), and aesthesiometry (for touch sensitivity). At the endpoint of 12 months post-operation, all animals were euthanized according to animal facility guidelines, and tissue samples of both operated and contralateral eyes were collected.

Samples from implanted and control corneas were processed for TEM as described in McTiernan et al. [14, 21, 22]. In brief, samples were prepared for TEM by fixing a quarter of each cornea in 2.5% glutaraldehyde solution in 0.1 M sodium cacodylate buffer (pH 7.4). After fixing, the quarters were cut into 1-mm wide strips. The strips were postfixed in 1% OsO_4 solution for 2 h, dehydrated through an ethanol series and embedded in EMbed 812 (Electron Microscopy Sciences, Hatfield, Pennsylvania). Ultrathin sections stained with lead citrate were imaged on a Tecnai G2 Spirit Bio Twin Microscope (FEI, Eindhoven, The Netherlands) at 120 kV.

In vivo confocal microscopy examinations were performed before surgery and at 3, 6, 9, and 12 months post-surgery. Images taken were used for nerve counts as described in McTiernan et al. [21]. When nerves where observed, they were defined as bright, slender, straight, or branched structures and were sufficiently different from the background intensity level. NeuronJ, a nerve tracing and analysis software, and FIJI were used together for measuring the total length of the observed nerves [23]. Corneal nerve densities were based on averaging the highest nerve density for each treatment group and time point from individual images.

Statistics

For all tests of hydrogels, a minimum of three samples was used in evaluations. For the in vivo

subcutaneous studies, 5 RHCI hydrogels, 4 HAM samples, and 3 fibrin clots were implanted. The additional RHCI and HAM samples were implanted just in case animals died from unrelated causes, as these samples were more difficult to obtain. As all animals remained healthy and survived, so, all samples were analyzed for potential adverse immune cell infiltration or activation by differential cell counts followed by a Kruskal-Wallis nonparametric test as described above.

The unit of analysis for the in vivo study in minipigs was the eye (RHCI n=4, syngeneic graft n=4, unoperated n=8). Clinical variables over time (Fig. 3a–f) were analyzed with a mixed effects model with matched stacking, no assumption of sphericity, and $\alpha = 0.05$ using a post hoc Tukey's multiple comparison test. Statistical analysis and graphing were performed using GraphPad Prism v8.4.3 (GraphPad Software LLC, San Diego, CA, USA).

Results

Physical and Mechanical Properties of RHCI Hydrogels

The properties of the aligned and random RHCI hydrogels, compared to HAM, are summarized in Fig. 1. Both types of collagen hydrogel and control HAM displayed a RI that approximates that of the human cornea (1.37–1.38). The rRHCI hydrogels allowed for light transmittance within the visual spectrum of over 91% (Fig. S1) while aRHCI hydrogels showed only 37% light transmission, appearing opaque (Fig. S1, 1a). Figure 1a also shows that the aRHCI hydrogels were prone to splitting along the direction of the collagen fibrils. HAM, which served as a control, showed light transmission of 66%. The opacity of the aRHCI hydrogels precluded its use for corneal implants, while it was tested for toxicity and biocompatibility as subcutaneous implants in rats, it was not tested as corneal implants in vivo. The rRHCI hydrogels used for corneal implantation, however, was robust, pliable, and easy to manipulate when molded into corneal-shaped and corneal-sized im

Both aligned and random hydrogels, as well as HAM, showed a predominantly elastic, rather than viscous behavior with storage moduli much higher than loss moduli. However, due to the very low thickness of HAM, reliable data from oscillatory rheology was not possible to obtain and therefore, eliminated from further comparisons. The G' of rRHCI gels was found to be 2.9 ± 0.03 kPa, whereas that of aRHCI hydrogels was found to be 0.383 ± 0.03 kPa indicating a 10-fold higher stiffness for the rRHCI (Fig. S3). The aRHCI hydrogels have slightly higher water content compared to their random counterparts. Moreover, the G" of the rRHCI hydrogels was found to be 0.158 ± 0.036 kPa resulting in a tanδ of 0.05 ± 0.01. Stress strain analysis shows that both RHCI hydrogels

display stress and strain values that are inferior to that of HAM membrane. These results reveal that HAM displayed roughly three times greater energy absorption compared to random RHCI hydrogels. Young's modulus indicates that the latter are much stiffer than the HAM. The aRHCI hydrogels were inherently too weak to allow stress-strain analysis

Collagenase degradation assays showed that aligned and random RHCI hydrogel degradation was complete by 8 h and 16 h respectively (Fig. S4). The degradation of HAM was slower, with complete degradation occurring after 24 h. Inoculation with P. aeruginosa showed that RHCI hydrogels, irrespective of fibril alignment or not, were 50- to 100-fold more resistant to microbial contamination for both strains of Pseudomonas (Table S3) compared to HAM. We recently showed in Haagdorens et al. that RHCI hydrogels were biocompatible with human corneal epithelial cells and supported their growth [14].

Ultrastructure

Surface scanning by AFM (Fig. 1d–f) confirmed the random arrangement of fibrils in rRHCI hydrogels, and the unidirectional alignment of the RHCI fibrils in the shear-mediated preparation of aRHCI. It was noted that the collagen fibrils in the aRHCI hydrogels are thicker (93.8 ± 30.6 nm in diameter) than the fibrils in the rRHCI hydrogels (23.6 ± 10.4 nm in diameter). This showed that the fibrils had assembled into distinct thicker bundles of fibrils or collagen fibers. Fibrils in the random hydrogel were very fine, but also matted in areas. HAM fibrils were more similar to aRHCI in thickness (112.6 ± 61.7 nm in diameter).

SEM (Fig. 1g–i) confirmed the unidirectional collagen orientation in the surface of aHCI hydrogels. The rRHCI hydrogels showed a smooth surface. SEM imaging of HAM revealed complete removal of amniotic epithelium and exposure of the underlying basement membrane. At the amniotic basement membrane, remaining cellular debris and extracellular matrix (ECM) could be seen between collagen fibers.

TEM of rRHCI hydrogels confirmed the presence of fine collagen fibrils distributed randomly throughout the sample (Fig. 1k) as revealed by AFM. In the aRHCI, the fibrils formed thick collagen bundles (Fig 1j) as seen in the cross-sectional views. They showed unidirectional alignment in contrast to the interpenetrating thin collagen fibrils.

In vivo Biocompatibility in Rats

After subcutaneous implantation of the rRHCI hydrogels in rats, the animals did not exhibit any general or implantation-site adverse symptoms. Upon recovery of the implants, there were no clear macroscopic signs of implant degeneration, and the RHCI hydrogels could easily be distinguished from the surrounding tissues. Based on grading of the H&E-stained samples (Fig. 5a–f), RHCI hydrogels were ruled as being slightly irritant, with an average grading score of 7.33, well comparable to controls with scores of 7.63 for fibrin, 9.75 for HAM and 7.93 for sham (Table S4). Transmission electron microscopy images of implanted hydrogels showed isotropic collagen fibers interspersed with capillaries and small blood vessels, along with fibroblasts (Fig. 2b–e). Microscopically, some degree of disintegration was evident, and the RHCI hydrogels were mainly infiltrated by lymphocytes, fibroblasts, and macrophages with some ingrowth of capillary vessels (Fig. 2f). Even though granulocytes were not identified in the H&E sections, some cells stained positive for anti-myeloperoxidase, a granulocyte marker, in the IF pictures (Fig. 2f). Statistical analysis of the prevalence of infiltrating cells showed statistically significant ($P \leq 0.05$) elevated levels of T-lymphocytes, von Willebrand factor (vWf) positive cells, macrophages, and granulocytes compared to HAM, but no significant difference compared to other groups (Fig. 2g). The plasma cell staining was higher in the RHCI group compared to both HAM and fibrin glue. No significant differences among groups were found in the myofibroblast counts.

In vivo Performance in Minipigs

Results for the clinical observations of syngeneic grafts and their unoperated contralateral untreated corneas were previously reported in McTiernan et al. as the same four animals served as controls for the two different studies [21]. Clinical results are summarized in Fig. 3. At 6 weeks post-operation, the RHCI implants were completely covered with regenerated epithelium, as noted from clinical observation and slit lamp. The corneal thickness in the RHCI group was close to unoperated ranges at 3 months, and indistinguishable from unoperated by 6 months onwards (Fig. 3a). Even though there looks to be a trend towards a thicker cornea in the RHCI group compared to the syngeneic graft, this difference was statistically non-significant.

There is a statistically significant amount of haze in the RHCI group (Fig. 3c) that decreased with time and was scored at zero in two out of the four animals at the 12-month point. At the 12-month point, the difference between groups is not statistically significant (Tukey's multiple comparisons α=0.05).

The subepithelial nerve plexus recovered fast, and at 12 months, nerve plexus morphology in the RHCI group resembled that of unoperated animals as seen in IVCM in Fig. 4. Nerve density of the corneal stroma, as noted based on IVCM, was close to normal ranges in both groups at 3 months onwards (Fig. 3e). One animal in the RHCI group had haze in the regenerated cornea that did not allow for imaging to obtain nerve counts. The missing datapoints were taken into account by using a mixed model rather than ANOVA for this comparison. All the pigs regained touch response in the operated eye prior to 12 months. Statistical analysis could not be performed due to uneven state of sedation of the animals during measurement.

Intraocular pressure was indistinguishable from unoperated eyes at all timepoints in both the RHCI group and the syngeneic grafts (Fig. 3b). The normal intraocular pressure (IOP) shows that there is no weakening of the cornea capable of causing long-term distortions or leakage, nor was the implant too rigid to cause increased pressure.

H&E sections showed that the stratified corneal epithelium and stroma have regenerated in the neo-corneas of all four pigs, to resemble those in the syngeneic grafts and untreated, healthy controls (Fig. 5g–l). Immunohistochemical staining showed full regeneration of a mucin-positive tear film and fully differentiated epithelial cells (Fig. 5). Antibodies against smooth muscle actin (α-SMA) showed the presence of positive cells in RHCI, most likely myofibroblasts, but not the syngeneic or control untreated corneas (Fig. 5y–ad).

Discussion

Plant-derived RHCI was successfully fabricated into aligned and random hydrogels. The RHCI was aligned to mimic the highly aligned, lamellar structure of collagen in the cornea. Unfortunately, the aRHCI hydrogels were opaque. Despite the same net weight of RHCI in the random and aligned gels, the aRHCI gels were thicker as the collagen assembled into thicker fibrils with variable spacing in between fibers. They also demonstrated extreme transverse mechanical weakness. The optical and mechanical deficits of the hydrogels in comparison to cornea is most likely due to the structural deficits of RHCI-only fibrils and a lack of perpendicular structural elements (for review, see Espana et al.) [24]. In the cornea, collagen protofibril formation is regulated through the incorporation of collagen V to create uniform protofibrils for subsequent fibrillar assembly [24]. In the absence of collagen V, collagen I produces thicker, branching, heterogeneous fibers like the ones observed by AFM and TEM in this study. These fibers are known to be incompatible with corneal transparency. Collagen fiber spacing also contributes to the aRHCI structural deficits.

The spacing of corneal collagen fibrils is regulated by small leucine-rich proteoglycans, preventing the compaction of the collagen fibrils seen in the aRHCI [24]. The high aRHCI fibril density also contributes to the limitations in light transmission through the hydrogels. Finally, the collagen fibrils in each lamellar layer of the cornea are aligned in different directions, providing uniform mechanical strength throughout the entire cornea [24]. The single layer, shear force alignment method used here was insufficient to produce the structural complexity required to fully mimic the human cornea and will undergo future modifications, in order to improve the transparency of the material.

By contrast, the rRHCI hydrogels were transparent and mechanically stronger in all directions. When compared to previously tested collagen hydrogels, the transparency of random RHCI hydrogels was equivalent to that of porcine collagen type I, yeast-sourced RHCI, RHCIII, and collagen-mimicking hydrogels [25,26,27,28,29]. Moreover, rRHCI hydrogels outperformed HAM and rat tail collagen type I gels in terms of light transmission and refractive index [30]. In this study, RHCI hydrogels degraded faster in collagenase than HAM. The data on HAM degradation times should however be interpreted carefully; in this study, HAM degraded much slower than earlier reported degradation times of 6–13 h [18, 20]. The variability in degradation speeds of HAM underscores the inconsistent state of donated HAM and the need for well-standardized carrier materials in ocular tissue engineering. Aligned RHCI degraded too quickly for future clinical purposes without further modifications to its chemical formulation [31]. The difference in degradation time between both types of RHCI hydrogel may be attributed to the difference in collagen fibril density. One would assume, it would take longer to degrade the densely packed fibers in the aRHCI; however, without the interpenetrating fibrils holding the aligned fibers together, the hydrogel disintegrates into isolated fibers. Given the dense fibrillar network in the rRHCI hydrogels, these hydrogels degraded slower than aRHCI. Collagenase resistance of rRHCI was comparable to reported resistance of pure RHCIII, porcine collagen type I, and rat tail collagen type I hydrogels, with 8 h, 12–20 h, and 8 h degradation time respectively [19, 20, 25, 32].

As demonstrated by Griffith et al., collagen hydrogels have a tendency of being more resistant to microbial contamination when compared to HAM or the human cornea [20, 33]. As we inoculated membranes with P. aeruginosa, a bacterium responsible for causing severe corneal ulcers, results confirmed the relative microbial resistance of RHCI compared to amniotic membrane. Microbial contamination of grafts is a serious and widespread problem in ocular surgery because it often causes devastating infections and loss of implanted material [20]. With a 100-fold resistance to microbial infection, RHCI has a clear advantage over HAM in a clinical setting, where substrates are manipulated repeatedly in clean rooms prior to transport to the operating theater.

By implanting RHCI hydrogels subcutaneously in rats, we demonstrated that they were biocompatible in mammals and elicit minimal inflammation. Furthermore, the recovered hydrogel implants had initiated partial degradation. As we and other groups previously reported intact hydrogel retrieval after 90 days of implantation, this might indicate that additional crosslinking or incorporation of interpenetrating phospholipids to RHCI might improve the stability of the implant [19, 25, 27, 28, 34]. There was formation of new collagen fibers within the implants. This suggests that infiltrating fibroblasts had begun to remodel the implant. Similar observations have been made in corneal implants that were implanted in pigs, where host keratocytes remodeled the implants' fibrillar structure [19, 35]. By computer analysis of immunofluorescent images, we were able to quantify leukocytosis and neovascularization of retrieved implants and compare results to the isoproterenol-based H&E grading system. Interestingly, no granulocytes could be identified in H&E sections, whereas anti-myeloperoxidase, a marker for granulocytes, showed to be focally positive by immunohistochemistry, showing that H&E histopathological examination should be supplemented by immunohistochemistry using known markers for target cells. In 2016, Van Essen et al. published their results on automated analysis of IF area staining for fish scale-derived collagen matrices that were implanted subcutaneously in rats for 11 weeks [36]. With reported area of stain of $<1\%$ for macrophages and T-lymphocytes, results are very similar to the values we found. Moreover, area of stain for granulocytes appears to be lower for RHCI hydrogels compared to reported values for fish scale matrices. The presence of α-SMA positive cells that are myofibroblast-like in the RHCI corneas are in keeping with the haze that was noted. They also correspond to the results from the subcutaneous study showing that RHCI was a mild irritant. It is possible that there may be traces of plant material that contributed to the irritation and activation of stromal cells.

Although there are collagens that are derived from bovine and porcine skin which are widely available and offer a potentially unlimited supply source, an important consideration for the use of xeno-derived collagen is the potential risk for allergic reactions to xenogeneic biomaterials [37] and zoonotic pathogen transmission [38] if tight processing controls are not adhered to. Overall, plant-derived RHCI was largely biocompatible and immune compatible. RHCI hydrogels promoted regeneration of corneal tissue and nerves when grafted into the corneas of minipigs. Finally, application of RHCI should not solely be restricted to ocular regeneration, as collagen type I is abundantly present throughout the body. Aligned RHCI, with its unique collagen alignment, might find its way in musculoskeletal tissue engineering, whereas random hydrogels might be explored in cutaneous or cardiac regeneration [39,40,41].

Conclusions

RHCI hydrogels made from random collagen fibrils were biocompatible and promoted corneal regeneration in minipigs. This shows that the plant-derived collagen serves as a viable source of collagen for tissue engineering and regenerative medicine applications, such as for promoting in situ tissue regeneration of the cornea after further optimization and testing.

Data Availability

Data collected and analyzed for this study are provided in the Electronic Supplemental Material. Other data generated during the current study are available from the corresponding authors on reasonable request. RHCI available from CollPlant Ltd.

References

(1) Gain P, Jullienne R, He Z, Aldossary M, Acquart S, Cognasse F, et al. Global survey of corneal transplantation and eye banking. JAMA Ophthalmol. 2016;134(2):167–73. https://doi.org/10.1001/jamaophthalmol.2015.4776.

(2) Holak SA, Holak HM, Bleckmann H. AlphaCor keratoprosthesis: postoperative development of six patients. Graefe's Arch Clin Exp Ophthalmol = Albrecht von Graefes Archiv für klinische und experimentelle Ophthalmologie. 2009;247(4):535–9. https://doi.org/10.1007/s00417-008-0964-7.

(3) Zerbe BL, Belin MW, Ciolino JB, Boston Type 1 Keratoprosthesis Study G. Results from the multicenter Boston Type 1 Keratoprosthesis Study. Ophthalmology. 2006;113(10):1779.e1-7. https://doi.org/10.1016/j.ophtha.2006.05.015.

(4) Casey TA. Osteo-odonto-keratoprosthesis. Proc R Soc Med. 1966;59(6):530–1.

(5) Schrage N, Hille K, Cursiefen C. Aktuelle Versorgungsmöglichkeiten mit Keratoprothesen. Ophthalmologe. 2014;111(11):1010–8. https://doi.org/10.1007/s00347-013-3009-5.

(6) Ghezzi CE, Rnjak-Kovacina J, Kaplan DL. Corneal tissue engineering: recent advances and future perspectives. Tissue Eng B Rev. 2015;21(3):278–87. https://doi.org/10.1089/ten.TEB.2014.0397.

(7) Griffith M, Alarcon EI, Brunette I. Regenerative approaches for the cornea. J Intern Med. 2016;280(3):276–86. https://doi.org/10.1111/joim.12502.

(8) Fagerholm P, Lagali NS, Merrett K, Jackson WB, Munger R, Liu Y, et al. A biosynthetic alternative to human donor tissue for inducing corneal regeneration: 24-month follow-up of a phase 1 clinical study. Sci Transl Med. 2010;2(46):46ra61. https://doi.org/10.1126/scitranslmed.3001022.

(9) Yang C, Hillas P, Tang J, Balan J, Notbohm H, Polarek J. Development of a recombinant human collagen-type III based hemostat. J Biomed Mater Res Part B Appl Biomater. 2004;69(1):18–24. https://doi.org/10.1002/jbm.b.20030.

(10) Vuorela A, Myllyharju J, Nissi R, Pihlajaniemi T, Kivirikko KI. Assembly of human prolyl 4-hydroxylase and type III collagen in the yeast Pichia pastoris: formation of a stable enzyme tetramer requires coexpression with collagen and assembly of a stable collagen requires coexpression with prolyl 4-hydroxylase. EMBO J. 1997;16(22):6702–12. https://doi.org/10.1093/emboj/16.22.6702.

(11) Stein H, Wilensky M, Tsafrir Y, Rosenthal M, Amir R, Avraham T, et al. Production of bioactive, post-translationally modified, heterotrimeric, human recombinant type-I collagen in transgenic tobacco. Biomacromolecules. 2009;10(9):2640–5. https://doi.org/10.1021/bm900571b.

(12) Abir R, Stav D, Taieb Y, Gabbay-Benziv R, Kirshner M, Ben-Haroush A, et al. Novel extra cellular-like matrices to improve human ovarian grafting. J Assist Reprod Genet. 2020;37(9):2105–17. https://doi.org/10.1007/s10815-020-01832-4.

(13) Andrée B, Ichanti H, Kalies S, Heisterkamp A, Strauß S, Vogt P-M, et al. Formation of three-dimensional tubular endothelial cell networks under defined serum-free cell culture conditions in human collagen hydrogels. Sci Rep. 2019;9(1):5437. https://doi.org/10.1038/s41598-019-41985-6.

(14) Haagdorens M, Cėpla V, Melsbach E, Koivusalo L, Skottman H, Griffith M, et al. In vitro cultivation of limbal epithelial stem cells on surface-modified crosslinked collagen scaffolds. Stem Cells Int. 2019;2019:7867613–7. https://doi.org/10.1155/2019/7867613.

(15) Zhong SP, Teo WE, Zhu X, Beuerman R, Ramakrishna S, Yung LYL. Development of a novel collagen–GAG nanofibrous scaffold via electrospinning. Mater Sci Eng C. 2007;27(2):262–6. https://doi.org/10.1016/j.msec.2006.05.010.

(16) Torbet J, Malbouyres M, Builles N, Justin V, Roulet M, Damour O, et al. Orthogonal scaffold of magnetically aligned collagen lamellae for corneal stroma reconstruction. Biomaterials. 2007;28(29):4268–76. https://doi.org/10.1016/j.biomaterials.2007.05.024.

(17) Zakaria N, Koppen C, Van Tendeloo V, Berneman Z, Hopkinson A, Tassignon MJ. Standardized limbal epithelial stem cell graft generation and transplantation. Tissue Eng Part C, Methods. 2010;16(5):921–7. https://doi.org/10.1089/ten.TEC.2009.0634.

(18) Van den Bogerd B, Ní Dhubhghaill S, Zakaria N. Characterizing human decellularized crystalline lens capsules as a scaffold for corneal endothelial tissue engineering. J Tissue Eng Regen Med. 2018;12(4):2020–8. https://doi.org/10.1002/term.2633.

(19) Koulikovska M, Rafat M, Petrovski G, Veréb Z, Akhtar S, Fagerholm P, et al. Enhanced regeneration of corneal tissue via a bioengineered collagen construct implanted by a nondisruptive surgical technique. Tissue Eng A. 2015;21(5-6):1116–30. https://doi.org/10.1089/ten.tea.2014.0562.

(20) Dravida S, Gaddipati S, Griffith M, Merrett K, Lakshmi Madhira S, Sangwan VS, et al. A biomimetic scaffold for culturing limbal stem cells: a promising alternative for clinical transplantation. J Tissue Eng Regen Med. 2008;2(5):263–71. https://doi.org/10.1002/term.91.

(21) McTiernan CD, Simpson FC, Haagdorens M, Samarawickrama C, Hunter D, Buznyk O, et al. LiQD Cornea: Pro-regeneration collagen mimetics as patches and alternatives to corneal transplantation. Sci Adv. 2020;6(25):eaba2187. https://doi.org/10.1126/sciadv.aba2187.

(22) Jangamreddy JR, Haagdorens MKC, Islam MM, Lewis P, Samanta A, Fagerholm P, et al. Short peptide analogs as alternatives to collagen in pro-regenerative corneal implants. Acta Biomater. 2018;69:120–30. https://doi.org/10.1016/j.actbio.2018.01.011.

(23) Meijering E, Jacob M, Sarria JC, Steiner P, Hirling H, Unser M. Design and validation of a tool for neurite tracing and analysis in fluorescence microscopy images. Cytometry A. 2004;58(2):167–76. https://doi.org/10.1002/cyto.a.20022.

(24) Espana EM, Birk DE. Composition, structure and function of the corneal stroma. Exp Eye Res. 2020;198:108137. https://doi.org/10.1016/j.exer.2020.108137.

(25) Merrett K, Liu W, Mitra D, Camm KD, McLaughlin CR, Liu Y, et al. Synthetic neoglycopolymer-recombinant human collagen hybrids as biomimetic crosslinking agents in corneal tissue engineering. Biomaterials. 2009;30(29):5403–8. https://doi.org/10.1016/j.biomaterials.2009.06.016.

(26) Islam MM, Cėpla V, He C, Edin J, Rakickas T, Kobuch K, et al. Functional fabrication of recombinant human collagen–phosphorylcholine hydrogels for regenerative medicine applications. Acta Biomater. 2015;12:70–80. https://doi.org/10.1016/j.actbio.2014.10.035.

(27) Liu W, Deng C, McLaughlin CR, Fagerholm P, Lagali NS, Heyne B, et al. Collagen-phosphorylcholine interpenetrating network hydrogels as corneal substitutes. Biomaterials. 2009;30(8):1551–9. https://doi.org/10.1016/j.biomaterials.2008.11.022.

(28) Islam MM, Ravichandran R, Olsen D, Ljunggren M, Fagerholm P, Lee CJ, et al. Self-assembled collagen-like-peptide implants as alternatives to human donor corneal transplantation. RSC Adv. 2016;6(61):55745–9. https://doi.org/10.1039/C6RA08895C.

(29) Rafat M, Xeroudaki M, Koulikovska M, Sherrell P, Groth F, Fagerholm P, et al. Composite core-and-skirt collagen hydrogels with differential degradation for corneal therapeutic applications. Biomaterials. 2016;83:142–55. https://doi.org/10.1016/j.biomaterials.2016.01.004.

(30) Tidu A, Ghoubay-Benallaoua D, Lynch B, Haye B, Illoul C, Allain JM, et al. Development of human corneal epithelium on organized fibrillated transparent collagen matrices synthesized at high concentration. Acta Biomater. 2015;22:50–8. https://doi.org/10.1016/j.actbio.2015.04.018.

(31) Spoerl E, Wollensak G, Reber F, Pillunat L. Cross-linking of human amniotic membrane by glutaraldehyde. Ophthalmic Res. 2004;36(2):71–7. https://doi.org/10.1159/000076884.

(32) Koh LB, Islam MM, Mitra D, Noel CW, Merrett K, Odorcic S, et al. Epoxy cross-linked collagen and collagen-laminin Peptide hydrogels as corneal substitutes. J Funct Biomater. 2013;4(3):162–77. https://doi.org/10.3390/jfb4030162.

(33) Deng C, Li F, Hackett JM, Chaudhry SH, Toll FN, Toye B, et al. Collagen and glycopolymer based hydrogel for potential corneal application. Acta Biomater. 2010;6(1):187–94. https://doi.org/10.1016/j.actbio.2009.07.027.

(34) Merrett K, Fagerholm P, McLaughlin CR, Dravida S, Lagali N, Shinozaki N, et al. Tissue-engineered recombinant human collagen-based corneal substitutes for implantation: performance of type I versus type III collagen. Invest Ophthalmol Vis Sci. 2008;49(9):3887–94. https://doi.org/10.1167/iovs.07-1348.

(35) Liu W, Merrett K, Griffith M, Fagerholm P, Dravida S, Heyne B, et al. Recombinant human collagen for tissue engineered corneal substitutes. Biomaterials. 2008;29(9):1147–58. https://doi.org/10.1016/j.biomaterials.2007.11.011.

(36) van Essen TH, van Zijl L, Possemiers T, Mulder AA, Zwart SJ, Chou CH, et al. Biocompatibility of a fish scale-derived artificial cornea: cytotoxicity, cellular adhesion and phenotype, and in vivo immunogenicity. Biomaterials. 2016;81:36–45. https://doi.org/10.1016/j.biomaterials.2015.11.015.

(37) Rieder E, Steinacher-Nigisch A, Weigel G. Human immune-cell response towards diverse xenogeneic and allogeneic decellularized biomaterials. Int J Surg. 2016;36(Pt A):347e51. https://doi.org/10.1016/j.ijsu.2016.06.042.

(38) Silvipriya K, Kumar K, Bhat A, Kumar B, John A, Lakshmanan P. Collagen: animal sources and biomedical application. J Appl Pharm Sci. 2015;5:123–7. https://doi.org/10.7324/JAPS.2015.50322.

(39) Docheva D, Müller SA, Majewski M, Evans CH. Biologics for tendon repair. Adv Drug Deliv Rev. 2015;84:222–39. https://doi.org/10.1016/J.ADDR.2014.11.015.

(40) Shahrokhi S, Arno A, Jeschke MG. The use of dermal substitutes in burn surgery: acute phase. Wound repair and regeneration : official publication of the Wound

Healing Society [and] the European Tissue Repair. Society. 2014;22(1):14–22. https://doi.org/10.1111/wrr.12119.

(41) Kochegarov A, Lemanski LF. New trends in heart regeneration: a review. J Stem Cells Regen Med. 2016;12(2):61–8. https://doi.org/10.46582/jsrm.1202010.

(42) Prescott HP. Tobacco, and its adulterations. Lancet. 1853;62(1561):103–7. https://doi.org/10.1016/S0140-6736(02)39999-9.

Acknowledgements

We thank Dr. Christopher McTiernan, University of Ottawa Heart Institute, for the nerve counts in Fig. 4E. We acknowledge Science Advances (AAAS) for reproduction of results in Fig. 4 from McTiernan et al. We thank Prof. Dr. Sorcha Ní Dhubhghaill for her help with the pig surgeries, Prof. Dr. Nadia Zakaria for administration and logistics, and Ms. Nezahat Bostan and Ms. Eline Melsbach for procurement of the amniotic membranes and cadaveric donor eyes. Ms. Sofie Thys is acknowledged for performing the scanning electron microscopy and Ms. Bieke Vanhoutte for assisting in the microbial challenge testing. The tobacco plant in the graphical abstract is adapted from "Tobacco and its adulterations", this rendering is in the public domain [42].

Funding

Open access funding provided by Linkoping University. This research was funded with research grants from The Research Foundation Flanders (#FWO - 11ZB315N) to MH; EuroNanoMed II (G0D5615N to MJT) for the REGENERATE project in partnership with the Swedish Research Council (529-2014-7490 to MKL) and the Research Council of Lithuania (EuroNanoMed2-01/2015 to RV), and the European Cooperation in Science and Technology (EU-COST BM1302). MG acknowledges salary and research support from her Canada Research Chair Tier 1 in Biomaterials and Stem Cell in Ophthalmology and a Caroline Durand Foundation Research Chair in Cellular Therapy in the Eye, as well as a Honorary Professorship at the School of Optometry and Vision formation.

Ethics declarations

Ethics Approval

The Declaration of Helsinki guidelines were applied and were approved by the Antwerp University Hospital Ethical Committee (EC: 14/30/319) for use of human amniotic membrane. Animal experiments in rats and Göttingen minipigs were performed in accordance with the Association for Research in Vision and Ophthalmology Statement for the Use of Animals in Ophthalmic and Vision Research and the Swedish Animal Welfare Ordinance and the Animal Welfare Act, after ethical approval was acquired from the local Linkoping ethical committee (Linköpings Djurförsöksetiska Nämnd).

Competing Interests

Dr. Oded Shoseyov is a founder and chief scientist at CollPlant which produces and markets tobacco-derived RHCI. Other authors have no competing interests.

Figure Legends

Figure 1. Structural properties of RHCI hydrogels compared to human amniotic membrane (HAM). a Aligned hydrogels are semi-translucent and have the tendency of splitting unidirectionally. b Random collagen hydrogels are optically transparent. c Control HAM serves as reference. AFM (d–f) and SEM (g–i) of hydrogels, showing that in random hydrogels, very fine collagen fibrils were present, resulting in a smooth surface as revealed by SEM. Cross-sectional TEM of the hydrogels with aligned fibers (j) showed thick RHCI fibers (arrow) interspersed with thin collagen fibrils (arrowhead). The collagen fibers show unidirectional alignment, whereas the interpenetrating fibrils are randomly dispersed (k). Fibers were of varying thickness, 75–200-nm diameter. In random hydrogels, only fine collagen fibrils are seen, although some clumping was seen in the AFM and TEM images. l Collagen fibers were randomly oriented in HAM, with fibers showing distinct collagen banding (inset). The inset table shows the optical and mechanical characteristics of RHCI hydrogels and human amniotic membrane (HAM). *The stress test was not performed on the aligned RHCI hydrogels. **not performed

Figure 2. Subcutaneous RHCI hydrogel implantation in rats for 3 months. a H&E staining showing a delaminating RHCI implant (i) with infiltration of blood vessels, leukocytosis, and fibrosis. b Low magnification TEM image of recovered implants shows the implanted hydrogel in close approximation to the subcutaneous muscle (M). c Detailed TEM imaging shows clear fibroblast infiltration (*) and deposition of collagen fibers in bundles. d Typical collagen periodic D-banding is present in collagen fibers. e Region of implant degradation characterized by loosely packed collagen fibers, interspersed with capillaries (arrow), leucocytes, and fibroblasts (*). f Representative images of immunostained samples for macrophages, T-cells, granulocytes, plasma cells, myofibroblasts, and blood vessels in implants. g Graphs showing the percentage of immune-positive staining areas for each marker, a red * indicates a significant difference from the RHCI group ($p<0.05$)

Figure 3. Clinical results comparing RHCI grafted corneas with syngeneic grafts and untreated controls. Please note that the plots for the syngeneic grafts and unoperated controls were previously reported in McTiernan et al., as the same animals served as benchmarks for both studies. A Pachymetry results indicating corneal thickness was comparable to unoperated controls. B Central corneal haze was reported according to a modified variant of McDonald-Shadduck scale of 0–4 (from least to most haze). Haze peaked between 6 weeks and 3 months and then decreases. By 12 months, the difference among groups have decreased to a nonsignificant level (by Tukey's multiple comparisons). C The excised corneal nerves in the RHCI group showed penetrance into the graft

area after six months of tissue regeneration. Overall, the regenerated nerve density for RHCI and syngeneic grafts was equivalent to the unoperated eye at 12 months. D There was increased corneal neovascularization observed. This is also shown by an ANOVA, but the post hoc test could however not identify any particular time-point where there was a difference between the RHCI group and the groups (B) Intraocular pressure was similar in all animals, with an increase over time as the animals matured. C, F The Schirmer tear tests showed no marked changes in tear production in any group

Figure 4. In vivo confocal microscope images of RHCI and syngeneic grafted corneas, compared to unoperated healthy corneas. Scale bars, 100 μm. Insets, 100 $\times$ 100 μm. The insets show epithelial cell morphology in detail. Sub-epithelial nerves (arrows) in regenerated RHCI implanted corneas form parallel bundles like those of unoperated corneas, while those of syngeneic grafts were disorganized. Stromal keratocytes were present in all three groups. The endothelial layers of operated corneas retained a healthy morphology

Figure 5. Columns 1–4 shows each of the individual animals in the RHCI group. Column 5 shows representative images from the syngeneic graft. Column 6 shows representative images from unoperated controls. a–f Eyes of all RHCI grafted pigs and controls, showing haze in a and b. g–l Hematoxylin and eosin stained sections show morphologies of regenerated neo-corneas are comparable to those of the controls. Mucin staining (m–r) shows that the animals in the RHCI group have intact tear films. Cytokeratin 12(Ck12) staining (s-x) shows differentiated corneal epithelial cells in all samples. y–ad α-Smooth muscle actin (α-SMA), a myofibroblast marker shows the presence of activated fibroblasts in RHCI corneas, particularly in the ones with haze

Figures

Figure 1.

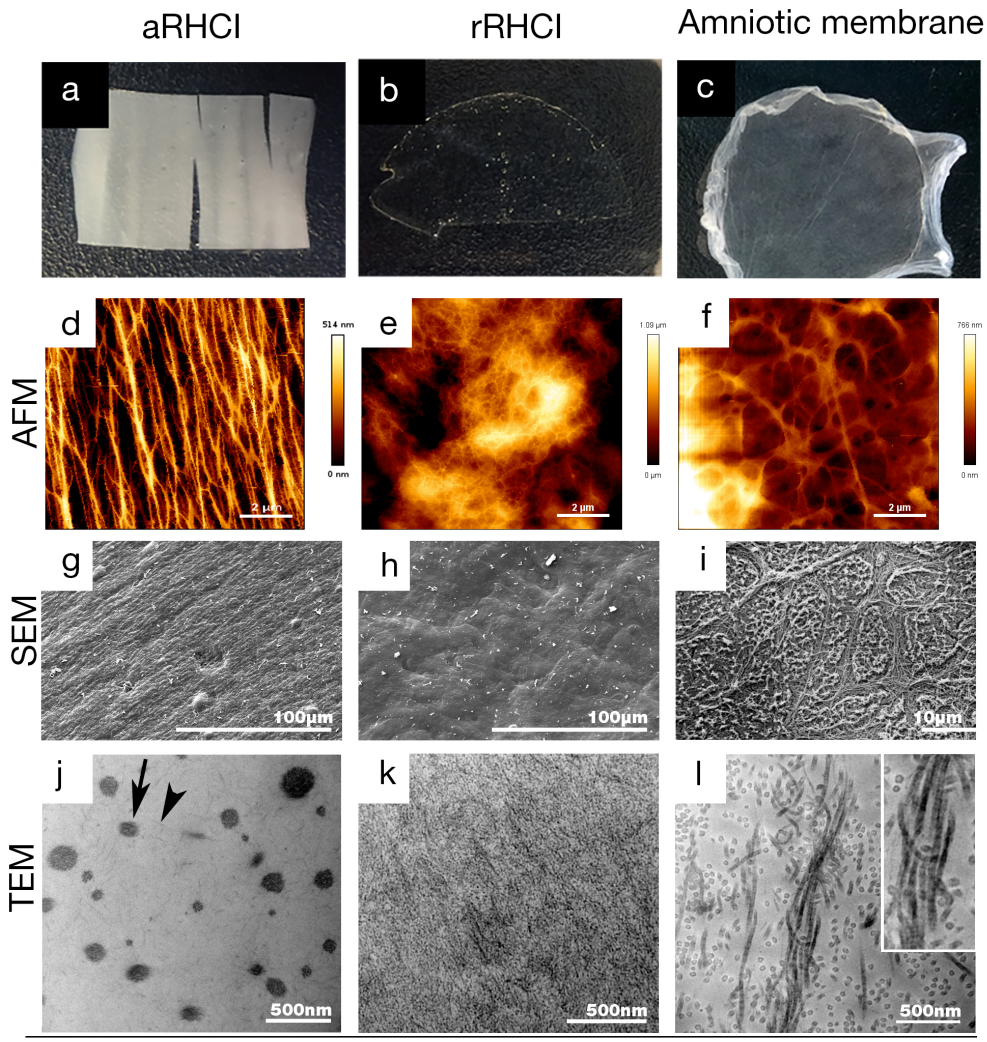

Properties	aRHCI	rRHCI	HAM	Human Cornea[1]
Water content (%)	92.21 ± 0.007	89.21 ± 0.003	87.68 ± 0.018	78
Transmission (%)	37.1	91.5	65.9	87
Tensile strength (MPa)	*	2.67±0.8	7.6±2.4	3.81 ± 0.4
Elongation at break (%)	*	28±6	68±10	**
Young's Modulus (MPa)	*	52.79±13.1	23.14±4.34	3-13

1: Fagerholm P, Lagali NS, Ong JA, Merrett K, Jackson WB, Polarek JW et al. Biomaterials. 2014;35(8):2420-7.

Figure 2.

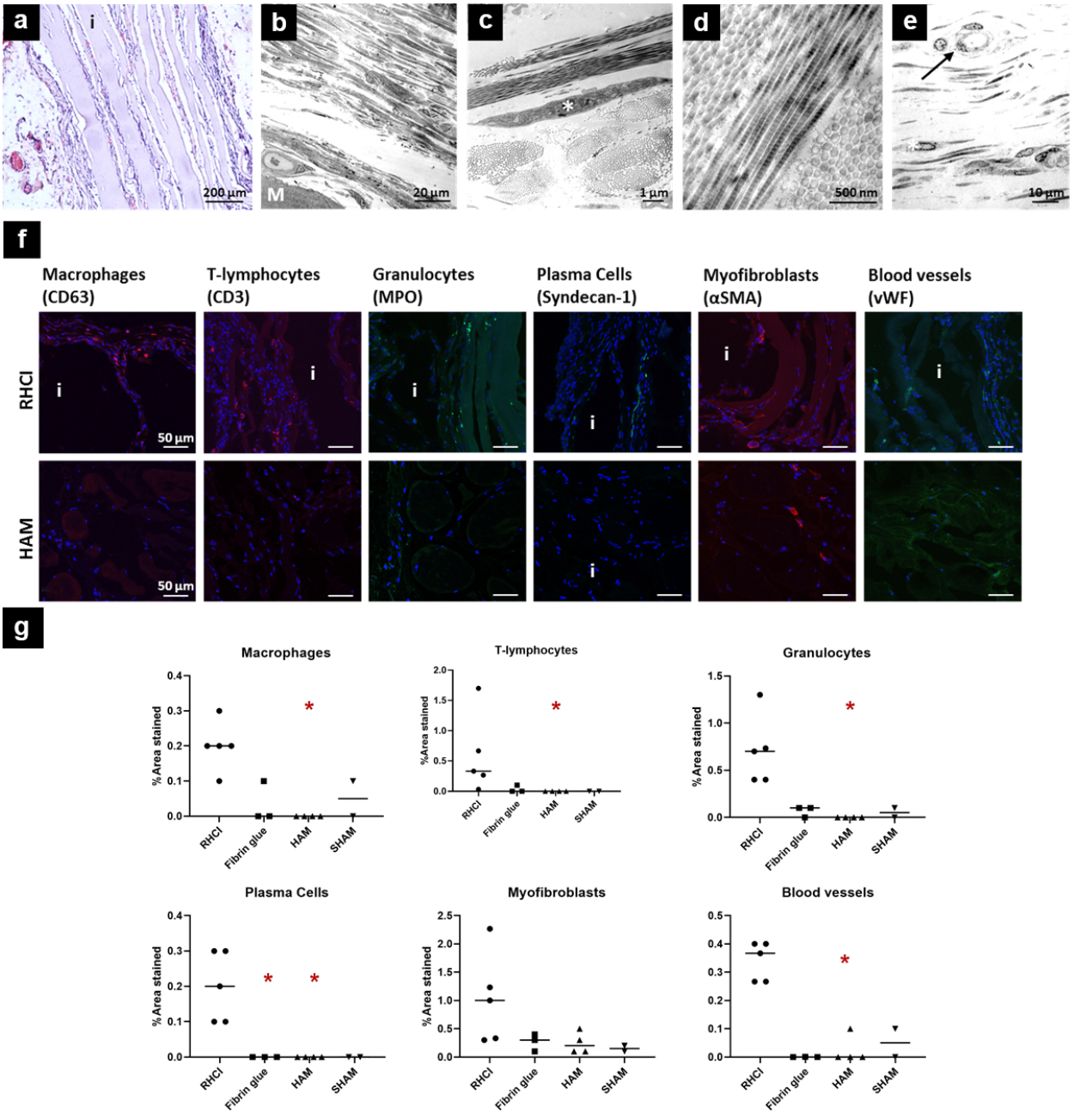
a
i
200 µm
b
M
20 µm
c
*
1 µm
d
500 nm
e
10 µm
f
Macrophages (CD63)
T-lymphocytes (CD3)
Granulocytes (MPO)
Plasma Cells (Syndecan-1)
Myofibroblasts (αSMA)
Blood vessels (vWF)
RHCI
HAM
50 µm
g
Macrophages
T-lymphocytes
Granulocytes
Plasma Cells
Myofibroblasts
Blood vessels
%Area stained
RHCI
Fibrin glue
HAM
SHAM

Figure 3.

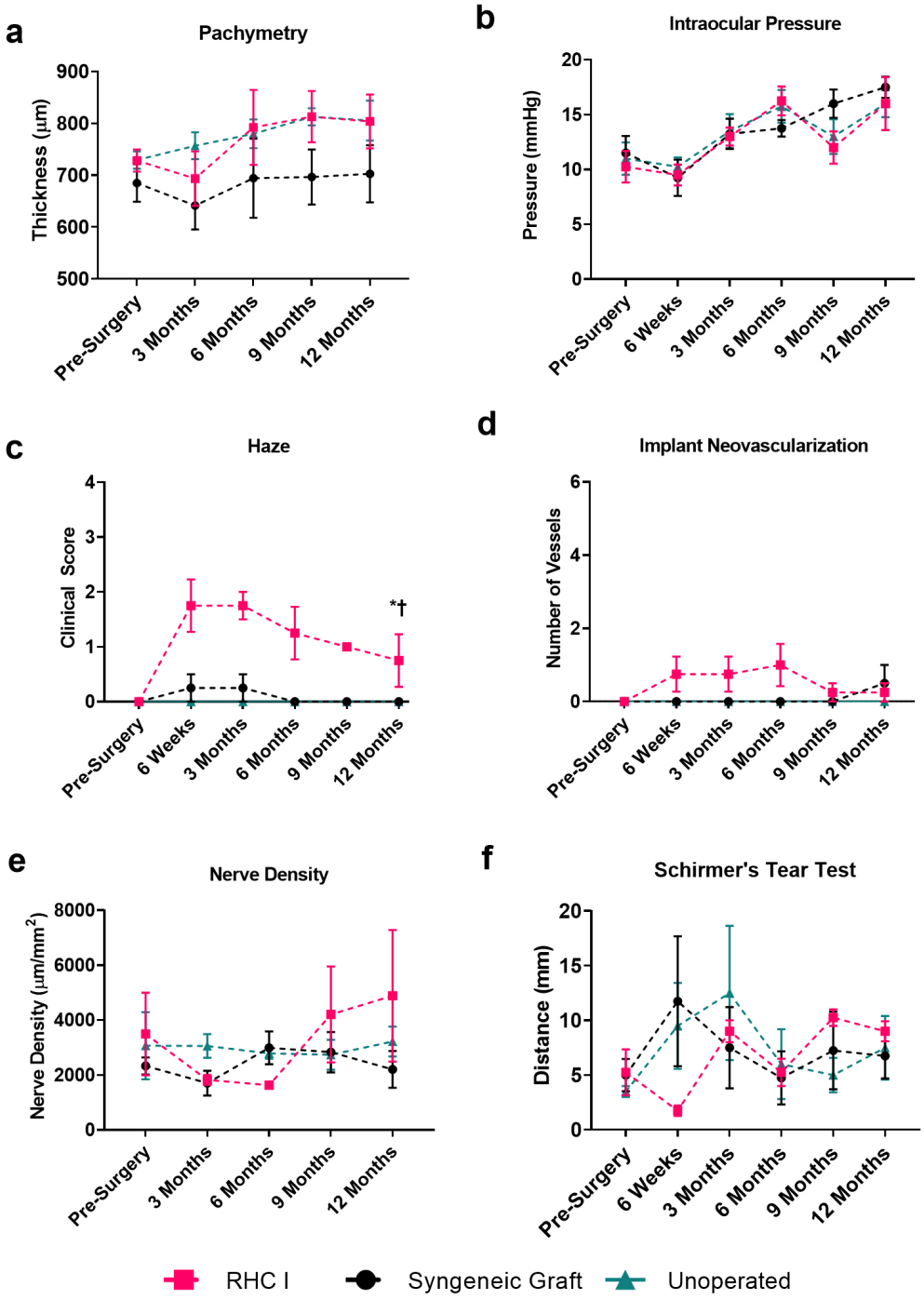
a
Pachymetry
Thickness (µm)
900
800
700
600
500
Pre-Surgery
3 Months
6 Months
9 Months
12 Months
b
Intraocular Pressure
Pressure (mmHg)
20
15
10
5
0
Pre-Surgery
6 Weeks
3 Months
6 Months
9 Months
12 Months
c
Haze
Clinical Score
4
3
2
1
0
*†
Pre-Surgery
6 Weeks
3 Months
6 Months
9 Months
12 Months
d
Implant Neovascularization
Number of Vessels
6
4
2
0
Pre-Surgery
6 Weeks
3 Months
6 Months
9 Months
12 Months
e
Nerve Density
Nerve Density (µm/mm²)
8000
6000
4000
2000
0
Pre-Surgery
3 Months
6 Months
9 Months
12 Months
f
Schirmer's Tear Test
Distance (mm)
20
15
10
5
0
Pre-Surgery
6 Weeks
3 Months
6 Months
9 Months
12 Months
RHC I
Syngeneic Graft
Unoperated

Figure 4.

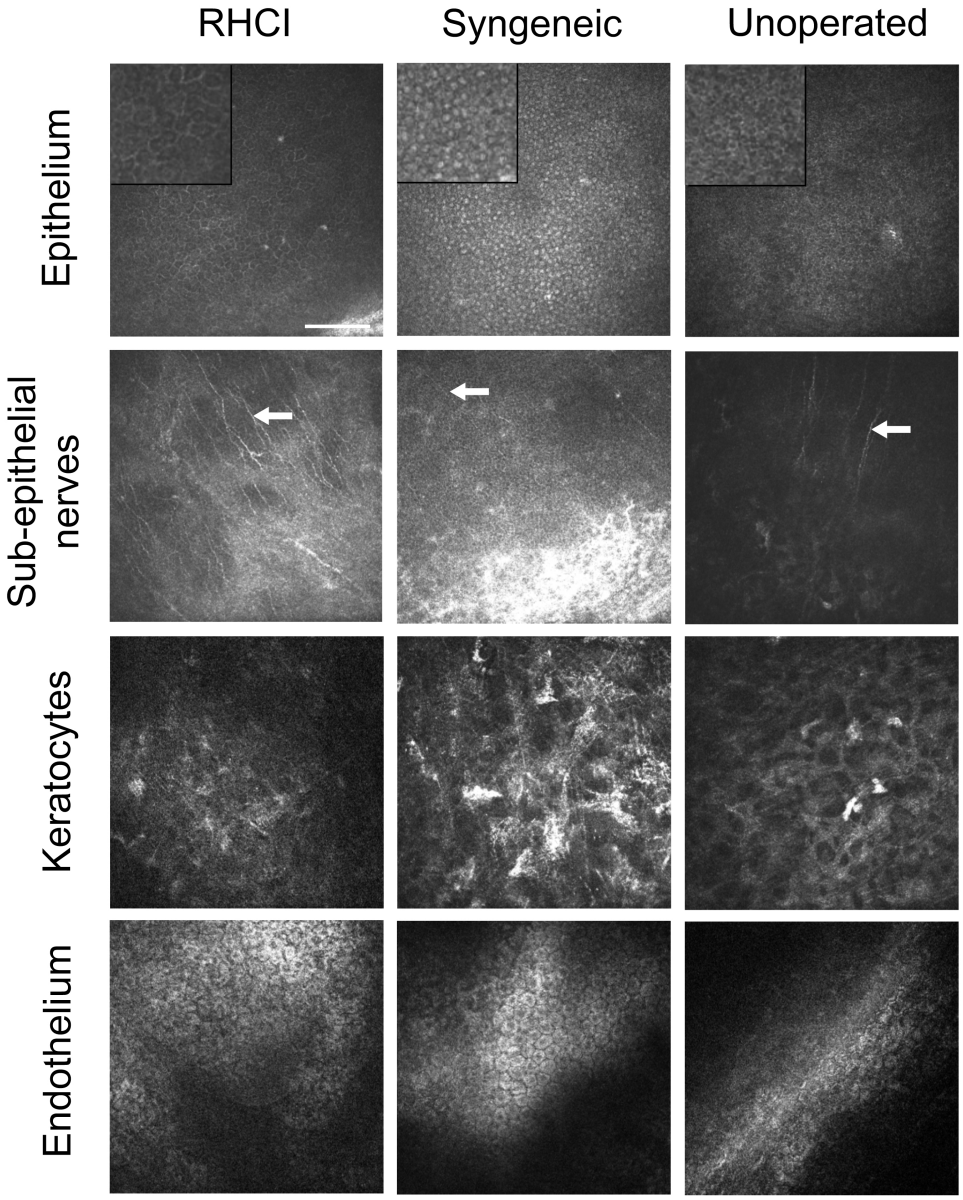
RHCI
Syngeneic
Unoperated
Epithelium
Sub-epithelial nerves
Keratocytes
Endothelium

Figure 5.

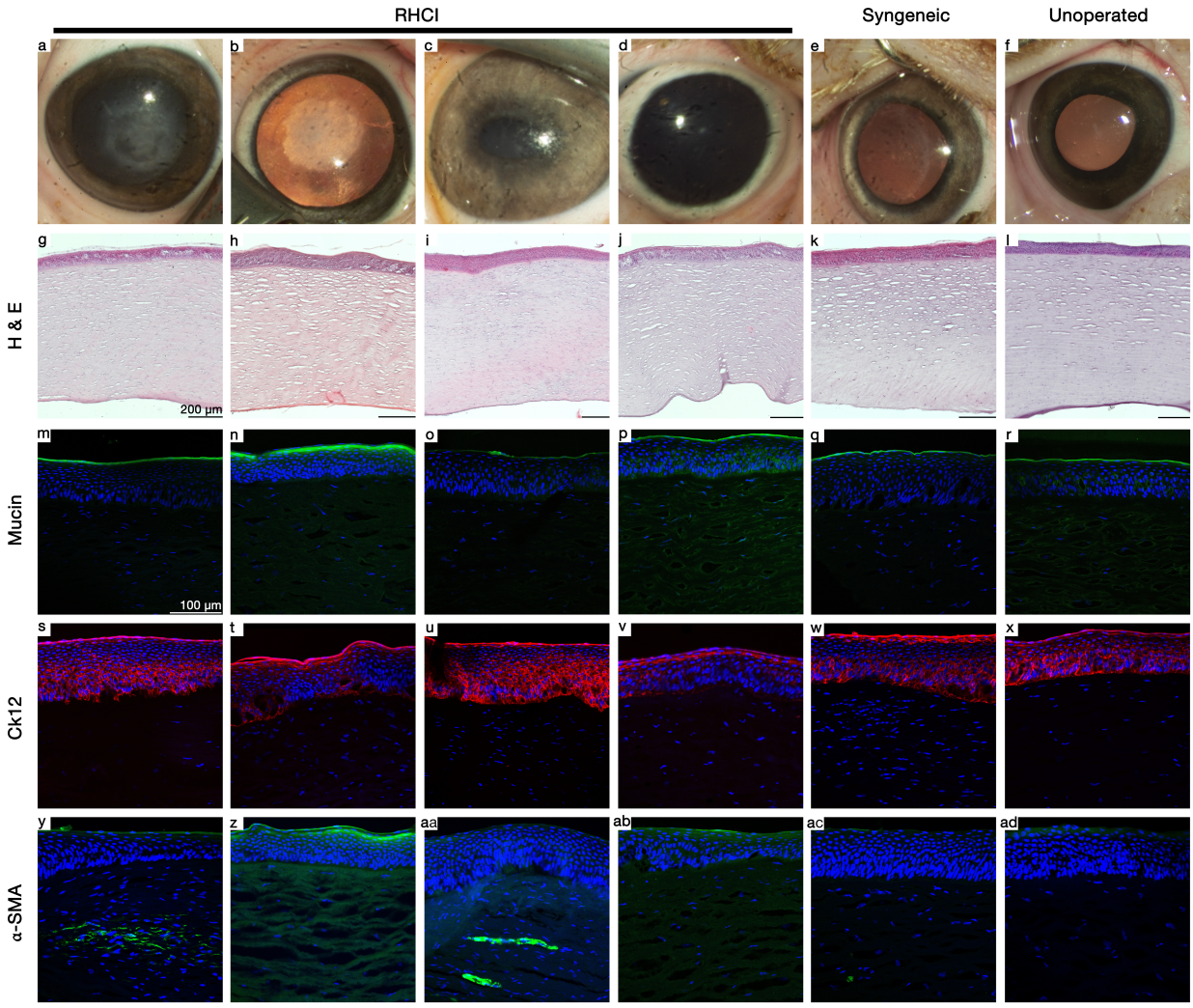

Supplementary Figures

Supplementary Figure 1.

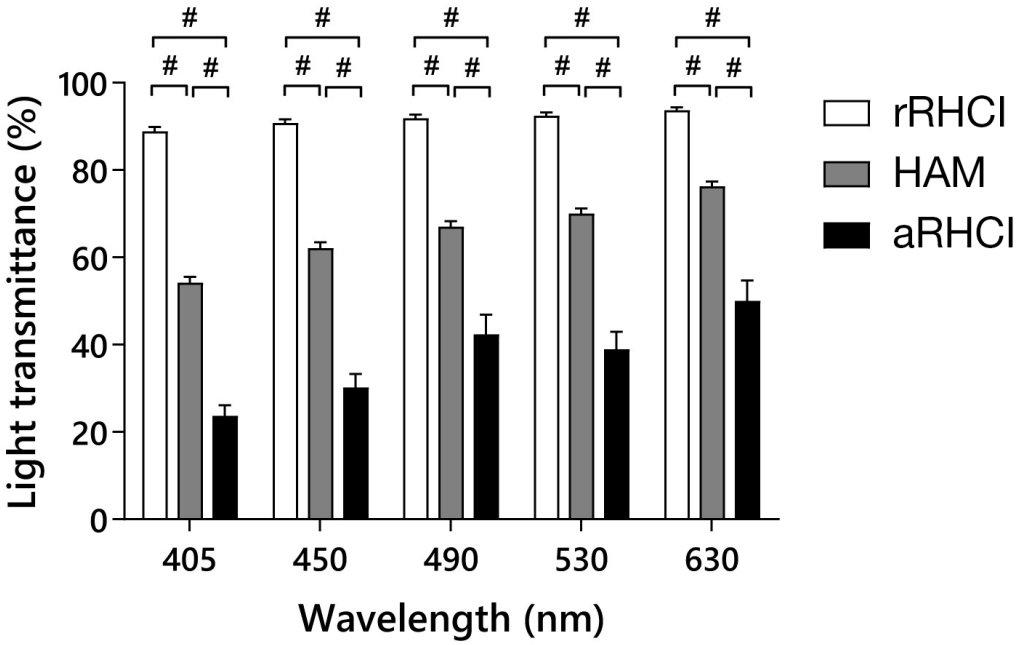

Supplementary Figure 2.

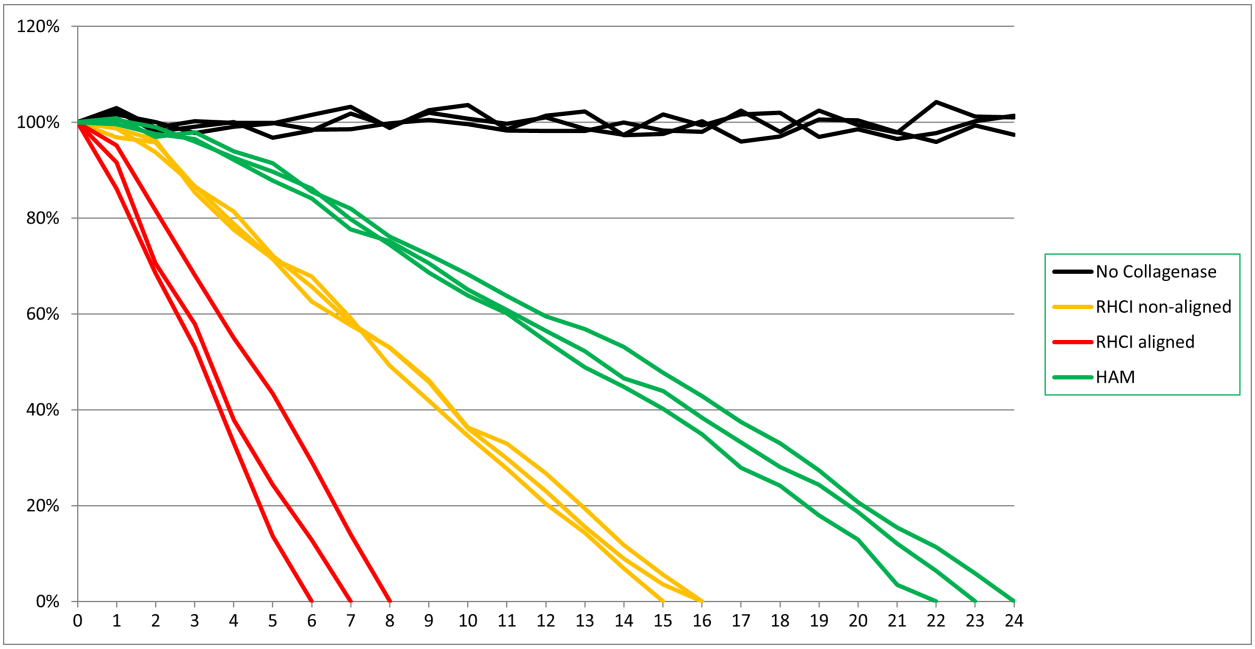

Supplementary Figure 3.

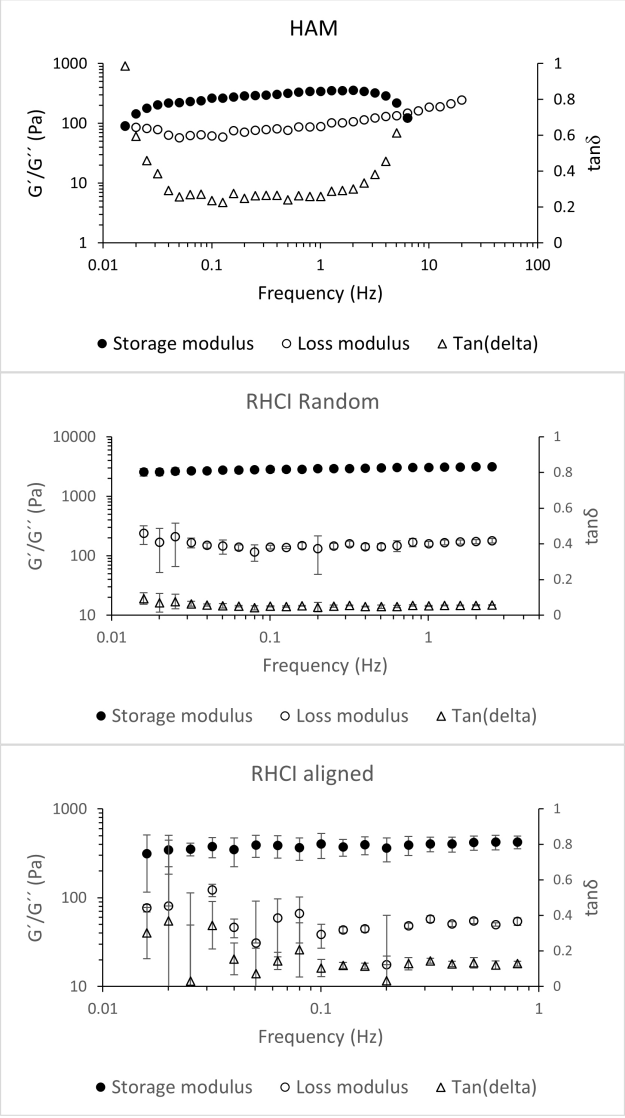

Supplementary Tables

Table S1. Method of *in vivo* biocompatibility grading of H&E slides from rat subcutaneous implantation at three months post-operation.

Cell Type/ Response	**Score**				
	0	**1**	**2**	**3**	**4**
Polymorphonuclear cells	0	Rare, 1-5/phf	6-20/phf	>21/phf	packed
lymphocytes	0	Rare, 1-5/phf	6-20/phf	>21/phf	packed
Plasma Cells	0	Rare, 1-5/phf	6-20/phf	>21/phf	packed
Macrophages	0	Rare, 1-5/phf	6-20/phf	>21/phf	packed
Giant Cells	0	Rare, 1-5/phf	6-20/phf	>21/phf	packed
Necrosis	0	Minimal	Mild	Moderate	Severe
Neovascularisation	0	1-3 focal capillaries	4-10 capillaries with supporting fibroblastic structure	>10, or broad band of capillaries with supporting structure	Numerous capillaries with supporting fibroblastic structure
Band of Fibrosis	0	Narrow	Moderate	Thick	Extensive
Fatty Infiltrate	0	Minimal fat associated with fibrosis	Layering of fat and fibrosis	Elongated and broad accumulation of fat cells at implant site	Extensive fat surrounding the whole implant

PHF: Per high power field (400x)

Under the conditions of this study, the test sample was considered as a non-irritant (0,0 up to 2,9) slight irritant (3,0 up to 8,9) moderate irritant (9,0 up to 15,0) severe irritant ($>$ 15)

Table S2. Antibodies used for immunohistochemistry

Antibody	**Dilution**	**Specificity**	**Reference**
Anti-ΔNp63	1:100	Delta Negative p63 isotype	NBP2-29467, Novus Bio, Littleton, Colorado
Anti-Coll-IV	1:100	Collagen type IV	Ab6586, Cambridge, UK Abcam,
Anti-KRT14	1:100	Cytokeratin 14	Ab9220, Abcam
Anti-Laminin	1:25	Laminin	Ab11575, Abcam
Anti-KRT3	1:100	Cytokeratin 3	Ab68260, Abcam
Anti-E-cad	1:100	E-cadherin	Ab1416, Abcam
Anti-INTB4	1:50	Integrin-β4	Ab110167, Abcam
Anti-Syndecan-1	1:100	Plasma Cells	Ab34164, Abcam
Anti-CD68	1:200	Macrophages	Ab955, Abcam
Anti-CD3	1:100	Lymphocytes	Ab16669, Abcam
Anti-Myeloperoxidase	1:100	Granulocytes	Ab9535, Abcam
Anti-vWF	1:500	von Willebrand Factor	Ab6994, Abcam
Anti-αSMA	1:50	Smooth muscle cells	Ab7817, Abcam
Donkey anti-Rabbit IgG (H+L), Cy3 conjugate	1:1000	Secondary antibody	711-165-152, ImmunoResearch Suffolk, UK Jackson (JI),
Donkey anti-Mouse IgG (H+L), Biotin conjugate	1:100	Secondary antibody	715-065-151, JI
FITC Streptavidin conjugated	1:100	Tertiary antibody	016-010-084, JI
Goat anti-rabbit IgG (H+L), Alexa Fluor 488 conjugate	1:1000	Secondary antibody	A-11008, Thermo Fisher Scientific
Goat anti-rabbit IgG (H+L), Alexa Fluor 594 conjugate	1:1000	Secondary antibody	A-11012, Thermo Fisher Scientific
Goat anti-Mouse IgG (H+L), Alexa Fluor 488 conjugate	1:1000	Secondary antibody	A-11029, Thermo Fisher Scientific

Antibody	**Dilution**	**Specificity**	**Reference**
Goat anti-Mouse IgG (H+L), Alexa Fluor 594 conjugate	1:1000	Secondary antibody	A-11005, Thermo Fisher Scientific

Table S3. Microbial susceptibility of HAM versus aligned and random RHCI hydrogels

Pseudomonas aeruginosa strain	Material	CFU			Average number of CFU/mL ± SEM
ATCC 15442 (1,9 x 10^8 CFU/mL)	HAM	5,4 x 10^7	9,0 x 10^7	1,0 x 10^7	5,1 ± 2,3 x 10^7
	RHCI random	2,2 x 10^5	2,0 x 10^5	0,9 x 10^5	1,7 ± 0,4 x 10^5
	RHCI aligned	4,1 x 10^5	3,4 x 10^5	3,0 x 10^5	3,5 ± 0,3 x 10^5
	TSB	3,4 x 10^{10}	3,5 x 10^{10}	3,7 x 10^{10}	3,5 ± 0,1 x 10^{10}
	PBS	8,3 x 10^7	5,3 x 10^7	8,1 x 10^7	7,2 ± 1,0 x 10^7
ATCC 9027 (8,9 x 10^8 CFU/mL)	HAM	9,0 x 10^7	2,1 x 10^8	3,1 x 10^8	2,0 ± 0,6 x 10^8
	RHCI random	0,2 x 10^6	1,6 x 10^6	2,9 x 10^6	1,5 ± 0,8 x 10^6
	RHCI aligned	7,0 x 10^6	5,9 x 10^6	5,1 x 10^6	6,0 ± 0,6 x 10^6
	TSB	2,3 x 10^{10}	4,5 x 10^{10}	3,6 x 10^{10}	3,4 ± 0,6 x 10^{10}
	PBS	4,0 x 10^7	3,7 x 10^7	1,7 x 10^7	3,1 ± 0,7 x 10^7

CFU: Colony Forming Unit; HAM: Human Amniotic Membrane; TBS: Tryptic Soy Broth; PBS: Phosphate Buffered Saline

Table S4. Results of in vivo biocompatibility grading of HE slides

Parameter	RHCI					HAM				Fibrin			Sham	
Implant present (P) or absorbed (A)	P	P	P	P	P	A	A	A	A	A	A	A	A	A
PMN cells	0,13	0,1	0	0,1	0	/	1,27	0,73	1,07	0,46	0,4	0,47	0,1	0,47
Lymphocytes	2,73	2,33	3,13	1,87	2,07	/	1,6	1,47	1,33	0,4	0,87	1,4	0,85	0,8
Plasma Cells	0,2	0,1	0	0,13	0	/	0,1	0,1	0,1	0	0,1	0,13	0	0
Macrophages	1,87	2,13	2	1,33	1,87	/	1,4 7	0,87	1,93	0,86	0,6	1,2	1,85	1,4
Giant Cells	0	0	0	0	0	/	0	0	0	0	0	0	0	0
Necrosis	0	0	0	0	0	/	0	0	0	0	0	0	0	0
Neovascular-isation	1,73	1,27	1,33	1,27	1	/	1,6	1,6	1,8	0,93	0,87	1,2	0,85	1,53
Fibrosis	1,53	1,87	1,87	1,33	1,27	/	4	4	4	4	4	4	4	4
Fatty Infiltrate	0	0,1	0	0	0	/	0,1	0,1	0	0,4	0,47	0,13	0	0
No. sites /slide examined	3	3	3	3	3	3	3	3	3	3	3	3	3	3
PMN: polymorphonuclear; /: quality of sample insufficient for grading														